

Decoding the molecular interplay of tissue regeneration and disease progression: Insights from liver and brain models

By:

Shruti

PhD20211

Under the Supervision of:

Dr. Jaspreet Kaur Dhanjal

Department of Computational Biology

Indraprastha Institute of Information Technology Delhi

June, 2026



Decoding the molecular interplay of tissue regeneration and disease progression: Insights from liver and brain models

By:

Shruti

PhD20211

A Thesis submitted

in partial fulfilment of the requirements for the degree of

Doctor of Philosophy

To the

Department of Computational Biology

Indraprastha Institute of Information Technology Delhi

June, 2026

Certificate

This is to certify that the thesis titled "**Decoding the molecular interplay of tissue regeneration and disease progression: Insights from liver and brain models**" being submitted by Ms. Shruti to the Indraprastha Institute of Information Technology Delhi, for the award of the degree of Doctor of Philosophy, is an original research work carried out by her under my supervision. In my opinion, the thesis has reached the standards fulfilling the requirements of the regulations relating to the degree.

The results contained in this thesis have not been submitted in part or full to any other university or institute for the award of any degree/diploma.



Date: June 21, 2026

Place: New Delhi

Dr. Jaspreet Kaur Dhanjal
Assistant Professor
Department of Computational Biology
Indraprastha Institute of Information Technology Delhi
New Delhi 110020

Declaration

"I acknowledge that I am fully responsible for the entire content of my thesis, including any sections assisted by online tools, including Artificial Intelligence-based tools. I accept full accountability for any violations of ethical standards in publications arising from the use of such tools.".

Month, Year	June, 2026
Student Name	Shruti
Roll Number	PhD20211
Advisor Name	Dr. Jaspreet Kaur Dhanjal



Indraprastha Institute of Information Technology Delhi
New Delhi 110020

Acknowledgments

I would like to express my sincere gratitude to my supervisor, **Dr. Jaspreet Kaur Dhanjal**, for her exceptional guidance, constant encouragement, and steadfast support throughout my doctoral studies. Her scientific acumen and insightful feedback have profoundly influenced the trajectory of this research; more importantly, I am grateful for her patience and for believing in my potential even during the moments I doubted myself. I am also deeply indebted to our collaborator from IIT Delhi, **Dr. Shilpi Minocha** for her invaluable suggestions, mentorship, and motivation, which significantly enhanced the quality and clarity of this work.

I would like to thank my internal committee members, **Prof. GPS Raghava** and **Dr. Vibhor Kumar**, for their invaluable guidance and insightful feedback throughout this research. Their constructive criticism and continued support have been instrumental in shaping the direction and quality of this thesis.

On a personal level, I want to thank the **University Grants Commission (UGC)** for the PhD fellowship that supported me financially. This fellowship gave me the freedom to carry out research.

I am deeply thankful to my lab mates, who made the lab feel like home. To **Samriddhi**, my companion from day one, thank you for growing alongside me through every milestone. We started this journey as novices and finished as peers, and I will always cherish the way we leaned on each other to reach the finish line. To **Rajeswari**, you have been more than a lab mate; thank you for being my "baby sister" and for supporting me with such a listening heart. My gratitude to **Prateek**, for capturing life through your lens and helping me find the joy necessary to survive the Ph.D. grind; to **Arnab**, for being the best seatmate and a truly lovely colleague; and to **Shivangi**, for your wonderful companionship and collaboration. Working alongside such dedicated individuals turned every challenge into a shared learning experience.

A special mention goes to my best friend and soulmate, **Mohima**. Thank you for your unwavering belief in me and for being the source of my strength whenever I faltered.

I owe my deepest gratitude to **my parents**, whose unconditional love, trust, and sacrifices have been the foundation of all my achievements. To my baby brother, **Ekansh**, thank you for being my constant cheerleader. Your innocence and belief in me kept me going, and having you by my side has made this journey so much sweeter.

Lastly, I wish to express my profound appreciation to my husband, **Anshul**. Your patience, understanding, and unwavering emotional support helped me stay grounded throughout this demanding pursuit. Thank you for your constant belief in my potential and for being my pillar of strength during the most difficult phases of this journey. This achievement is as much yours as it is mine.

I sincerely acknowledge the **Indraprastha Institute of Information Technology Delhi** for providing access to advanced computational resources, which were instrumental in the smooth execution of this thesis.

Lastly, I would like to acknowledge of AI tools for light headed editing of the content of my thesis.

This Ph.D. journey has been one of immense learning and personal growth, and I feel lucky to have had such caring people around when things got tough. Thanks to each person who lifted me up at various times.

Date: June 21, 2026 **Shruti**

Place: New Delhi PhD20211

Abstract

Abstract

Regeneration and disease progression involve context-dependent outcomes of shared molecular and cellular programs that maintain tissue homeostasis. Effective regeneration requires the precise activation and timely resolution of pathways regulating inflammation, metabolism, cell proliferation, and differentiation, whereas persistent or dysregulated activation of these same pathways can drive chronic disease and malignancy. Intervention will require understanding and applying conserved regulatory signals and targets for successful execution of failure of regenerative programs in disease.

The aim of this thesis is to find the molecular determinants that distinguish successful regeneration from pathological progression using integrated transcriptomic and functional analyses across tissues with contrasting regenerative capacities. The systems chosen for study, the liver and brain, serve as paradigm cases, where the liver represents a prototype of a robustly regenerating organ and the adult mammalian brain exemplifies an organ with severely limited regenerative potential. Zebrafish as a model organism offer the possibility to investigate neural regenerative capacity and metabolic challenges allowing the examination of both evolutionarily conserved and tissue-specific controls in these contexts.

In liver, coordinated regulation of both metabolism and cell cycle emerges as key to regenerative potential. Epigenetic co-regulator Host Cell Factor-1 (HCF-1) is found to function as a key integrator linking hepatic metabolic state to transcriptional networks conducive to both proliferative hepatocyte expansion and restoration of liver tissue. A lack of HCF-1 function, leads to a buildup of metabolic byproducts and inhibits regenerative responses to lead eventually to the pathogenic state of MAFLD (metabolic dysfunction-associated fatty liver disease). To further dissect the molecular events underlying disease onset, a high-fat diet–induced MAFLD zebrafish model was also established and characterized. This model enabled systematic analysis of transcriptional and metabolic changes associated with the transition from metabolic adaptation to pathological lipid accumulation and inflammation, shedding light on early regulatory failures leading to the development of MAFLD.

Parallelly, whole-brain transcriptomic profiling of zebrafish after traumatic injury shows that effective neural regeneration not only is accompanied by local neurogenic activation and also by a large scale and dynamic change in gene expression profile. The p38 MAPK pathway, specifically MAPK14a, is identified as a critical regulator of progenitor activation,

proliferation, and neuronal replacement. Functional inhibition of MAPK14a disrupts glial and neuronal progenitor responses, impairs neurogenesis and gliogenesis, and alters downstream Wnt/β-catenin and PI3K/AKT signaling, establishing MAPK14a as a nodal regulator of regenerative signaling.

Comparative analysis across multiple stages of regeneration and cancer progression reveals that early regenerative responses share striking transcriptional similarities with tumor-associated programs, including inflammation-driven signaling, metabolic reprogramming, and progenitor-like cellular states. However, a distinct divergence emerges during later stages of regeneration, when proliferative programs are actively terminated and replaced by processes associated with tissue reorganization, differentiation, and functional integration. In contrast, cancer fails to engage these terminal regulatory mechanisms, resulting in persistent proliferation and disruption of tissue architecture. By integrating longitudinal transcriptomic profiles of regenerating zebrafish brain with gene expression data from glioblastoma, this work identifies two distinct molecular programs associated with regenerative termination. These programs are characterized by coordinated cell-cycle exit and suppression of mitotic activity, rather than merely a gradual decline in proliferation. Their activation during late regeneration, but not in cancer, highlights critical regulatory control points that distinguish successful regenerative resolution from pathological proliferation.

Together, these findings provide a broader perspective on the molecular mechanisms underlying regeneration and their relationship with disease progression. Across the liver and brain, the studies highlight the importance of coordinated regulation of metabolic, inflammatory, and proliferative processes during tissue repair. Disruption of these regulatory mechanisms can alter regenerative responses and contribute to pathological outcomes, as observed in metabolic liver disease and glioblastoma. Overall, this thesis identifies molecular regulators and transcriptional programs associated with successful regeneration and provides insights into how their dysregulation may contribute to disease progression.

List of Abbreviations

ChIP-Seq: Chromatin Immunoprecipitation sequencing;

CpG: Cytosine-phosphate-Guanine;

DAVID: The Database for Annotation, Visualization and Integrated Discovery;

H3K4me3: Trimethylated histone H3; HET, Heterozygous;

HCF-1: Host Cell Factor 1;

KO: Knockout;

LINE: Long Interspersed Nuclear Element;

NASH: Non-alcoholic steatohepatitis;

NAFLD: Non-alcoholic fatty liver disease;

OGT: O-linked β-N-acetylglucosamine transferase;

POL2: RNA polymerase II;

PH: Partial hepatectomy;

srpRNA: Signal recognition particle RNA;

SMA: Smooth muscle α-actin;

TSS: Transcriptional start sites ;

CR: Calorie restriction;

DEG: Dysregulated genes;

ECM: Extracellular matrix;

ER: Endoplasmic reticulum;

GSEA: Gene set enrichment analysis;

GO: Gene ontology;

MAFLD: Metabolic dysfunction-associated fatty liver disease;

MASH: Metabolic dysfunction associated steatohepatitis;

PA: Palmitic acid;

UPR: Unfolded protein response;

Dc: Central zone of dorsal telencephalic area;

Dp: Posterior zone of dorsal telencephalic area;

Dm: Medial zone of dorsal telencephalic area;

Dl: Lateral zone of dorsal telencephalic area;

Vd: Dorsal nucleus of ventral telencephalic area;

Vv: Ventral nucleus of ventral telencephalic area;

BDNF: Brain-derived neurotrophic factor;

BMP: Bone morphogenic protein;

BrdU: 5-bromo-2'-deoxyuridine;

CNS: Central Nervous System;

dpl: days post lesion;

DUSP: dual-specificity phosphatases;

FGF: Fibroblast Growth factor;

GFAP: Glial fibrillary acidic protein;

GO: Gene Ontology;

GSEA: Gene set enrichment analysis;

KEGG: Kyoto Encyclopedia of Genes and Genomes;

NSC: Neural Stem Cells;

PCNA: Proliferating cell nuclear antigen;

RGC: Radial Glial Cells;

Shh: Sonic hedgehog;

SVZ: Subventricular zone;

TBI: Traumatic Brain Injury.

List of Additional Files

Additional file 4.1: Distribution of HCF-1, POL2 and H3K4me3 peaks and Genomic annotation by functional region of HCF-1, POL2 and H3K4me3 peak signals.

Additional file 4.2: HCF-1 peaks with different down trends; Biological Process (BP), Cellular Component (CC), Molecular Function (MF) and KEGG Pathways enriched in regions associated with HCF-1 peak signals decreasing over time; Motifs significantly enriched in HCF-1 binding sites.

Additional file 4.3: Annotation of peaks located in Intergenic regions.

Additional file 4.4: H3K4me3 peaks with different up trends; H3K4me3 peaks with different down trends; BP, CC, MF enriched in regions associated with H3K4me3 peak signals increasing and decreasing over time; KEGG Pathways enriched in regions associated with H3K4me3 peak signals increasing and decreasing over time.

Additional file 4.5: POL2 peaks with different up trends; POL2 peaks with different down trends; Biological Process, Cellular Component, Molecular Function enriched in regions associated with POL2 peak signals increasing and decreasing over time; KEGG Pathways enriched in regions associated with POL2 peak signals increasing and decreasing over time.

Additional file 4.6: Pathway enrichment analysis of the dysregulated genes (D0>>D7) common between POL2 and H3K4me3; Pathway enrichment analysis of the dysregulated genes (D0<<D7) common between POL2 and H3K4me3.

Additional file 4.7: Dysregulated genes from RNA-seq data upon loss of HCF-1. GO (Biological Processes, Molecular Functions, Cellular Components) enrichment analysis and KEGG Pathways associated with dysregulated genes.

Additional Figure 4.1: Loss of *Hcfc1* adversely impacts mitochondrial structure

Additional Figure 4.2: Loss of *Hcfc1* leads to reduction in expression of OXPHOS protein complexes in *Hcfc1*$^{hepKO/Y}$ knockout male mice

Additional Figure 4.3: Loss of *Hcfc1* leads to impairment in levels of electron transport chain complexes.

Additional file 5.1: Dysregulated genes associated with palmitic acid (PA) fed zebrafish. Gene Set Enrichment analysis (GSEA) for Gene Ontology and GSEA for KEGG pathways.

Additional file 5.2: Dysregulated genes associated with high fat diet fructose mouse model. Comparison between Fructose and Palmitic models for the categories.

Additional file 5.3: List of all overlapping dysregulated genes between high fat diet fructose and palmitic models. List of overlapping dysregulated genes with log2FC ≥ 1.0 or ≤ -1.0.

Additional file 5.4: Dysregulated genes associated with human MAFLD dataset. Common upregulated genes and downregulated genes between human and zebrafish model. GO enrichment analysis for common upregulated genes downregulated genes.

Additional File 6.1: List of dysregulated genes at different timepoints across brain regeneration in Zebrafish

Additional File 6.2: Gene Set Enrichment Analysis (GSEA): Enriched GO and KEGG terms across different timepoints in brain regeneration in Zebrafish

Additional File 6.3: List of genes in each module obtained from WGCNA

Additional File 6.4: Module-wise gene enrichment

Additional File 6.5: List of dysregulated genes in mouse traumatic brain injury and their functional enrichment

Additional File 7.1: Transcriptomic profiling and functional annotation data of brain regeneration and brain cancer.

Additional File 7.2: Intersection between regeneration and cancer.

Additional File 7.3: Therapeutic target mapping of inverse expression genes.

Additional File URLS: This file contains the corresponding URLs for each software application, tool, and Python or R package.

All additional files are available at:
https://drive.google.com/drive/folders/1I43LZYnCse28sTsy3F8ACRIbLs7scJDT?usp=drive_link

List of Figures

Figure 4.1. Circos plot showing genome-wide distribution of HCF-1, POL2, and H3K4me3 peaks at days 0, 4, and 7 (A); stacked bar plot of functional genomic annotations for these peaks (B).

Figure 4.2. Heatmaps of temporal HCF-1 peak trends with representative ChIP-Seq profiles, GO enrichment, pathway analysis, and top transcription factor motifs.

Figure 4.3. Donut chart of functional annotations (A) and sunburst chart of transcription factors (B) for intergenic HCF-1 peak regions.

Figure 4.4. Heatmaps of increasing and decreasing H3K4me3 peak trends with KEGG pathway and biological process enrichment analyses.

Figure 4.5. Heatmaps of increasing and decreasing POL2 peak trends with KEGG pathway and biological process enrichment analyses.

Figure 4.6. Immunofluorescence analysis of HCF-1 loss in hepatocytes following tamoxifen-induced *Hcfc1* knockout in mouse liver.

Figure 4.7. Histological assessment of liver injury showing steatosis, macrophage infiltration, and collagen deposition in *Hcfc1* knockout mice.

Figure 4.8. Pathway enrichment analysis of genes with concordant dysregulation patterns in POL2 and H3K4me3 peak signals.

Figure 4.9. GO and KEGG enrichment analyses, mitochondrial process treemap, and schematic of dysregulated mitochondrial genes upon HCF-1 loss.

Figure 5.1. Phenotypic and histological characterization of palmitic acid-supplemented zebrafish showing increased growth and hepatic lipid accumulation.

Figure 5.2. Altered expression of lipid metabolism, ER stress, UPR, oxidative phosphorylation, fatty acid oxidation, and inflammation genes in PA-fed zebrafish.

Figure 5.3. Differential expression analysis of MAFLD zebrafish liver transcriptome including volcano plot, hierarchical clustering, GSEA, and protein-protein interaction networks.

Figure 5.4. Relative mRNA expression of hepatic metabolic genes (*cyp7a1*, *cebpa*, *gck*, *rdh12*, *cetp*) in PA-fed versus control zebrafish livers.

Figure 5.5. Comparative analysis of GO terms, KEGG pathways, and concordantly dysregulated genes between palmitic acid and fructose MAFLD models.

Figure 5.6. Comparison of commonly dysregulated genes between human and zebrafish MAFLD models.

Figure 6.1. Characterization of zebrafish telencephalic stab-wound injury model showing PCNA expression, histology, and regeneration marker expression over time.

Figure 6.2. Immunohistochemical analysis of cell proliferation, neuronal differentiation, and glial activation during zebrafish brain regeneration.

Figure 6.3. Transcriptome profiling of zebrafish brain regeneration at 1, 4, and 7 dpl showing differential gene expression and functional enrichment dynamics.

Figure 6.4. Weighted gene co-expression network analysis revealing module clustering and biological pathway enrichment during brain regeneration.

Figure 6.5. Identification of hub genes and their functional associations across regeneration time points using network topology analysis.

Figure 6.6. Temporal expression heatmaps of cell cycle, MAPK, PPAR, and calcium signaling pathway genes during brain regeneration.

Figure 6.7. Cytoscape network visualization of enriched KEGG pathways among differentially expressed genes across all regeneration stages.

Figure 6.8. Integrated transcriptomic and pathway analysis of zebrafish brain regeneration with emphasis on cell cycle dynamics and MAPK signaling.

Figure 6.9. BIRB796-mediated inhibition of p38α MAPK signaling impairs proliferative and regenerative responses following zebrafish brain injury.

Figure 7.1: Temporal transcriptome analysis of zebrafish brain regeneration. Differential expression and GSEA reveal stage-specific gene regulation and pathway enrichment at 1, 3, and 14 dpl.

Figure 7.2: Transcriptomic profiling of zebrafish brain cancer. Volcano plots and GSEA identify cancer-specific DEGs and dysregulated GO terms and KEGG pathways.

Figure 7.3: Intersection of regeneration and cancer transcriptomes. Overlapping DEGs and shared biological terms between regenerative stages and brain cancer highlight common molecular programs.

Figure 7.4: Anti-regenerative, pro-cancer gene signatures. Genes downregulated during regeneration but upregulated in cancer are mapped to cancer hallmarks via Sankey and treemap visualizations.

Figure 7.5: FAM26F (CALHM6) predicts poor survival in glioblastoma. Elevated tumor expression and significant association with adverse prognosis across GEPIA2, CGGA, and TCGA cohorts.

Figure 7.6: FAM26F downstream network and functional enrichment. PPI, GO, and KEGG analyses of FAM26F-overexpression models reveal regulated effectors and implicated signaling pathways.

List of Tables

Table 4.1. Functional roles of significantly enriched transcription factors mapped to HCF-1-interacting intergenic regulatory sites.

Table 4.2. Liver regeneration-associated genes downregulated upon hepatocyte-specific *Hcfc1* loss.

Table 7.1. Identification of High-Confidence FAM26F Downstream Effectors via Reciprocal Expression Analysis.

Contents

Certificate ..... **iii**

Declaration ..... **iv**

Acknowledgments ..... **v**

Abstract ..... **viii**

List of Abbreviations ..... **xi**

List of Additional Files ..... **xiii**

List of Figures ..... **xv**

List of Tables ..... **xvii**

Chapter 1. Introduction **2**

1.1 Pathological Consequences of Dysregulated Regeneration 2

Chapter 2. Review of Literature **6**

2.1 Overview of Tissue Regeneration and Disease Progression 6

2.2 Comparative Models: Liver and Brain 9

2.3 Liver Regeneration and Metabolic Disease 9

2.3.1 Mechanisms of Liver Regeneration 9

2.3.2 HCF-1 as a Master Regulator of Liver Regeneration 10

2.3.3 From Regenerative Failure to MAFLD Pathogenesis 11

2.3.4 Animal Models of MAFLD 13

2.3.5 Zebrafish as a Novel Model for MAFLD 14

2.4 Brain Regeneration and Neurodegeneration 15

2.4.1 Zebrafish as a Model for Brain Regeneration 15

2.4.2 p38α MAPK in Brain Regeneration 16

2.4.3 The Continuum Between Regeneration and Carcinogenesis 17

2.5 Synthesis and Concluding Perspectives 19

Chapter 3. Thesis objectives **21**

3.1 Objectives 21

Chapter 4. HCF-1 as a molecular switch between liver regeneration and steatotic disease in a conditional knockout mouse model (*Mus musculus*). **22**

4.1 Graphical abstract 22

4.2 Background 23

4.3 Materials and methods 25

4.3.1 Experimental design and Data sources 25

4.3.2 ChIP-seq data processing and peak calling 26
4.3.3 Histological and Immunohistochemical Analyses 27
4.4 Results 27
4.4.1 Dynamic chromatin occupancy of HCF-1 during hepatocyte-specific depletion in mice 27
4.4.2 HCF-1 loss disrupts cell cycle, stress, immune, and lipid-metabolic regulatory networks 29
4.4.3 Potential binding partners of HCF-1 31
4.4.4 Annotation of HCF-1 peak signals localized in intergenic regions 32
4.4.5 Changes in gene expression profiles and its regulation by methylation upon loss of HCF-1 33
4.4.6 Hepatic HCF-1 depletion drives progressive liver injury and impairs hepatocyte proliferative capacity 38
4.4.7 Functional inactivation of HCF-1 leads to a disturbed metabolic and signaling networks in *Hcfc1* knockout mice 44
4.5 Discussion 48
4.6 Conclusion 50
Chapter 5. Dissecting the molecular landscape of MAFLD using a palmitic acid-supplemented high-fat diet zebrafish model (*Danio rerio*) 52
5.1 Graphical abstract 52
5.2 Background 53
5.3 Methods 55
5.3.1 Zebrafish care and diet protocol 55
5.3.2 Annexin V Staining (Apoptosis) 56
5.3.3 Reactive oxygen species (ROS) assay for estimating oxidative stress 56
5.3.4 Staining for endoplasmic reticulum (ER) stress 56
5.3.5 Histological staining 56
5.3.6 Immunoblotting (Western Blot) 56
5.3.7 Quantitative Real-time PCR (qPCR) 56
5.3.8 Whole genome transcriptomic profiling 56
5.3.9 Statistical analysis 57
5.4 Results 57
5.4.1 Palmitic acid (PA) supplementation induces hepatic steatosis and early liver injury in adult zebrafish 57
5.4.2 PA supplementation perturbs lipid metabolism and activates ER and mitochondrial stress pathways 58
5.4.3 PA supplementation disrupts oxidative phosphorylation and fatty acid oxidation 59
5.4.4 PA supplementation induces oxidative stress and inflammatory signaling 59
5.4.5 Mapping of PA-supplemented diet induced pathophysiological changes to alterations in transcriptome 60

5.4.6 Protein–protein interaction analysis identifies key regulatory nodes in MAFLD progression 64
5.4.7 Cross-species comparison reveals conserved molecular signatures of MAFLD 68
5.5 Discussion 71
5.6 Conclusion 74
Chapter 6. Molecular and cellular basis of brain regeneration in zebrafish *(Danio rerio*). 76
6.1 Graphical abstract 76
6.2 Background 77
6.3 Methods 78
6.3.1 Animal Handling and Injury Model. 79
6.3.2 Protein Analysis (Immunoblotting) 79
6.3.3 Histological and Immunofluorescence Assessment 79
6.3.4 RNA Analysis and Transcriptomic Profiling 80
6.3.5 Quantitative RT-PCR (qRT-PCR) 80
6.3.6 Transcriptomic Data Analysis 80
6.3.7 Weighted Gene Co-Expression Network Analysis 81
6.3.8 Statistical Analysis 82
6.4 Results 82
6.4.1 Establishment of telencephalic stab wound injury model to study brain regeneration in zebrafish 82
6.4.2 Transcriptome Profiling and functional annotation of the zebrafish telencephalon during different stages of brain regeneration 85
6.4.3 Weighted co-expression networks 92
6.4.4 Identification of key molecular players with high connectivity across stages of regeneration 93
6.4.5 Activation dynamics of proliferative genes across distinct regenerative phases 99
6.4.6 p38α MAPK is upregulated during brain regeneration in Zebrafish 101
6.4.7 Inhibition of MAPK14a leads to impairment of the progenitor response 105
6.5 Discussion 107
6.6 Conclusion 112
Chapter 7. Mapping the transcriptomic divergence between controlled regenerative exit and oncogenic persistence in zebrafish (*Danio rerio*) 114
7.1 Graphical abstract 114
7.2 Background 115
7.3 Methods 116
7.3.1 Transcriptome Analysis 116
7.3.2 Data Acquisition and Survival Analysis of Glioblastoma Cohorts 116

7.3.3 Identification of FAM26F-Regulated Downstream Effectors 117
7.4 Results 117
7.4.1 Transcriptomic Landscape of Brain Regeneration in Zebrafish 117
7.4.2 Overlap Between Regeneration and Brain Cancer 118
7.4.3 Divergence Between Regeneration and Cancer at Late Stages 122
7.4.4 Identification of FAM26F as a Novel Prognostic Marker 125
7.4.5 FAM26F Regulatory Network and Functional Mechanisms 127
7.5 Discussion 131
7.6 Conclusion 133
Chapter 8. Summary and future directions 135
Bibliography 139
Publications 163

Introduction

Chapter 1. Introduction

1.1 Pathological Consequences of Dysregulated Regeneration

The ability of multicellular organisms to maintain tissue integrity in response to injury, environmental stress, and aging depends on the coordinated regulation of tissue repair and regeneration. Tissue regeneration and disease progression can represent contrasting outcomes of shared molecular and cellular processes, with successful regeneration restoring tissue homeostasis and dysregulation of these processes contributing to pathological states. Regeneration involves the coordinated proliferation, differentiation, and organization of specific cell populations to restore tissue structure and function, whereas disease may arise when these responses are impaired, unresolved, or aberrantly sustained (1). Although regenerative ability is widespread across the animal kingdom, its extent varies considerably among species and tissues (2). Organisms such as planarians, salamanders, and zebrafish can regenerate complex structures and, in some cases, entire organs, whereas regenerative capacity in adult mammals is considerably more restricted (3). Understanding the molecular and cellular mechanisms that enable successful regeneration in highly regenerative organisms, and how these mechanisms become limited or dysregulated under pathological conditions, therefore represents an important area of biological and biomedical research.

Disease progression can be viewed as a gradual deviation from tissue homeostasis driven by cumulative alterations in cellular and molecular processes. Chronic disorders, including metabolic diseases, fibrosis, cancer, and neurodegenerative conditions, frequently involve regenerative responses that are either insufficient or fail to resolve appropriately. Inflammation, for example, is essential for initiating tissue repair, but its persistent activation can promote fibrosis and progressive tissue dysfunction. Similarly, activation and proliferation of stem or progenitor cells are fundamental to regeneration, whereas their uncontrolled or sustained proliferation can contribute to tumorigenesis (4). Thus, regeneration and disease are not necessarily governed by entirely distinct molecular mechanisms; rather, their outcomes depend on the context, magnitude, and temporal regulation of shared cellular programs. Advances in high-throughput transcriptomics, single-cell sequencing, spatial transcriptomics and epigenomic profiling have enabled these dynamic processes to be examined with increasing molecular and cellular resolution (5). These approaches have demonstrated that both regenerative and pathological states are characterized by coordinated and temporally changing

gene-expression programs rather than fixed cellular responses. Integrating these data with information on epigenetic regulation, metabolism, and intracellular signalling can therefore provide a more comprehensive understanding of how tissues transition between homeostasis, regeneration, and disease.

Studying systems where the processes of regeneration and disease are fundamentally at odds proves particularly beneficial in elucidating general and organ specific mechanisms involved in regeneration and disease. While for some aspects the general principles derived from these systems may not be organ specific, other details will clearly vary by organ.

Comparative analysis of tissues with markedly different regenerative capacities provides a useful framework for identifying both conserved and tissue-specific determinants of regeneration. The liver and brain represent contrasting examples among vertebrate organs. The liver possesses a remarkable ability to recover following injury through coordinated hepatocyte proliferation and interactions among epithelial, immune, and stromal cell populations. In contrast, the adult mammalian brain has limited capacity to replace lost neurons, and neuronal injury frequently results in persistent functional deficits (6). Studying these systems in parallel therefore provides an opportunity to examine how common regulatory principles are adapted to tissues with fundamentally different regenerative capacities.

In the liver, regeneration requires close coordination between metabolic state, transcriptional regulation, and cell-cycle progression. The epigenetic co-regulator Host Cell Factor-1 (HCF-1) has emerged as an important link between metabolic cues and transcriptional programs required for hepatocyte proliferation (7). Under chronic metabolic stress, however, these regulatory processes can become disrupted, contributing to lipid accumulation, inflammation, and progression of metabolic dysfunction-associated fatty liver disease (MAFLD) (8). Genome-wide transcriptomic and epigenomic analyses provide an opportunity to investigate how alterations in these regulatory networks influence the transition from metabolic homeostasis to disease and compromise regenerative capacity.

The brain provides a complementary system in which regenerative capacity differs substantially across species. Unlike the adult mammalian brain, the adult zebrafish brain retains extensive neurogenic potential throughout life. Following injury, specialized radial glial cells are activated and generate new neurons, enabling restoration of damaged neural tissue without the persistent inhibitory scarring characteristic of the mammalian central nervous system (9). Investigation of the molecular programs underlying this response has highlighted signalling

pathways, including p38 MAPK, that coordinate progenitor activation, proliferation, and subsequent neuronal regeneration. Such highly regenerative systems provide a useful framework for identifying molecular mechanisms that may be absent, restricted, or inadequately activated in tissues with limited regenerative capacity.

The relationship between regeneration and disease becomes particularly relevant in the context of cancer. Physiological regeneration requires transient activation of proliferative and developmental programs followed by their timely termination as tissue structure and function are restored. Tumorigenesis can involve persistent activation of many of these same processes, including cellular plasticity, progenitor-like states, inflammatory signalling, and proliferation (10). A critical distinction may therefore lie not only in the pathways that are activated, but also in whether proliferative programs are appropriately terminated. Comparative analysis of regenerating zebrafish brain and brain tumor transcriptomes provides a means to identify molecular programs that are activated during both processes but subsequently resolved during successful regeneration and persist in cancer (11). Such comparisons can help define regulatory mechanisms that distinguish controlled tissue repair from pathological proliferation and provide a broader understanding of how dysregulated regenerative programs contribute to disease progression.

Review of Literature

Chapter 2. Review of Literature

2.1 Overview of Tissue Regeneration and Disease Progression

The relationship between the tissue regeneration and pathologic disease is not just of interest to understand both the processes but is also very important for maintaining health. These processes represent the opposing fates of cellular function and molecular regulatory networks (12). One leads toward healing, and another, typically due to injury, towards destruction of normal cellular and tissue function. Understanding how tissues regenerate following injury and how diseases progress when this regeneration fails or becomes dysregulated lies at the heart of modern biomedical research. Insights gained into cellular remodeling and tissue equilibrium contribute toward the identification of novel therapeutic strategies for managing various chronic and degenerative disorders. Tissue regeneration represents the rebuilding of tissues by replacement of defective cell and tissue constituents with functioning counterparts a process present in various animal species. Yet regeneration ability shows vast and uneven distribution among species such as in lower vertebrates: zebrafish or salamanders, where they possess advanced capabilities for growth of many organs and tissues, and in some cases even of central-nervous tissue, which are dramatically absent in mammals (13). This level of difference has motivated extensive comparative research to identify the cellular and molecular mechanisms that underlie successful regeneration in highly regenerative species, with the goal of reawakening similar capacities in humans. Key signaling pathways such as fibroblast growth factor (FGF), Wnt/β-catenin and Notch have emerged as central regulators of regeneration across tissues, orchestrating processes like stem cell activation, proliferation and dedifferentiation (14). These conserved signals therefore become a new blueprint to engineer therapeutic treatments to boost human tissue repair capabilities beyond current levels.

From a scientific perspective regeneration has far reaching implications for the burgeoning field of regenerative medicine that aims to harness these mechanisms to help generate artificial or induce endogenous regeneration of lost tissues and organs. Progresses in stem cell studies, tissue engineering, gene manipulations and many more technologies have thus made various new approaches to replacing damaged tissues with functioning counterparts. These can be illustrated by understanding regenerative biology, which has allowed for therapies such as organoids and hepatocyte transfer to cirrhosis patients (15). Similarly, studies of neural and cardiac regeneration in model organisms have inspired efforts to induce regenerative responses

in the mammalian heart and central nervous system, these tissues previously thought to be incapable of repair. The translation of these discoveries from bench to bedside highlights how fundamental research on tissue regeneration can directly inform therapeutic innovation.

In parallel, understanding disease progression in the series of cellular, molecular, and systemic changes that drive a disease from its initial onset to advanced pathology is equally critical for improving human health. Diseases such as fibrosis, cancer, metabolic disorders and neurodegeneration represent aberrant forms of cellular behaviour, where normal regulatory networks governing proliferation, differentiation, and death become disrupted. Elucidating the molecular mechanisms that control disease progression helps in identifying early biomarkers, predicting prognosis, and designing effective therapeutic interventions. For instance, cancer progression has been conceptualized through the "hallmarks of cancer," which include sustained proliferative signaling, evasion of growth suppressors, and resistance to cell death all of which reflect hijacked regenerative and repair mechanisms (16). These insights underscore the notion that disease and regeneration share common signaling axes but differ in their regulation and outcome.

The intersection of regeneration and disease is particularly intriguing, as it illustrates how the same molecular pathways that promote repair can in pathological contexts drive uncontrolled tissue remodeling and tumorigenesis. Chronic inflammation, for example, is a double-edged sword: while it recruits immune cells that facilitate repair, persistent inflammation can induce fibrosis and organ dysfunction (17). Likewise, activation of stem cells is necessary for regeneration but dysregulation may lead to the formation of cancer stem cells and malignant growth. Thus, studying tissue regeneration not only informs our understanding of healing but also reveals how its dysregulation contributes to disease progression. This interplay is evident in fibrosis, where excessive extracellular matrix deposition replaces functional tissue, and in cancer, where regenerative signaling pathways are co-opted to sustain tumor growth and metastasis.

Another crucial aspect of studying regeneration and disease progression lies in understanding cellular plasticity the ability of cells to change their identity or function in response to environmental cues. During regeneration, differentiated cells may dedifferentiate or transdifferentiate to contribute to tissue repair as seen in the reprogramming of fibroblasts into cardiomyocytes or neurons. Conversely, in disease, similar reprogramming events can drive metastasis or drug resistance (16). Investigating the regulatory networks controlling cellular

plasticity is therefore essential for distinguishing between adaptive and maladaptive responses in tissues. Recent advances in single cell omics and spatial transcriptomics have revolutionized this field by enabling mapping of gene expression dynamics during regeneration and disease progression with an unprecedented resolution (18).

From a translational perspective, the convergence of regeneration and disease progression research offers significant potential for therapeutic discovery. For example, factors that enhance regenerative capacity such as growth factors, extracellular vesicles, and microRNAs are being explored as therapeutic agents to reverse degenerative diseases. On the other hand, inhibitors of aberrant regenerative signaling are being tested as anti-cancer and anti-fibrotic drugs. Understanding the delicate balance between regeneration and pathological remodeling enables the design of therapies that restore homeostasis without triggering uncontrolled growth or scarring (19). Moreover, regenerative biology provides the conceptual and experimental framework for developing bioengineered organoids, tissues, and synthetic models that can be utilized to study disease progression in a controlled environment.

In summary, the basic biological study of regeneration and disease progression has broad and concrete implications for medicine. It serves to bridge the knowledge of a naturally competent repair system with that of disease-induced damage, so that the universal cellular and signaling mechanisms involved in regeneration and disease may be identified and applied to combat disease. This fusion not only contributes to our basic understanding of life's resistance and repair abilities, but leads to developing novel treatments and therapies for all manner of degenerative diseases from organ failure to cancer. With ongoing breakthroughs and shifts in biomedicine, studying these fundamental phenomena continues to play a crucial role in discovering life's hidden regenerative and resilient nature, and ultimately, how best to harness this for therapeutic applications.

2.2 Comparative Models: Liver and Brain

To investigate the mechanisms distinguishing tissue regeneration from disease progression, two distinct yet complementary vertebrate organ systems are evaluated: the liver and the brain. These organs represent two extremes of regenerative capacity in vertebrates: the liver possesses remarkable regenerative potential, while the brain, particularly in mammals, exhibits limited ability to restore lost or damaged neurons. Comparing these systems provides unique insights into the molecular, cellular, and systemic mechanisms that govern tissue recovery and pathological remodeling. Understanding how regeneration succeeds in the liver but remains

constrained in the brain is critical for uncovering the fundamental principles of tissue plasticity and for identifying therapeutic strategies to enhance repair and counteract disease progression.

2.3 Liver Regeneration and Metabolic Disease

2.3.1 Mechanisms of Liver Regeneration

The liver is one of the most regenerative organs across vertebrate species, extensively characterized in rodents (mice and rats) and observed clinically in humans. It can restore up to 70% of its mass following two-thirds partial hepatectomy or toxic injury through tightly regulated mechanisms involving mature hepatocyte proliferation, hepatic progenitor cell mobilization, and signaling from non-parenchymal lineages, including resident Kupffer cells and hepatic stellate cells (15). In murine and human liver regeneration, the process begins with a priming phase wherein pro-inflammatory cytokines such as IL-6 and TNF-α activate STAT3 and NF-κB signaling cascades to transition quiescent G0 hepatocytes into the G1 phase of the cell cycle. This is followed by a robust proliferation phase driven primarily by the HGF/c-Met and Wnt/β-catenin pathways, which stimulate the expression of Cyclin D1 and promote DNA synthesis (20). Concurrently, the Hippo/YAP pathway acts as a crucial mechanical and biochemical sensor to regulate organ size, while metabolic reprogramming ensures that hepatocytes meet the high energetic demands of division without compromising systemic glucose and lipid homeostasis (21). Once the original liver mass is restored a set point often referred to as the "Hepatostat" the process is actively terminated through the growth-inhibitory signals of the TGF-β and Activin A pathways, which arrest the cell cycle and prevent pathological overgrowth (22–24). This process restores not only the size but also the functional complexity of the liver, maintaining metabolic and detoxification capacity. It is central to numerous physiological functions, including the processing of metabolites, detoxification of xenobiotics, and regulation of lipid and glucose metabolism (25). Owing to this multifunctionality, the liver is continually exposed to metabolic stress and xenobiotic insults, rendering it particularly susceptible to injury. The same metabolic complexity that supports regeneration also predisposes the liver to progressive diseases such as metabolic dysfunction-associated fatty liver disease (MAFLD), steatohepatitis (MASH), fibrosis, and cirrhosis. Thus, the liver exemplifies how the fine balance between regeneration and disease progression determines clinical outcomes.

2.3.2 HCF-1 as a Master Regulator of Liver Regeneration

Emerging studies have substantially expanded our understanding of HCF-1 as a master regulator of hepatocyte proliferation, chromatin organization, and metabolic homeostasis during liver regeneration (26,27). Initially identified as a host cell factor for herpes simplex virus replication, HCF-1 is a conserved metazoan transcriptional co-regulator encoded by the *Hcfc1* gene on the X chromosome (28). The HCF-1 precursor protein undergoes proteolytic cleavage mediated by O-linked β-N-acetylglucosamine transferase (OGT), yielding functional subunits that physically interact with diverse chromatin-modifying enzymes (29). Genome-wide analyses have demonstrated that HCF-1 is extensively co-occupied with E2F transcription factors at promoters of genes required for DNA replication, centrosome duplication, and mitotic progression, reinforcing its essential role in cell-cycle control (26).

The indispensability of HCF-1 in liver regeneration is underscored by its role as a metabolic-to-proliferative bridge, acting as a high-order scaffold that coordinates chromatin modification and metabolic signaling. Upon stimuli like partial hepatectomy or acute injury, HCF-1 enables quiescent hepatocytes to exit the G0 state by assembling Set1/MLL methyltransferase complexes (30). These complexes sustain high levels of H3K4 trimethylation and coordinate with KAT8/MOF to promote H4K16 acetylation at the promoters of E2F-responsive genes (31–33). This dual epigenetic action creates a "permissive" environment essential for the efficient "pause-release" of RNA Polymerase II, driving the expression of critical G1/S transition factors like Cyclin A2 and E1 (34). By integrating these transcriptional and metabolic cues, HCF-1 functions as a guardian of hepatic homeostasis, ensuring the timely replacement of damaged tissue while safeguarding long-term liver function (35).

In parallel, HCF-1 has been shown to play a crucial role in maintaining hepatic metabolic identity during regeneration (34)**.** The unique aspect of HCF-1 in the liver is its interaction with O-GlcNAc transferase (OGT) (36). Its interaction with OGT positions HCF-1 at the intersection of nutrient sensing and epigenetic regulation, allowing fluctuations in glucose and amino acid availability to be transduced into chromatin-based transcriptional programs. This HCF-1–OGT axis is particularly important in the regenerating liver, where rapid metabolic adaptation is required to balance detoxification, biosynthesis, and cell division. HCF-1 is not only a substrate for OGT-mediated proteolytic cleavage which activates HCF-1 for its cell cycle roles but it also acts as a scaffold to recruit OGT to metabolic regulators (37,38). Specifically, the HCF-1/OGT complex stabilizes PGC-1-alpha, a master regulator of gluconeogenesis and

mitochondrial biogenesis. This dual functionality allows HCF-1 to serve as a nutrient sensor, ensuring that the liver maintains its vital metabolic functions, such as glucose production, even as it undergoes the energetic stress of rapid tissue mass restoration (39).

However, when HCF-1 function is compromised, the regenerative machinery effectively stalls. HCF-1 depletion results in a failure to activate E2F-responsive gene networks following partial hepatectomy, leading to G1/S arrest and replication stress (40). Mechanistically, the loss of HCF-1 disrupts activating histone modifications and permits the accumulation of repressive chromatin states, thereby compromising transcriptional fidelity during regenerative responses. This failure to re-enter the cell cycle triggers a cascade of cellular stress and metabolic maladaptation, where the liver's metabolic workload is distributed across a diminishing number of functional hepatocytes, preventing the organ from restoring its functional mass (41).

2.3.3 From Regenerative Failure to MAFLD Pathogenesis

While liver regeneration represents the organ's reparative capacity, its failure or chronic overactivation leads to metabolic and inflammatory disorders such as MAFLD the most common chronic liver disease globally. MAFLD encompasses a spectrum of hepatic pathologies ranging from simple steatosis (fat accumulation) to MASH, fibrosis, cirrhosis, and hepatocellular carcinoma (42). The disease is characterized by excessive triglyceride accumulation in hepatocytes (≥5%), accompanied by inflammation, oxidative stress, and mitochondrial dysfunction (43). Though early-stage MAFL can be reversed through lifestyle interventions, persistent metabolic dysfunction drives irreversible progression toward MASH and fibrosis. The increasing global prevalence estimated to affect nearly one-third of adults and its association with systemic disorders such as cardiovascular disease and type 2 diabetes underscore its clinical significance (44). Consequently, experimental depletion of HCF-1 does not result in a simple lack of growth, but rather a collapse of lipid homeostasis and a rapid shift toward a MASH phenotype, with persistent DNA damage signaling, altered inflammatory gene expression, and heightened susceptibility to liver injury (35).

As mentioned above HCF-1 serves as a direct sensor of the cell's nutritional status, in a state of nutrient overload, excessive OGT activity leads to the hyper-GlcNAcylation of HCF-1 and its associated transcription factors (45). This modification alters the affinity of HCF-1 for its co-activators. Instead of promoting the G1/S transition, the GlcNAcylated HCF-1 complex preferentially stabilizes SREBP-1c and ChREBP (Carbohydrate Response Element Binding Protein) (35,46). This stabilization drives the transcription of *de novo* Lipogenesis (DNL)

enzymes, such as Fatty Acid Synthase (FASN) and Acetyl-CoA Carboxylase (ACC), thereby facilitating the rapid accumulation of intrahepatic triglycerides that defines early-stage MAFLD. The transition from simple steatosis to Metabolic Dysfunction-Associated Steatohepatitis (MASH) is characterized by a failure of hepatocytes to effectively replace damaged tissue. E2F1, typically a driver of the cell cycle, directly regulates the expression of lipogenic genes in the liver. As mentioned above, under normal conditions, HCF-1 assists E2F1 in driving the proliferative programs necessary for regeneration. However, in the context of insulin resistance and hyperinsulinemia hallmarks of MAFLD, the E2F1–HCF-1 complex is redirected (47). This redirection creates a molecular paradox: the hepatocytes receive signals to proliferate (high nutrient availability and insulin), but the HCF-1-mediated epigenetic machinery is occupied by lipogenic programs (48). This leads to what is colloquially termed a "stalled" liver. The hepatocytes undergo DNA replication stress and p53-mediated cell cycle arrest, leading to cellular senescence. As hepatocytes become senescent, they secrete the Senescence-Associated Secretory Phenotype (SASP), which includes proinflammatory cytokines and growth factors that paradoxically activate Hepatic Stellate Cells (HSCs), fueling the progression toward fibrosis and cirrhosis (49).

The collapse of the HCF-1-regulated network also impacts the mitochondrial compartment. As HCF-1 is required to stabilize PGC-1 alpha, its dysregulation leads to impaired mitochondrial biogenesis and compromised β-oxidation (50). When fatty acid oxidation is inhibited while lipogenesis is accelerated, the liver experiences a massive buildup of toxic lipid species, such as diacylglycerols and ceramides. These lipids trigger ER stress and mitochondrial Reactive Oxygen Species (ROS) production (51). This lipotoxicity further inhibits the proteolytic processing of HCF-1, creating a vicious cycle: compromised HCF-1 leads to poor mitochondrial health, which generates more ROS, further impairing HCF-1 function (52). This molecular feedback loop explains why MAFLD becomes significantly harder to reverse once it reaches the MASH stage; the epigenetic machinery required to resolve metabolic stress is impaired, effectively crippling the liver's regenerative potential.

2.3.4 Animal Models of MAFLD

In metabolic research, the High-Fat Diet (HFD) model is considered the most physiologically relevant method for studying Metabolic Dysfunction-Associated Fatty Liver Disease (MAFLD) because it closely mimics the over-nutrition and sedentary lifestyle typical of the modern human condition (44). Unlike older nutrient-deficient models that often cause weight

loss, the HFD model successfully replicates the systemic "metabolic syndrome" symptoms of MAFLD, including obesity, insulin resistance, and dyslipidemia. In this model, organisms are typically fed a diet where 45% to 70% of the total caloric intake is derived from fats often lard, beef tallow, or coconut oil sometimes supplemented with high levels of fructose or cholesterol to accelerate disease progression (53). Over a period of 12 to 36 weeks, the excessive intake of saturated fatty acids leads to the accumulation of triglycerides within hepatocytes, a condition known as steatosis. This lipid overload triggers lipotoxicity, oxidative stress, and chronic low-grade inflammation. As the diet continues, the liver may progress from simple "fatty liver" to Metabolic Dysfunction-Associated Steatohepatitis (MASH), characterized by hepatocyte ballooning and the recruitment of inflammatory cells, eventually leading to fibrosis and even hepatocellular carcinoma in long-term studies (54).

Historically, rodent models such as ob/ob and db/db mice, which possess spontaneous mutations in the leptin or leptin receptor genes, have been widely used to study the genetic underpinnings of obesity and steatosis (53). Similarly, the PTEN-null mouse model, where the phosphatase and tensin homolog gene is deleted in hepatocytes, has provided insights into how altered insulin signaling triggers steatohepatitis and tumor formation. Researchers also traditionally relied on dietary interventions like the methionine–choline-deficient (MCD) and choline-deficient L-amino acid-defined (CDAA) diets (55). While the MCD diet is highly effective at inducing rapid inflammation and fibrosis within weeks, it is often criticized for causing severe weight loss and lacking the insulin resistance characteristic of human MAFLD (56). The CDAA diet was developed as a refinement to maintain body weight while still promoting rapid fibrotic progression, though it still lacks the full metabolic profile of a standard high-fat diet (54).

Regarding the organisms studied, research into MAFLD utilizes a diverse array of animal models, each offering unique translational insights into the human disease. Mice, particularly the C57BL/6 strain, are the most common subjects because they are highly susceptible to diet-induced obesity and develop metabolic profiles similar to humans. Rats, specifically Wistar and Sprague-Dawley strains, are favored for their larger size, which facilitates more frequent blood sampling and surgical procedures (57). Beyond rodents, Rabbits are used to study the specific link between liver fat and atherosclerosis due to their human-like lipid metabolism. In more complex studies, large mammals like the Ossabaw mini-pig provide a high level of anatomical and metabolic similarity to humans, making them ideal for long-term cirrhosis research (58). In recent years, zebrafish (*Danio rerio*) has emerged as a powerful alternative

model organism due to its physiological, genetic, and metabolic conservation with mammals (59). The zebrafish liver becomes fully functional within four days post-fertilization, harboring hepatocytes, macrophages, and neutrophils that mirror mammalian counterparts, making it suitable for studying steatosis, inflammation, and regeneration (60).

2.3.5 Zebrafish as a Novel Model for MAFLD

Building upon these advantages, a novel adult zebrafish model of MAFLD was established through overfeeding combined with dietary supplementation of palmitic acid (PA), a saturated fatty acid known to provoke hepatic lipid accumulation and inflammatory signaling. Palmitic acid triggers lipotoxicity, insulin resistance, and oxidative stress, effectively mimicking early stages of human MASH (61). RNA-seq–based transcriptomic profiling revealed substantial overlap between the differentially expressed genes in this zebrafish model and human MAFLD datasets, reinforcing its translational relevance. Comparative analysis with a high-fructose-diet mouse model further demonstrated concordant activation of pathways associated with cholesterol biosynthesis, lipid metabolism, and mitochondrial function are key determinants of MAFLD pathogenesis. These findings highlight the zebrafish's capacity to faithfully reproduce molecular hallmarks of human fatty liver disease and provide a tractable system to study its progression and potential therapeutic targets.

Together, these complementary investigations evaluating murine HCF-1-mediated liver regeneration alongside diet-induced MAFLD modeling in zebrafish illustrate the dual nature of hepatic homeostasis, wherein pathways facilitating acute regenerative repair undergo maladaptive remodeling under chronic metabolic stress to drive progressive disease (62). The epigenetic landscape, exemplified by HCF-1's role in integrating transcriptional and metabolic cues, serves as a regulatory switch between regenerative and degenerative states. Similarly, the zebrafish MAFLD model provides an opportunity to dissect how metabolic overload and lipotoxic stress rewire transcriptional and mitochondrial networks, tipping the balance from adaptation to degeneration. Thus, studying these systems in parallel allows us to understand how the liver maintains, loses, and potentially regains its remarkable regenerative capacity in the face of metabolic dysfunction.

In essence, the liver stands as a powerful paradigm for studying the continuum between regeneration and disease progression. By integrating insights from epigenetic regulation, transcriptomics, and comparative model systems, we can elucidate the molecular determinants that govern hepatic resilience and vulnerability. Such understanding is essential not only for

developing targeted therapies for metabolic liver diseases but also for uncovering universal principles of regeneration applicable to other organ systems.

2.4 Brain Regeneration and Neurodegeneration

2.4.1 Zebrafish as a Model for Brain Regeneration

Another model explored to understand the molecular basis of tissue regeneration and disease progression is the brain, an organ that represents one of the most complex and least regenerative systems in higher vertebrates. In mammals, the central nervous system (CNS) exhibits extremely limited regenerative potential; neuronal loss resulting from trauma, stroke, or neurodegenerative diseases is largely irreversible due to inhibitory factors in the microenvironment, glial scar formation, and restricted neurogenesis confined to a few discrete regions. In contrast, the zebrafish (*Danio rerio*) possesses a remarkable ability to regenerate its CNS throughout life, offering a unique opportunity to study neuronal regeneration, neurogenesis, and repair mechanisms that may inform therapeutic approaches for human brain injuries and neurodegenerative disorders (63,64).

Regeneration of lost or damaged tissue is a fundamental biological process that enables the restoration of structural and functional integrity following injury. Across the animal kingdom, regenerative capacity varies dramatically from minimal in mammals to extensive in species such as planarians, salamanders, and zebrafish (65,66). Among vertebrates, zebrafish have emerged as an exceptional system to investigate regenerative biology due to their ability to regenerate multiple organs, including the heart, fins, spinal cord, and brain. This unique capacity makes zebrafish an invaluable model to explore the molecular and cellular mechanisms of regeneration, with potential translational relevance for promoting repair in mammalian systems.

Within the CNS, the zebrafish brain stands out for its extensive and lifelong neurogenic potential. Unlike the mammalian brain, where neurogenesis is limited to restricted niches such as the subventricular zone (SVZ) and the hippocampal dentate gyrus, the adult zebrafish brain contains at least 16 distinct proliferative zones along its rostro-caudal axis (9). These zones primarily consist of radial glial cells (RGCs) functional orthologs of mammalian ependymal and neural stem cells and neuroepithelial-like progenitors, both of which play central roles in neurogenesis and tissue repair. Following injury, these progenitors' populations become rapidly activated, proliferate, and migrate to the lesion site where they differentiate into neurons and

glial cells. The newly generated neurons successfully integrate into existing neural circuits, restoring structure and function without the formation of inhibitory glial scars a feature that starkly contrasts with mammalian injury responses (65).

Regeneration in the zebrafish brain can be experimentally modelled using controlled lesions such as telencephalic stab wounds, local ablations, or laser-induced injuries (64,67). These models enable systematic investigation of early transcriptional events and cellular responses that initiate repair. Several key signaling pathways have been identified as critical regulators of progenitor activation, proliferation, and differentiation during zebrafish brain regeneration. Among them, Sonic Hedgehog (Shh), Bone Morphogenetic Protein (BMP/TGF-β), Wnt/β-catenin, Notch, Aryl hydrocarbon receptor (AhR), and Fibroblast Growth Factor (FGF) pathways are known to orchestrate neural stem cell behavior both during development and regeneration (68). These developmental programs are reactivated upon injury, reflecting the principle that regenerative processes often "recapitulate development."

In addition to intrinsic signaling, inflammation plays a pivotal role in initiating and modulating brain regeneration. Upon injury, microglia and macrophages are rapidly activated and secrete cytokines that influence progenitor cell dynamics and tissue remodeling (69). Unlike mammals, where chronic inflammation hinders recovery, zebrafish exhibit a transient and tightly regulated inflammatory response that promotes regeneration by clearing debris and providing growth-promoting signals. Further, factors such as insulin signaling, brain-derived neurotrophic factor (BDNF), and steroid hormones have been implicated in regulating progenitor cell proliferation and differentiation, highlighting the complex interplay between metabolic, immune, and developmental cues during brain regeneration (70).

2.4.2 p38α MAPK in Brain Regeneration

Despite extensive research, the molecular mechanisms governing early stages of brain regeneration remain incompletely understood. To address this, a telencephalic stab wound injury model was established and validated in zebrafish, simulating traumatic brain injury (TBI) (71). This model allows precise spatial and temporal analyses of regenerative responses, using the contralateral, non-injured hemisphere as an internal control. Transcriptomic profiling through RNA sequencing at defined time points control, 1-day post-lesion (dpl), 4 dpl, and 7 dpl revealed a dynamic cascade of gene expression changes. Among the most significantly enriched pathways were the mitogen-activated protein kinase (MAPK) signaling pathways, with the p38 MAPK cascade emerging as a key mediator of regeneration.

The p38 MAPK pathway is well-known for regulating cellular stress responses, proliferation, and differentiation, particularly within the neural lineage (72). It modulates neuronal function by influencing protein translation, ion channel regulation, and neurotransmitter receptor activity (73). Interestingly, this pathway demonstrates dual functional roles: while moderate activation promotes neural stem cell proliferation and neurogenesis, excessive activation can trigger neurotoxicity and apoptosis. Studies in mammals have shown that p38α MAPK activation in the SVZ enhances progenitor proliferation and neurogenesis, whereas its loss reduces neuronal precursor expansion (72). However, aberrant or sustained activation of p38α MAPK has been implicated in neurodegenerative conditions such as Parkinson's, Alzheimer's, and Huntington's diseases, as well as in chemically induced neurotoxicity models (74).

Transcriptomic analyses highlight the central role of p38α MAPK in coordinating the transcriptional programs required for zebrafish brain regeneration. This pathway likely integrates injury-induced stress responses with developmental signaling networks, ensuring controlled proliferation and differentiation of neural progenitors. These findings not only elucidate a novel regulatory axis in zebrafish neurogenesis but also provide potential therapeutic insight into enhancing neural regeneration in mammals while mitigating risks of aberrant cell growth.

2.4.3 The Continuum Between Regeneration and Carcinogenesis

The ability of the zebrafish brain to harness these potent signaling pathways without descending into malignancy suggests that the biological relationship between tissue regeneration and carcinogenesis is increasingly viewed not as two distinct phenomena, but as a regulatory continuum where shared molecular pathways are deployed toward different outcomes (75). At the foundation of this comparison is the "wound that never heals" hypothesis, first articulated by Harold Dvorak, which posits that tumors co-opt the physiological programs of wound repair that is angiogenesis, inflammation, and rapid cell proliferation but fail to execute the terminal "off-switch" that characterizes healthy tissue recovery (76). In a regenerative context, cells undergo a transient period of dedifferentiation and rapid cycling, yet this process remains under strict spatiotemporal control, governed by intact checkpoint proteins like p53 and pRb (77,78). Conversely, in carcinogenesis, the loss of these regulatory signals allows the regenerative state to become constitutive, leading to an immortalized progenitor-like phenotype that drives tumor growth and eventual metastasis.

The molecular machinery driving both processes is centered on highly conserved developmental signaling axes, namely the Wnt/β-catenin, Notch, and Sonic Hedgehog (Shh) pathways (79). In physiological regeneration, these pathways are activated in a pulsatile manner to expand the stem cell pool and guide tissue patterning (80). For instance, during liver regeneration or limb repair in lower vertebrates, these pathways are silenced via negative feedback loops once the target architecture is achieved. In malignancy, however, these same pathways are pathologically sustained through genetic mutations or epigenetic silencing of inhibitors (e.g., *APC* mutations in colorectal cancer or *PTCH1* mutations in medulloblastoma). This creates a state of "frustrated regeneration" where the cell is trapped in a loop of perpetual expansion, utilizing Epithelial-Mesenchymal Transition (EMT) not for wound re-epithelialization, but for systemic invasion (81).

In the mammalian brain, this intersection is particularly complex due to the organ's geographically restricted regenerative capacity. Research into the "cell of origin" for brain tumors suggests that Glioblastoma Multiforme (GBM) often arises from the hijacking of Neural Stem Cells (NSCs) residing in the subventricular zone (SVZ) (82). As the most aggressive primary malignancy of the central nervous system, GBM is defined by its extreme intra-tumoral heterogeneity and a profound capacity for diffuse infiltration into the surrounding parenchyma. This malignancy is sustained by a subpopulation of glioma stem cells (GSCs) that exploit the neurogenic niche's protective signals to maintain a state of treatment-resistant quiescence (83). Recent comparative transcriptomic studies between regenerating zebrafish brains and glioblastomas have revealed a striking "Early Convergence / Late Divergence" model. At the onset of injury, both the regenerating brain and the developing tumor show nearly identical metabolic and proliferative gene modules. However, by the 14-day mark, the zebrafish brain converges back to a homeostatic state, while the human glioma continues to express the "day 3" proliferative profile indefinitely. This metabolic persistence is often marked by the Warburg effect, where the tumor indefinitely utilizes biosynthetic pathways meant only for transient tissue repair (84). This divergence is largely driven by "epigenetic locking," where mutations in histone modifiers (such as the H3K27M onco-histone) freeze the cells in a fetal-like, highly plastic state, preventing the chromatin from closing and thus blocking the path to terminal differentiation (48,85).

Ultimately, the study of brain regeneration offers a roadmap for "differentiation therapy." If glioblastoma is a regenerative process that has lost its way, the therapeutic goal is to re-engage the dormant developmental switches that force Glioma Stem Cells (GSCs) to complete their

journey and become mature, non-cycling neurons or glia (86). By understanding how regenerative species like the axolotl or zebrafish manage rapid neural proliferation without falling into malignancy, we may uncover how to restore the "off-switch" in human brain cancer, effectively turning a lethal disease back into a manageable healing process (83).

Comparative transcriptomic analyses between regenerating zebrafish telencephalon (at 1 dpl, 4 dpl, and 7–14 dpl) and brain cancer models reveal striking parallels and distinctions. In this context, studying brain regeneration in zebrafish not only advances our understanding of neuronal repair but also provides a conceptual framework for investigating the delicate balance between regeneration and disease progression.

2.5 Synthesis and Concluding Perspectives

By studying regeneration in the liver and brain, this work uses two distinct organ systems to investigate the broader molecular principles governing tissue regeneration, homeostasis, and disease progression. In the liver, the epigenetic regulation of regeneration by HCF-1 was investigated alongside the establishment of a zebrafish model of MAFLD to understand how disruption of metabolic and regenerative processes contributes to disease. In the brain, the p38α MAPK signaling pathway was investigated as a nodal regulator of regenerative neurogenesis in zebrafish and in the context of its dysregulation in mammalian neurological conditions. This integrated approach, spanning different tissues and model systems, highlights how molecular pathways involved in physiological tissue repair may contribute to pathological outcomes when their regulation is disrupted or persistently activated. Collectively, this research aims to define key regulatory determinants of successful regeneration and to understand how alterations in these mechanisms contribute to the loss of tissue homeostasis and disease progression.



Objectives

Chapter 3. Thesis objectives

3.1 Objectives

To systematically investigate the molecular and cellular mechanisms governing tissue regeneration and its dysregulation in disease, this thesis is structured around four interconnected objectives.

3.1.1 HCF-1 as a molecular switch between liver regeneration and steatotic disease in a conditional knockout mouse model (*Mus musculus*).

3.1.2 Dissecting the molecular landscape of MAFLD using a palmitic acid-supplemented high-fat diet zebrafish model (*Danio rerio*).

3.1.3 Molecular and cellular basis of brain regeneration in zebrafish (*Danio rerio*).

3.1.4 Mapping the transcriptomic divergence between controlled regenerative exit and oncogenic persistence in zebrafish (*Danio rerio*).

Chapter 4. HCF-1 as a molecular switch between liver regeneration and steatotic disease in a conditional knockout mouse model (*Mus musculus*).

4.1 Graphical abstract

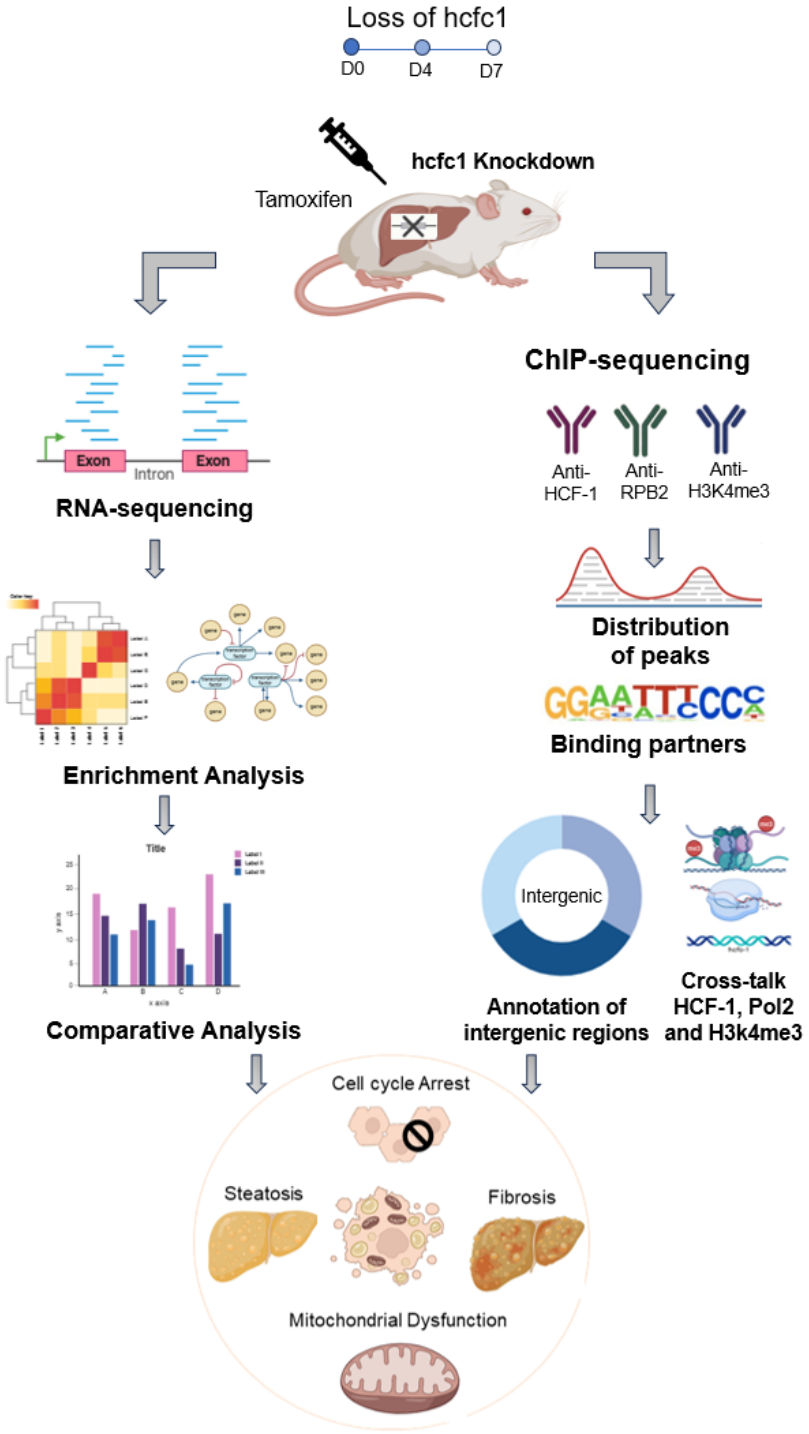

4.2 Background

In vertebrates, the liver is a central metabolic organ, act as a core site for the regulation of glucose and lipid metabolism, clearance of toxins, and the synthesis of essential plasma proteins. Unlike most mammalian tissues, the liver also possesses a remarkable capacity for regeneration, allowing restoration of tissue mass and function after injury through coordinated proliferation, metabolic reprogramming, and epigenetic remodeling of mature hepatocytes and progenitor cells (87,88). Maintaining this regenerative capacity while preserving metabolic homeostasis is critical for liver health, as failure to properly resolve regenerative responses underlies chronic liver diseases such as steatosis, fibrosis, and hepatocellular carcinoma (89–91).

A protein named Host Cell Factor-1 (HCF-1) now stands out because it helps connect cell growth in the liver with normal metabolic activity and positioning it as a central player of liver regeneration and disease susceptibility. Genetic and functional perturbation of HCF-1 disrupts liver repair programs, leading to impaired regenerative responses and progressive metabolic dysfunction, highlighting its essential role in preserving tissue integrity during stress and injury.

Initially identified as a host-cell factor required for herpes simplex virus gene expression, HCF-1 is now recognized as a highly conserved metazoan transcriptional co-regulator with fundamental roles in mammalian physiology. The *Hcfc1* gene, located on the X chromosome, encodes the HCF-1 protein in mice (92). HCF-1 is synthesized as a large 2045–amino acid precursor that undergoes site-specific proteolytic cleavage mediated by O-linked β-N-acetylglucosamine transferase (OGT), generating functional N- and C-terminal subunits that assemble into active regulatory complexes (93,94).

At the molecular level, HCF-1 functions as a central epigenetic scaffold, physically linking sequence-specific DNA-binding transcription factors with a wide array of chromatin-modifying enzymes. These include histone demethylases such as KDM1A (LSD1) (95,96) and PHF8 (97)), histone H3 lysine-4 methyltransferases including SET1 and MLL complexes (98), the histone acetyltransferase KAT8 (MOF) (99), the ubiquitin hydrolase RNF2 (BAP-1) (100), the histone deacetylase complex SIN3A (101), the glycosyl transferase OGT (50,102), and the protein phosphatase PPA1 (40). Through these interactions, HCF-1 localizes preferentially to the transcriptional start sites (TSSs) of numerous genes, where it coordinates transcriptional initiation and chromatin state. Consistent with this central role, HCF-1 has been implicated in

diverse biological processes including development, differentiation, and embryonic stem cell pluripotency (26,103).

HCF-1 is also indispensable for cell proliferation, both *in vitro* and *in vivo*. Genetic studies in mice have demonstrated that HCF-1 is required during embryogenesis and for post-injury tissue repair, particularly in the liver (27). During liver regeneration following two-thirds partial hepatectomy, quiescent hepatocytes must re-enter the cell cycle to restore tissue mass. Strikingly, HCF-1–deficient hepatocytes are unable to do so, rendering them incapable of contributing to liver regeneration (104). These findings establish HCF-1 as a core regulator of hepatocyte proliferative competence.

In additional roles than those in cell cycle control, HCF-1 is crucial for modulating metabolism. Mutations in *HCFC1* have been identified in X-linked human disorders characterized by neurodevelopmental defects and cobalamin metabolism abnormalities (105,106), highlighting its broader physiological importance. In the liver, HCF-1 modulates glucose homeostasis. Its knockdown improves glycemic control in diabetic rats, whereas stabilization of HCF-1 increases hepatic glucose production (50). These metabolic functions are of particular relevance in the context of Metabolic Dysfunction Associated Fatty Liver Disease (MAFLD), a global health burden characterized by excessive lipid accumulation in hepatocytes and progressive metabolic stress. MAFLD can advance to Metabolic Dysfunction Associated Steatohepatitis (MASH), which is marked by chronic inflammation, fibrosis, and eventual cirrhosis.

Consistent with these clinical and metabolic roles, hepatocyte-specific impairment of HCF-1 function in mice is sufficient to induce MAFLD and MASH, demonstrating that HCF-1 is not merely associated with metabolic liver disease but is causally required for maintaining hepatic metabolic stability. Together, these findings position HCF-1 at the intersection of cell proliferation, metabolic regulation, and epigenetic control, yet the molecular mechanisms by which it integrates these processes in hepatocytes remain incompletely understood.

A murine model (*Mus musculus*) was selected as the experimental system for this objective because the structural architecture, metabolic zoning, and regenerative kinetics of the mammalian liver closely parallel human hepatic physiology. Mice provide well-established Cre-loxP genetic tools for hepatocyte-specific and temporally controlled gene disruption, facilitating direct mechanistic interrogation of essential genes without confounding embryonic lethality. Furthermore, the extensive genomic annotation and validated ChIP-grade reagent

availability in the mouse make it uniquely suited for high-resolution epigenomic profiling of transcriptional co-regulators such as HCF-1. Given the indispensable role of HCF-1 in coordinating mammalian liver regeneration and metabolic homeostasis, the hepatic HCF-1 cistrome was systematically mapped in adult mice using ChIP-seq to define its genomic binding landscape and identify its primary transcriptional targets. Integration of these data with RNA Polymerase II (Pol II) occupancy profiles enabled direct correlation between HCF-1 loss and dynamic changes in transcriptional activity across the genome. Building on prior work demonstrating that HCF-1 depletion disrupts H3K4me3 patterns (107), we further examined how HCF-1 recruitment shapes local epigenetic states during regeneration and disease progression.

Together, this multi-omics framework establishes HCF-1 as a pivotal epigenetic integrator that links metabolic cues to transcriptional programs governing hepatocyte proliferation and liver repair. By defining how HCF-1 controls the transition between regenerative and pathological states, this work places HCF-1 at the core of the regeneration–disease continuum that underlies MAFLD progression and hepatic failure.

4.3 Materials and methods

4.3.1 Experimental design and Data sources

All *in vivo* mouse handling, tamoxifen induction, tissue harvesting, and histological and immunohistochemical analyses were carried out in the laboratory of collaborator Dr. Shilpi Minocha at the Indian Institute of Technology (IIT) Delhi, while animal breeding and tissue collection were conducted under approved institutional ethics protocols at the University of Lausanne, Switzerland (Prof. Winship Herr). Experimental procedures and sample preparation were performed by co-first author Debashruti Bhattacharya and colleagues at IIT Delhi. The work presented in this thesis focused on genome-wide bioinformatics processing, ChIP-seq peak calling, temporal motif enrichment analysis, integration of transcriptomic and epigenomic datasets, pathway and network analyses, and biological interpretation of the resulting data. Experimental procedures are described below for completeness and reproducibility.

4.3.1.1 Mouse Models and Tissue Collection

Mice were housed in compliance with EU and national legislation at the University of Lausanne, typically four to five per cage at at 23 °C, with a 12-hour light/dark cycle and ad libitum food/water. Mice were anesthetized with isoflurane and euthanized by cervical

dislocation. Tamoxifen treatment and tissue collection occurred between Zeitgeber Time ZT2 to ZT3 (ZT0 being the start of the light cycle). For all experiments with *Hcfc1*$^{hepKO/Y}$ (KO) males, *Hcfc1*$^{lox/Y}$ male mice were chosen as controls, whereas for *Hcfc*$^{1hepKO/+}$ (HET) females, *Hcfc1*$^{lox/+}$ female mice were used.

4.3.1.2 Chromatin isolation, immunoprecipitation, and preparation of high throughput sequencing

Chromatin was isolated from the liver of individual male Alb-Cre-ERT2^{tg}; *Hcfc1*$^{lox/Y}$ male mice at 0, 4, and 7-days following tamoxifen-induced deletion of the *Hcfc1* allele. Chromatin was immunoprecipitated and prepared for high-throughput sequencing as described (108) using the anti-HCF-1 (Bethyl Laboratories, A301-400A; RRID: AB_961015) H12, anti-RPB2 (Santa Cruz Biotechnology, sc-673–18), and anti-H3K4me3 (Abcam, ab8580) (102,109). Parallel Input DNA samples were processed for each time point (Day 0, 4, and 7) to serve as essential background controls for normalization and to account for local variations in chromatin accessibility. Following library preparation, the samples underwent high-throughput sequencing using the Illumina HiSeq 2500 platform to generate paired-end reads, ensuring high-resolution mapping of DNA fragments and improved alignment across repetitive genomic regions.

4.3.2 ChIP-seq data processing and peak calling

Raw data were cleaned using Trim Galore (v0.6.4) (110) and were checked for quality using FastQC (v0.11.8) (111). STAR aligner (v2.7.9a) was deployed to align the reads to the mouse reference genome (mm10) once they had passed quality control (112). Random, chimeric and uncharacterised reads were removed. Regions from the ENCODE blacklisted list were discarded for further analysis (113). Only the fragments with 255 (unique mapping) and 3 (maps to 2 locations in the target) and 1 (maps to more than 2 locations in the target) MAPQ score were considered. All the fragments bigger than 2 kb were discarded. The module "callpeak" in MACS2 (Model-based Analysis for ChIP Sequencing v2.0) was used to identify regions of ChIP-seq enrichment over the background in an unbiased manner (114). The parameters were adjusted according to different markers, HCF-1 and POL2 in narrow peak mode, H3K4me3 in broad peak mode, with q-value of 0.1. Further, differential peaks were identified using HOMER (v4.11) and intersect function in BEDTools (v2.30.0) (115). Motifs enrichment in peak regions was searched using the findMotifsGenome.pl script in the HOMER suite of tools. For biological interpretation of the results from the ChIP-Seq experiments, gene

ontology and pathway analysis was implemented using web-based tool DAVID (The Database for Annotation, Visualization and Integrated Discovery) (116).

4.3.3 Histological and Immunohistochemical Analyses

To validate computational findings, histological data generated at IIT-Delhi were integrated with the genomic analyses. These included immunohistochemistry (IHC), Sirius Red staining, and Oil Red O staining, which were used to assess hepatocyte proliferation, fibrosis, and lipid accumulation, respectively.

4.3.3.1 Immunohistochemistry (IHC)

IHC was performed on 4-µm paraffin-embedded liver sections following deparaffinization, rehydration, antigen retrieval (citrate buffer), and blocking with 2% normal goat serum. Sections were incubated with primary and secondary antibodies (listed) and counterstained with DAPI before mounting.

4.3.3.2 Sirius Red Staining

Sirius Red staining was used to visualize collagen deposition and assess hepatic fibrosis. Sections were rehydrated, treated with phosphomolybdic acid, stained with Sirius Red, and counterstained with Mayer's hematoxylin.

4.3.3.3 Oil Red O Staining

To assess lipid accumulation, 8-µm liver cryosections were used. The sections were air-dried, fixed, rinsed with isopropanol, stained with Oil Red O, washed, and co-stained with hematoxylin (nuclei appearing blue).

4.3.3.4 Statistical analysis

All experiments were performed with a minimum of three biological replicates. IHC data were quantified using ImageJ, and histological measurements are reported as mean ± SEM. Statistical significance was assessed using a two-tailed Student's t-test in GraphPad Prism, with $p < 0.05$ considered statistically significant.

4.4 Results

4.4.1 Dynamic chromatin occupancy of HCF-1 during hepatocyte-specific depletion in mice

Host Cell Factor 1 (HCF-1) serves as an essential metazoan transcriptional co-regulator that coordinates cell-cycle progression and metabolic homeostasis. Previous studies established that

global genetic deletion of *Hcfc1* is embryonic lethal, while hepatocyte-specific depletion impairs liver regeneration and induces rapid steatotic liver injury. However, the immediate chromatin-level mechanisms and dynamic regulatory targets of HCF-1 in adult liver tissue have remained largely uncharacterised. To define the direct cistromic alterations and transcriptional networks controlled by HCF-1 *in vivo*, chromatin immunoprecipitation followed by high-throughput sequencing (ChIP-seq) was performed in a conditional knockout mouse model (*Mus musculus*). Genome-wide occupancy profiles for HCF-1, RNA Polymerase II (POL2), and trimethylated histone H3 lysine 4 (H3K4me3) were systematically mapped in liver tissue harvested at day 0 (pre-depletion baseline), day 4 (intermediate depletion), and day 7 (complete hepatocyte-specific HCF-1 loss) following tamoxifen administration in Alb-Cre-ERT2^{tg}; *Hcfc1*$^{lox/Y}$ male mice.

Circos plots revealed a genome-wide redistribution of all three chromatin marks over time (**Figure 4.1A**). Genomic annotation showed that although HCF-1 is classically associated with transcription start sites (TSSs), only ~28% of HCF-1 peaks were promoter-proximal, compared with ~32% of H3K4me3 and ~42% of POL2 peaks (**Figure 4.1B)** indicating that HCF-1 also functions extensively at distal regulatory elements.

Approximately 390 HCF-1 peaks were detected at day 0, and these progressively declined by days 4 and 7, demonstrating efficient and temporal loss of HCF-1 occupancy after hepatocyte-specific gene deletion (**Figure 4.1A**). Heatmap analysis revealed five distinct dynamic patterns of HCF-1 occupancy (**Figure 4.2A**) (i) continuous decline (D0 > D4 > D7), (ii) transient loss with partial recovery (D0 > D4 < D7), (iii) early loss with stabilization (D0 > D4 = D7), (iv) transient gain (D0 < D4 > D7), and (v) delayed loss (D0 = D4 > D7). Across all categories, the dominant trend was progressive HCF-1 depletion. This was illustrated at representative loci including Denr and Pura, where HCF-1 binding declined steadily from day 0 to day 7, accompanied by concordant losses of POL2 and H3K4me3 (**Figure 4.2B**), indicating coordinated transcriptional silencing.

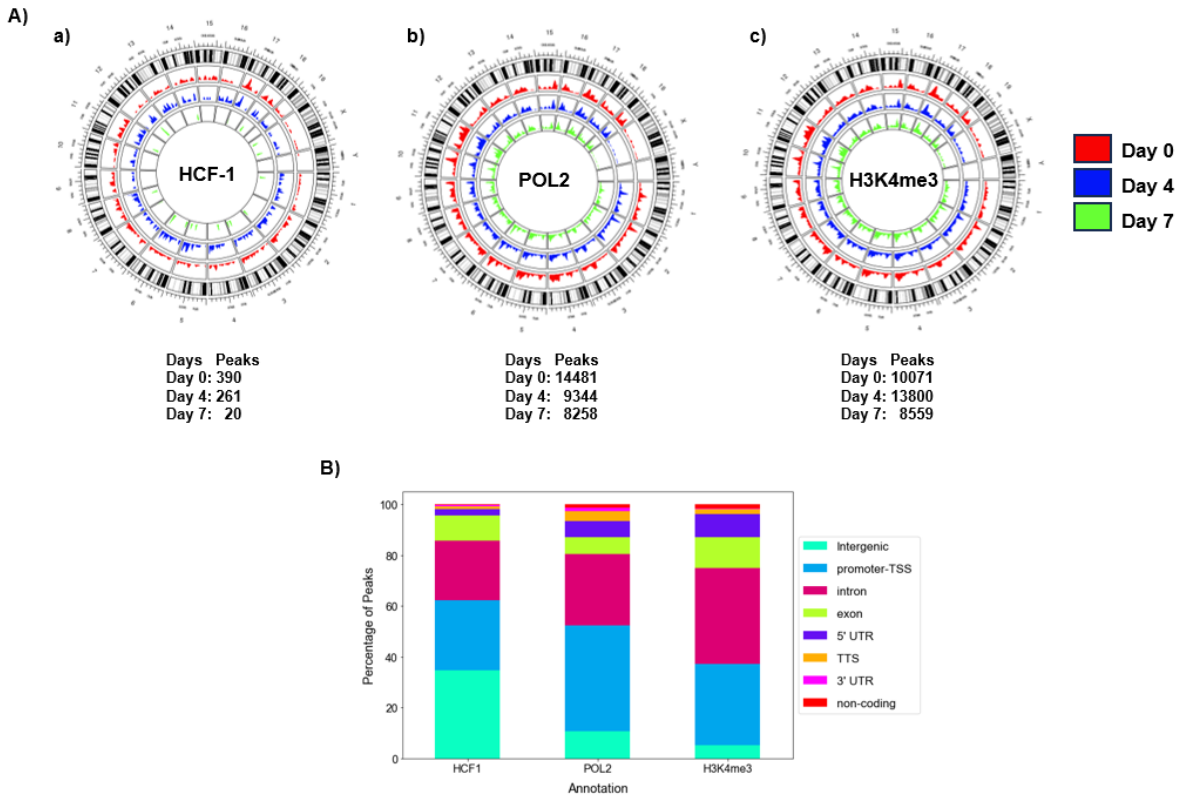

Figure 4.1: **A** Circos plot depicting the distribution of a) HCF-1 b) POL2 and c) H3K4me3 peaks. Red, blue and green colors represent day 0, day 4 and day 7 respectively. Bioconductor package circlize was used with mm10 as the reference genome. **B** Stacked bar plot showing the genomic annotation by functional region of HCF-1, POL2 and H3K4me3 peak signals. Annotation was obtained from HOMER. Associated data is available in Additional file 4.1.

4.4.2 HCF-1 loss disrupts cell cycle, stress, immune, and lipid-metabolic regulatory networks

To determine the biological programs directly regulated by HCF-1, dysregulated ChIP-seq peak signals identified from the day 0, day 4, and day 7 comparisons were mapped to their associated genes and subjected to gene ontology and pathway enrichment analyses (**Figure 4.2C&D**). These HCF-1–associated genes were enriched across multiple core biological processes and signalling pathways.

Strong enrichment was observed for processes related to mitosis and transcription, as well as cell-cycle regulation, cell proliferation, and multicellular organismal development, indicating that HCF-1 is centrally involved in maintaining hepatocyte proliferative and regenerative capacity. In parallel, significant enrichment was detected in MAPK signalling, lipid and atherosclerosis pathways, adaptive immune system signalling, sphingolipid signalling, transcriptional regulation, and cellular responses to stress and external stimuli.

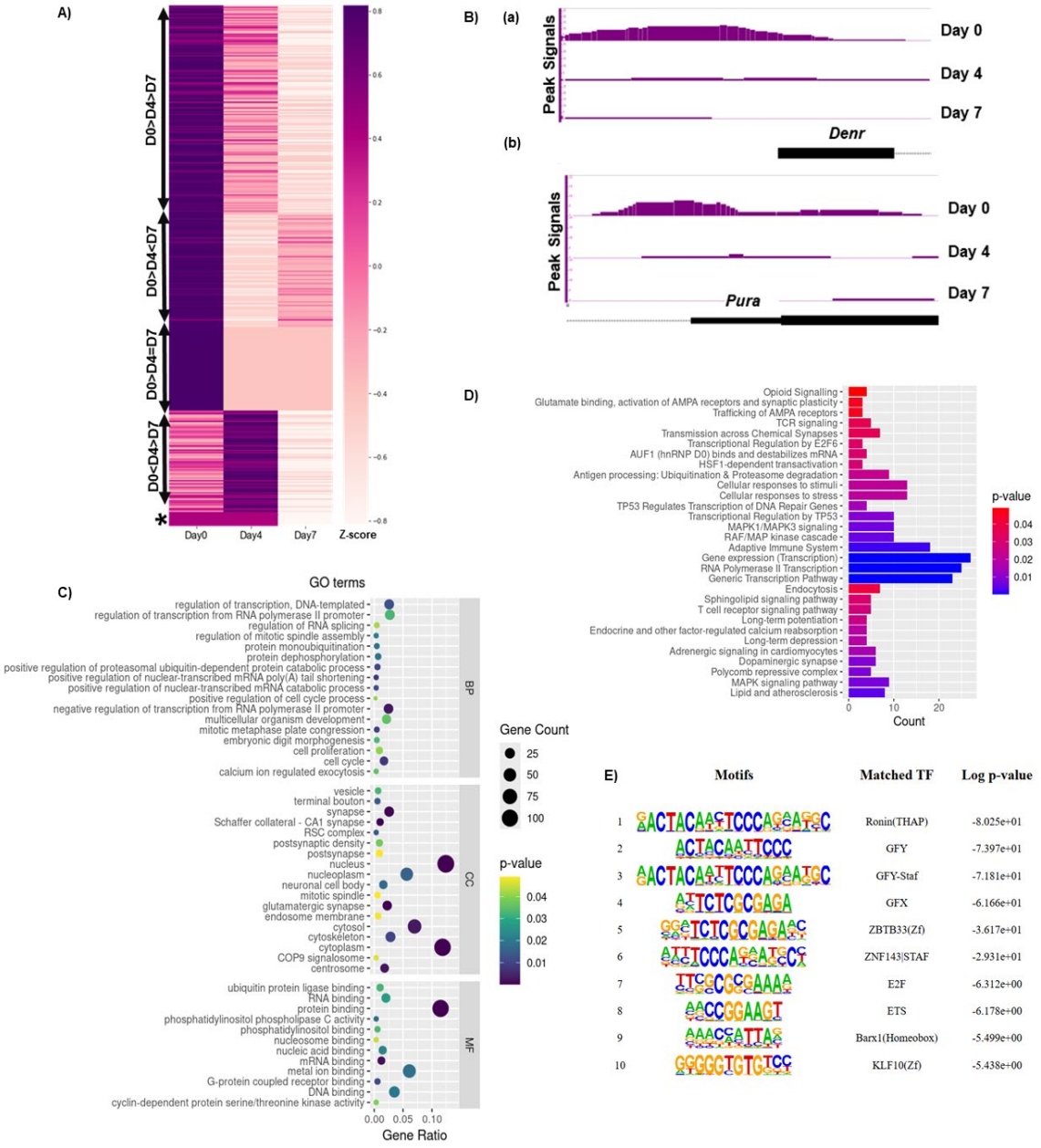

Figure 4.2: A Heatmap displaying decreasing trends [D0 > D4 > D7], [D0 > D4 < D7], [D0 > D4 = D7], [D0 < D4 > D7] in HCF-1 peak signals. Here * represent the [D0 = D4 > D7] trend. The color key indicates the associated row z-score. **B** Visual representation of HCF-1 ChIP-Seq profiles mapped on the genes *Denr* and *Pura* for day 0, 4 & 7 showing continuous decrease trends [D0 > D4 > D7] **C** Gene ontology (GO) of the genes i.e. Biological process (BP), Molecular Function (MF) and Cellular component (CC) associated with regions where HCF-1 peak signals were decreasing with time. **D** Pathway analysis of the genes associated with regions where HCF-1 peak signals were decreasing with time. The enrichment in a specific process and pathway was measured by DAVID. The p-value was determined by Fisher's Exact test. **E** Top ten transcription factor motifs overrepresented in HCF-1 peak regions, found using HOMER. Associated data is available in Additional file 4.2.

Dysregulation of these pathways has direct relevance to MAFLD pathogenesis. Altered MAPK and stress-response signalling compromises hepatocyte survival and adaptive injury responses, increasing susceptibility to inflammation and oxidative damage. Enrichment of developmental

and regenerative pathways suggests that loss of HCF-1 impairs tissue maintenance and regenerative repair, limiting the liver's ability to recover from injury—an established risk factor for progression toward fatty liver disease.

Perturbation of lipid- and sphingolipid-associated pathways is particularly significant, as these pathways regulate lipid synthesis, transport, and storage, all of which are central to hepatic steatosis. Dysregulated cellular localisation and transport pathways further promote lipid accumulation within hepatocytes. In addition, altered immune and inflammatory signalling contributes to hepatic inflammation and insulin resistance, both hallmarks of MAFLD progression.

Collectively, these results demonstrate that HCF-1 regulates an integrated network of proliferative, metabolic, immune, and stress-response pathways required to preserve liver homeostasis. Disruption of this network following *Hcfc1* loss destabilizes the balance between regeneration and metabolic control, thereby creating a molecular environment that promotes lipid accumulation, inflammation, and progressive MAFLD.

4.4.3 Potential binding partners of HCF-1

As a transcriptional co-regulator, HCF-1 does not bind DNA directly but is recruited to chromatin through interactions with sequence-specific transcription factors and chromatin-associated complexes. To identify candidate factors mediating HCF-1 chromatin recruitment in murine hepatocytes, motif enrichment analysis was performed on the genomic coordinates defined by HCF-1 ChIP-seq peaks. The identification of enriched sequence motifs indicates the overrepresentation of specific transcription-factor binding sites but does not in itself demonstrate physical protein-protein interactions with HCF-1 *in vivo*; hence, these factors represent putative or potential binding partners. The top ten significantly enriched DNA motifs ($p \leq 0.01$) within HCF-1-bound regions are presented in **Figure 4.2E**, together with their corresponding transcription factors. Notably, this analysis recovered motifs corresponding to established binding partners of HCF-1, including THAP, KLF10, E2F, and ZNF143, which have been reported in the literature to physically or functionally cooperate with HCF-1 in transcriptional regulation (117,118). These factors are key regulators of cell-cycle progression, transcriptional initiation, and chromatin organization, consistent with the observed role of HCF-1 in hepatocyte proliferation and regenerative control.

In addition to these validated partners, the motif analysis also identified several additional transcription factors not previously linked to HCF-1 in liver, suggesting the existence of

previously unrecognized regulatory partnerships that may contribute to metabolic, stress-response, and differentiation programs in hepatocytes. The complete catalogue of significantly enriched motifs and their corresponding transcription factors is provided in **Additional File 4.2**.

Together, these results define the transcription factor network that recruits HCF-1 to its genomic targets in liver, supporting its function as an epigenetic scaffold that integrates cell-cycle, metabolic, and stress-responsive transcriptional programs.

4.4.4 Annotation of HCF-1 peak signals localized in intergenic regions

A substantial fraction of HCF-1 ChIP-seq peaks mapped to intergenic regions, genomic intervals located between annotated genes making their functional interpretation non-trivial **Figure 4.3A**. Because such regions can harbour distal regulatory elements, repetitive elements, or epigenetically active domains, we performed a systematic annotation of these HCF-1–bound loci using HOMER, which displays chromatin state annotations generated from ChIP-seq of histone modifications. This analysis revealed that a large proportion of intergenic HCF-1 peaks were associated with specific sequence and chromatin features, including- (i) Simple repeats, (ii) Short Interspersed Nuclear Elements (SINEs), (iii) Long Interspersed Nuclear Elements (LINEs), (iv) Low-complexity regions, (v) CpG-rich regions, (vi) Signal recognition particle RNA (srpRNA), (vii) Satellite DNA, (viii) Young repetitive elements (YREP_Mm), (ix) tRNA loci, and (x) other intergenic regulatory regions. These findings indicate that HCF-1 is not restricted to canonical promoters or gene bodies but is also extensively recruited to regulatory intergenic domains, which are increasingly recognized as important hubs for epigenetic control and transcriptional regulation.

To further define the regulatory potential of these HCF-1–bound intergenic regions, we interrogated their transcription-factor occupancy using ORegAnno, which links sequence features to experimentally validated transcription-factor binding sites (119). This analysis mapped a distinct set of transcription factors to these intergenic HCF-1 peaks (**Figure 4.3B**). Functional characterization of the significantly enriched transcription factors revealed that they are involved in chromatin remodelling, DNA methylation, transcriptional regulation, and related epigenetic processes (**Table 4.1**).

Collectively, these data demonstrate that HCF-1 occupies a diverse repertoire of intergenic regulatory landscapes, where it is positioned to modulate chromatin structure and transcriptional programs through interactions with multiple transcriptional and epigenetic

regulators. This expanded binding profile further supports a role for HCF-1 as a global epigenetic coordinator in the liver.

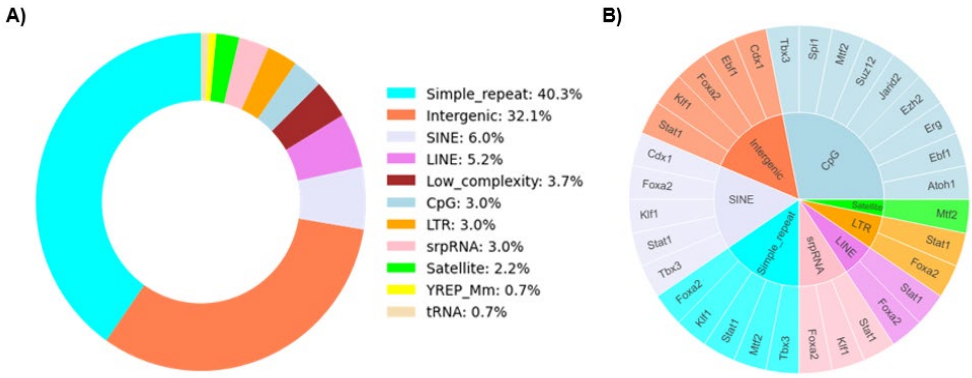

Figure 4.3: A Donut chart representing the percentage of functional annotation of intergenic regions with HCF-1 peak signals. Epigenomic resource of HOMER was utilized for the annotation. **B** Sunburst chart displaying the transcription factors mapped for the annotated intergenic sites with HCF-1 peak signals. Associated data is available in Additional file 4.3.

4.4.5 Changes in gene expression profiles and its regulation by methylation upon loss of HCF-1

Loss of HCF-1 resulted in widespread disruption of transcriptional programs controlling hepatocyte proliferation and genome maintenance. Consistent with the progressive decline in HCF-1 ChIP-seq peak intensities observed in the *Hcfc1* knockout (KO) livers over time, we identified a large set of cell-cycle–associated genes that became significantly dysregulated.

Table 4.1. Functional role of significantly enriched transcription factors mapped to regulatory sites present in the intergenic region interacting with HCF-1.

Transcription Factor	**Function**
Stat1	Signal transducer and transcription activator that mediates cellular responses to interferons (IFNs), cytokine KITLG/SCF and others, and growth factors. Also leads to activation of the JAK-STAT signaling pathway.

Foxa2	Involved in longevity regulating pathway. Involved in the development of multiple endoderm-derived organ systems such as the liver, pancreas, and lungs. Essential for hepatic specification and bile duct formation, IL-6 induced fibrinogen beta transcriptional activation. Transcription activator for number of liver genes such as AFP, albumin, tyrosine aminotransferase, PEPCK etc. Onset of diabetes- Involved in glucose homeostasis, regulates fat metabolism, activates transcriptional programs of lipid metabolism and ketogenesis at low insulin state.
Klf1/elkf	Transcription regulator of erythrocyte development. Binds to the CACCC box in the beta-globin gene promoter and activates transcription. When SUMOylated, acts as a transcriptional repressor by promoting interaction with CDH2/MI2beta and also represses megakaryocytic differentiation.
Tbx3	Involved in signaling pathways regulating pluripotency of stem cells.
Cdx1	Plays a role in transcriptional regulation. Involved in activated KRAS-mediated transcriptional activation of PRKD1 in colorectal cancer (CRC) cells.
Mtf2	Regulates the transcriptional networks during embryonic stem cell self-renewal and differentiation. Enhances PRC2 H3K27me3 methylation activity.
Spi1	Controls hematopoietic cell fate by decompacting stem cell heterochromatin and allowing other transcription factors to enter otherwise inaccessible genomic sites.
Jarid2	Regulator of histone methyltransferase complexes that plays an essential role in embryonic development, including heart and liver development. Binds DNA and mediates the recruitment of the PRC2 (Polycomb Repressive Complex 2 Subunit) complex to target genes in embryonic stem cells, thereby playing a key role in stem cell differentiation and normal embryonic development.
Ezh2	This gene encodes a member of the Polycomb-group (PcG) family. PcG family members form multimeric protein complexes, which are involved in maintaining the transcriptional repressive state of genes over successive cell generations.

Suz12	Polycomb group (PcG) protein. Component of the PRC2 complex, which methylates 'Lys-9' (H3K9me) and 'Lys-27' (H3K27me) of histone H3, leading to transcriptional repression of the affected target gene.The PRC2 complex may also serve as a recruiting platform for DNA methyltransferases, thereby linking two epigenetic repression systems.
Erg	This gene encodes a member of the erythroblast transformation-specific (ETS) family of transcriptions factors. All members of this family are key regulators of embryonic development, cell proliferation, differentiation, angiogenesis, inflammation, and apoptosis.
Ebf1	Enable DNA-binding transcription activator activity, RNA polymerase II-specific and RNA polymerase II cis-regulatory region sequence-specific DNA binding activity.
Atoh1	Enables sequence-specific double-stranded DNA binding activity. Predicted to be involved in neuron differentiation; positive regulation of neuron differentiation; and regulation of transcription by RNA polymerase II.

Among the most prominent were *Ppp2r5b* (protein phosphatase 2 regulatory subunit B), *Brd7* (bromodomain containing 7), *Cdk12* (cyclin-dependent kinase 12), *Cdc27* (cell division cycle 27), and *Cdk6* (cyclin-dependent kinase 6). These genes are key regulators of DNA repair, cell-cycle progression, and genomic stability, processes that are essential for maintaining tissue homeostasis and enabling effective liver regeneration.

In parallel, integration of POL2 and H3K4me3 ChIP-seq profiles revealed that a large number of genes involved in liver regeneration were located within genomic regions showing a progressive loss of transcriptional activity and active chromatin marks between day 0 and day 7 following *Hcfc1* deletion. A representative subset of these genes and their biological functions is summarized in **Table 4.2**. These data indicate that loss of HCF-1 is strongly associated with a coordinated reduction in both RNA polymerase II occupancy and H3K4me3-marked promoter enrichment at genes involved in hepatocyte proliferation and liver regeneration. It should be noted that while these changes in gene expression and promoter chromatin marks are identified via high-confidence ChIP-seq analysis, direct transcript-level expression changes for individual regeneration genes were not independently validated by quantitative RT-PCR in this cohort, representing an area for future experimental validation.

HCF-1 is known to function as both a transcriptional activator and repressor depending on its chromatin context and binding partners (120), and this dual role was reflected in the epigenetic landscape of HCF-1–deficient livers. Genome-wide analysis of H3K4me3 revealed a large cohort of genes exhibiting significant alterations in promoter methylation patterns, as illustrated in the heatmaps shown in **Figure 4.4A and 4.4B.** Functional annotation of these differentially methylated genes (**Figure 4.4C and 4.4D**) demonstrated strong enrichment for pathways involved in insulin resistance, fatty acid metabolism, chromatin remodelling, liver regeneration, cholesterol metabolism, and lipid metabolic processes.

Table 4.2: Genes associated with liver regeneration were found to be downregulated upon loss of *Hcfc1*.

Genes	**Function**	**References**
Genes enriched in regions where POL2 peak signals decreased over time		
A1cf	APOBEC1 complementation factor, involved in RNA editing and alternative splicing regulation. Plays a role in post-transcriptional modification and mRNA processing	(121)
Adam10	A Disintegrin and Metalloprotease 10, involved in cell adhesion, migration, plays a role in Notch signaling.	(122)
E2f3	Transcription factor that regulates the cell cycle, involved in promoting cell proliferation and DNA synthesis.	(123)
Egfr	Epidermal Growth Factor Receptor, receptor tyrosine kinase, involved in cell growth, proliferation, and survival.	(124)
Foxo3	Forkhead Box O3, transcription factor, plays a role in regulating cell cycle arrest, apoptosis, DNA repair, and oxidative stress response.	(125)
Gab1	Grb2-associated binder 1, adaptor protein involved in signaling cascades, interacts with various receptor tyrosine kinases and acts as a scaffold to transmit signals for cell growth, differentiation, and survival.	(126)
Ghr	Growth Hormone Receptor, involved in growth promotion, metabolism regulation, and cell proliferation.	(127)
Jun	Component of the transcription factor complex AP-1 (Activator Protein 1), involved in processes like cell proliferation, differentiation, apoptosis, and response to stress signals.	(128)

Mcl1	Myeloid Cell Leukemia-1, anti-apoptotic protein, inhibits caspase activation and promotes cell survival.	(129)
Nfatc3	Nuclear Factor of Activated T Cells, Cytoplasmic 3, transcription factor, plays a role in immune response, cell differentiation, and development.	(130)
Nfe2l2	Nuclear factor erythroid 2-related factor 2, transcription factor, plays a central role in cellular defense against oxidative stress.	(131)
Nr0b2	Nuclear Receptor Subfamily 0 Group B Member 2, nuclear receptor that functions as a transcriptional corepressor, plays a role in liver development, metabolism, and bile acid homeostasis.	(132)
Onecut1	One Cut Homeobox 1, transcription factor involved in the development and differentiation of various tissues, including the liver, pancreas, and neural tissues.	(133)
Pdpk1	3-Phosphoinositide Dependent Protein Kinase-1, serine/threonine protein kinase, involved in the activation of various kinases, including protein kinase B (AKT), and regulates processes like cell proliferation, survival, and metabolism.	(134)
Plg	Plasminogen, synthesized and secreted by the liver and is involved in the fibrinolytic system, which is responsible for the breakdown of blood clots.	(135)
Ppara	Peroxisome Proliferator-Activated Receptor Alpha, nuclear receptor, regulates the expression of genes involved in fatty acid metabolism, lipid transport, and inflammation.	(136)
Rxra	Retinoid X Receptor Alpha, nuclear receptor, involved in gene regulation, particularly in developmental processes, cellular differentiation, and metabolism.	(137)
Socs3	Suppressor of Cytokine Signaling 3, negative feedback inhibitor of cytokine signaling, involved in development and maintaining tissue homeostasis.	(138)
Tgfb1	Transforming Growth Factor Beta 1, cytokine, regulates cell growth, differentiation, apoptosis, and immune responses.	(139)

Txnip	Thioredoxin Interacting Protein, inhibits the activity of thioredoxin, a key regulator of redox signaling, involved in cellular responses to oxidative stress, glucose metabolism, and apoptosis.	(140)
Genes enriched in regions where h3k4me peak signals decreased with time.		
E2f1	Transcription factor, regulates cell cycle progression and cell proliferation, involved in apoptosis, DNA repair, and differentiation processes.	(123)
Fabp1	Liver fatty acid-binding protein (L-FABP), involved in the uptake, transport, and metabolism of fatty acids in hepatocytes.	(141)
Fadd	Fas-associated death domain protein, adaptor protein involved in mediating apoptosis, or programmed cell death.	(142)
Nr1i2	Nuclear receptor protein that acts as a transcription factor, primarily expressed in the liver and intestine and is involved in the regulation of drug metabolism and detoxification.	(143)
Pdpk1	3-phosphoinositide-dependent protein kinase-1, key regulator of the phosphoinositide 3-kinase (PI3K) signaling pathway and is involved in the activation of various downstream kinases, including Akt (protein kinase B), S6K (p70 ribosomal protein S6 kinase), and PKC (protein kinase C). These kinases regulate multiple cellular processes, such as cell survival, growth, proliferation, and metabolism.	(134)

Importantly, these same biological processes were independently identified through analysis of differential POL2 peak dynamics (**Figure 4.5**), providing convergent evidence that loss of HCF-1 disrupts both epigenetic marking and transcriptional output at genes that coordinate hepatocyte proliferation and metabolic homeostasis. Together, these findings establish HCF-1 as a central regulator linking chromatin state, transcriptional control, and metabolic-regenerative balance in the liver.

4.4.6 Hepatic HCF-1 depletion drives progressive liver injury and impairs hepatocyte proliferative capacity

To establish the physiological consequences of HCF-1 loss in the liver, all *in vivo* and histological experiments were performed by our collaborators at IIT-Delhi and are included here to provide a complete biological framework for the computational analyses described

above. Hepatocyte-specific deletion of HCF-1 was induced by tamoxifen administration to 10–14-week-old Albumin-Cre-ERT2^{tg}; *Hcfc1*$^{lox/Y}$ male mice and Albumin-Cre-ERT2^{tg}; *Hcfc1*$^{lox/+}$ female mice, generating *Hcfc1*$^{hepKO/Y}$ (KO) males with complete hepatocyte loss of HCF-1 and *Hcfc1*$^{hepKO/+}$ (HET) females with mosaic HCF-1 expression due to X-chromosome inactivation. As previously demonstrated (34,144), in these mouse strains the Albumin-Cre-ERT2^tg allele enables tamoxifen-inducible, hepatocyte-specific deletion of the *Hcfc1* gene.

Before tamoxifen induction, all HNF4α-positive hepatocytes uniformly expressed HCF-1 (red arrows, **Figure 4.6A**). By 7 days after induction, a marked hepatocyte-specific loss of HCF-1 was observed in both HET females (**Figure 4.6B**) and KO males (**Figure 4.6C**).

In heterozygous females, the X-linked nature of the *Hcfc1* gene resulted in random X-chromosome inactivation, producing a mosaic liver composed of approximately 50% HCF-1-positive hepatocytes (red arrows) and 50% HCF-1-negative hepatocytes (white arrows), while non-hepatocytes (HNF4α-negative) retained HCF-1 expression (yellow arrows). In contrast, *Hcfc1*$^{hepKO/Y}$ male mice exhibited a complete loss of HCF-1 in all hepatocytes, with HCF-1 expression preserved only in non-parenchymal cells (yellow arrows, **Figure 4.6C**). Quantification of immunostained sections across mouse cohorts (n = 4 biological replicates per group) confirmed a significant reduction in the percentage of HCF-1-positive hepatocytes in both heterozygous females (46.2 ± 7.1%, $p \leq 0.001$) and knockout males (0.0 ± 0.0%, $p \leq 0.0001$) relative to control animals (100.0 ± 0.0%), as assessed by a two-tailed Student's t-test (**Figure 4.6D**).

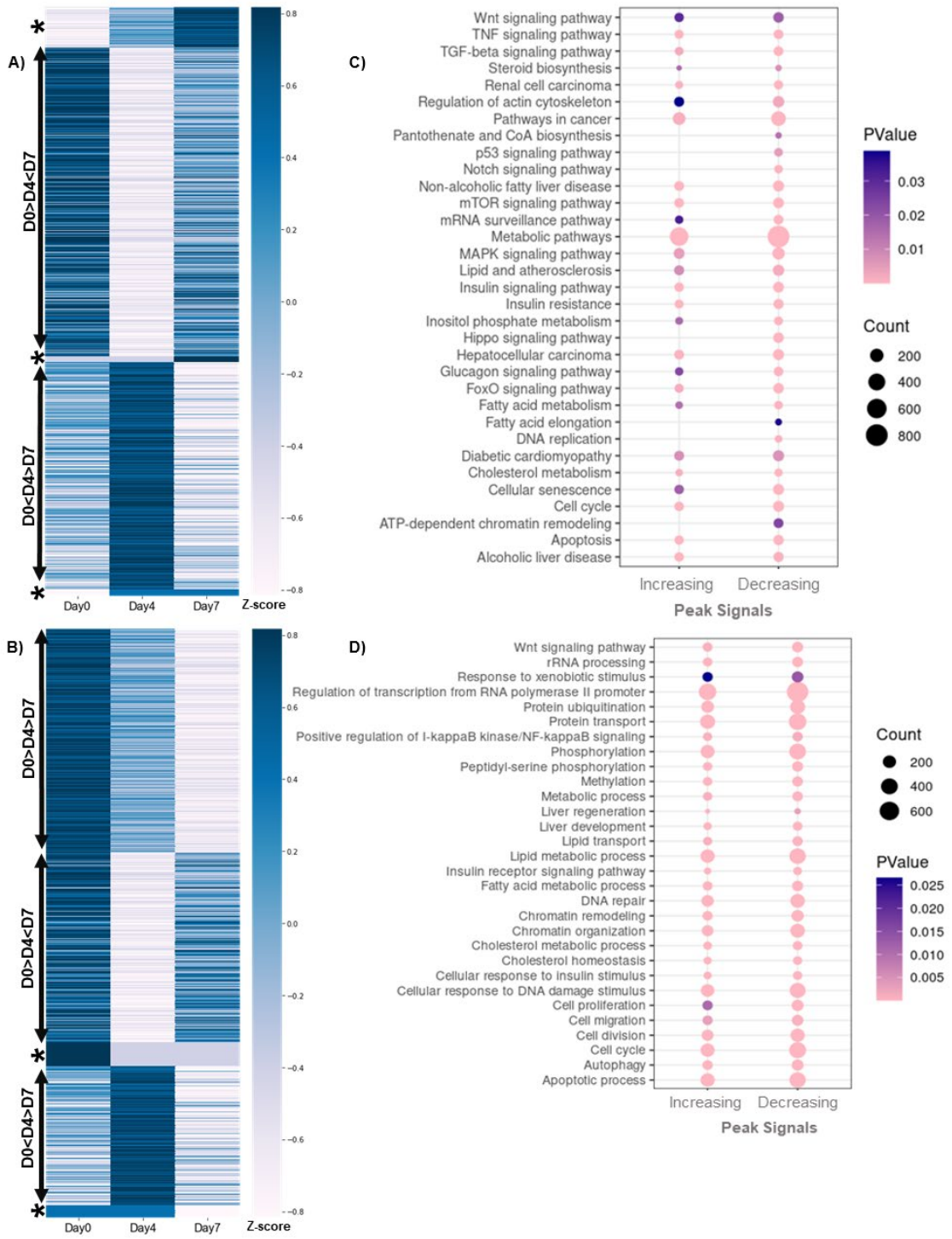

Figure 4.4: A Heatmap displaying increasing trends [D0 > D4 < D7], [D0 < D4 > D7] in H3K4me3 peak signals. Here * represent the [D0 < D4 < D7], [D0 = D4 < D7], [D0 < D4 = D7] trends. The color key indicates the associated row z-score. **B** Heatmap displaying decreasing trends [D0 > D4 > D7], [D0 > D4 < D7], [D0 < D4 > D7] in H3K4me3 peak signals. Here * represent the [D0 > D4 = D7], [D0 = D4 > D7] trends. The color key indicates the associated row z-score. **C** KEGG pathway analysis of the genes associated with regions where H3K4me3 peak signals increased and decreased over time. **D** Biological Process analysis of the genes associated with regions where H3K4me3 peak signals increased and decreased over time. The enrichment of genes for different GO terms and pathways was found using DAVID. All the data associated with these figures is included in Additional file 4.4.

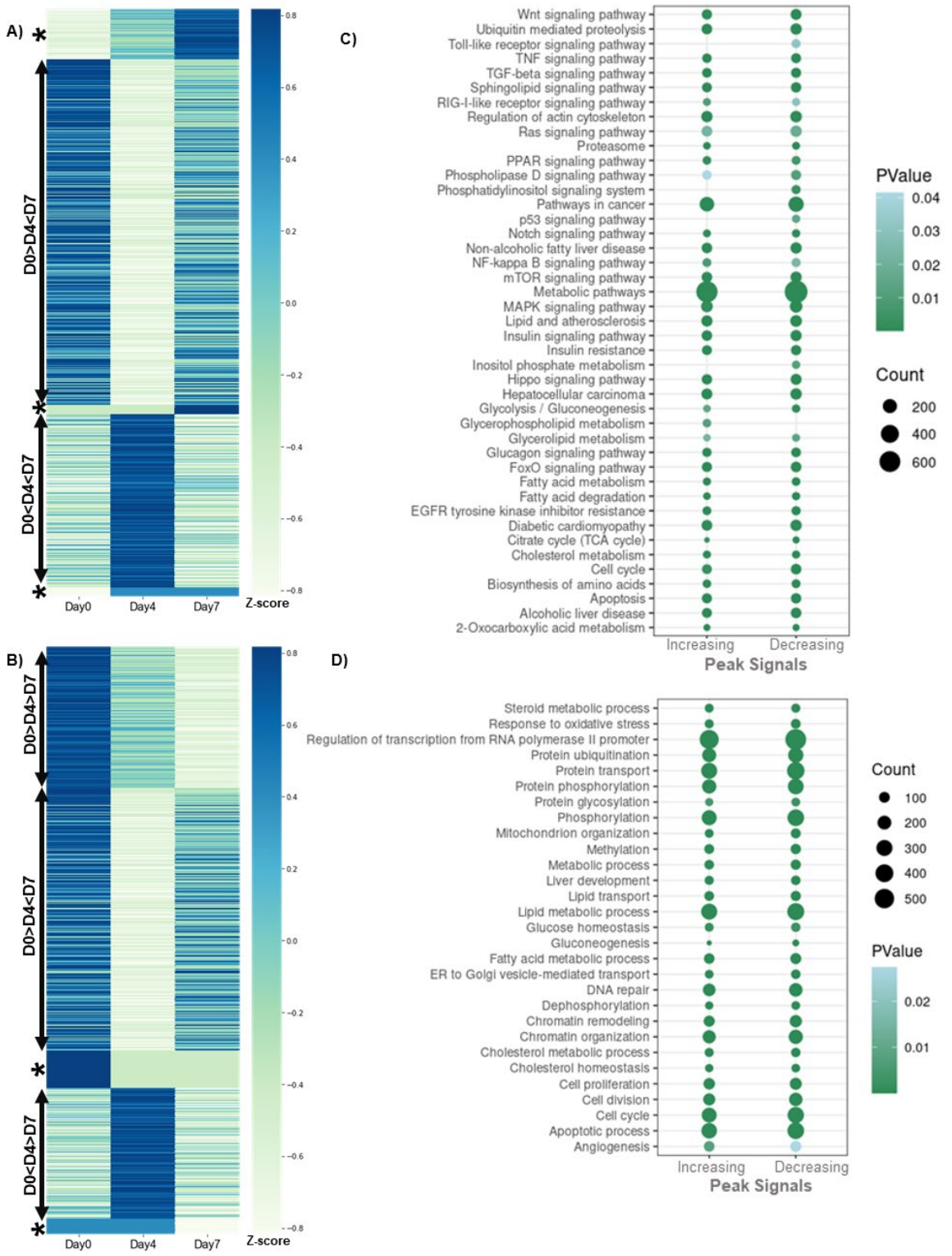

Figure 4.5: A Heatmap displaying increasing trends [D0 > D4 < D7], [D0 < D4 > D7] in POL2 peak signals. Here * represent the [D0 < D4 < D7], [D0 = D4 < D7], [D0 < D4 = D7] trends. The color key indicates the associated row z-score. **B** Heatmap displaying decreasing trends [D0 > D4 > D7], [D0 > D4 < D7], [D0 < D4 > D7] in POL2 peak signals. Here * represent the [D0 > D4 = D7], [D0 = D4 > D7] trends. The color key indicates the associated row z-score. **C** KEGG pathway analysis of the genes associated with regions where POL2 peak signals increased and decreased over time. **D** Biological Process analysis of the genes associated with regions where POL2 peak signals increased and decreased over time. The enrichment of genes for different GO terms and path ways was found using DAVID. All the data associated with these figures is included in Additional file 4.5.

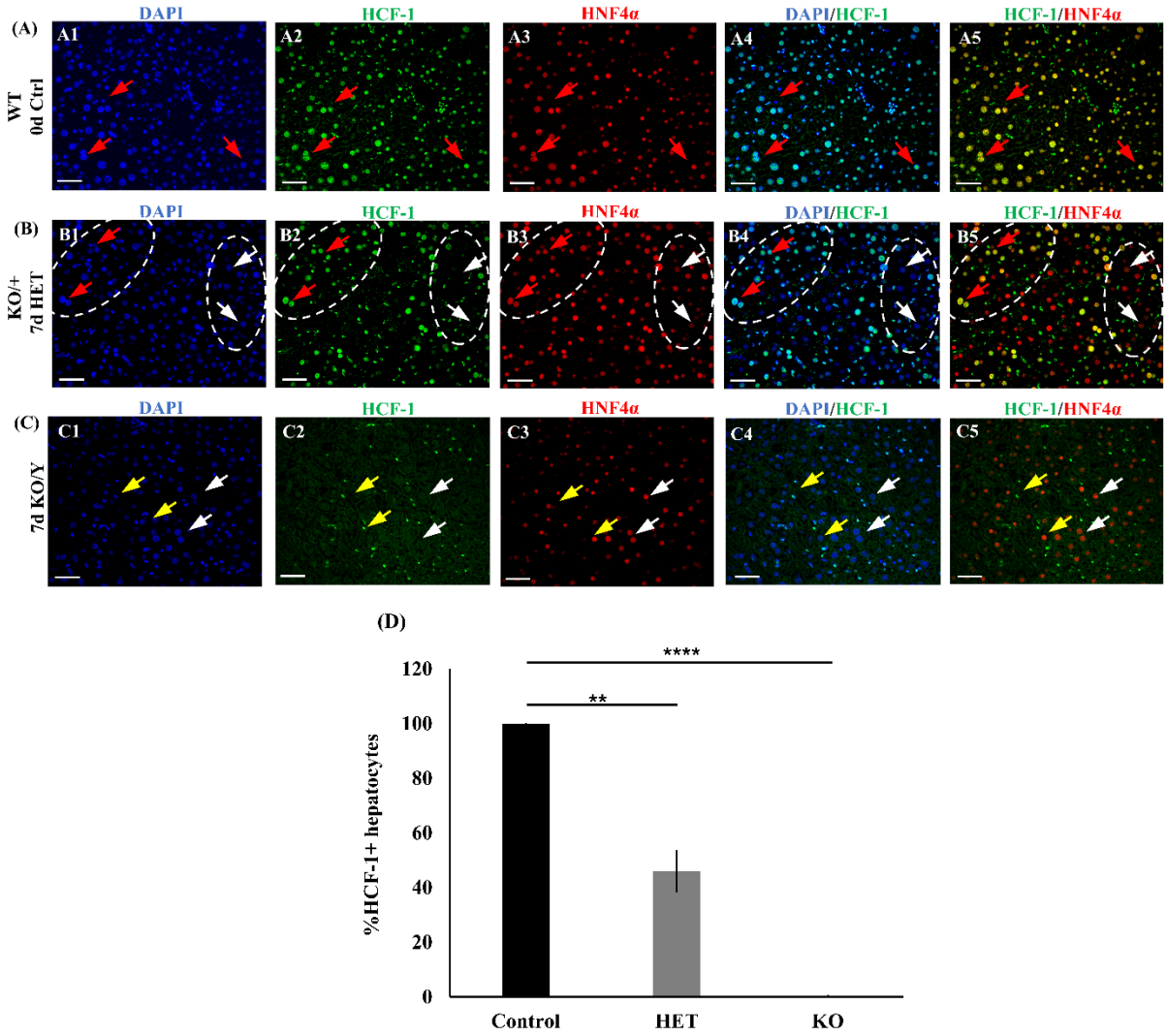

Figure 4.6: Tamoxifen induction leads to rapid loss of hepatocyte-specific HCF-1 expression in *Hcfc1*$^{hepKO/+}$ female and *Hcfc1*$^{hepKO/Y}$ male livers. Immunofluorescence analysis of HCF-1 and hepatocyte specific marker (HNF4α) of 10-week old control (0d Ctrl WT; panels **A**), heterozygous Alb-Cre-ERT2tg; *Hcfc1*$^{hepKO/+}$ female (7d HET; panel **B**) and knockout Alb-Cre-ERT2tg; *Hcfc1*$^{hepKO/Y}$ male livers (7d KO; panel **C**) 7 days post-tamoxifen treatment. The paraffin embedded sections of livers (panels **A, B**, and **C**) were stained with DAPI (blue), anti-HNF4a (red), anti-HCF-1 (green). In panels **A**, and **B** the red arrows point to HCF-1-positive and HNF4α-positive hepatocytes. White arrows in panels **B** and **C** point to HCF-1-negative and HNF4α-positive hepatocytes. Yellow arrows in panel **C** point towards HCF-1-positive and HNF4α-negative non-hepatocytes. The indented circles in B reflect some of the visible HCF 1-positive and negative hepatocyte clusters. Percentages of HCF-1 positive hepatocytes (panel **D**, n = 4) were calculated for 0 d Ctrl WT, heterozygous Alb-Cre-ERT2tg; *Hcfc1*$^{hepKO/+}$ female and knockout Alb-Cre-ERT2tg; *Hcfc1*$^{hepKO/Y}$ male mice livers. Student's t-test was used to calculate the significance. (**, $p \leq 0.001$;***, $p \leq 0.0001$; n.s., $p > 0.05$)

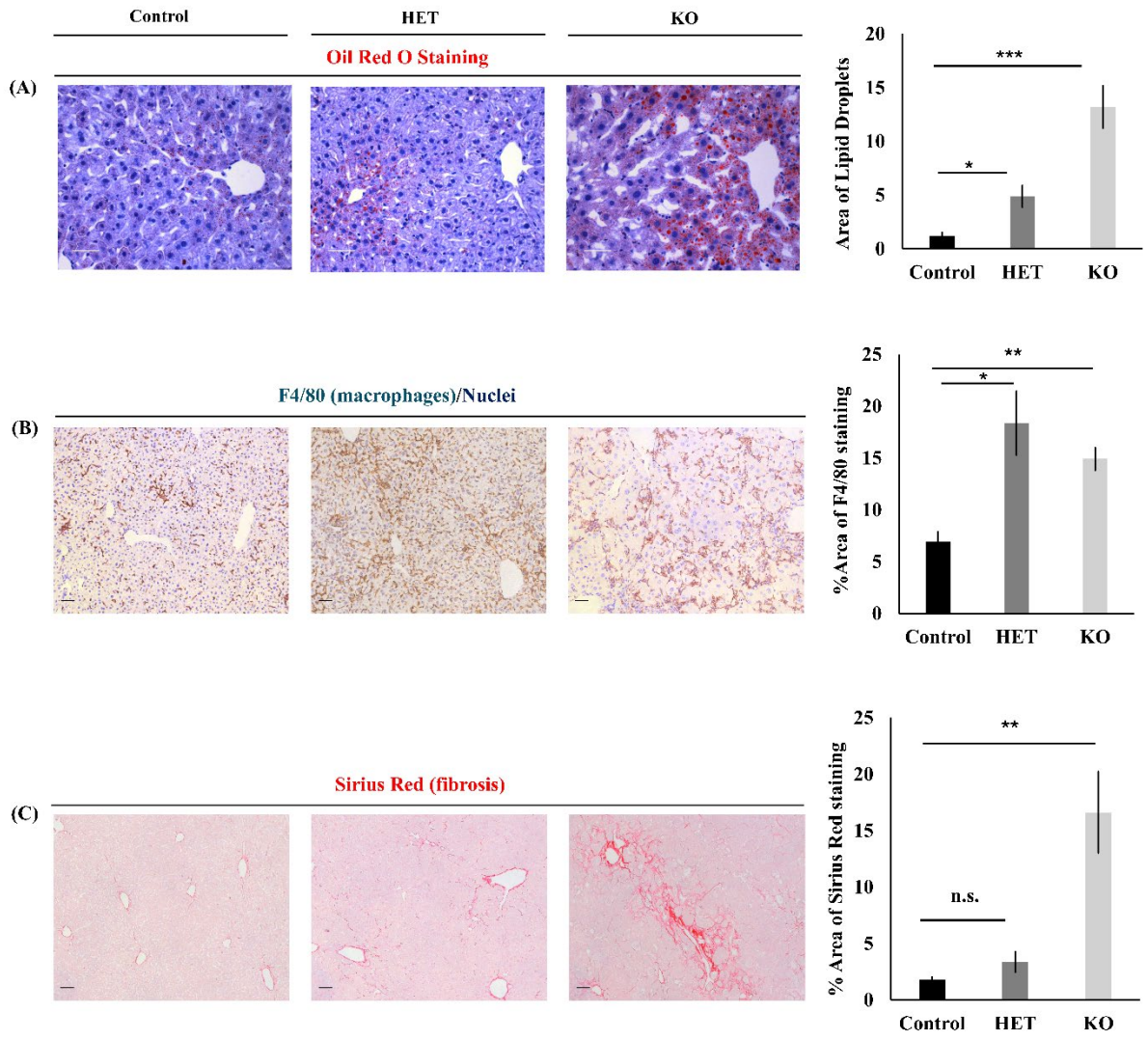

Figure 4.7: *Hcfc1* knock-out leads to severe liver injury. Comparison of cryosections (**A**) and paraffin-embedded sections (**B and C**) of control livers (0d; left), heterozygous Alb-Cre-ERT2tg; *Hcfc1*$^{hepKO/+}$ female (middle) and knockout Alb-Cre-ERT2tg; *Hcfc1*$^{hepKO/Y}$ livers (right). **A** The presence of steatosis was estimated by Oil Red O staining of cryo-sections from control, heterozygous Alb-Cre-ERT2tg; *Hcfc1*$^{hepKO/+}$ female and knockout Alb-Cre-ERT2tg; *Hcfc1*$^{hepKO/Y}$ livers. Scale bar 50 µm. Quantifications show significant increase in area of lipid droplets in heterozygous Alb-Cre-ERT2tg; *Hcfc1*$^{hepKO/+}$ female and Alb Cre-ERT2tg; *Hcfc1*$^{hepKO/Y}$ knockout male livers in comparison to control (n = 4, ***, $p \leq 0.0001$; *, $p \leq 0.05$,) **B** DAB immunostaining for macrophage marker F4/80 (brown). The sections were also stained with hematoxylin (blue). Scale bar 25 µm. Quantifications show significant increase in percentage area of F4/80 staining in heterozygous Alb-Cre-ERT2tg; *Hcfc1*$^{hepKO/+}$ female and Alb-Cre-ERT2tg; *Hcfc1*$^{hepKO/Y}$ knockout male livers in comparison to control (n = 4, **, $p \leq 0.001$; *, $p \leq 0.05$,) **C** Sirius red staining of paraffin embedded sections. Scale bar 25 µm. Quantifications show significant increase in percentage area of sirius red staining in Alb-Cre-ERT2tg; *Hcfc1*$^{hepKO/Y}$ knockout male livers in comparison to control, while non-significant increase in case of heterozygous Alb-Cre-ERT2tg; *Hcfc1*$^{hepKO/+}$ female in comparison to Control (n = 4; **, $p \leq 0.001$; n.s., $p > 0.05$). Student's t-test was used to calculate the significance.

Histological analysis of liver sections from both male and female *Hcfc1*^{hepKO} mice revealed rapid and progressive liver pathology. By 7 days post-tamoxifen induction, Oil Red O staining revealed a statistically significant expansion of lipid droplet area in heterozygous females (4.9

± 0.9%, $p \leq 0.05$) and knockout males (13.2 ± 2.0%, $p \leq 0.0001$) compared to controls (1.2 ± 0.2%; n = 4 mice per group, two-tailed Student's t-test; **Figure 4.7A**). Concurrently, F4/80 macrophage immunostaining showed a significant increase in positive staining area in heterozygous females (18.4 ± 2.3%, $p \leq 0.05$) and knockout males (15.1 ± 1.0%, $p \leq 0.001$) relative to controls (6.9 ± 0.9%; n = 4 mice per group, two-tailed Student's t-test; **Figure 4.7B**). Sirius Red staining demonstrated a marked increase in collagen deposition in knockout males (16.6 ± 3.7%, $p \leq 0.001$; n = 4 mice per group, two-tailed Student's t-test), while heterozygous females exhibited a non-significant increase (3.4 ± 1.1%, $p > 0.05$) relative to controls (1.8 ± 0.4%; **Figure 4.7C**). Together, these features—lipid accumulation, inflammation, and fibrosis recapitulate core hallmarks of MAFLD.

These pathological changes closely mirror the molecular disruptions identified in our computational analyses. Differential peak analysis across days 0, 4, and 7 following *Hcfc1* deletion revealed enrichment of dysregulated genes in MAPK signalling, lipid and atherosclerosis pathways, and the adaptive immune system (**Figure 4.2C and 4.2D**). Such pathway perturbations are known to impair hepatocyte proliferation and tissue regeneration while simultaneously driving lipid dysregulation, oxidative stress, inflammation, and insulin resistance, the core processes underlying MAFLD progression.

Collectively, the integration of *in vivo* pathology from IIT-Delhi with multi-omics computational analyses demonstrates that hepatocyte-specific loss of HCF-1 destabilizes the balance between regeneration and metabolic homeostasis, leading to steatosis, immune cell infiltration, and fibrosis, and thereby driving progressive liver injury characteristic of MAFLD.

4.4.7 Functional inactivation of HCF-1 leads to a disturbed metabolic and signaling networks in *Hcfc1* knockout mice

Genes exhibiting coordinated changes in H3K4me3 and POL2 occupancy between day 0, day 4, and day 7 following *Hcfc1* deletion were analysed to define the molecular consequences of HCF-1 loss. Pathway enrichment using g:Profiler and EnrichmentMap identified metabolic pathways and cell-proliferation-associated processes as the most significantly enriched KEGG categories (**Figure 4.8A and 4.8B; Additional File 4.6**), demonstrating that HCF-1 depletion is associated with widespread alterations in both hepatic metabolic networks and regenerative gene profiles. While the identified perturbations in mitochondrial biological processes (**Figure 4.9**) and electron transport chain genes stem from computational enrichment and secondary RNA-seq analysis without primary *de novo* cellular respirometry assays conducted herein, they

are strongly consistent with published literature establishing direct mitochondrial respiratory defects upon hepatic *Hcfc1* inactivation. These functional metabolic perturbations warrant further biochemical and metabolic flux validation in future studies.

To extend these observations, RNA-seq data from a previously published study were analysed, comparing *Hcfc1*$^{hepKO/Y}$ male livers with *Hcfc1*$^{lox/Y}$ control males and *Hcfc1*$^{hepKO/+}$ heterozygous females. This analysis identified 521 upregulated and 654 downregulated transcripts in *Hcfc1*-deficient livers (**Additional File 4.7**). Gene ontology enrichment using DAVID showed that upregulated genes were associated with oxidoreductase activity, mitochondrial translation, cholesterol metabolism, autophagy, and innate immune responses (**Figure 4.9A**). In contrast, downregulated genes were linked to protein ubiquitination, apoptotic processes, lipid metabolism, chromatin remodelling, DNA repair, and mitochondrial organisation (**Figure 4.9C**), reflecting a broad collapse of cellular homeostasis.

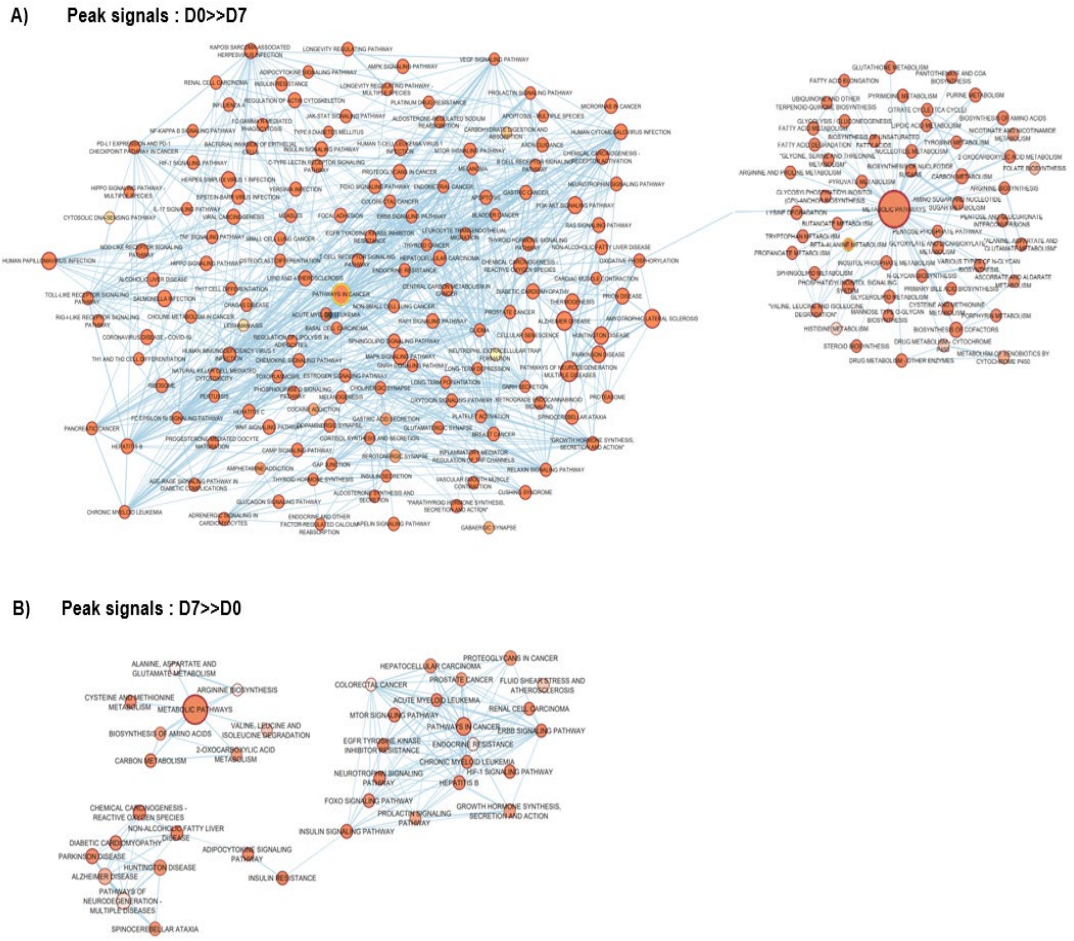

Figure 4.8: Pathway enrichment analysis of the dysregulated genes **A** D0 > > D7 and **B** D7 > > D0 found to be common in POL2 and H3K4me3 peak signals. g:Profiler and Cytoscape plugin EnrichmentMap were used for the analysis. Additional file 4.6 contains data associated with these figures.

KEGG pathway analysis further refined these functional alterations. Upregulated transcripts were enriched in fatty-acid degradation, alcoholic liver disease, lysine degradation, β-alanine metabolism, and aminoacyl-tRNA biosynthesis pathways (**Figure 4.9B**), consistent with a stress-adapted metabolic state. Conversely, downregulated transcripts were enriched in PPAR signalling, fatty-acid metabolism, peroxisome function, and linoleic-acid metabolism (**Figure 4.9D**), which are central pathways governing normal hepatic lipid handling.

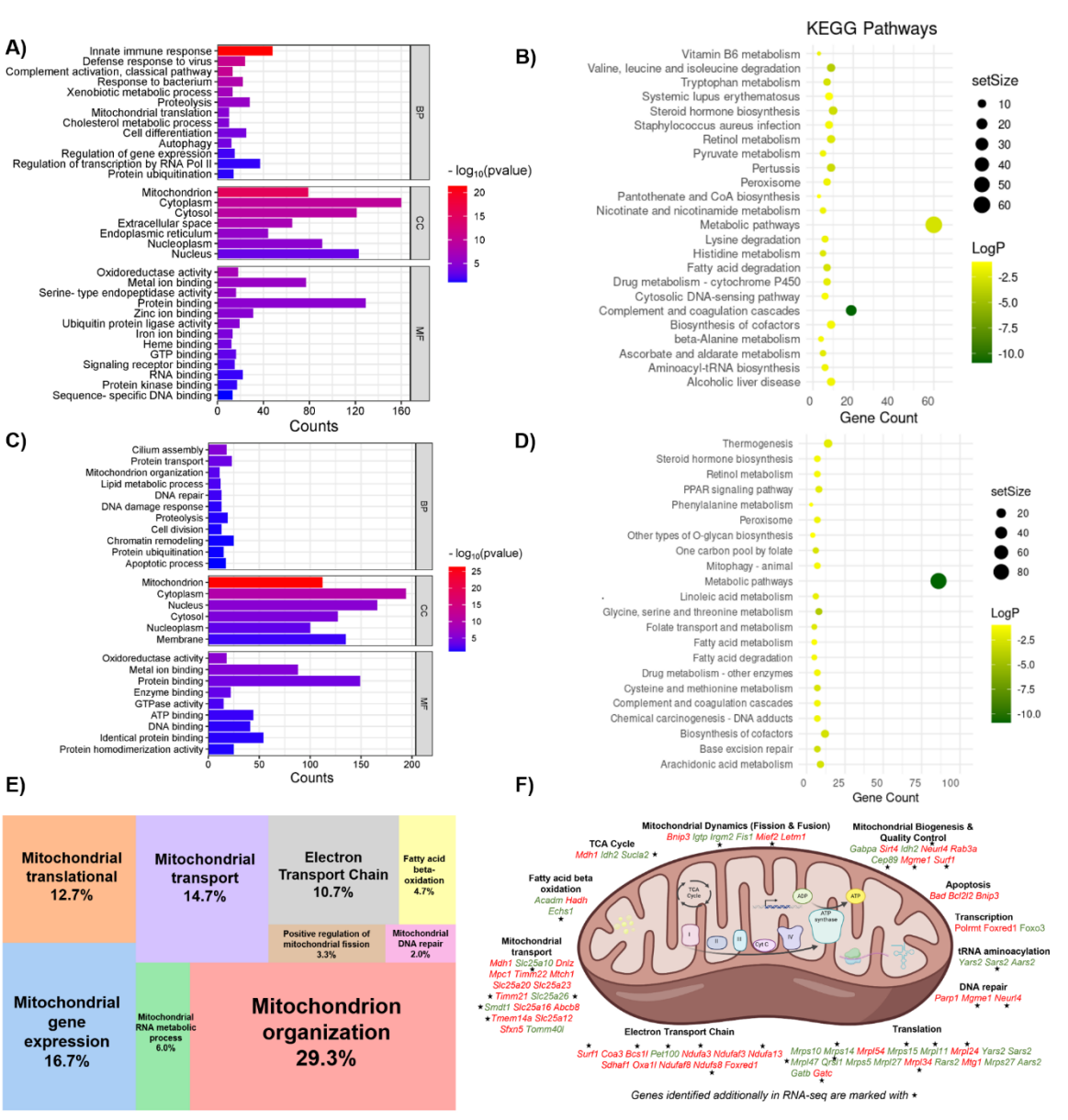

Figure 4.9: GO enrichment analysis shows biological process (BP), cellular component (CC) and molecular functions (MF) linked with **A** upregulated genes and **C** downregulated genes. The larger the bar chart is, the higher the enrichment degree of each process, and the color of the bar plot map represents the significance (p-value). The dot plot represents the KEGG pathways on the y-axis and gene count on the x-axis for **B** upregulated genes **D** down regulated genes. Greater the gene count corresponds to a greater dot. The colour of the dot varies based on the p-value. The enrichment of genes for different GO terms and pathways was found using DAVID. **E** The treemap illustrates mitochondrial processes linked to dysregulated genes. **F** A schematic representation of a

mitochondrion shows functionally annotated genes, indicating upregulation (green) or downregulation (red) resulting from the loss of HCF-1. Additional file 4.7 contains data associated with these figures.

Cellular-component analysis revealed a strong enrichment for mitochondrial pathways, including fatty-acid β-oxidation, mitochondrial translation, electron-transport-chain activity, mitochondrial RNA metabolism, mitochondrial fission, and mitochondrial DNA repair **(Figure 4.9E).** These disruptions were visualised in a functional mitochondrial map **(Figure 4.9F),** highlighting coordinated dysregulation of genes governing mitochondrial structure and bioenergetics.

Cellular-component analysis revealed a strong enrichment for mitochondrial pathways, including fatty-acid β-oxidation, mitochondrial translation, electron-transport-chain activity, mitochondrial RNA metabolism, mitochondrial fission, and mitochondrial DNA repair (**Figure 4.9E**). These disruptions were visualised in a functional mitochondrial map (**Figure 4.9F**), highlighting coordinated dysregulation of genes governing mitochondrial structure and bioenergetics.

These transcriptomic and epigenomic alterations were reflected in structural and biochemical mitochondrial defects. Using electron microscopy, liver tissue of *Hcfc1*$^{hepKO/Y}$ demonstrated distorted mitochondrial morphology, together with lipid accumulation detectable as early as four days after tamoxifen induction (**Additional Fig. 4.1**). Immunoblotting with anti-OXPHOS antibodies revealed a significant reduction in NDUFB8 (complex I), SDHB (complex II), and ATP5α (complex V), while UQCRC2 (complex III) remained largely unchanged (**Additional Fig. 4.2**). Immunofluorescence analysis confirmed markedly reduced levels of ATP5α, MTCO1, and total OXPHOS proteins in *Hcfc1*-deficient livers (**Additional Fig. 4.3**), indicating a global impairment of oxidative phosphorylation.

Disruption of mitochondrial energy production provides a mechanistic explanation for lipid accumulation, defective fatty-acid β-oxidation, and the rapid transition from MAFLD toward MASH following HCF-1 loss. The strong concordance between RNA-seq, ChIP-seq, mitochondrial ultrastructure, and OXPHOS protein analyses demonstrates that HCF-1 is a central regulator of hepatic metabolic integrity.

Taken together, these results show that HCF-1 is a central epigenetic coordinator that integrates chromatin state, transcriptional activity, and metabolic regulation in hepatocytes. Loss of HCF-1 disrupts POL2 recruitment and H3K4me3 landscapes at genes governing cell-cycle progression, mitochondrial function, and lipid metabolism, leading to impaired regeneration

and progressive metabolic dysfunction. The convergence of transcriptomic, epigenomic, and histopathological evidence demonstrates that HCF-1 defines a molecular boundary between effective liver repair and pathological progression toward MAFLD.

4.5 Discussion

MAFLD stands for metabolic dysfunction–associated fatty liver disease, a condition characterized by a broad clinical picture that includes ranging from simple steatosis to steatohepatitis (MASH) which may progress to fibrosis, cirrhosis and hepatocellular carcinoma (HCC) (145–147). Despite its growing clinical burden, the molecular mechanisms that govern MAFLD initiation, progression, and recovery remain incompletely understood.

One way to begin addressing this knowledge gap is to determine the function of the evolutionarily conserved metazoan co-transcription factor HCF-1 in hepatocytes, and its function as a hub for epigenetic regulation of metabolism and regeneration.

The liver is distinguished by an extraordinary ability to regenerate, a process that has been extensively characterized using models such as partial hepatectomy (PH), in which liver mass is restored to its original liver-to-body weight ratio through a tightly controlled proliferative response (62,148,149). Through studying genetic and pharmacological perturbation studies in mice, we have identified multiple transcription factors, cytokines, growth factors, and intracellular signalling cascades that orchestrate hepatocyte proliferation and tissue restoration following injury (150,151,152–154). However, the molecular mechanisms that determine when regeneration is initiated, sustained, or terminated remain incompletely defined. Importantly, pathological contexts such as chronic injury, fibrosis, and steatosis as observed in MAFLD can substantially impair regenerative capacity (154–157). These studies presented here place HCF-1 as a previously underappreciated determinant of this balance between regeneration and degeneration.

HCF-1 has been extensively linked to cell-cycle control, chromatin regulation, and transcriptional coordination in diverse cellular contexts (158–160). Hepatocyte-specific loss of HCF-1 produces a rapid and spontaneous recapitulation of MAFLD, as previously reported (34), and this phenotype is strongly reinforced by the present epigenomic and transcriptomic analyses. The early onset of steatosis following HCF-1 depletion highlights its essential role in maintaining mitochondrial integrity, lipid handling, and metabolic homeostasis. Prior work has shown that HCF-1 loss disrupts oxidative phosphorylation, β-oxidation, gluconeogenesis, and

the stability of key metabolic regulators such as PGC-1α (34,50,161), thereby placing HCF-1 at the core of mitochondrial and hepatic metabolic control. Consistent with this, HCF-1–deficient hepatocytes fail to mount an effective regenerative response even following two-thirds partial hepatectomy, underscoring the requirement for HCF-1 in hepatocyte proliferative competence (144).

The mechanistic basis of this phenotype is clarified by the integrated RNA-seq and ChIP-seq analyses. Loss of HCF-1 was shown to cause widespread disruption of promoter-associated H3K4me3 and RNA polymerase II (POL2) occupancy at genes governing mitochondrial function, cell-cycle progression and lipid metabolism. H3K4me3 is a canonical mark of transcriptionally active promoters, and its perturbation in the absence of HCF-1 strongly suggests that HCF-1 serves as a master organizer of transcriptionally permissive chromatin in hepatocytes. The close correspondence between altered H3K4me3 landscapes, POL2 redistribution, and transcriptomic dysregulation suggests a unified framework, that HCF-1 exerts its effects primarily through coordinated epigenetic and transcriptional control.

These chromatin-level alterations provide a plausible mechanistic explanation for the downstream metabolic and regenerative defects. These changes in chromatin make sense of why metabolism and growth go awry afterward. Disruption of H3K4me3 at promoters of mitochondrial and metabolic genes is expected to impair oxidative phosphorylation, fatty acid β-oxidation, and mitochondrial biogenesis, leading to lipid accumulation, oxidative stress, and hepatocyte injury. Similarly, altered regulation of cell-cycle and DNA-repair genes compromises hepatocyte proliferation, thereby limiting the ability of the liver to recover from injury. Together, these effects explain the rapid transition from steatosis to inflammation, fibrosis, and failure of regeneration observed following HCF-1 loss.

The role of HCF-1 as an epigenetic integrator is further supported by previous reports linking HCF-1 to histone-modifying complexes and transcriptional co-activators (158,162–164). Although this study focused on promoter-associated H3K4me3, additional chromatin features such as H3K27ac and enhancer activity may also contribute to HCF-1–dependent gene regulation. Future studies integrating histone acetylation landscapes and mapping direct interactions between HCF-1 and chromatin-modifying enzymes through co-immunoprecipitation or proteomics would further refine this regulatory framework.

A striking biological insight from this study is the sex-specific consequence of HCF-1 depletion. Male *Hcfc1*$^{hepKO/Y}$ mice, in which all hepatocytes lack HCF-1, exhibit rapid liver

failure and death, whereas heterozygous *Hcfc1*$^{hepKO/+}$ females retain sufficient HCF-1–positive hepatocytes to support regeneration. This mosaicism allows partial preservation of hepatic proliferative capacity, highlighting a fundamental constraint imposed by HCF-1 deficiency: HCF-1–negative hepatocytes are intrinsically incapable of contributing to liver regeneration. This creates a powerful experimental model in which MAFLD development and regenerative failure occur simultaneously, providing a unique system to dissect the genetic and epigenetic determinants of both processes.

The dysregulated gene networks identified in this study further reinforce the centrality of HCF-1 in liver biology. Though different in function, affected genes (by HCF-1 loss) link together through roles in energy handling, cell growth pathways, programmed cell death, mitochondrial operation, DNA structure changes, and cell-cycle regulation. These dysregulated genes were enriched in pathways related to metabolism, stimulus response, intracellular localisation and transport, developmental processes, cellular homeostasis, and signal transduction, all of which are tightly linked to MAFLD pathogenesis. The convergence of these pathways provides a coherent explanation for the complex and progressive phenotype observed in HCF-1–deficient livers.

So, summing up, what we've found shows that HCF-1 tightly controls how genes are turned on in liver cells (hepatocytes), their ability to support normal function, balance of energy-related activities, yet also limits how fast these cells grow back after damage. Loss of HCF-1 destabilizes promoter-associated chromatin architecture, disrupts POL2-mediated transcription, impairs mitochondrial and lipid metabolism, and prevents effective liver regeneration, thereby driving rapid MAFLD progression. Identification of the specific HCF-1–dependent gene networks and chromatin regulators involved in these processes offers a promising foundation for developing therapeutic strategies aimed at restoring liver function in metabolic liver disease.

4.6 Conclusion

When HCF-1 is eliminated only in liver cells (hepatocytes), it recapitulates the metabolomic, biochemical, and histopathological hallmarks of MAFLD and drives its progression toward MASH, establishing HCF-1 loss as a profound insult to liver homeostasis. In addition to inducing severe metabolic dysfunction and mitochondrial impairment, HCF-1 deficiency abolishes the regenerative capacity of the liver following partial hepatectomy. At the molecular level, depletion of HCF-1 disrupts promoter-associated H3K4me3 marks and RNA polymerase

II occupancy, leading to coordinated misregulation of genes governing metabolism, signalling, chromatin remodelling, methylation, and cell-cycle control. These epigenetic and transcriptional perturbations provide a mechanistic basis for the rapid onset of steatosis, hepatocyte injury, and regenerative failure observed in HCF-1–deficient livers. Collectively, this work establishes HCF-1 as a central epigenetic integrator of hepatic metabolism and regeneration and highlights its pivotal role in maintaining liver health and preventing MAFLD progression.

The findings presented in this chapter are published in *BMC Genomics.*

Kaushal, S*., Bhattacharya, D*., Kumar, S., Herr, W., Dhanjal, J. K., & Minocha, S. (2025). Epigenetic modifications in the murine liver upon depletion of transcriptional coregulator host cell factor 1. BMC genomics, 26(1), 654. https://doi.org/10.1186/s12864-025-11786-5

***** *equal contribution*

Chapter 5. Dissecting the molecular landscape of MAFLD using a palmitic acid-supplemented high-fat diet zebrafish model (*Danio rerio*).

5.1 Graphical abstract

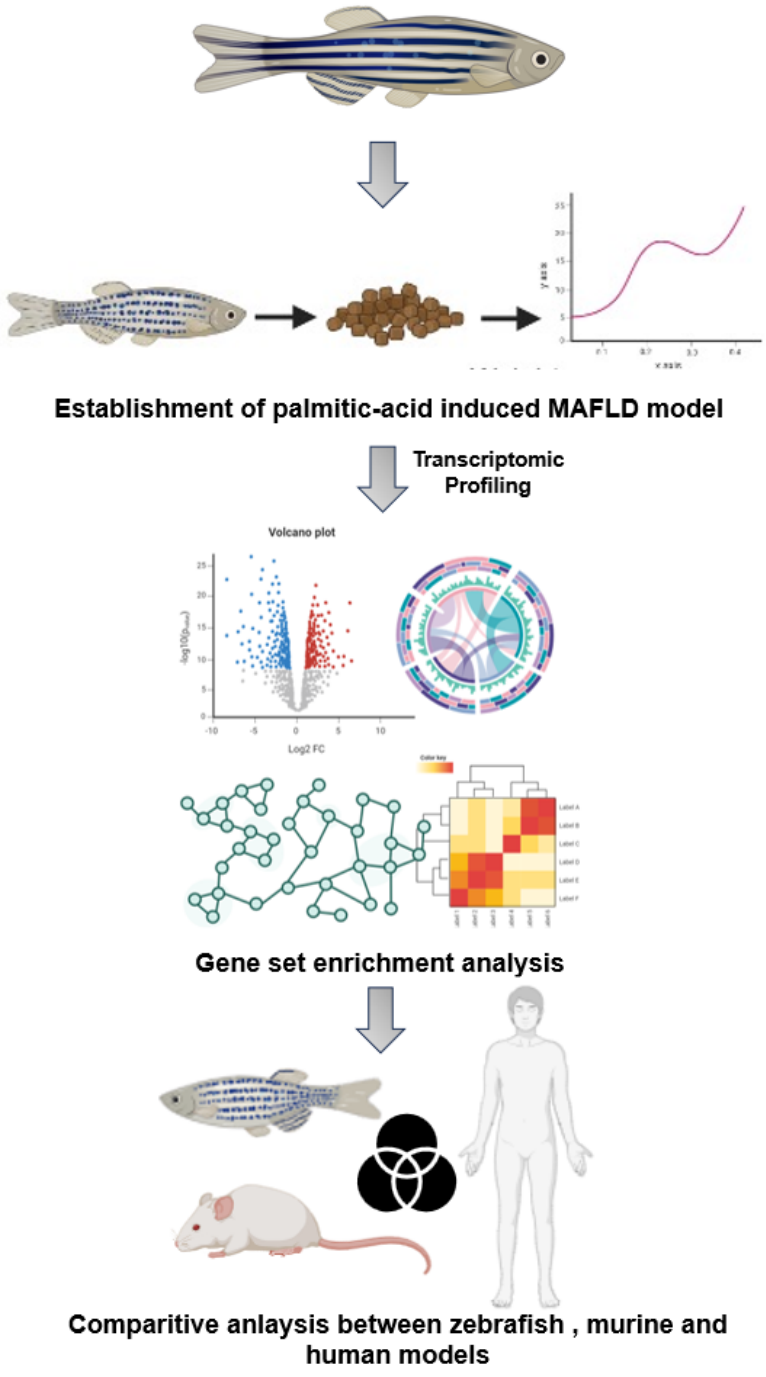

5.2 Background

Metabolic dysfunction–associated fatty liver disease (MAFLD) encompasses a broad spectrum of hepatic disorders, ranging from metabolic dysfunction–associated fatty liver (MAFL) to the more severe and progressive metabolic dysfunction–associated steatohepatitis (MASH) (165–167). Simple fatty liver is characterized by hepatic steatosis, in which hepatocytes accumulate more than 5% triglycerides (168,169). Although MAFL is frequently reversible with rigorous calorie restriction and sustained physical activity, in certain cases it may progress to MASH, a condition marked by liver injury and inflammation (55,170). Continued disease progression can lead to fibrosis, cirrhosis, and, ultimately, hepatocellular carcinoma (171). MAFLD, often regarded as the hepatic manifestation of metabolic syndrome, is a complex disorder that has garnered increasing scientific attention due to its rising global prevalence (172). It is estimated to affect approximately 32% of adults worldwide (173). MAFLD is frequently associated with a range of comorbidities, including cardiovascular disease, coronary artery disease, cancer, renal failure, and liver failure (155,167) Despite extensive investigation, the underlying pathophysiology and molecular mechanisms driving this heterogeneous disease remain incompletely understood.

Historically, the pathogenesis of MAFLD has been studied primarily using rodent models, including nutritional models such as the methionine choline–deficient (MCD) diet, choline-deficient L-amino acid–defined (CDAA) diet, and high-cholesterol diet; genetic models such as ob/ob, PTEN-null, PPARα knockout, and db/db mice; and combination models, for example db/db mice fed an MCD diet (168,174–176). However, these models present intrinsic limitations, including high maintenance costs, prolonged experimental timelines, and physiological differences that constrain their translational relevance to human MAFLD. Moreover, none fully recapitulates the multifactorial complexity of the disease.

Whereas the preceding chapter utilized a murine model to investigate the epigenetic consequences of a specific genetic lesion (*Hcfc1* deletion) in the mammalian liver, this chapter employs an adult zebrafish (*Danio rerio*) model to study diet-induced metabolic dysfunction. Each model organism provides complementary scientific advantages that directly align with the overarching objectives of this thesis. The mouse model is uniquely suited for mammalian genetic knockouts, cell-type-specific Cre-loxP drivers, and chromatin immunoprecipitation studies due to the depth of murine genomic annotation. Conversely, the adult zebrafish provides an exceptionally tractable, cost-effective *in vivo* platform for diet-induced systemic metabolic

studies. Lipid and carbohydrate metabolic pathways, hepatic cellular architecture (hepatocytes, biliary cells, and resident macrophages), and nuclear receptor signaling cascades are remarkably conserved between zebrafish and mammals. Crucially, the ease of dietary manipulation in zebrafish allows the administration of specific saturated fatty acids, such as palmitic acid, to model diet-induced steatosis, lipotoxicity, and inflammatory progression without the confounding secondary pathologies often observed in nutrient-deficient rodent diets (59,177). Integrating both models allows cross-species comparative analysis to discern conserved, fundamental molecular drivers of fatty liver disease (59,178). The zebrafish liver becomes fully developed within four days of fertilization and contains cell types such as hepatocytes, neutrophils, and macrophages that function analogously to their mammalian counterparts, thereby facilitating studies of inflammation and steatosis (179). The conservation of gene expression patterns and the presence of orthologues for most human genes involved in carbohydrate and lipid metabolism further support the use of zebrafish as a physiologically relevant model for dyslipidaemia-related disorders, including MAFLD (180).

MAFLD has been extensively investigated in zebrafish using a range of genetic (foie gras, ducttrip, hi559), transgenic (liver-specific overexpression of YY1 and cannabinoid receptor 1; heart-specific overexpression of IL6), and dietary (high-fructose diet and high-cholesterol diet) models (61,181–183). Diet-induced MAFLD models in zebrafish are considered clinically relevant, as the pathophysiology of obesity in zebrafish closely resembles that observed in mammals (177). In the present work, a novel zebrafish model of MAFLD is described, generated through overfeeding and supplementation with a diet rich in palmitic acid. Saturated fatty acids such as palmitic acid are known to induce inflammation and hepatic lipid accumulation (184,185), making them particularly relevant for modelling steatosis and early MASH-like conditions. Palmitic acid has been implicated in cellular damage, inflammation, insulin resistance, and dyslipidaemia (184–186). The lipid accumulation and metabolic abnormalities observed in human MAFLD are effectively reproduced in this model.

To gain a comprehensive understanding of the molecular alterations associated with disease development, extensive transcriptome profiling was performed using RNA sequencing (RNA-seq). Transcriptome analysis revealed notable parallels between the differentially expressed genes identified in the palmitic acid–supplemented zebrafish model and those reported in human MAFLD datasets, underscoring the translational relevance of this approach. Cross-species comparison with a mouse MAFLD model induced by a high-fructose diet further demonstrated the upregulation of pathways associated with cholesterol biosynthesis, lipid

metabolism, and related enzymatic activities in both systems. In addition, significant perturbations were observed in key regulatory pathways governing mitochondrial and hepatic metabolism, which are known to play central roles in the development and pathophysiology of MAFLD. Collectively, these findings strengthen the utility of zebrafish as a model for elucidating the complex molecular landscape of fatty liver disease and provide insights into conserved and species-specific mechanisms underlying MAFLD pathogenesis and progression.

5.3 Methods

All zebrafish husbandry, palmitic acid dietary interventions, tissue harvesting, flow cytometric Annexin V assays, ROS measurements, and histological and fluorescence-based staining were performed by collaborators in the laboratory of Dr. Shilpi Minocha at the Indian Institute of Technology (IIT) Delhi, specifically by co-first author Debashruti Bhattacharya and laboratory colleagues. The work presented in this thesis focused on whole-genome RNA-seq data processing, differential expression analysis, Gene Set Enrichment Analysis (GSEA), protein–protein interaction network construction using STRING, and cross-species comparative analyses integrating zebrafish data with murine and human MAFLD datasets. Experimental procedures are described below for completeness and reproducibility.

5.3.1 Zebrafish care and diet protocol

Adult wild-type zebrafish (6–8 months old) were maintained at 28.5 °C under a 14-h light/10-h dark cycle in accordance with Institutional Animal Ethics Committee regulations. Fish were sex-matched and acclimatized for three weeks before being randomly assigned to two groups (n = 20 per group). The control group received Tetramin flakes twice daily. For the test group, a palmitic acid (PA)–supplemented Tetramin diet was prepared by dissolving 7% (w/w) palmitic acid in diethyl ether and administering it four times daily. The overfeeding protocol was continued for eight weeks. Body weight measurements were performed after anesthetizing fish with 0.02% (w/v) MS222 (tricaine) for 45–60 seconds.

5.3.2 Annexin V Staining (Apoptosis)

Apoptosis (early and late) and necrosis in liver cells were evaluated using Annexin V and Propidium Iodide (PI) dyes, followed by flow cytometry. Liver tissue was dissociated into a single-cell suspension using trypsin prior to staining.

5.3.3 Reactive oxygen species (ROS) assay for estimating oxidative stress

Intracellular ROS levels were measured using the cell-permeable fluorescent dye DCFH-DA, which is oxidized to the fluorescent product DCF. Fluorescence intensity was recorded at an excitation wavelength of 484 nm and an emission wavelength of 535 nm.

5.3.4 Staining for endoplasmic reticulum (ER) stress

NBD-Oct dye was applied to 4 μm–thick paraffin-embedded liver sections to assess endoplasmic reticulum (ER) stress.

5.3.5 Histological staining

Hematoxylin and eosin (H&E) staining was performed on 4 μm–thick paraffin sections to evaluate general liver morphology. For lipid-specific staining, Oil Red O (ORO) and BODIPY were used on cryosections of 8 μm and 5 μm thickness, respectively, to examine hepatic neutral lipid accumulation. ORO-stained lipids red and nuclei blue (with hematoxylin), whereas BODIPY stained lipids green and nuclei blue (with DAPI). Quantification was performed using ImageJ software.

5.3.6 Immunoblotting (Western Blot)

Immunoblotting was used to detect specific proteins in liver lysates, with 70 μg of protein loaded per lane. Target proteins included PCNA, Sirt1, SREBP1c, PGC1α, OXPHOS, C/EBPα, and β-actin as the loading control.

5.3.7 Quantitative Real-time PCR (qPCR)

Total RNA was isolated using the Trizol method. Complementary DNA (cDNA) synthesis was performed using 1 μg of RNA. qPCR reactions were carried out using iTaq Universal SYBR® Green Supermix. The housekeeping gene used for normalization was gapdh, and relative fold changes were calculated using the ΔΔCt method.

5.3.8 Whole genome transcriptomic profiling

Total RNA was isolated from two control and three PA-supplemented diet–fed zebrafish livers using the RNeasy Lipid Tissue Mini Kit (Cat. No. 74804; Qiagen), following the manufacturer's protocol. RNA quality was assessed by agarose gel electrophoresis and RNA integrity number (RIN) scoring. Only samples with RIN values above 7 were processed further for sequencing on the Illumina NovaSeq 6000 platform. Raw sequencing data were trimmed

using Trim Galore (v0.6.4) and assessed for quality using FastQC (v0.11.8). High-quality reads were aligned to the zebrafish reference genome GRCz11 (danRer11) using the STAR aligner (v2.7.9a). Transcript counts were generated using featureCounts (v2.0.3) (112,187). Normalization and differential expression analysis were performed using the DESeq2 package (v1.42.0) in Bioconductor. Wald tests were applied for the MAFLD versus control comparison. Genes with a log2 fold change ≥ 1.0 were considered upregulated, and those with a log2 fold change ≤ −1.0 were considered downregulated, with a q value < 0.05. Gene set enrichment analysis (GSEA), Gene Ontology (GO), and KEGG pathway enrichment analyses were performed using the clusterProfiler R package (v4.10.0) (112,187). Protein–protein interaction (PPI) analysis was conducted using the STRING database (188).

5.3.9 Statistical analysis

All experiments were performed with at least three biological replicates unless otherwise stated. Data are presented as mean ± SEM. Statistical significance was assessed using a two-tailed Student's t-test using GraphPad Prism software, with $p < 0.05$ considered statistically significant.

5.4 Results

5.4.1 Palmitic acid (PA) supplementation induces hepatic steatosis and early liver injury in adult zebrafish

To establish a diet-induced model of metabolic dysfunction–associated fatty liver disease (MAFLD), only male zebrafish between 5 and 6 months of age were selected in order to minimize potential sex- and age-related variation in metabolic responses. All animals were weight-matched at baseline to ensure a uniform starting population. The experimental group was overfed a standard diet supplemented with 7% palmitic acid (PA) for a duration of 8 weeks (**Figure 5.1A**).

Body weight was monitored longitudinally to assess diet-induced obesity. A steady and statistically significant increase in body weight was observed in the PA-supplemented group (n = 24 fish per group; baseline: 0.17 ± 0.01 g; 1 month: 0.35 ± 0.02 g, $p \leq 0.0001$; 2 months: 0.51 ± 0.03 g, $p \leq 0.0001$; two-tailed Student's t-test), whereas control fish maintained stable weight (baseline: 0.15 ± 0.01 g; 2 months: 0.17 ± 0.01 g, $p > 0.05$; **Figure 5.1B,C**). As shown in **Figure 5.1D**, PA feeding induced a significant elevation in the liver-to-body weight ratio (n = 10 fish per group; control: 2.3 ± 0.5%; PA-fed: 7.2 ± 0.9%; $p \leq 0.01$, two-tailed Student's t-test),

demonstrating marked hepatomegaly. Though, an elevated level of PCNA immunodetection indicated only a moderate increase in cell proliferation, suggesting that liver enlargement was primarily attributable to lipid accumulation rather than enhanced cellular proliferation.

Histopathology was performed on PA treated fish to elucidate the structural changes of the liver. Hematoxylin–eosin (H&E) staining of liver sections revealed mild architectural disorganization in PA-fed zebrafish, indicative of early hepatic injury (**Figure 5.1E**). ORO staining of cryosections demonstrated extensive lipid droplet deposition in PA-fed livers compared with controls **(Figure 5.1F)**, and quantitative analysis confirmed a significant increase in lipid-stained area (**Figure 5.1G**). BODIPY staining further corroborated these findings, revealing a marked increase in neutral lipid accumulation in PA-fed liver sections (green stain) relative to controls (**Figure 5.1H and I**). Collectively, these results establish that PA supplementation effectively induces hepatic steatosis and moderate tissue disorganization, recapitulating a MAFLD-like phenotype in adult zebrafish.

5.4.2 PA supplementation perturbs lipid metabolism and activates ER and mitochondrial stress pathways

To elucidate the molecular mechanisms underlying PA-induced hepatic steatosis, transcriptional changes in pathways associated with lipid metabolism, endoplasmic reticulum (ER) stress, unfolded protein response (UPR), oxidative stress, and mitochondrial function were examined.

The mRNA expression levels of key lipogenic and cholesterol biosynthetic enzymes fatty acid synthase (*fasn*), acetyl-CoA carboxylase (*acc*), 3-hydroxy-3-methylglutaryl-CoA reductase *(hmgcra*), and 3-hydroxy-3-methylglutaryl-CoA synthase 1 (*hmgcs1*) were significantly elevated in PA-fed animals **(Figure 5.2A)**. These enzymes catalyze rate-limiting steps in fatty acid and cholesterol biosynthesis, indicating enhanced *de novo* lipogenesis and dysregulated cholesterol metabolism, both hallmarks of MAFLD (189–191).

Given the established role of lipid overload in triggering ER stress, the expression of ER stress–responsive genes was assessed. Growth arrest and DNA damage–inducible gene 45 alpha (*gadd45a*), activating transcription factor 6 (*atf6*), DNA damage–inducible transcript 3 (*ddit3*), and X-box binding protein 1 (*xbp1*) were significantly upregulated in PA-fed livers **(Figure 5.2B)**. These transcriptional changes are indicative of activation of the unfolded protein response (UPR) and ER stress signaling cascades (192,193).

Mitochondrial dysfunction and activation of the mitochondrial UPR (UPR^{mt}) were also evident. Expression of mitochondrial chaperones and proteases, including heat shock protein 60 (*hspd1*), caseinolytic mitochondrial matrix peptidase proteolytic subunit (*clpp*), and lon peptidase 1 (*lonp1*), was significantly increased (**Figure 5.2C**), reflecting a compensatory stress response aimed at restoring mitochondrial proteostasis.

Fluorescent staining of liver sections with the ER-specific polarity-sensitive dye NBD-Oct further demonstrated a progressive increase in ER lipid content in PA-fed animals at both 1-month and 2-month time points, consistent with sustained lipotoxic stress within the ER lumen.

5.4.3 PA supplementation disrupts oxidative phosphorylation and fatty acid oxidation

Transcriptional profiling of mitochondrial oxidative phosphorylation (OXPHOS) genes revealed broad dysregulation. Genes encoding components of mitochondrial complexes I (*nd1*), III (*uqcrc2*), IV (*cox4i1*), and V (*atp5f1b*) exhibited a downward trend in expression, although these changes did not reach statistical significance. In contrast, complex II (*sdha*) was significantly downregulated (**Figure 5.2D**), suggesting impaired electron transport chain function and compromised mitochondrial bioenergetics.

In parallel, genes involved in mitochondrial and peroxisomal fatty acid β-oxidation were significantly upregulated. Carnitine palmitoyltransferase 1a (*cpt1a*), which facilitates mitochondrial import of long-chain fatty acids, showed increased expression. Additional fatty acid oxidation regulators, including medium-chain acyl-CoA dehydrogenase (*acadm*), peroxisome proliferator-activated receptor gamma (*pparg*), and peroxisome proliferator-activated receptor alpha b (*pparab*), were also significantly elevated (**Figure 5.2E**). These findings indicate a compensatory upregulation of fatty acid oxidation pathways in response to excess lipid availability.

5.4.4 PA supplementation induces oxidative stress and inflammatory signaling

Enhanced fatty acid oxidation and mitochondrial dysfunction are known to increase reactive oxygen species (ROS) production. Consistently, transcription of the antioxidant enzyme glutathione peroxidase 1a (*gpx1a*) was significantly increased in PA-fed animals (**Figure 5.2F**), suggesting activation of cellular antioxidant defenses.

Direct measurement of intracellular ROS using DCFDA fluorescence revealed a significant increase in ROS levels in the PA-fed group compared to controls (**Figure 5.2G**), confirming the presence of heightened oxidative stress.

Pro-inflammatory signaling was concurrently activated, as evidenced by significantly elevated mRNA levels of interleukin-1β (*il1β*) and interleukin-8 (*il8*), along with a modest but non-significant increase in transforming growth factor β (*tgfβ*) (**Figure 5.2F**). These cytokines are key mediators of hepatic inflammation and fibrogenic progression, indicating early transition toward a more advanced MAFLD phenotype (194,195). Taken together, these molecular and histopathological findings demonstrate that chronic PA. supplementation induces a coordinated pathological response involving dysregulated lipid metabolism, ER stress and UPR activation, mitochondrial dysfunction, impaired oxidative phosphorylation, compensatory fatty acid oxidation, oxidative stress, and pro-inflammatory signaling.

5.4.5 Mapping of PA-supplemented diet induced pathophysiological changes to alterations in transcriptome

To map PA-induced pathophysiological changes onto global transcriptional alterations, whole-transcriptome profiling was performed using RNA sequencing of total RNA isolated from control and PA-supplemented adult zebrafish livers. Following preprocessing and normalization, differentially expressed genes (DEGs) were identified using the DESeq2 package. In total, 1,137 genes (792 upregulated and 345 downregulated) were identified as differentially expressed based on fold-change thresholds, while 1,055 genes (768 upregulated and 287 downregulated) were identified based on log2 fold-change cutoffs. A volcano plot illustrating significantly dysregulated genes ($p < 0.05$) and their respective log2 fold changes is shown in **Figure 5.3A**.

Notably dysregulated genes included cholesterol 7α-hydroxylase (*cyp7a1*), fatty acid synthase (*fasn*), CCAAT enhancer binding protein alpha (*cebpa*), glucokinase (*gck*), retinol dehydrogenase 12 (*rdh12*), and cholesteryl ester transfer protein (*cetp*). These expression patterns were independently validated by quantitative real-time PCR **(Figure 5.4)**. All of these genes have been previously implicated in MAFLD pathogenesis, confirming the biological relevance of the observed transcriptional changes (196–201). Hierarchical clustering of highly dysregulated genes ($q < 0.05$; $-1.0 \geq \log2FC \geq +1.0$) is presented in **Figure 5.3B**.

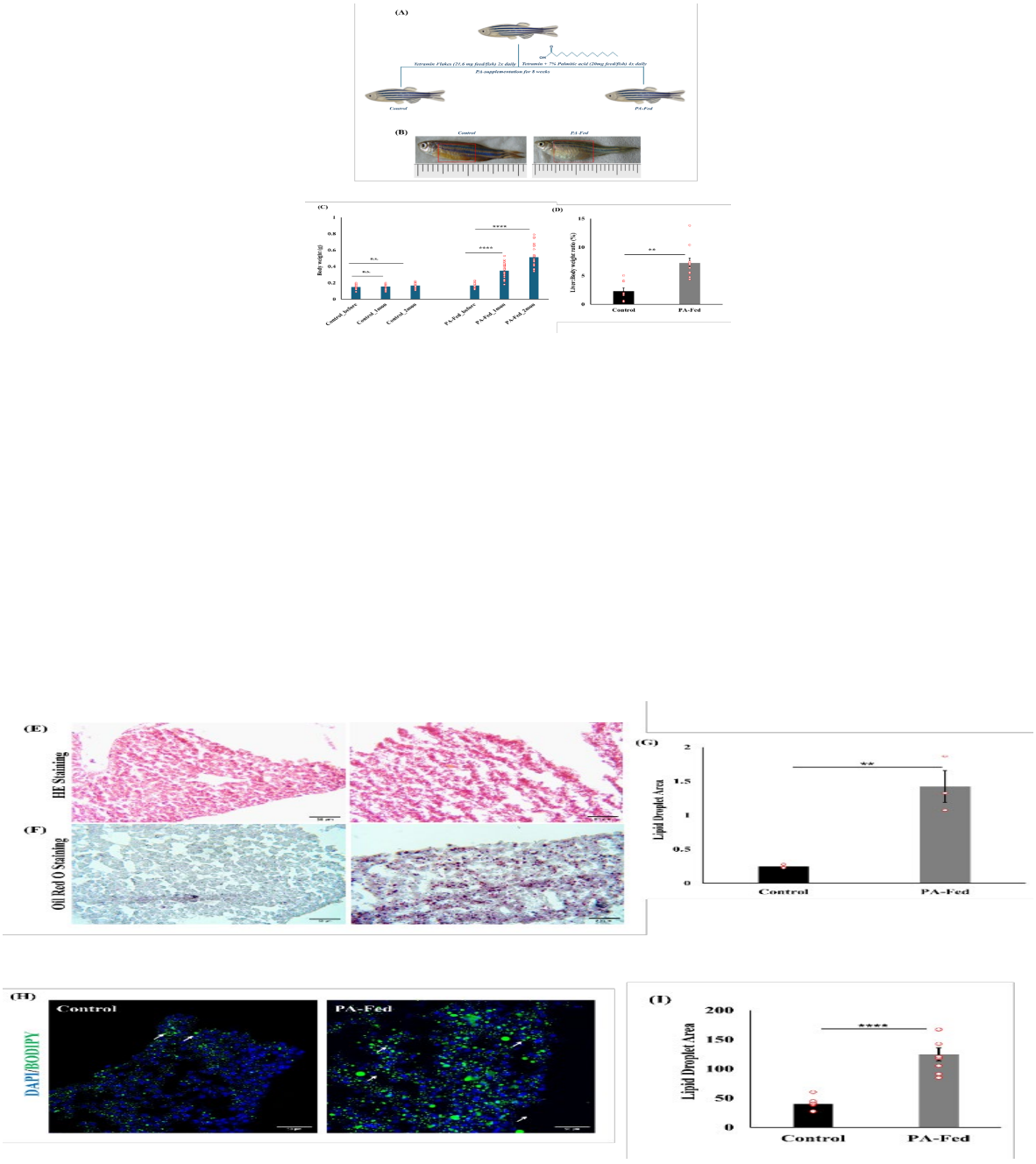

Figure 5.1: PA-supplementation leads to increase in body length, body weight and lipid accumulation in liver. A Schematic representation of the PA-supplementation paradigm. **B** Increased body length of test group upon PA-supplementation in comparison to control group. **C** Assessment of body weight of adult zebrafish fed

with control diet or PA supplemented diet (n = 24). **D** Assessment of Liver-to-body weight ratio (n = 10). **E** Hematoxylin and Eosin staining of adult control and PA-fed 4 µm thick paraffin embedded liver tissue sections show increased accumulation of lipid droplets. **F** Oil Red O staining of adult control and PA-fed 8 µm thick liver cryosections (40 × magnification, images captured using DEBRO DIM 150, inverted microscope). Scale Bar: 50 µm. **G** Quantification of Oil Red O staining of control and PA-fed sections (quantified using ImageJ). **H** BODIPY staining of adult control and PA-fed 5 µm thick liver cryosections (63 × magnification, images captured using Confocal Leica DMi microscope). Scale Bar: 50 µm I Quantification of BODIPY staining of control and PA-fed sections (quantified using ImageJ).

Gene set enrichment analysis (GSEA) revealed significant overrepresentation of biological processes including lipid transport, lipid localization, cholesterol metabolic processes, insulin secretion, unsaturated fatty acid metabolism, and lipid biosynthesis. Enriched molecular functions included phospholipase activity, lipase activity, and glycosaminoglycan binding (**Figure 5.3D**). KEGG pathway analysis demonstrated significant enrichment of MAPK signaling, calcium signaling, fatty acid biosynthesis, cell cycle regulation, cellular senescence, and arachidonic acid metabolism (**Figure 5.3C**). These pathways are integral to inflammation, cell survival, and lipid metabolism, underscoring the complex interplay between metabolic and stress-response networks in MAFLD progression. The complete list of DEGs and associated GSEA results is provided in **Additional File 5.1**.

To explore the potential biological function of DEGs, Gene Set Enrichment analysis (GSEA) was conducted using the ClusterProfiler (v4.10.0) package. As expected, the DEGs showed significant enrichment in biological processes (GO) such as lipid transport, lipid localization, cholesterol metabolic process, insulin secretion, unsaturated fatty acid metabolic process, and lipid biosynthetic process, to name a few. Furthermore, phospholipase activity, lipase activity, glycosaminoglycan binding were notably enriched terms in GO molecular functions as shown in **Figure 5.3D**. According to KEGG enrichment analysis, pathways such as MAPK signaling pathways, calcium signaling pathway, fatty acid biosynthesis, cell cycle, cellular senescence and arachidonic acid metabolism were found to be overrepresented (**Figure 5.3C**). These pathways are integral to the development of MAFLD, as they influence inflammation, cell survival, and lipid metabolism. The presence of these pathways in our analysis underscores the complex interplay between these cellular processes in the progression of hepatic injury and steatosis. The complete list of DEGs and their associated GSEA are included in **additional file 5.1**. GSEA analysis did not show a direct association of some of the highly dysregulated genes with the onset or progression of MAFLD.

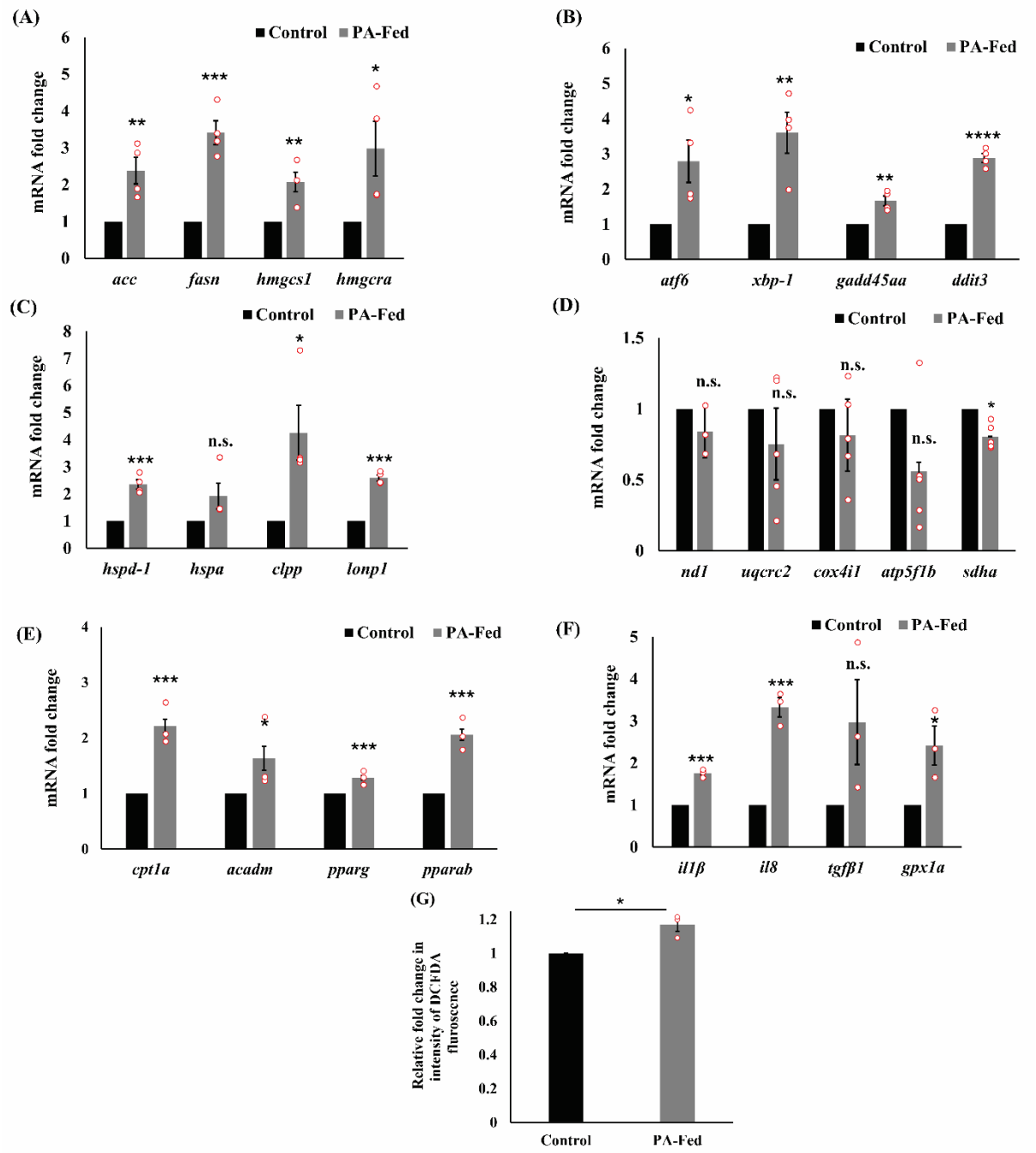

Figure 5.2: PA-supplementation leads to perturbed expression of genes associated with lipid metabolism, ER stress and unfolded protein response. Relative mRNA expression of **A** Lipid metabolism associated genes (n=4), **B** ER stress associated genes (n=4) and **C** Unfolded Protein Response-associated genes (n=4) and **D-** Oxidative phosphorylation genes in adult (n=5) control and PA-fed groups. **E** Genes associated with fatty acid oxidation (n=3) and **F** Genes associated with inflammation and antioxidant response system (n=3). **G** Relative fold change in the intensity of DCFDA fluorescence in PA-Fed group in comparison to control (n=3). Values are given as mean ± SEM. Student's t-test was performed to determine statistical significance. *$p < 0.05$, **$p < 0.01$, ***$p < 0.001$, ****$p < 0.0001$. acc, acetyl-CoA carboxylase; fasn, fatty acid synthase; hmgcs1, 3-hydroxy-3-methylglutaryl-CoA synthase 1; hmgcra, 3-hydroxy-3-methylglutaryl-CoA reductase; scd, stearoyl- CoA desaturase; atf6, activating transcription factor 6; xbp1, X-box binding protein 1; gadd45a, growth arrest and DNA-damage-inducible gene 45 alpha; ddit3, DNA damage-inducible transcript 3; il1β, interleukin-1β; hspd1, heat shock 60 protein 1; hspa9, heat shock protein 9; clpp, caseinolytic mitochondrial matrix peptidase proteolytic subunit; lonp1, lon peptidase 1; uqcrc2, cytochrome b-c1 complex subunit 2, mitochondrial; cox4i1, cytochrome

c oxidase subunit 4 isoform 1, mitochondrial, atp5f1b; ATP synthase subunit beta, mitochondrial, sdha; succinate dehydrogenase, cpt1a; carnitine palmitoyl transferase 1, acadm; medium-chain specific acyl-CoA dehydrogenase, mitochondrial, pparg; peroxisome proliferator-activated receptor gamma, pparab; peroxisome proliferator-activated receptor alpha b, il8; interleukin 8, tgfβ; transforming growth β, gpx1a; glutathione peroxidase 1a.

5.4.6 Protein–protein interaction analysis identifies key regulatory nodes in MAFLD progression

Protein–protein interaction (PPI) networks were constructed using STRING for all dysregulated protein-coding genes ($q < 0.05$; $-1.0 \geq \log2FC \geq +1.0$). The resulting interaction map is shown in **Figure 5.3E**.

Among the most highly upregulated genes was *inha* (**Figure 5.3B**), encoding the alpha subunit of inhibin, a member of the TGF-β superfamily involved in SMAD-mediated signaling. INHA is expressed by multiple immune cell types including NK cells ($CD56^+$ NK cells), dendritic cells, B cells, and T lymphocytes (such as Th17 and regulatory T cells), where it modulates their development, maturation, and function (202–204). Previous studies have demonstrated its involvement in various types of cancer, where it shapes the immune suppressive tumor microenvironment (202). More specifically its role in hepatocellular carcinoma has also been established (205). Its primary interactor ID3, encoded by *id3*, was downregulated and has been shown to regulate hepatoblast proliferation and differentiation (206). Another INHA interactor, CHRNA4B (encoded by *chrna4b*), was upregulated and has been linked to metabolic dysfunction–associated steatohepatitis (MASH) (207). CHRNA4B further interacts with GLT8D1, a glycosyltransferase implicated in MAFLD pathogenesis (208).

Another highly dysregulated gene identified in the protein–protein interaction network was *gc*, encoding the vitamin D–binding protein, which has been reported to attenuate liver injury and regulate glucagon secretion (209), The interaction network of GC included several upregulated partners, namely *cela1.6, cela1.3, slc4a8, cldni, cpa1, cpb1, c6ast4*, and *prss59.1*, along with a set of downregulated interactors, including *sb:cb37, ces2a, serpina7, zgc:174259*, and *proca*. Notably, recent evidence has implicated chymotrypsin-like elastase (CELA) in the regulation of lipid metabolism (210), supporting the functional relevance of the GC–CELA interaction in the context of hepatic lipid homeostasis. Carboxylesterase 2a (*ces2a*), which was significantly downregulated in this dataset, has been shown to promote hepatic steatosis and insulin resistance when deleted, through impairment of diacylglycerol and lysophosphatidylcholine catabolism (211). CES2A further interacts with glucokinase (*gck*), the primary hexokinase isoform expressed in hepatocytes. Glucokinase catalyzes the phosphorylation of glucose

entering the cell *via* GLUT transporters, converting it into glucose-6-phosphate (G6P), thereby directing glucose flux into multiple anabolic and catabolic pathways (212). Hepatic glucokinase activity is tightly regulated by hormonal signals, intracellular glucose metabolites, and binding partners, including 6-phosphofructo-2-kinase/fructose-2,6-bisphosphatase (PFK2/FBP2). Dysregulation of glucokinase expression and activity has been strongly associated with type 2 diabetes and metabolic dysfunction–associated fatty liver disease (213). Consistent with these observations, *gck* was found to be highly upregulated in the present dataset, further supporting a coordinated disruption of glucose and lipid metabolic pathways in the PA-induced MAFLD model. Several interacting partners of *gck* were further identified, including *pfkma, mat2ab, abcb5*, and *klb*, all of which exhibited increased expression in the present dataset. The functional relevance of these interactions is supported by prior evidence demonstrating that the TGF-β1/p65/MAT2A axis regulates liver fibrogenesis through modulation of intracellular S-adenosylmethionine (SAM) levels (214). In addition, genetic variation in abcb5 has been associated with an increased risk of hepatocellular carcinoma (HCC) (215).

The primary interactors of ABCB5 included proteins encoded by *jag1b, epcam, ccnb1, igsf9ba, itga6b*, and *proca*. Among these, *igsf9ba* and *proca* were downregulated, whereas all other interactors were upregulated in the present analysis. Cyclin B1 (*ccnb1*) has been reported to promote hepatocellular carcinoma development by facilitating DNA replication and cell-cycle progression (216). In the interaction network, CCNB1 was found to associate with proteins encoded by upregulated genes (*smcr8b, mid1ip1l, itgb4, cldne, ctrl, r3hdml*) and downregulated genes (*diabloa, ccdc141, col5a1, vsx1, foxh1, and cep55l*). Midline-1 interacting protein 1 (MID1IP1) has previously been shown to promote cancer metastasis through FOS-like 1–mediated matrix metalloproteinase-9 signaling in hepatocellular carcinoma (217), highlighting the oncogenic potential of this interaction module. The transcription factor foxh1, which exhibits DNA-binding transcriptional repressor activity and regulates cell growth and migration/invasion *via* mTOR signaling, has also been implicated in hepatocellular carcinoma development (220). FOXH1 was found to interact with proteins encoded by dysregulated genes including *ccdc103, mef2b, tfap2c*, and *oplah*. In addition, reduced expression of *col5a1* was observed. COL5A1, a collagen-related gene implicated in liver fibrosis (221), interacted with proteins encoded by dysregulated genes *itgb4, ccnb1, tox3*, and *slc35c2*, further supporting the presence of a fibrotic and pro-tumorigenic transcriptional signature.

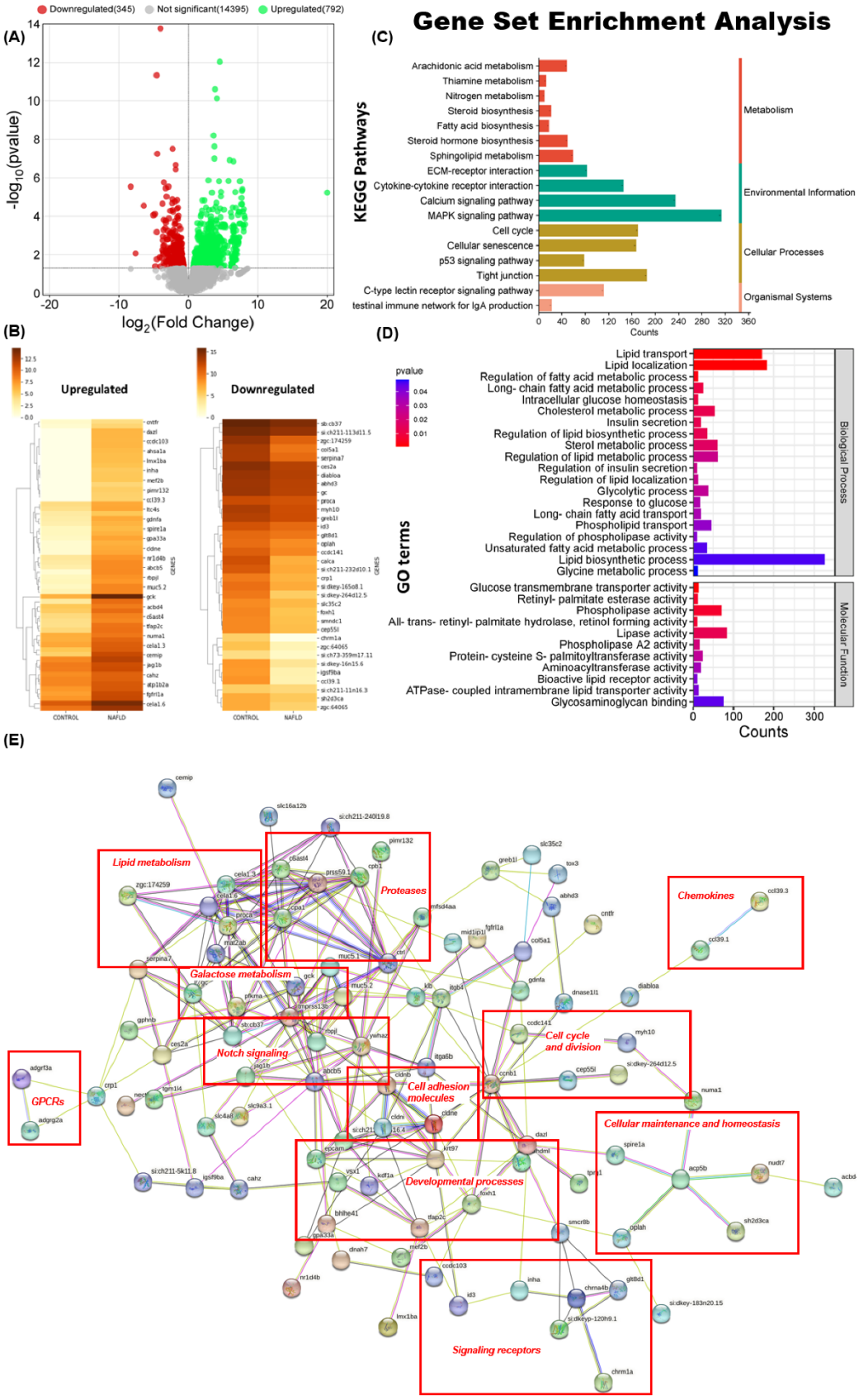

Figure 5.3: Identification and annotation of differentially expressed genes. A Volcano plot of DEGs for MAFLD vs control transcriptomic data. The volcano plot shows the fold-change (x-axis) versus the significance (y-axis) of the identified genes. The significance (p value) and the fold-change were converted to − log10 (p value)

and log2 (fold-change), respectively. The vertical and horizontal dotted lines show the cut-off of log2 Fold change = ± 1.0, and of p value < 0.05, respectively. There were 792 upregulated genes (upper-right, dots coloured green), and 345 downregulated genes (upper-left, dots coloured red). **B** Hierarchical clustering map of DEGs. The horizontal axis shows the names of each group (control and MAFLD) and the vertical axis shows the clusters of DEGs. The left clustermap shows upregulated DEG's while the right one shows downregulated DEG's. Colours towards brown represent high expression values and colours towards yellow represent low expression values. Here q value < 0.05 and log2Fold-change = ± 1.0 is taken as level of significance parameters. Constructed with seaborn package in python. **C** GSEA KEGG pathway analysis of DEGs. The dot plot represents the KEGG pathways on the y-axis and enrichment scores on the x-axis. The dot represents the gene count; greater gene count corresponds to a greater dot. The colour of the dot varies based on the p value. **D** GSEA Gene Ontology analysis of DEGs. The bar plot shows the gene counts (x-axis). GO terms, biological processes and molecular functions are on the y-axis. The colour of the bar varies based on the significance of p value. Constructed with SR plot. **E** STRING analysis showing protein–protein interaction between the proteins encoded by dysregulated genes. Some of these are GPCRs, chemokines, proteases, cell adhesion molecules and signaling receptors. Several are involved in galactose metabolism, lipid metabolism, Notch signaling, the cell cycle and division, developmental processes, as well as cellular maintenance and homeostasis.

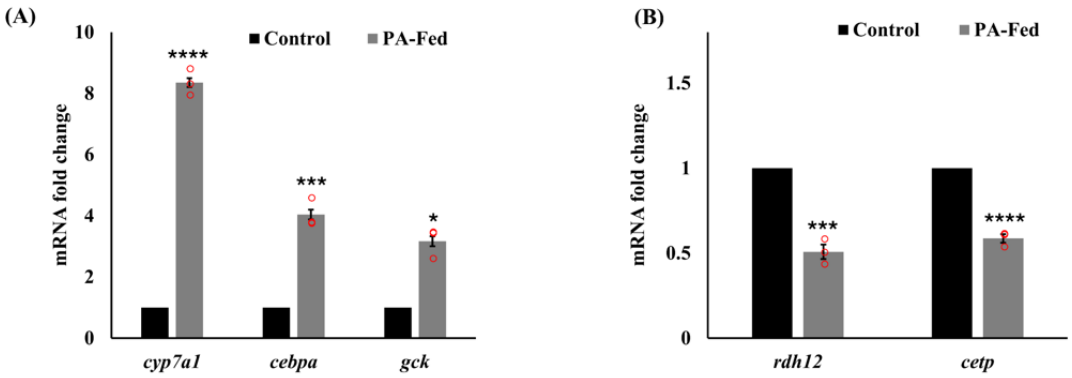

Figure 5.4: Relative expression of **A** *cyp7a1, cebpa, gck* and **B** *rdh12* and *cetp* in adult PA-fed livers in comparison to control (n=3). Values are given as mean ± SEM. Student's t-test was performed to determine statistical significance. ***p < 0.001, ****p < 0.0001. *cyp7a1*, cholesterol 7a-hydroxylase; *cebpa*, CCAT enhancer binding protein alpha; *gck*, glucokinase; *rdh12*, retinol dehydrogenase 12; *cetp*, cholesteryl ester transfer protein.

Collectively, this interaction-based analysis revealed the dysregulation of pathways previously associated with MAFLD, including lipid metabolism, cholesterol metabolism, inflammation, and insulin secretion. Perturbation of these pathways provides mechanistic insight into how altered transcriptional programs contribute to hepatic steatosis and liver injury. In addition, analysis of the MAPK signaling pathway, the arachidonic acid pathway and calcium pathway further illustrated the complexity of signaling between lipid metabolism, cell survival and inflammation when studying MAFLD progression, and helped understand how changes induced by PA lead to cell stress, lipids accumulation and hepatocellular damage.

The identification of key regulatory genes such as *inha*, which interfaces with immune signaling pathways, and *gc*, which is involved in glucose metabolism and lipid catabolism, illustrates the coordinated disruption of interconnected molecular networks in MAFLD.

Together, these findings provide new insight into the mechanisms driving insulin resistance, altered lipid metabolism, and chronic inflammation, hallmark features of MAFLD (**Figure 5.3E)**. Overall, this study delineates the transcriptional and network-level alterations associated with PA supplementation and offers a deeper understanding of how these molecular perturbations contribute to MAFLD pathogenesis.

5.4.7 Cross-species comparison reveals conserved molecular signatures of MAFLD

Building on the transcriptomic findings, a cross-species comparative analysis was performed between the PA–supplemented zebrafish model and a high-fructose diet–induced MAFLD mouse model (accession number PRJNA766592, European Nucleotide Archive). Indeed the overlap was quite compelling, with numerous biological pathways consistently dysregulated in both species including those related to lipid localization, sterol processing, lipid synthesis, cholesterol homeostasis, oxidoreductase and lipase activity. As illustrated in **Figure 5.5A–D**, these pathways were significantly enriched in both models, highlighting shared molecular mechanisms underlying lipid accumulation and hepatic injury. Additional overlapping biological processes are provided in **Additional File 5.2**.

To further delineate conserved molecular drivers of disease, genes that were commonly expressed and showed significant and concordant differential expression across both datasets were examined. Among the 6,742 genes expressed in both models, 38 genes met stringent selection criteria ($\log_2$FC $\geq$ 1.0 or ≤ -1.0) and exhibited consistent directional changes, as shown in **Figure 5.5E**. Key regulators of *de novo* lipogenesis (DNL), including *fasn, elovl6*, and *acaca*, were significantly upregulated, supporting their established role in hepatic lipid accumulation (218). In parallel, pro-inflammatory and fibrotic mediators such as *s100a11, inhbb*, and *fpr1* were also upregulated, underscoring the activation of chronic inflammatory and fibrogenic signaling pathways (219–221). Altered expression of cell-cycle regulators, including *cdkn1a, mki67*, and *cenpf*, pointed to aberrant hepatocyte proliferation and ongoing cellular injury, while dysregulation of *vldlr* and *pklr* reflected perturbations in lipid and glucose metabolism, respectively (222–224). Notably, *cyp17a1* and *sulf1*, both of which have been linked to metabolic dysfunction and oxidative stress, were also dysregulated, further implicating these genes in the exacerbation of hepatic steatosis (225,226). The complete list of overlapping genes is provided in **Additional File 5.3**.

Collectively, these findings underscore a conserved molecular landscape underpinning MAFLD pathogenesis in both the PA-fed zebrafish and high-fructose diet mouse models.

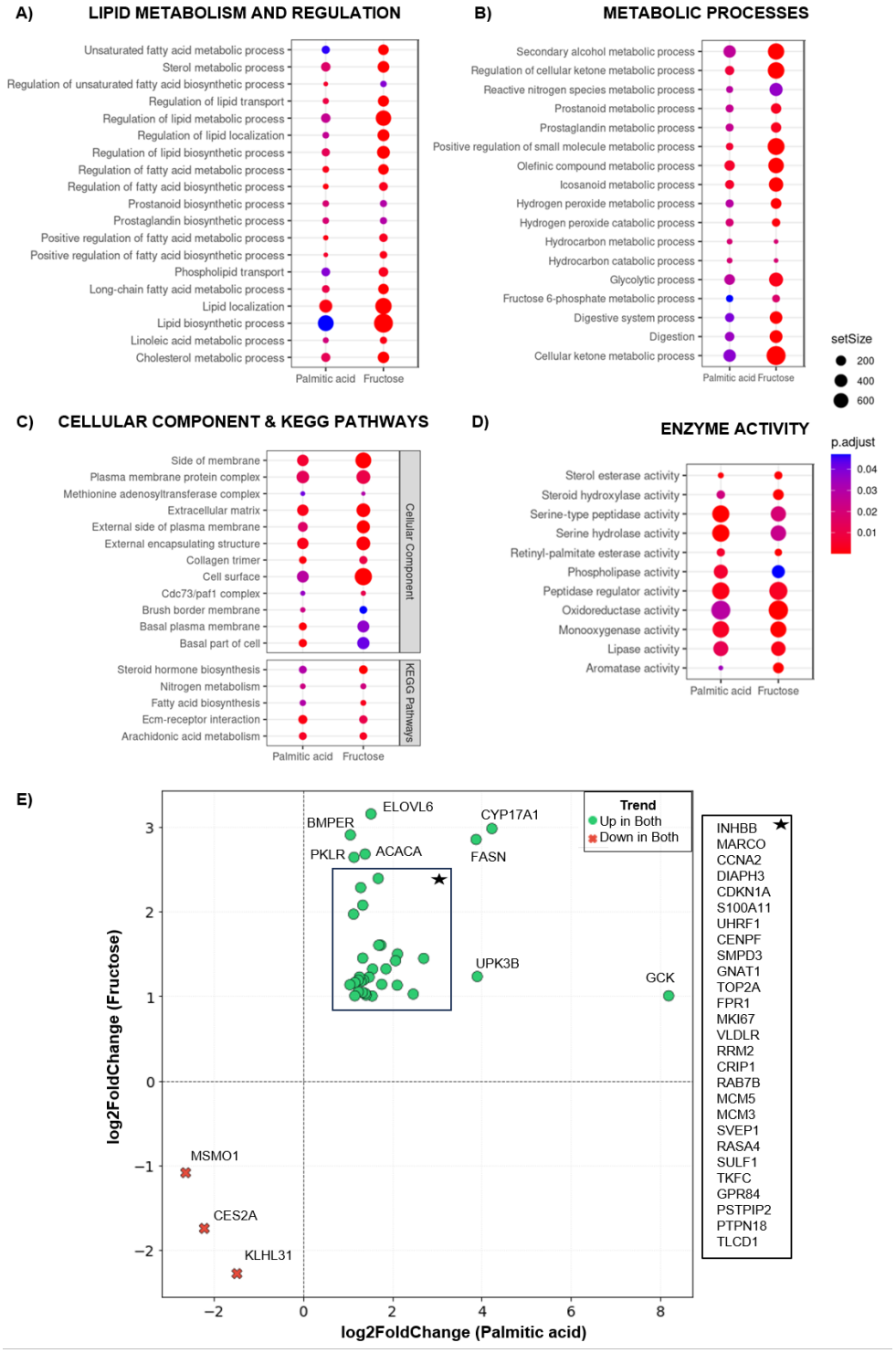

Figure 5.5: Comparison between palmitic acid- and fructose-based model: The dot plots depict the overlap between the categories **A** GO biological process: Lipid metabolism and regulation **B** GO biological process: Other metabolic processes **C** Cellular component and KEGG pathways **D** GO molecular function: Enzyme activity in palmitic acid and fructose based MAFLD model. The vertical items are the names of GO terms, and the length of horizontal graph represents the gene ratio. The depth of the colour represents the adjusted p-value. The area of

circle in the graph means gene counts. Constructed with ggplot2 in R package tidyverse. **E** The scatter plot illustrates commonly dysregulated genes with concordant trends in both the high-fructose diet mouse model (x-axis) and palmitic acid (PA)-fed zebrafish model (y-axis). Green dots indicate upregulated genes, while red crosses represent downregulated genes. Constructed with seaborn package.

Despite distinct dietary etiologies, both systems converged on common transcriptional programs that culminate in dyslipidaemia, inflammation, and liver injury. Integrative analysis of this data set showed that diet induced disorders in lipid metabolism cause pathology in liver tissues across species, demonstrating a key bridge for translational research across species ranging from animal models to disease states. Furthermore, analysis of human data was expanded using transcriptome data obtained from human subjects with MAFLD (accession: PRJNA558102, European Nucleotide Archive). This comparison revealed significant concordance between the differentially expressed genes identified in PA-fed adult zebrafish and those observed in human MAFLD patients (**Figure 5.6 and Additional File 5.4**). Genes involved in *de novo* lipogenesis (e.g., *hmgcs1* and *fasn*) and inflammation (e.g., *tgfβ1*) were upregulated in both species. In addition, genes associated with extracellular matrix remodeling and fibrogenesis, including *epcam*, *lamc2*, and *itgb6*, were also consistently upregulated in both models.

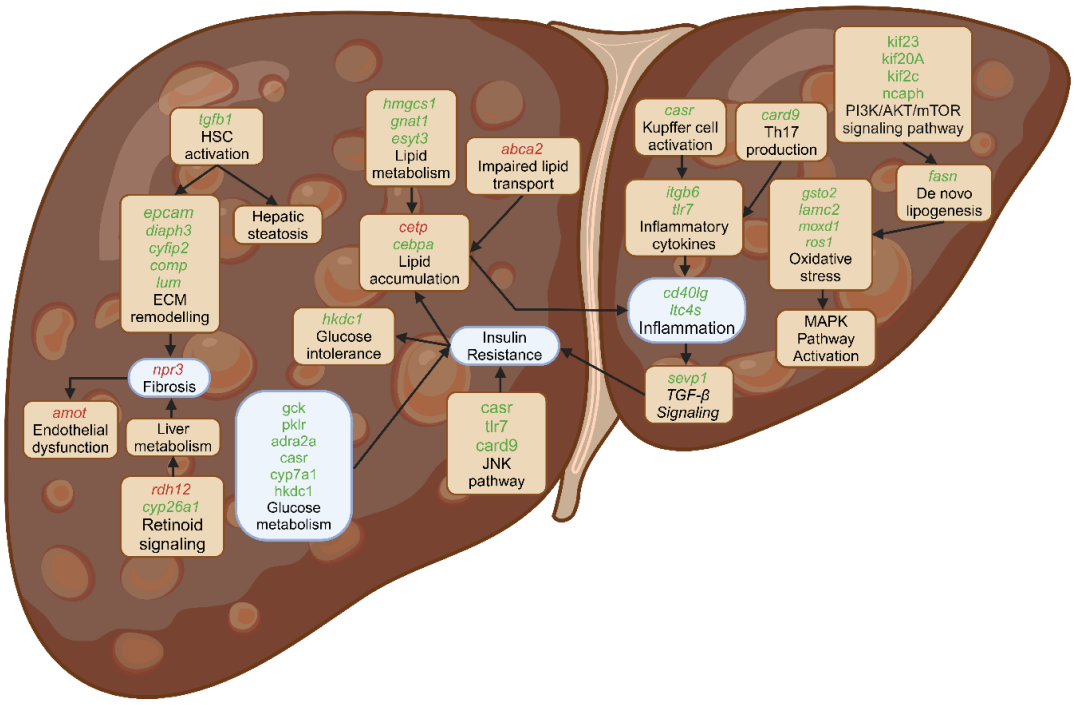

Figure 5.6: Comparison of human and zebrafish MAFLD models: Genes elevated in both models are highlighted in green, while downregulated genes are highlighted in red. The figure is created using BioRender.

The shared dysregulation of these metabolic, inflammatory, and fibrotic gene networks highlights the clinical relevance of the PA-fed zebrafish model for studying MAFLD. These

findings demonstrate that this model captures core transcriptional features of human MAFLD, thereby reinforcing its utility for investigating disease mechanisms and identifying conserved molecular targets with translational potential.

5.5 Discussion

The condition of metabolic dysfunction-associated fatty liver disease (MAFLD) is becoming a global burden affecting millions of people worldwide, children and adults alike. Animal models with both genetic and diet-based components have been widely used, yet the pathogenesis is not yet elucidated. Zebrafish has gained increasing recognition as a valuable experimental model for MAFLD research owing to its strong functional and molecular conservation with the mammalian liver. Upon exposure to environmental triggers such as hepatotoxins or fat-enriched diets, zebrafish develop hepatic steatosis that progresses to metabolic dysfunction–associated steatohepatitis (MASH) and, in advanced stages, hepatocellular carcinoma (HCC), following pathophysiological trajectories similar to those observed in human MAFLD/MASH (182,227).

In this study, a diet-induced zebrafish MAFLD model was established using chronic overfeeding with a high-fat, palmitic acid (PA)–supplemented diet to recapitulate key histopathological and metabolic features of the disease. Excessive consumption of a 7% PA-supplemented diet resulted in robust induction of hepatic steatosis in adult zebrafish. The feeding paradigm was designed to mimic high-fat dietary conditions prevalent in human MAFLD, thereby providing a physiologically relevant experimental context. Model validation was achieved through integrated phenotypic, histological, and molecular assessments, including body weight measurements, histological staining, Oil Red O and BODIPY lipid staining, apoptosis and proliferation analyses, and gene and protein expression profiling. These approaches collectively confirmed marked hepatic lipid accumulation, dysregulation of lipid metabolism, activation of cellular stress pathways, and mitochondrial dysfunction, hallmarks of MAFLD pathogenesis. Lipid loading of the endoplasmic reticulum in PA fed fish further supported the inductions of severely steatotic conditions which validated this model for mechanistic studies on MAFLD.

Obesity-associated MAFLD is tightly linked to dyslipidemia and increased hepatic free fatty acid (FFA) flux, placing the liver under sustained metabolic stress. Approximately 26% of the FFA flux in MAFLD has been attributed to hepatic *de novo* lipogenesis (DNL) (168,228). Consistent with this, PA-fed zebrafish exhibited significantly elevated expression of genes

involved in hepatic DNL and cholesterol biosynthesis, indicating profound disruption of lipid metabolic homeostasis. These transcriptomic changes were corroborated at the protein level by increased expression of SIRT1, SREBP-1c, and CEBPA, key regulators of hepatic lipid metabolism (229).

SIRT1, an NAD^+-dependent deacetylase, plays a central role in metabolic regulation by deacetylating transcription factors such as PPARα, PGC1α, ChREBP, and SREBP-1c, thereby modulating lipid and glucose metabolism (230,231). Although reduced SIRT1 activity has been associated with MAFLD progression in several models, its regulation is context-dependent and influenced by nutritional status (232–234). Under conditions of nutrient excess, as in the PA-supplemented model, elevated hepatic fatty acid and cholesterol synthesis may increase the NAD^+/NADH ratio, thereby enhancing SIRT1 activity (233,234). SIRT1-mediated deacetylation of PGC1α and SREBP-1c augments their transcriptional activity, promoting gluconeogenesis and *de novo* lipogenesis, respectively (235,236). In addition, SREBP-1c activation has been linked to ER stress and the unfolded protein response (UPR) (199, 237). In agreement with these mechanisms, the PA-fed model exhibited upregulation of multiple ER stress–associated genes and a marked increase in SREBP-1c protein levels, together with elevated PGC1α expression. These findings indicate a coordinated disruption of hepatic metabolic regulation and underscore the relevance of this model in capturing early pathogenic events in MAFLD.

ER stress and mitochondrial dysfunction are widely recognized as central contributors to MAFLD pathogenesis (238,239). Impaired ER-to-Golgi trafficking, defective triglyceride assembly and secretion as very-low-density lipoproteins (VLDLs), and altered calcium homeostasis activate ER stress pathways and trigger an adaptive UPR (240–242). Concurrently, defective mitochondrial β-oxidation and enhanced ω-oxidation of fatty acids increase reactive oxygen species (ROS) production, thereby promoting oxidative stress, inflammation, hepatocyte death, and progressive liver injury (243). The PA-fed zebrafish model exhibited significant activation of ER stress and UPR pathways, increased ROS generation, induction of antioxidant response genes, and elevated inflammatory signaling, collectively accounting for the severe hepatic injury observed. In addition, reduced expression of mitochondrial oxidative phosphorylation (OXPHOS) complex genes and proteins indicated compromised mitochondrial function. This observation aligns with previous studies reporting an initial adaptive mitochondrial response in MAFLD that becomes progressively impaired during

MASH progression (244–246). Comparable impairments in oxidative phosphorylation have also been documented in multiple rodent MAFLD models (247–250).

To assess whether PA-induced adult zebrafish liver pathology can be reversed a calorie restriction paradigm was applied in PA-fed adult zebrafish. This intervention was designed to emulate dietary strategies commonly employed in clinical management of MAFLD. Calorie restriction effectively attenuated hepatic steatosis, as evidenced by histological and gene expression analyses, demonstrating that the induced phenotype is metabolically plastic and responsive to dietary modulation. These findings are consistent with reports showing that caloric restriction improves liver health and reduces fat deposition through multiple metabolic pathways (55,177). The responsiveness of this model to caloric intervention highlights its utility for evaluating dietary, pharmacological, and combinatorial therapeutic strategies aimed at preventing or reversing MAFLD.

To further define the molecular perturbations caused by PA treatment in steatotic zebrafish livers, we analyzed changes in the transcriptome of adult steatotic zebrafish livers. Differential expression analysis revealed enrichment of genes involved in lipid transport, lipid localization, cholesterol metabolism, lipid biosynthesis, glucose metabolism, and retinoic acid metabolism. These perturbations were corroborated by increased expression of lipid metabolic genes (*acc, fasn, cebpa, hmgcs1, hmgcra*, and *cyp7a1*) and decreased expression of *rdh12*, consistent with known MAFLD-associated metabolic derangements. KEGG pathway analysis further identified enrichment of MAPK signaling, calcium signaling, cellular senescence, and p53 signaling pathways. These pathways have previously been linked to hepatic lipotoxicity, oxidative stress, ER stress, inflammation, and fibrogenesis (42,251,252).

Additional enrichment of ECM–receptor interaction and cytokine–cytokine receptor interaction pathways reflected the activation of profibrogenic and inflammatory programs, consistent with stellate cell activation and cytokine-mediated liver injury (252, 253–256). Other enriched pathways included steroid biosynthesis, arachidonic acid metabolism, sphingolipid metabolism, and cell cycle regulation, all of which have been implicated in MAFLD progression (257).

Beyond revalidating known MAFLD-associated genes, the analysis also identified novel candidate genes exhibiting pronounced dysregulation following PA exposure. Highly upregulated genes included (i) inhibin subunit alpha *(inha*, log2fold change 19.898), belonging to the TGF-β superfamily of proteins; (ii) ciliary neurotrophic factor receptor (*cntfr*, log2fold

change 4.106), a member of type 1 cytokine receptor family; (iii) cyclin B1 (*ccnb1*, log2fold change 7.972), known to show increased expression in HCC patients; (iv) transcription factors including LIM homeobox transcription factor 1, beta a (*lmx1ba*, log2fold change 7.768); and (v) myocyte enhancer factor 2b (*mef2b*, log2fold change 7.291) (258). Genes that showed prominent downregulation included (i) procollagen, type V, alpha 1 (*col5a1*, log2fold change − 4.024); (ii) calcitonin/calcitonin-related polypeptide alpha (*calca*, log2fold change − 5.031); and (iii) 5-oxoprolinase, ATP hydrolsying (*oplah*, log2fold change − 1.93), to name a few. *Col5a1* has formerly been identified as a basement membrane associated gene involved in the pathogenesis and progression of MAFLD (259). *Calca* that functions in maintaining calcium and chloride ion homeostasis has been implicated in cholestatic liver injury (260,261) while *oplah* is involved in glutathione metabolism and shows lower expression in MASH (261,262). These findings expand the molecular landscape of MAFLD and nominate new candidates for mechanistic and translational investigation.

5.6 Conclusion

The development of a palmitic acid (PA)–supplemented zebrafish model represents a robust and physiologically relevant *in vivo* platform for investigating metabolic dysfunction–associated fatty liver disease. This model faithfully recapitulates key histopathological, metabolic, and molecular features of MAFLD, including hepatic steatosis, dysregulated lipid metabolism, ER stress, mitochondrial dysfunction, oxidative stress, and inflammatory activation.

Comprehensive transcriptomic profiling revealed extensive reprogramming of metabolic, inflammatory, and fibrotic gene networks and identified both established and novel candidate genes implicated in MAFLD pathogenesis. Cross-species comparisons with high-fructose diet–induced MAFLD mouse models and human MAFLD transcriptomic datasets demonstrated strong conservation of dysregulated pathways governing lipid metabolism, inflammation, and liver injury, thereby validating the translational relevance of this zebrafish model.

The ability to modulate the PA-induced hepatic phenotype through caloric restriction highlights the metabolic plasticity of this system and its potential as an *in vivo* platform for testing therapeutic and dietary interventions. However, certain limitations of the present study should be noted. Although whole-liver RNA sequencing identified extensive transcriptional alterations and key regulatory hub genes (such as *inha*, *gc*, and *gck*), single-cell resolution was not performed to dissect cell-type-specific responses between hepatocytes, Kupffer-like

macrophages, and stellate cells. Furthermore, several computationally nominated network hubs and predicted cross-species regulatory axes remain to be functionally validated through targeted genetic knockouts or CRISPR-mediated perturbations in zebrafish. Future studies focused on single-cell transcriptomic dissection, targeted mutagenesis of novel candidate genes, and dynamic *in vivo* metabolic flux analyses will be crucial to fully leverage this model for translational therapeutics in MAFLD.

The findings presented in this chapter are published in *Scientific Reports.*

Bhattacharya, D*., **Kaushal, S*.,** Chakraborty, B., Raha, A., Dutta, T., Shekhar, H., Koner, A. L., Kumar, S., Ramachandran, R., Kaur Dhanjal, J., & Minocha, S. (2025). Zebrafish model of palmitic acid induced MAFLD recapitulates pathways conserved in mice and humans. Scientific reports, 15(1), 33343. https://doi.org/10.1038/s41598-025-13154-5

***** *equal contribution*

Chapter 6. Molecular and cellular basis of brain regeneration in zebrafish (*Danio rerio*).

6.1 Graphical abstract

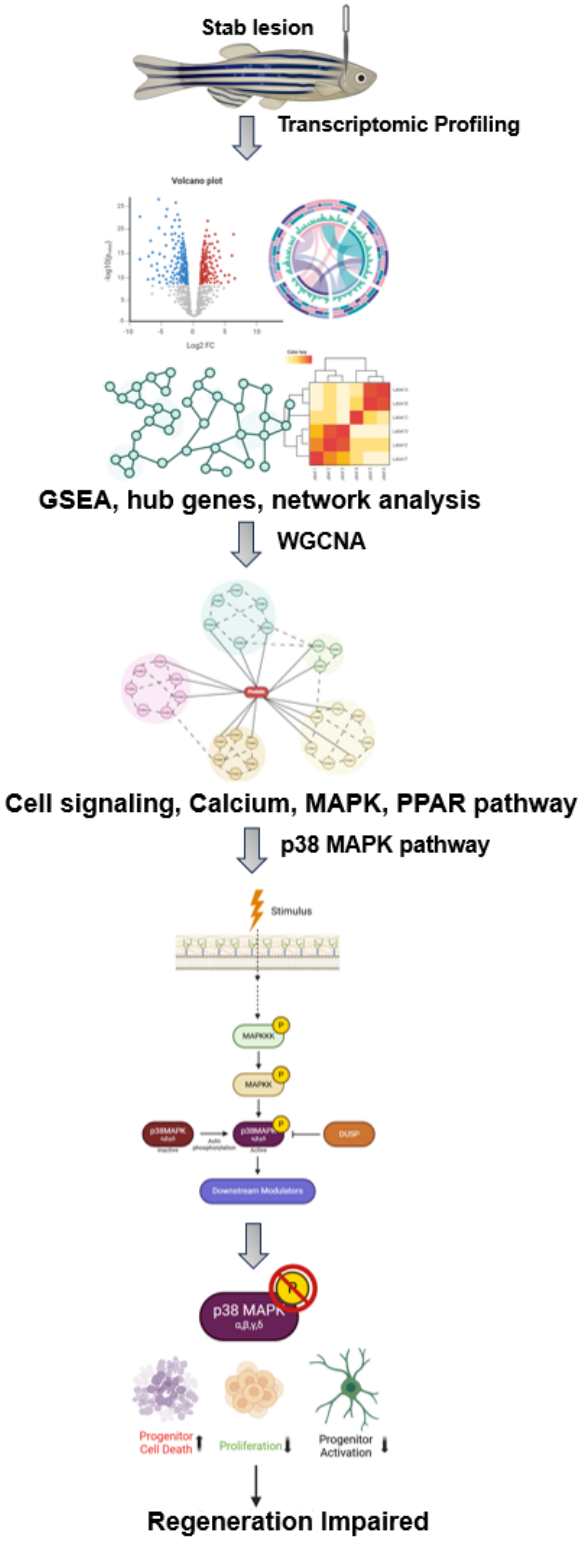

6.2 Background

Although the regeneration of lost or damaged tissue is a fundamental biological process observed across diverse organisms, tremendous variation exists in regenerative proficiency and the underlying molecular mechanisms across the animal kingdom. While mammals in general exhibit relatively poor regenerative capacity, there are several vertebrates (most notably zebrafish *Danio rerio*) with impressive multiorgan regenerative ability including some components of the mammalian brain (9,63). Zebrafish have gained importance both as an *in vivo* model system for the analysis of regeneration at the cellular and molecular level, and as a source of promising translationally relevant regenerative signals for the use in regenerative therapies for mammals (65,66).

The adult zebrafish brain displays considerable and sustained neurogenic potential, which is topographically distinct along the brain's rostro-caudal axis by the existence of 16 distinct regions of proliferation which, located immediately around the central ventricular system, are defined by radially oriented glial-like cells functionally equivalent to mammalian ependymal cells together with neuroepithelial-progenitor cells, providing a neuronal replacement pool subsequent to brain damage (263–265). In response to injury, the radially aligned glia become activated, proliferate, terminally differentiate and produce neurons which re-enter existing neural circuits within a brain environment which is devoid of sustained scarring glial formations which has been credited with facilitating repair of damaged neural tissue (65).

The regenerative capacity of the zebrafish brain can be stimulated through numerous types of injury models (focal ablations and stab wound lesions) allowing detailed analyses of the initial injury-driven transcriptional responses involved in regeneration (64,67). In addition, many and highly related signaling cascades that have been implicated in regulation of homeostatic versus regenerative neurogenesis in the zebrafish have been identified, including the reactivated Shh, BMP/TGFβ, Wnt/β-catenin, AhR, Notch, and FGF signaling pathways during injury in the zebrafish brain (68,266–269). Also contributing to neurogenesis, the inflammation response following injury and disease has been found to upregulate a protective neurogenic response during injury (69,270). Studies using both zebrafish and mammals have further defined roles for the pathways in insulin, brain derived neurotrophic factor (BDNF) and steroid signaling in progenitor proliferation, commitment and quiescence. (271,272). These studies, however, have not greatly advanced our understanding of the initial steps of brain regeneration; such as the signals linking injury-induced transcriptional responses to the activation of progenitor cells.

To investigate this, the current study presents and validated a telencephalic stab wound model in adult zebrafish (273). This paradigm relies upon the intact contralateral hemisphere to serve as an internal control thus facilitating exact comparisons of injured versus uninjured expression profiles across a variety of readouts at successive time points. RNA-seq profiles were collected at 4 time points across regeneration for injured compared with uninjured brains: uninjured brains, 1 dpl, 4 dpl, and 7 dpl, allowing the characterization of temporal change in gene expression that defines a regenerative response. Pathway enrichment analysis showed that the regenerating brains showed highly and significantly enriched activation of MAPK signaling pathways with a p38 MAPK signaling response.

The p38 MAPK signaling pathway has gained a great deal of attention due to its established role in the control of proliferation, migration, and differentiation of neural stem and progenitor cells (72,274,275). This pathway controls neuronal function through modulation of ion channel activity, regulation of protein translation and control of glutamate receptor signaling (73). Interestingly, p38 MAPK signaling in mammals is thought to possess context-dependent effects: sustained or inappropriate activation has been implicated in neurodegeneration (Parkinson's disease, Alzheimer's disease, and Huntington's disease), while transient or regulated activation increases neural precursor proliferation and neurogenesis (73,74,276). Activation of p38α MAPK in the subventricular zone of the mouse has been shown to stimulate neural precursor proliferation and neurogenesis, while deletion of p38α has been linked to decreased neural precursor proliferation (72). In excess, as has been demonstrated using cadmium neurotoxicity models, p38 MAPK activation has neurodestructive effects (277).

Though much remains unknown about rebuilding damaged brain tissue, a key role emerges for p38 alpha mitogen activated protein kinase in zebrafish recovery. Through combining transcriptomic profiling with a well-established telencephalic stab wound injury paradigm, insights appear into how reconstruction unfolds at molecular level inside central nervous system tissue. Such evidence shifts existing views on how mammals repair brain injury while opening possibilities for tracing universal molecular strategies applicable to human injuries.

6.3 Methods

All *in vivo* zebrafish maintenance, telencephalic stab-wound surgeries, tissue harvesting, Western blotting, and immunohistochemical analyses were carried out by collaborators in the laboratory of Dr. Shilpi Minocha at the Indian Institute of Technology (IIT) Delhi, under animal care and ethics approval IISERM/SAFE/PRT/2024/031 (IISER Mohali). Wet-lab experiments

were performed by co-first author Sidharth Bhasin and laboratory colleagues. The work presented in this thesis focused on bioinformatics analyses, including raw RNA-seq data processing, differential gene expression analysis, Gene Ontology and KEGG pathway enrichment analyses, network analysis using CytoHubba and WGCNA, and integrated biological interpretation of the resulting data. Experimental procedures are described below for completeness and reproducibility.

6.3.1 Animal Handling and Injury Model.

Adult fish were kept in controlled labs between 25-28 degrees Celsius, with a light cycle lasting 14 hours and then 10 hours of darkness. Water pH sat between 7.0 and 7.5. Rules set by IISER Mohali guided all care plans. Approval number IISERM/SAFE/PRT/2024/031 supported those choices. Before any procedures, general anesthesia used MS-222. A small gauge needle, sterilized, went straight up through skull bones into the brain's right half (telencephalon). Depth reached about two millimeters. After that, fish returned to their tank filled with water used for cleaning. How long afterward depended on research needs; endpoints varied. When time ended, each survived the transition into lethal conditions used later for analysis.

6.3.2 Protein Analysis (Immunoblotting)

Brain tissues were harvested and homogenized in RIPA lysis buffer in the presence of a protease inhibitor and a protein phosphatase inhibitor. Protein concentrations were determined using a bicinchoninic acid (BCA) assay. Equal amounts of protein were mixed with Laemmli sample buffer, denatured by boiling, and resolved on 8 to 12% SDS–polyacrylamide gels. Proteins resolved by gel electrophoresis were transferred to nitrocellulose, blocked with 5% bovine serum albumin (BSA). Membranes were incubated with primary antibodies against phospho-p38 MAPK, phospho-HSP27, total p38 MAPK, phospho-AKT, total HSP27, phospho-MK2, total MK2, c-Jun, total AKT, β-actin and β-catenin followed by incubation with appropriate horseradish peroxidase (HRP), conjugated secondary antibodies. Protein bands were visualized using enhanced chemiluminescence detection.

6.3.3 Histological and Immunofluorescence Assessment

Adult zebrafish exposed to a 5 mM BrdU bath for 4 h before being killed and then labelled. Brains were dissected and fixed in 4% paraformaldehyde (PFA), followed by dehydration through graded ethanol and xylene washes. Tissues were subsequently embedded in paraffin and sectioned at 5 μm thickness using a rotary microtome.

Hematoxylin and Eosin (H&E) Staining: Hematoxylin and Eosin (H&E) staining of paraffin sections, whereby dewaxed sections are rehydrated and then sequentially stained with hematoxylin (nuclear), eosin (cytoplasmic), dehydrated, cleared and mounted and observed under brightfield microscopy.

Immunofluorescence Staining: Frozen sections were thawed, dewaxed, rehydrated, then subjected to antigen retrieval by boiling in 10 mM sodium citrate buffer, (pH 6.0), followed by blocking. Non-specific binding was blocked using 1X normal goat serum. Sections were incubated overnight at 4°C with primary antibodies against Huc/D, BrdU, S100β, PCNA, Olig2, and GFAP, followed by incubation with appropriate fluorescently conjugated secondary antibodies. Nuclei were counterstained with DAPI (1 μg/mL). Slides were mounted and imaged using a Leica SP8 confocal microscope at 63X magnification.

6.3.4 RNA Analysis and Transcriptomic Profiling

Five adult zebrafish brains were pooled to constitute one biological replicate, with three independent biological replicates analysed per time point, for each experimental time point.
Frozen swiftly after dissection, the tissues stayed intact until RNA was extracted using a method from QIAGEN RNeasy Lipid Tissue Mini Kit, including on-column DNase digestion to eliminate genomic DNA contamination. Samples, with RNA quality (RIN) rated 8 or higher moved forward for downstream analysis.
Ribosomal RNA was depleted prior to library preparation. Strand-specific RNA sequencing libraries were generated using the NEBNext® Ultra™ II Directional RNA Library Prep Kit following the manufacturer's protocol. Paired-end sequencing (2 × 150 bp) was performed on the Illumina NovaSeq 6000 platform.

6.3.5 Quantitative RT-PCR (qRT-PCR)

Complementary DNA (cDNA) was synthesized from 1 μg of total RNA using standard reverse transcription protocols. Quantitative real-time PCR was carried out using iTaq™ Universal SYBR® Green Supermix. The ribosomal protein gene rpl13a was used as an internal control for normalization. Relative gene expression levels were calculated using the comparative ΔΔCt method.

6.3.6 Transcriptomic Data Analysis

Raw sequencing reads were processed using Trim Galore (v0.6.4) for adapter trimming and quality filtering, followed by quality assessment using FastQC (v0.11.8). High-quality reads

were aligned to the zebrafish reference genome GRCz11 (danRer11) using the STAR aligner (v2.7.9a). Gene-level read counts were generated using featureCounts (v2.0.3).

Normalization of read counts and differential gene expression analysis were performed using the DESeq2 package (v1.42.0) implemented in R/Bioconductor. Wald tests were applied to identify differentially expressed genes (DEGs) at each post-injury time point relative to the uninjured control. Genes with an absolute $\log_2$ fold change ≥ 1.0 and an adjusted p-value < 0.05 were considered statistically significant.

Gene set enrichment analysis (GSEA) was conducted using the clusterProfiler package (v4.10.0). Enriched Gene Ontology (GO) terms and KEGG pathways were analysed across all time-point comparisons to identify shared and time-specific biological processes.

Protein–protein interaction (PPI) networks for statistically significant DEGs were constructed by importing interaction data from the STRING database (version 12) into Cytoscape (v3.9.1). Key network nodes and hub genes were identified using the CytoHubba plugin (v0.1). Additionally, ClueGO (v2.5.10) and CluePedia (v1.5.10) were employed to generate functionally grouped networks and to perform integrative enrichment analysis by combining GO terms and KEGG pathways, enabling a pathway-centric interpretation of transcriptional changes across all regeneration stages.

6.3.7 Weighted Gene Co-Expression Network Analysis

A scale-free gene co-expression network was constructed using the Weighted Gene Co-expression Network Analysis (WGCNA) package implemented in R (278). WGCNA was performed on a filtered and normalized gene expression matrix derived from the zebrafish brain regeneration transcriptomic dataset. Raw count data were first transformed using the variance-stabilizing transformation (VST) function from the DESeq2 package (279) to minimize the dependence of variance on mean expression levels. Genes with missing values and those exhibiting zero variance across samples were excluded from further analysis. Following filtering, a total of 29,831 genes were retained for network construction.

Pairwise gene co-expression similarities were calculated using the average linkage method, resulting in a co-expression similarity matrix. That matrix turned into an adjacency matrix, using a power of $\beta = 6$ so it looked like an unweighted scale-free network. From there, it became a topological overlap matrix (TOM), which measures the relative interconnectedness between genes by considering both direct and shared network connections (280).

Gene modules, defined as clusters of genes exhibiting highly similar expression patterns, were identified using the dynamic hybrid tree-cutting algorithm based on TOM-derived dissimilarity. Module detection was performed using a minimum module size of 30 and a deepSplit parameter of 2. A dendrogram cut height of 0.4 was applied to delineate initial modules, and modules with highly similar expression profiles were subsequently merged based on the dissimilarity of their corresponding module eigengenes (MEs).

Module eigengenes, defined as the first principal component of each gene module, were used to represent the dominant expression pattern of the genes within each module. Functional annotation and enrichment analysis of genes within individual modules were performed using the DAVID bioinformatics resource (280) to identify overrepresented biological processes and pathways associated with brain regeneration.

6.3.8 Statistical Analysis

Most experiments were performed using at least three independent biological replicates (n = 3), unless otherwise explicitly stated. For RNA sequencing and quantitative real-time PCR analyses, one biological replicate consisted of pooled tissue from five adult zebrafish brains. Data are presented as mean ± standard error of the mean (SEM). Statistical significance for two-group comparisons was assessed using a two-tailed Student's t-test, with $p < 0.05$ considered statistically significant.

6.4 Results

6.4.1 Establishment of telencephalic stab wound injury model to study brain regeneration in zebrafish

A reproducible and well-characterized telencephalic stab wound injury model was established to investigate the temporal dynamics of brain regeneration in adult zebrafish (**Figure 6.1A**). A precise mechanical lesion was generated by vertically piercing the right dorsal-lateral telencephalon at a shallow angle with a fine 30-gauge needle, thus affecting the surrounding neuropil and neurogenic niche. The intact left hemisphere was internal contralateral sham control and served as a control for comparison of proliferative changes after mechanical lesion.

Tissue repair and regeneration was analyzed using histological assessments over several post-lesion time points (4, 7, 14 and 30 dpl). By 4 dpl the lesion could be visualized as a compact mass of cell at the site of the pokes, and is thought to reflect acute tissue destruction. Later time points show a decreasing size of the lesion over time. By 14 dpl a considerable amount of

remodeling of the tissue had taken place and closure of the site of the poke is seen, suggesting regeneration. By 30 dpl essentially all telencephalon had regenerated and only minor signs of the initial lesion can be seen (**Figure 6.1C**).

During the regenerative response proliferating cell nuclear antigen (PCNA) immunoreactivity was utilized to quantitatively study cell proliferation (see **Figure 6.1B**); a large number of immunoreactive cells were seen in the injured hemispheres during the recovery period indicating the involvement of a vigorous proliferative event.

These data further elucidate the molecular pathways involved in regeneration by comparing gene expression levels of important markers of neurogenesis and progenitor cells *via* real-time PCR and immunoblotting (**Figure 6.1D&E**). Quantitative RT-PCR analysis demonstrated that radial glial progenitor markers were significantly upregulated at 7 dpl relative to uninjured controls (*sox2*: 1.78 ± 0.20-fold, $p \leq 0.01$; *olig2*: 1.55 ± 0.14-fold, $p \leq 0.01$; *gfap*: 2.96 ± 0.27-fold, $p \leq 0.001$; n = 4 biological replicates with 5 pooled brains per replicate, two-tailed Student's t-test; **Figure 6.1D**). Concurrently, transcripts required for neuronal precursor differentiation exhibited marked induction (*tbr2*: 1.76 ± 0.16-fold, $p \leq 0.05$; *neurod1*: 1.40 ± 0.04-fold, $p \leq 0.01$; n = 3 biological replicates with 5 pooled brains each, two-tailed Student's t-test; **Figure 6.1E**), confirming post-injury neurogenesis.

Immunofluorescence techniques making use of cell-type-specific markers were further employed to elucidate the spatial patterning of proliferation during regeneration (**Figure 6.2A**). Proliferating cells were labeled by BrdU incorporation following a 4-hour pulse prior to tissue collection. At 4 dpl, quantification revealed a statistically significant increase in BrdU-positive cells within the injured telencephalic hemisphere compared with uninjured controls (control: 9.3 ± 1.5 cells; 4 dpl: 56.5 ± 6.6 cells; n = 4 fish per group, $p \leq 0.001$, two-tailed Student's t-test; **Figure 6.2B**). Similarly, the number of NeuroD1-positive differentiated neurons at 7 dpl increased significantly in the injured hemisphere (control: 55.7± 8.1 cells; 7 dpl: 142.5 ± 9.8 cells; n = 4 fish per group, $p \leq 0.001$, two-tailed Student's t-test; **Figure 6.2C**), while GFAP mean fluorescence intensity at 14 dpl was markedly elevated (control: 4.8 ± 1.2; 14 dpl: 33.0 ± 3.4; n = 4 fish per group, $p \leq 0.001$, two-tailed Student's t-test; **Figure 6.2D**). BrdU staining showed an increase in BrdU-positive cells with an increased extension of BrdU staining into the damaged parenchyma at 7 dpl, signifying an increase in cell production with persistent damage-induced cell division. A decrease in the intensity of BrdU immunostaining observed at 14 dpl seemed to reflect the reduction of proliferative activity observed in the injured

telencephalon, yet proliferation levels remain statistically higher in damaged brains compared with sham brains.

The onset of radial glial progenitor activity was analyzed with an immunohistochemistry-based detection of glial fibrillary acidic protein (GFAP). At 7 dpl GFAP staining was much stronger in the injured hemisphere, especially in the injured area and along neurogenic zone borders. By 14 dpl, GFAP staining could be detected throughout the injured telencephalon (**Figure 6.2A**, panel F), differing significantly from the sparse staining in the sham-injured hemisphere (**Figure 6.2A**, panel E; **Figure 6.2D**), indicating widespread activation of progenitor cells after injury.

Taken together, these data indicate that after a stab wound injury, the telencephalon in the adult zebrafish mounts a organized regenerative response that is accompanied by a pronounced increase in neurogenesis-associated markers, progenitor marker upregulation and activation of radial glial progenitors. These data validate use of this system to study cellular and molecular responses to brain damage in zebrafish following traumatic brain injury.

The process of neurogenesis was analyzed with NeuroD1 immunostaining, revealed in **Figure 6.2A** (panel C of **Figure 6.2A** was the uninjured control; **Figure 6.2C** shows quantification), was greatly elevated in injured telencephalons at 7 dpl, and at 14 dpl it persisted to a higher degree than the uninjured telencephalon (**Figure 6.2A**, panel D).

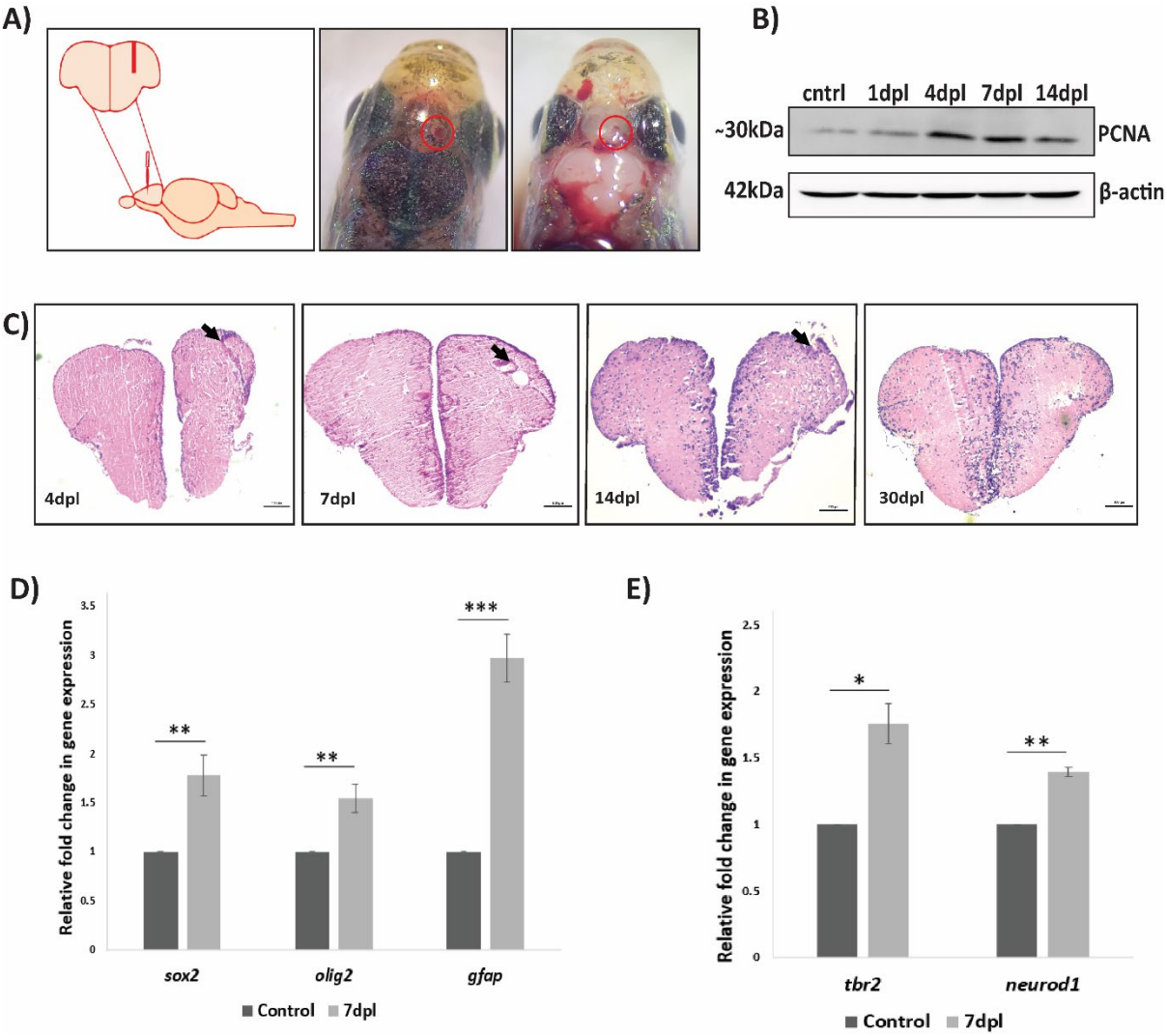

Figure 6.1: Telencephalic stab-wound injury model A Schematic representation of the stab-wound injury, with the injury site marked by the red circle. **B** Western blot analysis of Proliferating Cell Nuclear Antigen (PCNA) expression at different time points (control, 1 dpl, 4 dpl, 7 dpl, and 14 dpl). β-actin was used as a loading control. **C** Histological assessment of the injury at multiple time points (4 dpl, 7 dpl, 14 dpl, and 30 dpl) using Hematoxylin and Eosin (HE) staining. The black arrow indicates the injury site and the accumulation of cells observed at the injury location. **D** qRT-PCR of regeneration-specific markers Sox2, Olig2, and GFAP, showing significant upregulation at 7 dpl. Results are shown as mean ± SEM (n=4; 5 brains pooled for each sample). **E** qRT-PCR analysis of neuronal differentiation markers Tbr2 and NeuroD1 at 7 dpl, showing significant upregulation of both markers. Results are shown as mean ± SEM (n=3; 5 brains pooled for each sample). Significance is represented as * for P-value<0.05, ** for p-value<0.01 and *** for p-value<0.001 for all the quantifications cntrl; control; dpl, days post-lesion.

6.4.2 Transcriptome Profiling and functional annotation of the zebrafish telencephalon during different stages of brain regeneration

While histological and molecular analyses revealed robust cellular proliferation and neurogenesis following telencephalic injury, these approaches do not capture the global transcriptional programs that coordinate distinct phases of brain regeneration. Regeneration is

a highly dynamic, multistep process involving the coordinated regulation of inflammatory signaling, metabolic reprogramming, progenitor activation, and neuronal differentiation, many of which cannot be resolved by marker-based analyses alone. Therefore, an unbiased, genome-wide transcriptomic approach was employed to systematically identify injury-induced gene expression changes and signaling pathways underlying early regenerative responses in the zebrafish telencephalon.

Comparative analysis with uninjured controls revealed extensive transcriptional remodeling at all post-lesion stages. A total of 986 genes were significantly upregulated at 1 dpl, increasing to 2,551 genes at 4 dpl, followed by a reduction to 1,351 upregulated genes at 7 dpl. These temporal patterns correspond to distinct phases of regeneration, namely early injury response (1 dpl), peak proliferative activity (4 dpl), and tissue remodeling (7 dpl) (**Figure 6.3A–C**). The complete list of differentially expressed genes (DEGs) across time points is provided in **Additional File 6.1**.

PCA clearly separated the transcriptomic profiles obtained from the control samples and the profiles from each of the stages. The stage-based grouping of profiles was highly reproducible; profiles at each time point formed very tight groups. Volcano plots illustrating log2 fold change versus statistical significance highlighted distinct gene expression signatures at each regenerative stage (**Figure 6.3A–C**).

In order to determine the functional impact of the observed changes in gene expression, GSEA was applied for Gene Ontology (GO) terms and KEGG pathways at each time point.

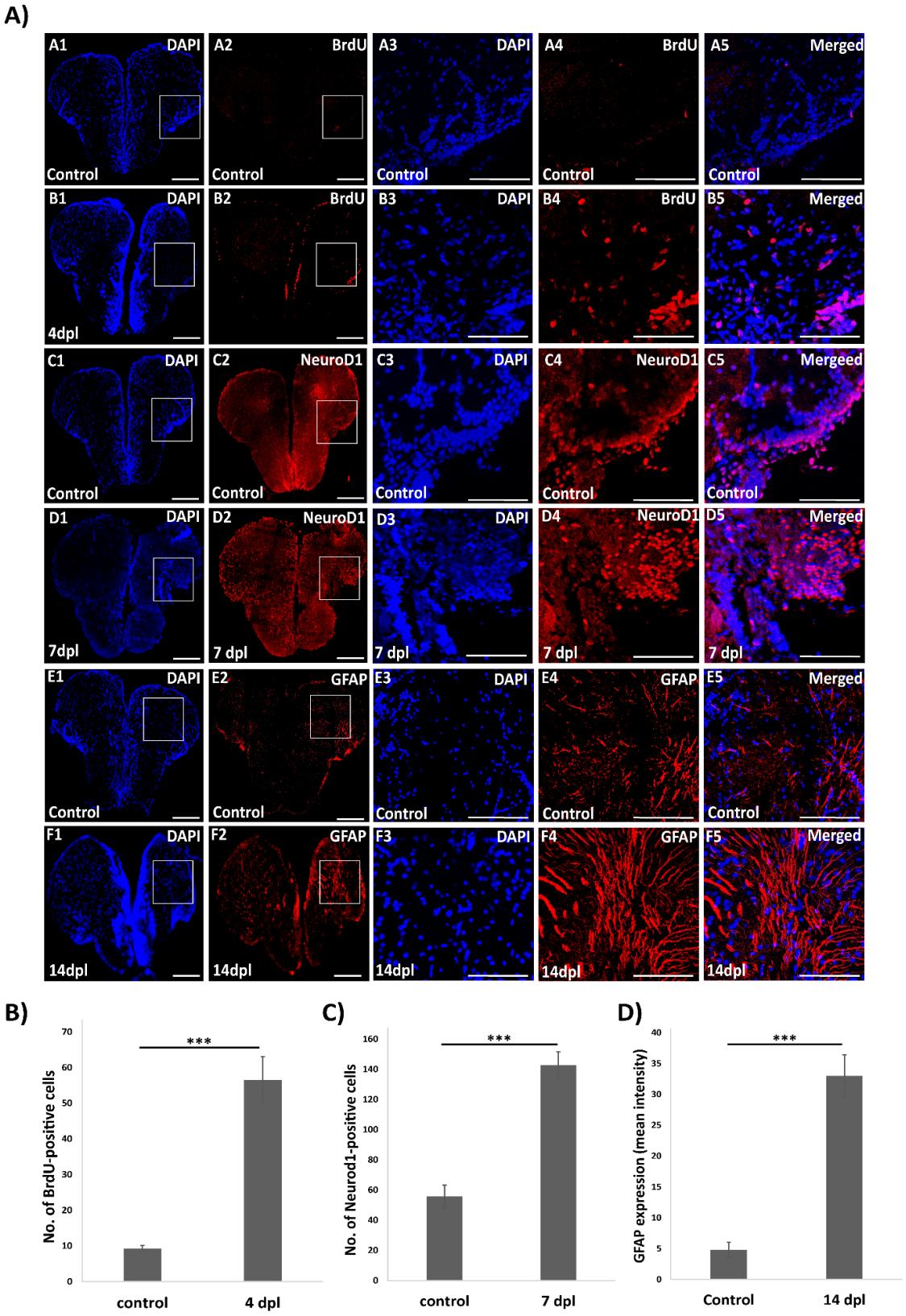

Figure 6.2: Zebrafish brain regeneration upon telencephalic stab-wound injury. **A** Immunostaining of uninjured control zebrafish brain and regenerating zebrafish brain at 4 dpl, 7 dpl and 14 dpl using antibodies against BrdU, NeuroD1, and GFAP. The area marked by square (A1-A2, C1-C2, E1-E2; scale bar = 100 µm) is shown at higher magnification (A3-A5, C3-C5, E3-E5; scale bar = 50 µm). The area marked by square (B1-B2, D1-D2, F1-F2; scale bar = 100 µm) is shown at higher magnification (B3-B5, D3-D5, F3-F5; scale bar = 50 µm).

These images highlight active cell proliferation (BrdU), neuronal differentiation (NeuroD1), and radial glial cell activation (GFAP) in response to injury. **B** Quantification of BrdU-positive cells in the telencephalon of control and regenerating (4 dpl) brains (n=4). **C** Quantification of NeuroD1-positive cells in control and regenerating (7 dpl) brains (n=4). D) Quantification of GFAP expression in control and regenerating (14 dpl) brains (n=4). Data are presented as mean ± SEM. Significance is represented as * for p-value<0.05, ** for p-value<0.01 and *** for p-value<0.001 for all the quantifications. dpl, days post-lesion.

Differentially regulated pathways at all the time points indicated processes involved in cell growth, cell death, signal transduction, metabolic shift and neurogenesis which suggest the changing demands on the biological system with the process of regeneration. In **Additional File 6.2**, a comprehensive list of the processes that are regulated differentially at each time point is provided. Importantly, signaling pathways critical to regeneration including MAPK, FoxO, PPAR and calcium signaling were consistently regulated, showing the importance of the former for an initial regenerative response post-brain injury.

6.4.2.1 Inflammatory response dynamics during regeneration

Acute inflammation is known to play a critical role in zebrafish brain regeneration by promoting progenitor activation, supporting neurogenesis, and facilitating tissue repair (270,281) Consistent with this, several inflammation-associated genes were differentially expressed at 1 dpl, 4 dpl, and 7 dpl. Quantitative RT-PCR validation confirmed the injury-induced upregulation of *hmox1a, il6*, and *il1b*. The increased expression of pro-inflammatory mediators such as *il1b*, involved in leukocyte recruitment, and *il6*, associated with neuroprotection and axonal regeneration, reflects rapid activation of the innate immune response following injury (282–285). Concurrent upregulation of the oxidative stress–responsive gene hmox1a suggests activation of cytoprotective mechanisms to mitigate injury-induced oxidative damage (286). In addition, elevated expression of *pparg*, a gene with established neuroprotective functions and a known regulator of microglial activation, supports its involvement in initiating inflammation-driven regenerative signaling (287).

The decrease in nuclear receptor nr4a1 a negative regulator of the pro-inflammatory signaling pathway could have led to an initial short phase of pro-inflammatory signaling that stimulates regeneration (288). Similarly, decreased expression of *park7* (the function of which is in redox-sensing to control oxidative stress) could have allowed the action of pro-regenerative signals at the onset of recovery (289). Lower *cxcr4b* expression would indicate control over the mobilisation of inflammatory cells (macrophage recruitment to injury sites). In sum, all of these observations indicate that inflammatory responses during zebrafish brain regeneration are under extremely tight regulation characterized by both fast induction and equally fast resolution once regeneration programs are triggered.

6.4.2.2 Early response genes are enriched at 1 dpl

Pathways significantly enriched by 1 dpl at GSEA analysis contained early injury responses such as cell cycle regulation, neurogenesis, gliogenesis, angiogenesis, and cellular differentiation. Genes that upregulated angiogenesis, for example, *angptl4, e2f7,* and *vegfbb* were upregulated significantly at this stage, which was as previously reported of rapidly vascular remodeling following a brain injury in zebrafish (290–292). These findings suggest that angiogenic processes are initiated at very early stages of regeneration.

In contrast, genes associated with gliogenesis, axon growth, and synaptic signaling, including *stat3, ncam3*, and *fosb*, were downregulated, potentially reflecting a transient suppression of differentiation programs immediately following injury (293–295). Additional enrichment of oxidative phosphorylation, ErbB signaling, and FoxO signaling pathways highlights metabolic and stress-responsive adaptations during early regeneration. Processes related to nitrogen metabolism, protein export, and programmed cell death further underscore the activation of repair mechanisms and restructuring of central nervous system architecture. Enrichment of MAPK, PPAR, insulin signaling, and wound healing pathways emphasizes the initiation of coordinated molecular programs driving early tissue repair (**Figure 6.3D–E**).

6.4.2.3 4 dpl corresponds to the onset of the proliferative phase of neurogenesis

By 4 dpl, the transcriptome was dominated by pathways associated with robust cell proliferation and metabolic activity. GSEA identified enrichment of VEGF signaling, the pentose phosphate pathway, and the tricarboxylic acid (TCA) cycle, reflecting increased biosynthetic and energetic demands. Pathways which encompassed processes such as gliogenesis, organ growth, CNS development and cell cycle progression were among the most enriched.

Several key cell cycle regulators were upregulated, for example, *bub1*, to arrest the cell cycle at the spindle checkpoint; (296)), *sass6,* involved in centriole duplication; (297)), and *stil,* involved in dopaminergic neuron proliferation and regeneration; (298)). Additionally, other regulators of proliferation and genome maintenance such as, *spdl1* (299), *rad54b* (300), and *cenpf* (301), were also elevated. Enrichment of pathways related to synapse organization, endothelial cell proliferation, and G1/S phase transition further supports extensive progenitor expansion at this stage (**Figure 6.3F**). Continued signaling *via* the pathways of FoxO, PPAR, MAPK and ErbB indicates their sustained activity at this proliferative phase (**Figure 6.3G**).

6.4.2.4 7 dpl reflects a transition toward tissue remodeling and differentiation

Transcriptional profiles were altered towards those associated with immune function, tissue remodeling, and differentiation by 7 dpl. Pathways such as, inflammatory mediators *cxcl18b* (282), *c6* (302)), and *rig1/ddx58* (303) continued but controlled immune activity during later stages of brain regeneration, were found to be enriched. Furthermore, upregulated expression of *nr1d1* a factor needed to guide excitatory neuronal migration to synaptic network formation, suggested that by day 7, brain regeneration was progressing towards neuronal function (304).

Pathway enrichment such as for calcium signalling, the signalling system important for neural cell proliferation/differentiation, in addition to neuron projection morphogenesis and glial cell development, were observed at this stage (**Figure 6.3H–I**). Along with glial lineage specification pathway, and pathways for CNS development, organ growth, cell signaling all indicated active tissue remodelling in place. Pathway enrichment for pentosephosphate pathway and MAPK pathway indicate sustained regulatory and metabolic support during latter phase of regeneration.

Many processes were consistently enriched throughout all the time points (insulin signaling pathway, PPAR, MAPK etc), signifying that these processes are critical components of the regenerative program in the adult CNS. Ferroptosis-related pathways were significantly enriched during regeneration; however, downregulation of ferroptosis-promoting genes such as *ncoa4* and *tfr1* suggests that suppression of ferroptotic cell death favors neurogenesis (305,306). It has been observed at 4 dpl there was an upregulation of apoptotic pathways and at 7 dpl both ferroptosis/necroptosis pathways suggesting balance between cell survival and death for the repair.

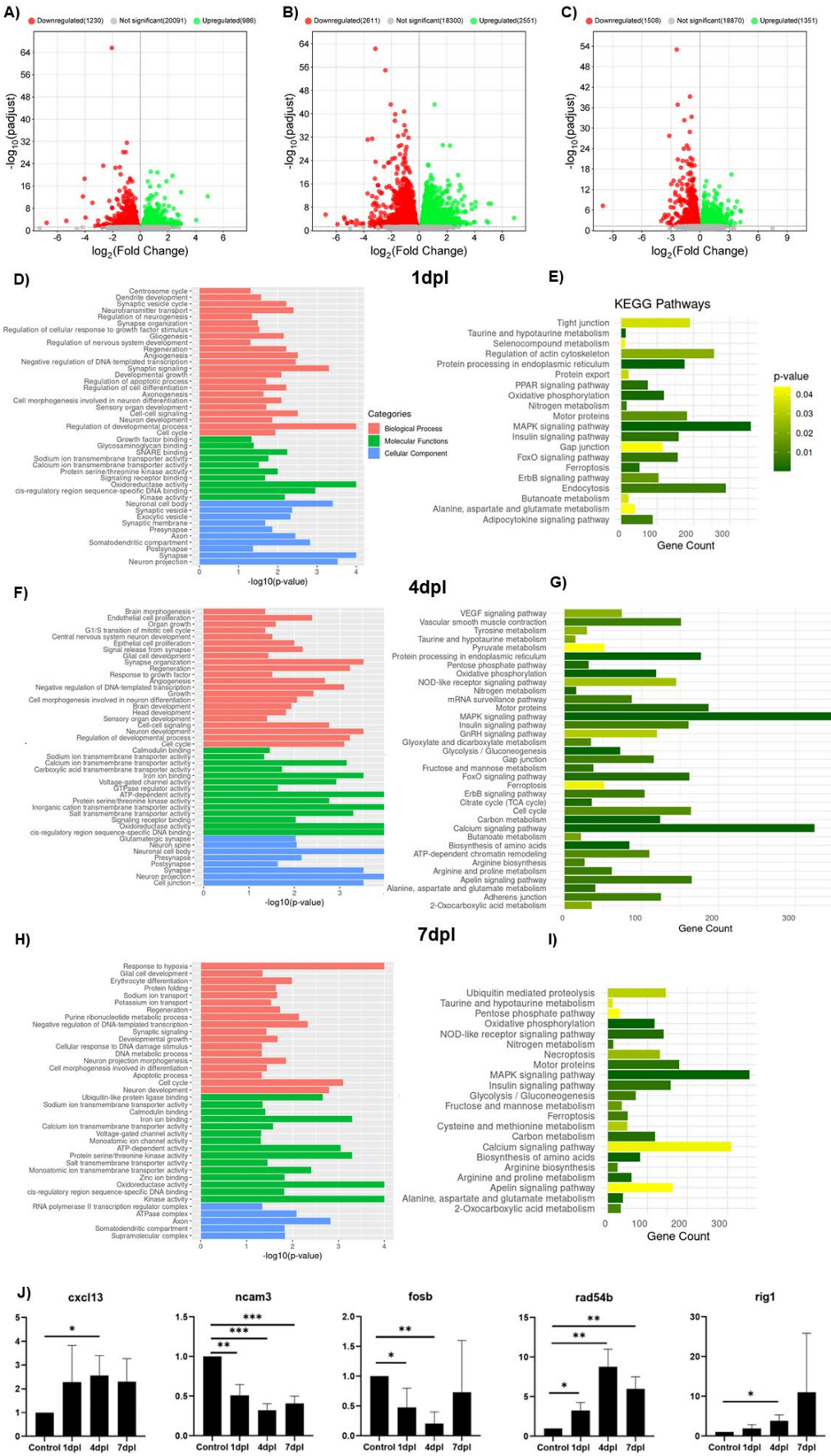
A)
Downregulated(1230)
Not significant(20091)
Upregulated(986)
-log10(padjust)
log2(Fold Change)
B)
Downregulated(2611)
Not significant(18300)
Upregulated(2551)
-log10(padjust)
log2(Fold Change)
C)
Downregulated(1508)
Not significant(18870)
Upregulated(1351)
-log10(padjust)
log2(Fold Change)
D)
1dpl
Centrosome cycle
Dendrite development
Synaptic vesicle cycle
Neurotransmitter transport
Regulation of neurogenesis
Synapse organization
Regulation of cellular response to growth factor stimulus
Gliogenesis
Regulation of nervous system development
Regeneration
Angiogenesis
Negative regulation of DNA-templated transcription
Synaptic signaling
Developmental growth
Regulation of apoptotic process
Regulation of cell differentiation
Axonogenesis
Cell morphogenesis involved in neuron differentiation
Sensory organ development
Cell-cell signaling
Neuron development
Regulation of developmental process
Cell cycle
Growth factor binding
Glycosaminoglycan binding
SNARE binding
Sodium ion transmembrane transporter activity
Calcium ion transmembrane transporter activity
Protein serine/threonine kinase activity
Signaling receptor binding
Oxidoreductase activity
cis-regulatory region sequence-specific DNA binding
Kinase activity
Neuronal cell body
Synaptic vesicle
Exocytic vesicle
Synaptic membrane
Presynapse
Axon
Somatodendritic compartment
Postsynapse
Synapse
Neuron projection
Categories
Biological Process
Molecular Functions
Cellular Component
-log10(p-value)
E)
KEGG Pathways
Tight junction
Taurine and hypotaurine metabolism
Selenocompound metabolism
Regulation of actin cytoskeleton
Protein processing in endoplasmic reticulum
Protein export
PPAR signaling pathway
Oxidative phosphorylation
Nitrogen metabolism
Motor proteins
MAPK signaling pathway
Insulin signaling pathway
Gap junction
FoxO signaling pathway
Ferroptosis
ErbB signaling pathway
Endocytosis
Butanoate metabolism
Alanine, aspartate and glutamate metabolism
Adipocytokine signaling pathway
p-value
Gene Count
F)
4dpl
Brain morphogenesis
Endothelial cell proliferation
Organ growth
G1/S transition of mitotic cell cycle
Central nervous system neuron development
Epithelial cell proliferation
Signal release from synapse
Glial cell development
Synapse organization
Regeneration
Response to growth factor
Angiogenesis
Negative regulation of DNA-templated transcription
Growth
Cell morphogenesis involved in neuron differentiation
Brain development
Head development
Sensory organ development
Cell-cell signaling
Neuron development
Regulation of developmental process
Cell cycle
Calmodulin binding
Sodium ion transmembrane transporter activity
Calcium ion transmembrane transporter activity
Carboxylic acid transmembrane transporter activity
Iron ion binding
Voltage-gated channel activity
GTPase regulator activity
ATP-dependent activity
Protein serine/threonine kinase activity
Inorganic cation transmembrane transporter activity
Salt transmembrane transporter activity
Signaling receptor binding
Oxidoreductase activity
cis-regulatory region sequence-specific DNA binding
Glutamatergic synapse
Neuron spine
Neuronal cell body
Presynapse
Postsynapse
Synapse
Neuron projection
Cell junction
-log10(p-value)
G)
VEGF signaling pathway
Vascular smooth muscle contraction
Tyrosine metabolism
Taurine and hypotaurine metabolism
Pyruvate metabolism
Protein processing in endoplasmic reticulum
Pentose phosphate pathway
Oxidative phosphorylation
NOD-like receptor signaling pathway
Nitrogen metabolism
mRNA surveillance pathway
Motor proteins
MAPK signaling pathway
Insulin signaling pathway
GnRH signaling pathway
Glyoxylate and dicarboxylate metabolism
Glycolysis / Gluconeogenesis
Gap junction
Fructose and mannose metabolism
FoxO signaling pathway
Ferroptosis
ErbB signaling pathway
Citrate cycle (TCA cycle)
Cell cycle
Carbon metabolism
Calcium signaling pathway
Butanoate metabolism
Biosynthesis of amino acids
ATP-dependent chromatin remodeling
Arginine biosynthesis
Arginine and proline metabolism
Apelin signaling pathway
Alanine, aspartate and glutamate metabolism
Adherens junction
2-Oxocarboxylic acid metabolism
Gene Count
H)
7dpl
Response to hypoxia
Glial cell development
Erythrocyte differentiation
Protein folding
Sodium ion transport
Potassium ion transport
Regeneration
Purine ribonucleotide metabolic process
Negative regulation of DNA-templated transcription
Synaptic signaling
Developmental growth
Cellular response to DNA damage stimulus
DNA metabolic process
Neuron projection morphogenesis
Cell morphogenesis involved in differentiation
Apoptotic process
Cell cycle
Neuron development
Ubiquitin-like protein ligase binding
Sodium ion transmembrane transporter activity
Calmodulin binding
Iron ion binding
Calcium ion transmembrane transporter activity
Voltage-gated channel activity
Monoatomic ion channel activity
ATP-dependent activity
Protein serine/threonine kinase activity
Salt transmembrane transporter activity
Monoatomic ion transmembrane transporter activity
Zinc ion binding
Oxidoreductase activity
cis-regulatory region sequence-specific DNA binding
Kinase activity
RNA polymerase II transcription regulator complex
ATPase complex
Axon
Somatodendritic compartment
Supramolecular complex
-log10(p-value)
I)
Ubiquitin mediated proteolysis
Taurine and hypotaurine metabolism
Pentose phosphate pathway
Oxidative phosphorylation
NOD-like receptor signaling pathway
Nitrogen metabolism
Necroptosis
Motor proteins
MAPK signaling pathway
Insulin signaling pathway
Glycolysis / Gluconeogenesis
Fructose and mannose metabolism
Ferroptosis
Cysteine and methionine metabolism
Carbon metabolism
Calcium signaling pathway
Biosynthesis of amino acids
Arginine biosynthesis
Arginine and proline metabolism
Apelin signaling pathway
Alanine, aspartate and glutamate metabolism
2-Oxocarboxylic acid metabolism
Gene Count
J)
cxcl13
ncam3
fosb
rad54b
rig1
Control 1dpl 4dpl 7dpl

Figure 6.3: Transcriptome profiling and functional annotation of the telencephalon during 1 dpl, 4 dpl, 7 dpl stages of zebrafish brain regeneration. **A-C** Volcano plots of differentially expressed genes (DEGs) comparing injured samples at **A** 1 dpl, **B** 4 dpl, and **C** 7 dpl with uninjured controls. The x-axis represents Log_2(fold-change), and the y-axis represents $-Log_{10}$(p-adjusted value). Vertical dashed lines mark the fold-change thresholds (≥1 for upregulated, ≤−1 for downregulated), and the horizontal dashed line marks the significance cutoff (p-adjusted < 0.05). Significant upregulated genes are shown in green (upper-right), and downregulated genes in red (upper-left). At 1 dpl, 986 genes were upregulated, and 1230 were downregulated. At 4 dpl, 2551 genes were upregulated, and 2611 were downregulated. At 7 dpl, 1351 genes were upregulated, and 1508 were downregulated. **D-I** Gene Set Enrichment Analysis (GSEA)-based functional annotations for GO terms and KEGG pathways at **D–E** 1 dpl, **F–G** 4 dpl, and **H–I** 7 dpl. At 1 dpl **D–E,** enriched processes include cell cycle regulation and protein processing; at 4 dpl **F–G,** angiogenesis, vascular remodeling, and immune signaling are prominent; and at 7 dpl **H–I,** pathways related to neurogenesis, synaptic signaling, and metabolic regulation dominate**. J** Validation of RNA-seq data using qRT-PCR for selected genes in uninjured control brains, 1dpl, 4 dpl and 7 dpl regenerating brains (n=3; pooled 5 for each sample per time point). Significance is represented as * for p-value<0.05, ** for p-value<0.01 and *** for p-value<0.001 for all the quantifications. The observed qPCR trends corroborate the transcriptomic findings, highlighting the reliability of the differential expression analysis. Note: Full lists of DEGs and enriched pathways are provided in Additional Files 6.1 and 6.2, respectively. Scale and axes in the volcano plots are consistent across panels for comparative analysis. dpl: days post-lesion.

Validating RNA sequencing data using qPCR showed downregulation of *ncam3* and *fosb*, as well as upregulation of *rad54b* and *rig1*, which aligned with the expression profile measured by RNA sequencing, thus confirming the concordance between transcriptomics and targeted expression analysis **(Figure 6.3J).** From these findings emerges a broad outline of the zebrafish brain transcriptional programs governing regeneration including separate transcriptomes for the response to injury (1 dpl), proliferation (4 dpl), and tissue remodeling (7 dpl), as well as numerous common upstream pathways which are used throughout the regenerative process.

6.4.3 Weighted co-expression networks

To supplement timepoint-specific differential expression and GO enrichment analysis, weighted gene coexpression network analysis (WGCNA) was applied to find highly interconnected gene co-expression modules across 1,4,7days post-lesion (dpl). Using a dynamic 'cutree' approach with a tree-cutting threshold of 0.4, a total of 20 co-expression modules (see **Figure 6.4 A–B; Additional File 6.3**) were detected. The cyan module was the largest cluster (6,363 genes), and the brown4 module was the smallest cluster (150 genes). The degree of connectivity of genes in each module was found to be significantly high intra-modularly.

Module–trait correlation analysis revealed clear temporal associations between specific modules and distinct stages of regeneration. Modules including greenyellow, cornflowerblue, lightskyblue4, blue1, and coral3 showed strong positive correlations with the early injury phase at 1 dpl. In contrast, midnightblue, blueviolet, deeppink1, cyan, and coral4 modules were most strongly associated with the proliferative phase at 4 dpl. Modules such as lightblue4, deeppink,

honeydew1, blue4, and chocolate3 exhibited significant correlations with the remodeling phase at 7 dpl.

Function annotation of the 20 modules with Gene Ontology and KEGG pathway enrichment analysis, provided stage-specific processes (**Figure 6.4C–D; Additional File 6.4**). The most remarkable feature seen at 1dpl was that cornflowerblue and greenyellow modules showed overlaps with inflammatory response and transcription pathways. Meanwhile, the blue1 module at this stage has a striking overlap with Wnt signal pathways and extracellular matrix organization. At the stage of 4dpl, the cyan module which associated strongly with this stage orchestrates a wealth of processes, including synaptic re-organization, cell division and survival signaling pathways like MAPK and mTOR. By 7dpl, the honeydew1 and lightblue4 modules overlap strongly with neurogenic processes and imminure pathways, such as TLR signal.

This stage dependence was strongly highlighted when we performed KEGG pathway analysis, which showed strong enrichment of re-programming of metabolic pathways at the injury associated modules of 1dpl, supremacy of the signaling pathways of proliferation and cell survival at the 4dpl associated modules, and a rise in neuro-immune interaction pathways by 7dpl. Collectively, these findings highlight dynamic, coordinated transcriptional reprogramming across successive stages of zebrafish brain regeneration and are consistent with previously reported molecular transitions during CNS repair.

6.4.4 Identification of key molecular players with high connectivity across stages of regeneration

Regeneration is a highly coordinated process that relies on the activation of interconnected molecular networks. Within these networks, a subset of genes with high connectivity, commonly referred to as hub genes often function as critical regulatory nodes that integrate signals from multiple pathways to control cellular behaviours such as proliferation,

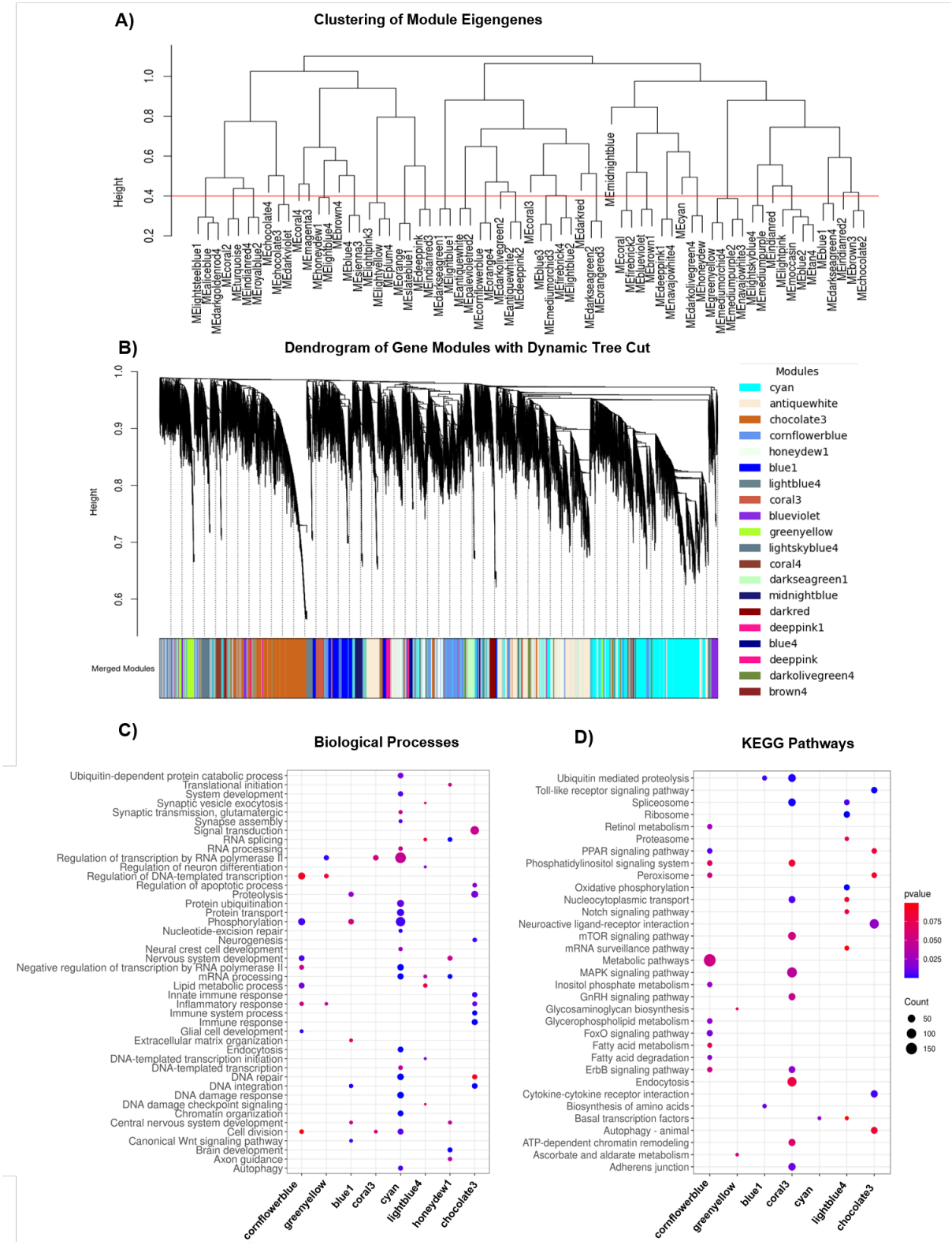

Figure 6.4: A Clustering of module eigengenes. A cut-line (0.4) was selected for the module dendrogram, and some modules were merged according to the dissimilarity (<0.4) of estimated module eigengenes. **B** A cluster dendrogram that presents 20 gene co-expression merged modules was built based on the dissimilarity of the topological overlap. The subsequent analysis is conducted in accordance with merged modules. **C** Biological Processes and **D** KEGG pathways enrichment of the highly correlated module.

migration, differentiation, and tissue remodeling. Identifying these hub genes provides mechanistic insight into the regulatory architecture underlying regeneration and highlights potential targets for functional validation.

To identify key molecular regulators operating at different stages of zebrafish brain regeneration, protein–protein interaction (PPI) network analyses were performed for differentially expressed genes (DEGs) identified at 1,4 and 7days post-lesion (dpl). Stage-specific DEG lists were converted into PPI networks using the STRING database and subsequently imported into Cytoscape for network visualization and analysis. Hub genes were identified using the degree centrality algorithm implemented in the CytoHubba plugin, which ranks genes based on the number of direct interactions within the network.

At 1 dpl, hub genes were predominantly associated with DNA replication and early cell cycle regulation. These included *ttk* (mitotic checkpoint kinase), *bub1* (chromosome alignment and segregation), *mcm4* (DNA replication licensing), *prc1b* (cytokinesis), *aspm* (mitotic spindle organization and neural progenitor proliferation), *dlgap5* (cell cycle progression), *plk1* (mitotic entry and progression), *aurka* (centrosome maturation and spindle assembly), and *cdc6* (initiation of DNA replication). The prominence of these genes indicates rapid activation of cell cycle entry and genomic maintenance mechanisms immediately following injury.

At 4 days post-laying, the gene hub landscape indicates maximum proliferative activity and adaptation to metabolic needs. The following genes constitute major hub *cdca8* (chromosomal passenger complex), *plk1, cdc20* (activator of the anaphase-promoting complex), *exo1* (DNA repair and recombination), *ttk, bub1, aspm, gapdhs* (glycolysis and metabolic regulation), and *ndufab1a* (mitochondrial energy metabolism). Co-enrichment of genes involved in cell division and those metabolically active in the above dataset hints at the energy intensive and biosynthetically active proliferating progenitor cell population seen at day 4.

Hubs by 7 dpl signal the emergence of late proliferative genes, immune modulatory effects, tissue remodeling processes. Prominent hubs included *aspm, nuf2* (kinetochore function and chromosome segregation), *aurka, plk4* (centriole duplication), *prc1b, mcm4, fancm* (Fanconi anemia DNA repair pathway), *usp18* (immune regulation *via* deubiquitination), and *dhx58*

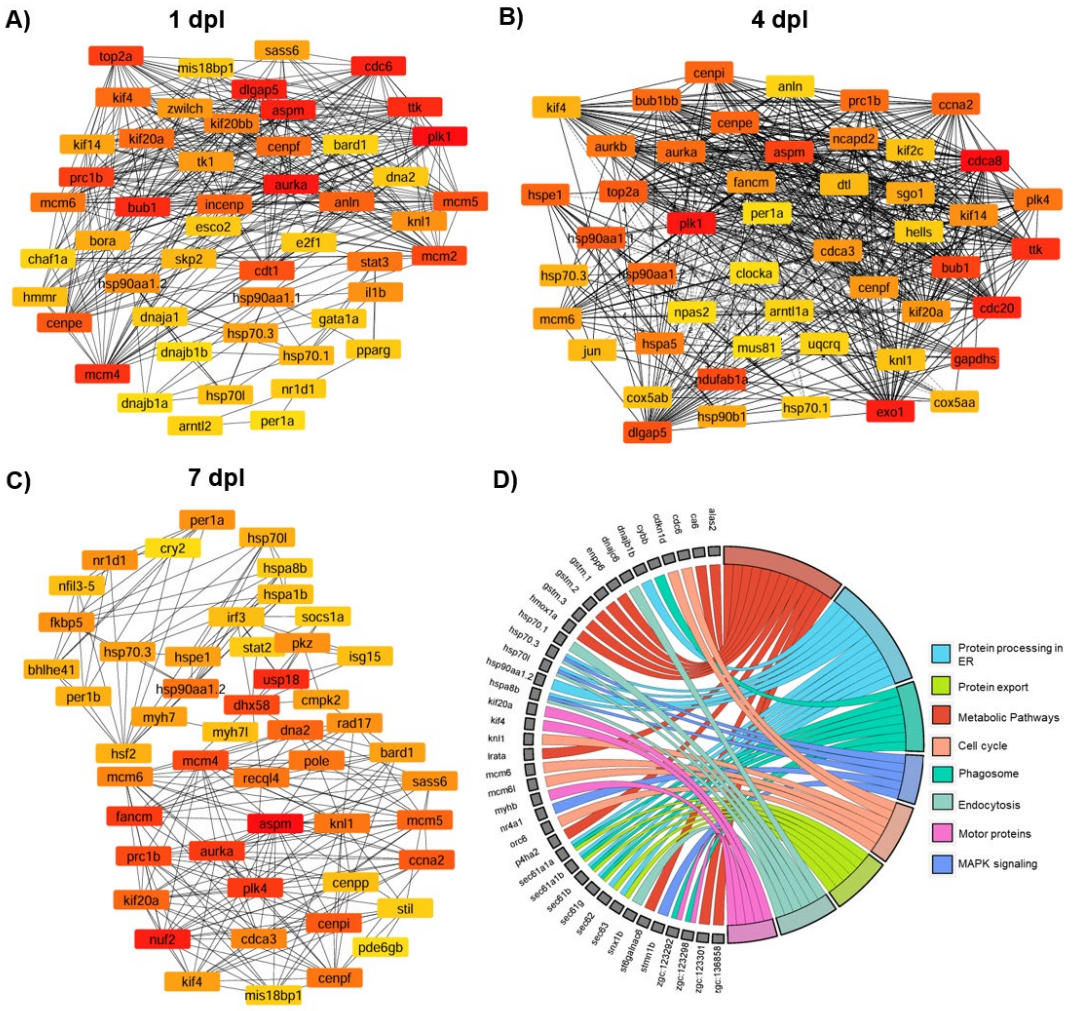

Figure 6.5: Identification and functional enrichment of hub genes: The hub genes were identified using the model-Degree for **A** Day1 **B** Day4 and **C** Day7 with the Cytoscape plug-in CytoHubba. The darker the color of the node, the more critical the gene, indicating the gene is more important in the network. **D** Chord plot shows the common hub genes across the three time points and their associated functions. The picture is illustrated using SR plot. dpl: days post-lesion

(innate antiviral and inflammatory responses). These findings, in a tightly regulated interplay between continued proliferative activity, genomic stability, and the immune response, provide a snapshot of what happens during the renovation portion of the repair process (**Figures 6.5A–C**).

Chord diagram analysis (**Figure 6.5D**) revealed that hub genes shared across all time points were enriched in pathways related to protein processing in the endoplasmic reticulum, protein export, metabolic pathways, cell cycle regulation, phagosome formation, endocytosis, motor proteins, and MAPK signaling. These signalling pathways play major roles in cellular

communication, immune response, cell proliferation and cell survival thereby indicating they are critically important in sustaining a regenerative ability throughout the process.

For a broader view of functional interactions between regenerating genes, DEGs from all the three time points are pooled and subjected to IPA-based PPI and functional interaction networks (see **figure 6.7**) using ClueGO and CluePedia plugins in cytoscape. This analysis revealed tightly interconnected networks involving cell cycle regulation, neuroactive ligand–receptor interactions, cytokine–cytokine receptor signaling, calcium signaling, PPAR signaling, MAPK signaling, cell adhesion molecules (CAMs), apoptosis, phagosome formation, and ferroptosis. The enrichment of these pathways highlights their collective role in maintaining cellular homeostasis and enabling effective regeneration. Calcium and PPAR signaling were seen to be critical adaptive metabolic change inducers enabling cells to respond to stimuli, and the presence of cell proliferation and apoptosis regulating pathways such as MAPK and apoptosis indicated successful maintenance of homeostasis during regeneration.

In an attempt to clarify the temporal dynamics of these network connections, gene expression patterns for core signaling pathways were compared at 1, 4 and 7 dpl (**Figure 6.6**). Within the cell cycle pathway, genes involved in DNA replication initiation and S-phase entry such as *mcm2, mcm4, e2f1, skp2, esco2, cdc6, cdc14aa*, and *cdt1* were strongly expressed at 1 dpl, indicating rapid engagement of repair-associated proliferation. At 4 dpl, genes associated with mitosis and spindle assembly (*aurkb, cdc20, dbf4, bub1bb, sgo1, mtbp*) were predominantly upregulated, consistent with active cell division. By 7 dpl, expression of *mad2l2* and *tfdp1b* suggested a shift toward mitotic checkpoint control and transcriptional regulation.

The genes *ttk, bub1* and *plk1*, were present at both day 1 and day 4, indicating a persistent role of these genes in checkpoints, while *mcm4* and *mcm5* established links from early replication to later cell cycle processes. Persistent expression of *knl1* and *mcm6* across all time points indicated stable involvement in chromosome alignment and replication, whereas *cdkn1d* remained consistently low, suggesting limited inhibitory regulation of proliferation during regeneration.

MAPK signaling showed maximal activation at 4 dpl, with elevated expression of *cacna1sb, rps6kal, rasgrp2, cacna2d4a, cacna1ab, cacna1fa*, and *erbb3b*. These genes collectively regulate calcium influx, RAS/MAPK activation, and growth factor signaling. Early regenerative signaling was supported by strong fgf17 expression at 1 dpl, while inflammatory mediator il1b was highly expressed at both 1 and 4 dpl, linking inflammation to MAPK-driven

repair. Several stress-response genes (nr4a1, hsp70 family members) remained low across time points, suggesting limited involvement during later recovery phases.

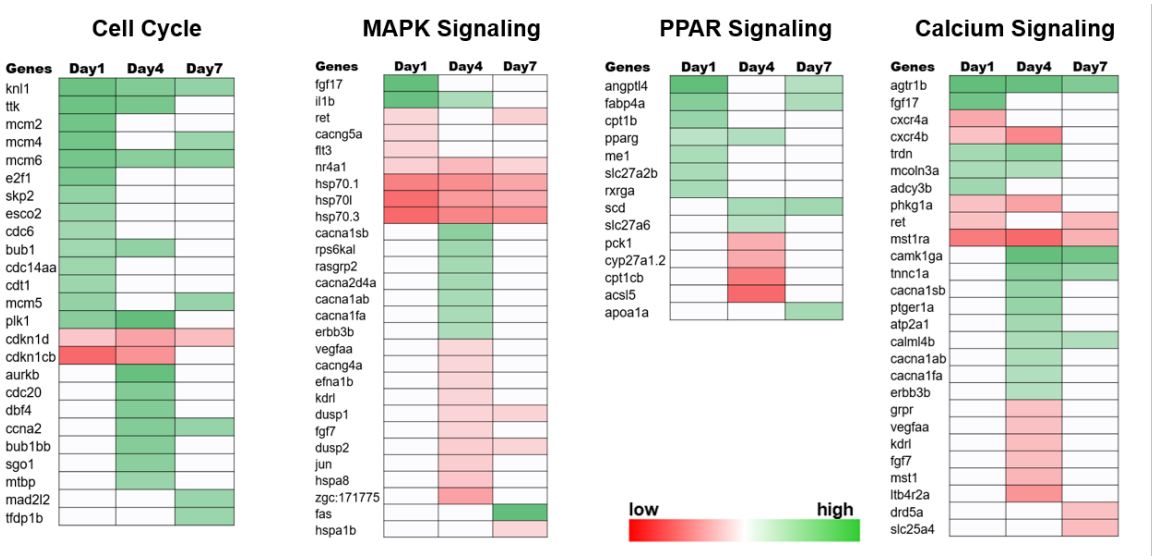

Figure 6.6: The color map shows the day wise expression of the genes in the pathways Cell cycle, MAPK signaling pathway, PPAR signaling pathway, and calcium signaling pathway. The red the color the lower the expression, the greener the color higher the expression.

PPAR signaling exhibited pronounced temporal regulation, reflecting changing metabolic demands during regeneration. At 1 dpl, lipid metabolism related genes (*cpt1b, me1, slc27a2b, rxrga*) were strongly expressed, indicating activation of fatty acid transport and oxidation. Pparg expression at 1 and 4 dpl highlighted its role in metabolic control during early and mid-regeneration. At later stages, *angptl4* and *fabp4a* were upregulated at both 1 and 7 dpl, while *scd* expression at 4 and 7 dpl suggested sustained lipid remodeling. Downregulation of genes such as *pck1, cyp27a1.2, cpt1cb*, and *acsl5* at 4 dpl reflected a metabolic shift accompanying peak proliferation.

Calcium signaling seemed to be active at 4 dpl, with elevated expression of *cacna1sb, cacna1ab, cacna1fa, ptger1a, atp2a1*, and *erbb3b*, which are involved in voltage-, store-operated or receptor-mediated calcium influxes and subsequent intracellular signaling pathways. The expression of calcium/calmodulin-dependent proteins (*camk1ga, tnnc1a, calml4b*) at 4 and 7 dpl was consistent with ongoing cell differentiation/remodeling processes. Suppression of *agtr1b* at all timepoints, along with consistent upregulation of mst1ra, further indicated a regulated signal.

In summary, these analyses show a dynamic molecular control system that coordinates different phases of the post-injury regenerative response of the zebrafish brain. It seems that these phases

can be controlled by a set of overlapping, but distinct network, including key genes (such as those regulating cell cycle) and signal pathways like MAPK, PPAR, and calcium signaling, that act at particular points in time. As with the previously mentioned studies, the tightly regulated sequence of signal activation and inactivation, reflects the high degree of specificity that must exist in any effective post-injury brain repair system.

6.4.5 Activation dynamics of proliferative genes across distinct regenerative phases

The use of GSEA-based GO and KEGG pathway analyses enabled us to describe the time-course of activity within molecular processes, components, and functions of zebrafish brain regeneration. However, such a systems-level view only highlighted stage-specific enrichments at the pathway level without indicating gene-level regulation governing these dynamic transitions. Analysis focusing on temporal gene expression of several key proliferative and regeneration-associated genes clarified how general signaling pathways convert into specific transcriptional changes capable of causing cellular processes like neurogenesis, axonal growth, and neuronal differentiation. Gene-specific enrichment analysis demonstrated the persistence of various processes across all time points, (glial proliferation, synaptic signaling, organization of synapses, neuron-axon and dendritic development, and neuron axon morphogenesis; (**Figure 6.8A**). These findings underscore the continuous and coordinated remodeling of neural architecture throughout regeneration. Additional enrichment of axon guidance receptor activity and neuropeptide hormone activity, along with cellular components such as neuron projections, somatodendritic compartments, and neuronal cell bodies, further highlights the molecular complexity underlying regenerative competence.

Although certain processes such as dendritic morphogenesis were preferentially enriched during later differentiation stages, regeneration-associated terms including tissue regeneration and developmental growth were evident throughout the time course. Notably, insulin-like growth factors (IGF-I and IGF-II), well-established regulators of brain development, neuronal growth, and cell survival (307,308), were prominently enriched during the differentiation phase.

Given the demand for rapid cellular expansion following injury, activation of cell cycle–related programs was expected across regenerative stages. To investigate this, we examined the temporal expression dynamics of key cell cycle regulatory genes (**Figure 6.8B**). Aurora kinase A (*aurka*) and Aurora kinase B (*aurkb*), which play critical roles in spindle assembly,

centrosome maturation, and axonal outgrowth, exhibited pronounced upregulation at 4 dpl (309–311), coinciding with peak proliferative activity. In contrast, *rgcc*, a regulator of neural stem cell fate decisions (312), showed maximal expression at 7 dpl, suggesting a role in facilitating the transition from proliferation to neuronal differentiation. The tumor suppressor gene *wdr76*, known to limit excessive proliferation through RAS degradation (313,314), peaked at 4 dpl and declined by 7 dpl, indicating its involvement in fine-tuning proliferative control during regeneration.



Figure 6.7: Network representation of DEG's combined across all the time points. The cytoscape ClueGO and Cluepedia plugin was used to identify enriched KEGG pathways amongst all statistically significant proteins across all the time points. Nodes containing proteins from related KEGG terms are colored the same.

Consistently, several additional cell cycle regulators including *dsn1, chaf1a, stil, sass6, spdl1*, and *wdhd1* were selectively enriched at 4 dpl, supporting their contribution to the rapid cell division characteristic of the proliferative phase (297,299) In parallel, sustained expression of Minichromosome Maintenance (MCM) complex components, essential for DNA replication

licensing (315), was observed across all time points. Such prolonged upregulation of *mcm2, mcm4*, and *mcm6* emphasizes their indispensable function to sustain proliferative ability as part of continuous tissue repair and regeneration.

These gene-specific results dovetailed perfectly with the broad pathway- specific findings, outlining a highly ordered temporal program governing proliferation, differentiation and remodelling in regeneration. The stage-specific up-regulation of proliferative controls highlights how precisely regenerative events are controlled and has created a useful paradigm linking transcription with success in neurogenesis and neural repair in the regenerating zebrafish brain.

6.4.6 p38α MAPK is upregulated during brain regeneration in Zebrafish

A comparative pathway enrichment analysis was carried out across three stages of regeneration (one, four and seven days postlesion, dpl) to elucidate the molecular mechanisms driving zebrafish brain regeneration. These analysis results provide an insight into how the regenerative mechanisms are regulated over time with separate signature patterns observed at each of the stages analysed. In particular, analysis of 1 dpl data revealed significant enrichment of pathways including PPAR signalling and adipocytokine signaling which has indicated an early inflammation and metabolic response to the damage respectively. At 4 dpl, corresponding to the proliferative phase characterized by extensive cellular reorganization and transcriptional regulation, pathways including VEGF signaling, polycomb repressive complex regulation, mRNA surveillance, and ATP-dependent chromatin remodeling were selectively enriched. By 7 dpl, pathways associated with tissue remodeling and regulated cell death, including necroptosis and ubiquitin-mediated proteolysis, were preferentially enriched, consistent with differentiation-associated processes.

Several pathways were either consistently enriched across multiple stages or shared between adjacent time points, indicating broader roles in brain regeneration. FoxO and ErbB signaling pathways were enriched at both 1 and 4 dpl, consistent with their involvement in early stress responses and proliferative signaling. During the transition from 4 to 7 dpl, enrichment of apelin signaling, mitophagy, autophagy, NOD-like receptor signaling, and calcium signaling pathways was observed, underscoring their importance in cellular maintenance, immune modulation, and differentiation during later regenerative phases.

Notably, a subset of pathways was consistently enriched across all three time points, including ferroptosis, oxidative phosphorylation, insulin signaling, MAPK signaling, and alanine,

aspartate, and glutamate metabolism (**Figure 6.8C**). MAPK signaling pathway was notably up-regulated, indicating the crucial function of signaling in orchestrating cellular responses during zebrafish brain regeneration; both temporal considerations and the persistent requirement of MAPK signaling for ongoing neurogenesis are thereby highlighted.

In light of these results, a further analysis into the function of the mitogen-activated protein kinase/extracellular signal-regulated kinase (ERK/MAPK) signal transduction pathway in zebrafish brain regeneration was performed. ERK/MAPK signal transduction pathway controls cellular processes including survival, proliferation, and differentiation by influencing gene expression and many metabolic signal transduction cascades. Previous studies have demonstrated the essential role of ERK/MAPK signaling during neurodevelopment, particularly as neural progenitor cells derived from the embryonic mesoderm progress through successive stages of neural differentiation (315).

Across all three regenerative stages, MAPK signaling was consistently enriched as both a KEGG pathway and a molecular process (**Figure 6.8A, C**), indicating a broad regulatory role in restorative neurogenesis. Detailed analysis of the MAPK cascade revealed dynamic regulation of several key genes. Upregulated genes included *rps6kal, cacna1ab, erbb3b, rasgrp2, ins, fgf17, cacna2d4a, fas*, and *il1b*, all of which contribute to cellular communication, growth factor signaling, inflammatory responses, and regeneration. Specifically, calcium voltage-gated channel subunit alpha1 B (cacna1ab) and calcium channel subunit alpha2delta (cacna2d4a) are integral to calcium signaling, which is essential for neurogenesis and synaptic function during repair (316,317). Rps6kal plays a role in mRNA translation and cell growth (318), while erbb3b and rasgrp2 facilitate vascular development and growth factor–mediated proliferation and differentiation (319–321). The growth factors fgf17 and ins support neuronal survival and growth and have been shown to be critical for zebrafish brain regeneration (322,323). Additionally, fas and il1b are involved in inflammatory and immune responses, which are essential during the early stages of wound healing (324,325).

Conversely, several MAPK-associated genes including *nr4a1, vegfaa, kdr, kdrl, hsp70, ret, flt3, dusp1*, and *dusp2* were downregulated across the regenerative time course, indicating shifts in signaling priorities. Dual-specificity phosphatases *dusp1* and *dusp2*, which negatively regulate MAPK signaling through dephosphorylation of active MAPKs (326,327), exhibited reduced expression, suggesting sustained MAPK pathway activation during regeneration. Decreased expression of nr4a1, a nuclear receptor involved in stress responses and apoptosis (328),

reflects suppression of apoptotic signaling in favor of regeneration. Angiogenesis-related genes *vegfaa* and its receptors *kdr* and *kdrl*, which are critical during early regeneration but diminish as vascular remodeling stabilizes (329,330), also showed reduced expression at later stages. Similarly, reduced expression of *hsp70*, associated with stress responses and protein stability (331), suggests attenuation of cellular stress as regeneration progresses. Downregulation of *ret* and *flt3*, both involved in neuronal development and signaling (332), further indicates refinement of proliferative and differentiation cues during regeneration. Collectively, these expression patterns illustrate the tightly regulated orchestration of MAPK signaling necessary for effective brain regeneration (**Figure 6.8D**) (333,334).

To further delineate MAPK pathway involvement, MAPK14a (p38α MAPK), a well-characterized isoform of the p38 MAPK family implicated in neural stem cell migration, proliferation, differentiation, and cell death, was examined. MAPK14a exhibited significant phosphorylation at 1 and 4 dpl, consistent with early wound repair and proliferative phases of regeneration. By 14 dpl, phosphorylation levels returned to baseline (**Figure 6.8E, G**), indicating resolution of pathway activation.

In addition, increased activation of downstream p38α MAPK substrates was observed during regeneration (335). Phosphorylated MAPKAPK2 (MK2) levels were elevated at 1, 4, and 7 dpl relative to uninjured controls and declined by 14 dpl (**Figure 6.8F, H**). Activated MK2 is known to phosphorylate heat shock protein 27 (HSP27), thereby promoting its activity (336). Consistent with this mechanism, phosphorylated HSP27 levels increased significantly at 1 and 4 dpl and remained elevated at 7 dpl compared to controls (**Figure 6.8F, J**). Furthermore, p38α MAPK-dependent activation of transcription factors was evident, including c-Jun, a key component of the AP-1 transcriptional complex that regulates gene expression, cell survival, and proliferation (337,338). Immunoblot analysis showed elevated c-Jun levels at 1 dpl, reduced levels at 4 dpl, and re-elevation at 7 dpl relative to uninjured brains (**Figure 6.8F, I**), consistent with transcriptomic expression patterns. The data show sustained activation, and highly regulated temporal pattern of the MAPK signaling cascade during brain regeneration in zebrafish and identify p38α MAPK as an essential regulator of wound response and proliferation during initial phases of regeneration.

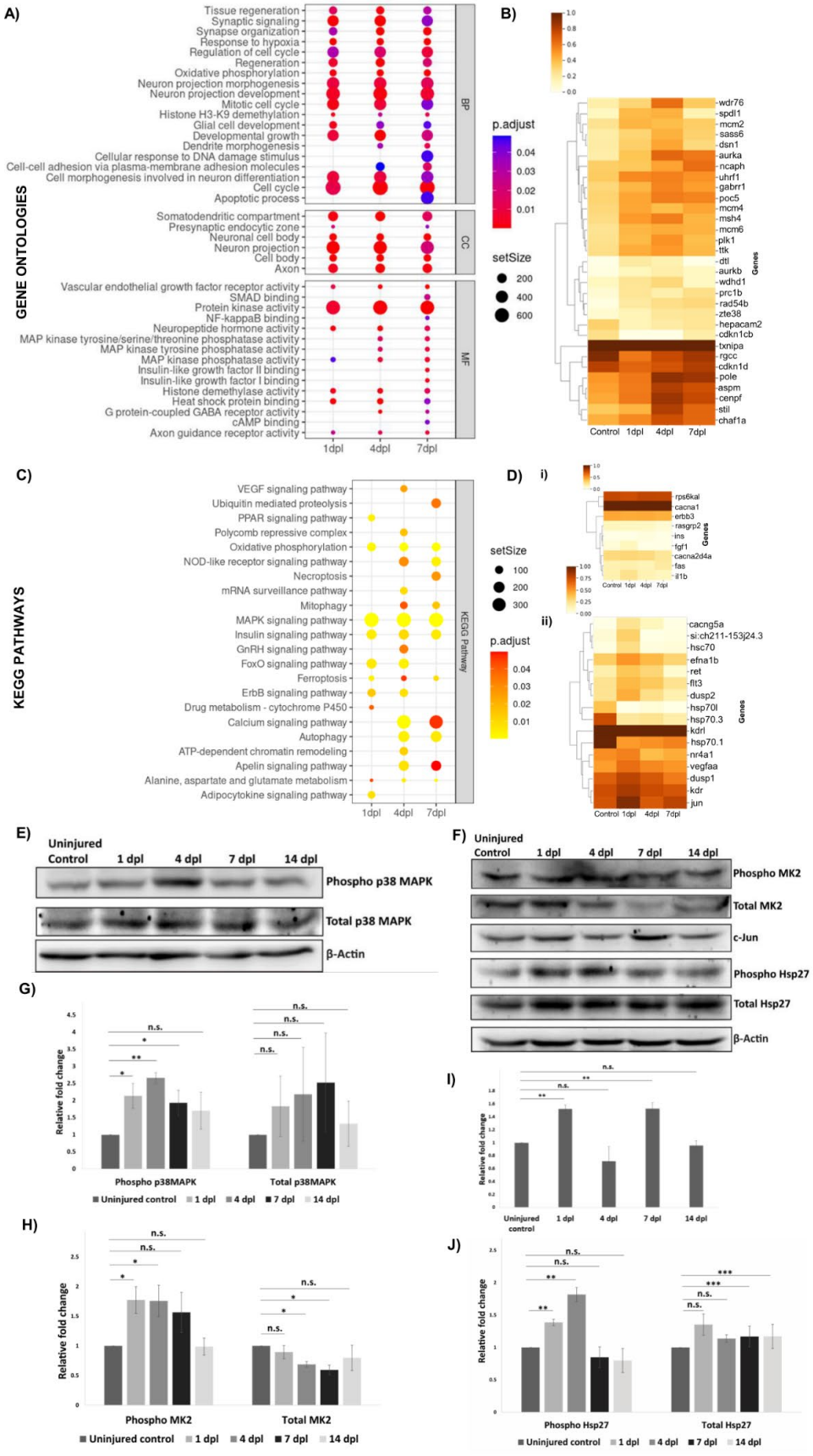

Figure 6.8: Transcriptomic and Pathway Insights into Zebrafish Brain Regeneration. **A** Gene Ontology (GO) enrichment analysis of biological processes (BP), molecular functions (MF), and cellular components (CC) across

the three regenerative stages (1, 4, and 7 days post-lesion; dpl). The vertical axis lists the enriched GO terms, while the horizontal bars represent the gene ratios associated with each term. The color depth indicates an adjusted p-value, while the circle size relates to the gene count contributing to each term**. B** Heatmap showing the expression levels of key cell cycle-related genes at 1, 4, and 7 dpl. Stage-specific activation patterns, such as peak expression of proliferation markers (aurka, aurkb, wdr76, etc.) at 4 dpl and sustained expression of MCM proteins, reflect dynamic cellular processes during brain regeneration. **C** Overview of KEGG pathways enriched across the three regeneration stages. The visualization underscores the pathways driving key biological processes during zebrafish brain regeneration. **D** Heatmaps showing the expression of genes related to the MAPK signaling pathway: i) upregulated genes and ii) downregulated genes, across the three stages, emphasizing the dynamic regulation of this critical pathway. **E** Immunoblot analysis showing the levels of phosphorylated (active) and total p38α MAPK protein during zebrafish brain regeneration. **F** Immunoblot analysis showing the levels of phosphorylated (active) and total MK2 and Hsp27 along with c-Jun protein during zebrafish brain regeneration. β-actin was used as the loading control for both E-F panels. **G** Quantification of Phosphorylated (active) and total p38α MAPK levels during regeneration is shown as a bar graph (n=3). **H** Quantification of Phosphorylated (active) and total MK2 levels during regeneration is shown as a bar graph (n=3). **I** Quantification of c-Jun levels during regeneration is shown as a bar graph (n=3). **J** Quantification of Phosphorylated (active) and total HSP27 levels during regeneration is shown as a bar graph (n=3). Significance is represented as n.s. for p-value>0.05, * for p-value<0.05, ** for p-value<0.01 and *** for p-value<0.00. dpl: days post-lesion.

6.4.7 Inhibition of MAPK14a leads to impairment of the progenitor response

Following the identification of MAPK14a (p38α MAPK) activation during zebrafish brain regeneration and its potential relevance to regeneration, pharmacological inhibition experiments were performed. The spatiotemporal roles of inhibited MAPK14a at the telencephalic injury site were examined through administration of BIRB796, a potent selective inhibitor of p38 MAPKs (**Figure 6.9A**). The efficacy of BIRB796 in inhibiting MAPK14a activity was confirmed by immunoblot analysis, which demonstrated a dose-dependent reduction in phosphorylated p38α MAPK levels (**Figure 6.9B, C**). Consistent with this inhibition, levels of downstream p38α MAPK substrates including phosphorylated MK2, phosphorylated Hsp27, and c-Jun were significantly reduced in the regenerating brain by 4 dpl following BIRB796 treatment (**Figure 6.9D, H**).

To analyze the effect of MAPK14a inhibition on proliferation, we used PCNA immunofluorescence. Compared to DMSO-treated controls, BIRB796-treated zebrafish exhibited a marked reduction in PCNA-positive cells within the injured telencephalon, indicating significantly impaired proliferative activity (**Figure 6.9I**, panels A2–A2′; quantified in **Figure 6.9J**). In addition, a notable decrease in GFAP-positive and S100B-positive cells was observed in the damaged hemisphere following MAPK14a inhibition (**Figure 6.9I**, panels C2–C2′ and D2–D2′; quantified in **Figure 6.9L, M**), suggesting compromised activation of glial progenitor populations. Together, these findings indicate that MAPK14a activity is required for

glial progenitor cell activation and proliferation during regeneration, and that its inhibition disrupts this essential response, leading to incomplete tissue repair.

Consistent with impaired progenitor activation, neuronal recovery was also adversely affected by MAPK14a inhibition. Immunostaining for the neuronal marker HuC/D revealed a reduced neuronal population in the injured hemisphere of BIRB796-treated fish compared to controls (**Figure 6.9I**, panels B2–B2′; quantified in **Figure 6.9K**). This reduction indicates that inhibition of MAPK14a significantly compromises neuronal replacement and limits the establishment of an effective regenerative response in the zebrafish brain.

The effect of inhibited MAPK14a upon oligodendrocyte precursors was further determined by the use of anti-Olig2 immunostaining, a marker of oligodendrocyte precursor cells. A pronounced decrease in Olig2-positive cells was detected in the injured hemisphere following MAPK14a inhibition, suggesting that MAPK14a contributes to the maintenance and expansion of the oligodendrocyte progenitor pool, which is critical for remyelination and structural restoration of the regenerating brain.

To investigate whether MAPK14a inhibition had any influence on cellular longevity, TUNEL staining to detect apoptosis was carried out. A modest increase in apoptotic cells was observed in the posterior region of the dorsal telencephalon (Dp) of the injured hemisphere following MAPK14a suppression. This region is considered functionally analogous to the subgranular zone (SGZ) of the mammalian hippocampus, suggesting that MAPK14a inhibition may exacerbate regenerative deficits by promoting progenitor cell loss in specific neurogenic niches.

Additional experiments were carried out to uncover additional roles that p38α MAPK regulates in relation to other regeneration signaling mechanisms in the brain. The Wnt/β-catenin signaling pathway is known to play a critical role in early wound healing and regenerative responses in the zebrafish brain (269). Immunoblot analyses revealed upregulation of β-catenin during regeneration. Consistent with previous reports demonstrating that p38 MAPK modulates β-catenin levels through regulation of GSK3β activity (339), BIRB796-mediated inhibition of p38α MAPK resulted in a reduction of β-catenin levels.

A final signaling pathway under analysis was PI3K/AKT which is vital for neuronal cell bodies survival and brain growth during the larval stages of zebrafish (340), was examined. Total AKT levels remained unchanged during regeneration, whereas phosphorylated AKT levels were elevated, indicating pathway activation. Notably, phosphorylated AKT levels were

significantly reduced at 4 dpl in BIRB796-treated regenerating brains compared to DMSO-treated controls, suggesting that MAPK14a functions upstream of, or in coordination with, the PI3K/AKT pathway to promote neurogenesis. These findings support the existence of extensive signaling crosstalk, whereby MAPK14a modulates multiple regenerative pathways, including Wnt/β-catenin and PI3K/AKT signaling.

Collectively, our observations establish that MAPK14a acts as an essential regulator of neural progenitor activation, proliferation and survival during brain regeneration of zebrafish; inhibiting it impairs gliogenic precursor amplification, neuronal recovery and oligodendrogenic precursor maintenance in addition to lightly increasing precursor cell death, demonstrating how MAPK14a directs an adaptive regenerative response and pointing to the obligatory nature of its function in integrating crucial signaling pathways and promoting recovery.

6.5 Discussion

Zebrafish brain regeneration allows the detailed analysis of cellular and molecular events driving efficient repair of damaged tissue. The zebrafish telencephalon has been the subject of numerous analyses aimed at elucidating mechanisms regulating neurogenesis, but far less is understood about the transcriptomic transitions that mark the earliest regenerative stages following injury in this system. The present study addresses this gap by providing a comprehensive transcriptomic characterization of early telencephalon regeneration, encompassing wound healing as well as early and peak proliferative phases. By analysing whole-brain transcriptional responses, this work captures injury-induced systemic molecular adaptations and enables the identification of key genes and pathways that regulate the regenerative process.

Injuries have been generated to cause acute damage to the adult zebrafish central nervous system (CNS), and among the most investigated regions is the telencephalon owing to the tissue's impressive regenerative capacities. A stab wound injury into the medial telencephalon was used in this study. The injury affects both postmitotic neurons residing in the brain parenchyma and radial glial progenitors along with ependymoglial cells with neural stem-cell like properties in the dorsal VZ. Consequently, this model provides valuable insight into progenitor cell activation and regenerative dynamics following injury. Transcriptomic analysis was carried out at three critical times 1 day post-lesion (dpl), the wound healing phase; 4 dpl,

at the onset of proliferation; and 7 dpl, at a high point of proliferation. One of the major advantages of this experiment was our analysis of the cell proliferation phases in detail.

A subset of highly conserved time-dependent gene expression profile emerged during this process; the greatest number of differentially expressed genes was found at 4 dpl, fewer genes were differentially expressed at 7 dpl, and an intermediate degree of differential expression was observed at 1 dpl. This pattern reflects the progressive engagement of distinct biological processes as regeneration proceeds. At 1 dpl, pathways associated with inflammation and immune signaling, including PPAR and NOD-like receptor pathways, were prominently enriched, consistent with the requirement for rapid resolution of the injury response. Insulin and calcium signaling pathways, which are implicated in cellular stress responses and tissue repair, were also activated at this stage. Concurrently, genes involved in DNA replication and cell cycle initiation, such as *mcm2, mcm4*, and *e2f1*, were upregulated, indicating early priming of progenitor cells for proliferation. By 4 dpl, pathways related to angiogenesis, neurogenesis, and cell cycle regulation were strongly enriched, reflecting the transition toward active tissue regeneration. The enhanced expression of the mitotic promoters *aurkb*, *cdc20*, and *dbf4* at the time points we analyzed indicated a shift towards extensive cell cycling and amplification of precursor populations. In addition, the overall profile of gene expression suggested that cell cycle progression was a regulated process that involved feedback mechanisms. The identification of hub genes such as *plk1*, which plays a critical role in cell cycle progression and genomic stability, further highlights the importance of tightly regulated mitotic control during this stage. At 7 dpl, when proliferation peaks, genes associated with differentiation and tissue remodeling, including *mad2l2* and *tfdp1b*, were enriched. Additionally, pathways related to ferroptosis and ubiquitin-mediated proteolysis were activated, suggesting a transition from proliferative expansion toward differentiation and functional integration of newly generated cells.

These studies clearly demonstrate the temporal sequence of a finely regulated regeneration that occurs across these intervals. The signaling networks involved in DNA repair and proliferation during early regeneration transition to a differentiated tissue at a later time point. While certain mechanisms remain constant, some pathways remain quiescent while others take precedence at different stages of regeneration. The progression from inflammation and DNA replication at 1 dpl to proliferation and tissue formation at 4 dpl, followed by differentiation and maturation at 7 dpl, underscores the precision and complexity of the regenerative response in zebrafish brain tissue. The concurrent activation of multiple signaling pathways, including MAPK,

insulin, and calcium signaling, suggests extensive pathway crosstalk that likely fine-tunes progenitor activation, proliferation, and survival. Notably, many of the pathways engaged during regeneration overlap with those active during embryonic brain development, indicating that developmental programs are reactivated to support injury repair. The MAPK signaling pathway, particularly MAPK14a (p38α MAPK), emerged as a key regulator of the regenerative response following brain injury. MAPK14a expression was significantly induced within 1 d of injury and showed an enduring decrease with regeneration progression and recovery as well as increasing levels of differentiative markers on 14 dpl when the rate of proliferation is at its highest (7 dpl). This temporal activation profile is consistent with the established role of p38 MAPKs as mediators of inflammatory signaling and cellular stress responses, both of which are prominent features of traumatic brain injury (69,270) To further contextualize these findings, transcriptomic data from a mouse hippocampal traumatic brain injury model at 3 days post-injury (3 dpi) were examined. This implies that this pathway is conserved among both model organisms and traumatic brain injury paradigms, as observed in the KEGG pathway and GO biological process enrichments analysis (**Additional File 6.5**) (341).

This cross-species enrichment underscores the relevance of MAPK signaling as a central regulatory axis in traumatic brain injury. Consistent with these observations, previous studies have demonstrated that p38α promotes the migration and proliferation of adult neural progenitor cells within mammalian neurogenic regions such as the subventricular zone (SVZ) and subgranular zone (SGZ), processes essential for brain repair (72). Moreover, forced expression of p38α has been shown to restore age-associated declines in neural progenitor cell proliferation through modulation of Wnt signaling pathways, while increased intracellular p38α levels enhance progenitor migration without affecting cell survival or differentiation, highlighting its potential role in facilitating progenitor recruitment to injury sites (342). Collectively, these findings position MAPK14a as a conserved and functionally relevant regulator of endogenous brain repair mechanisms.

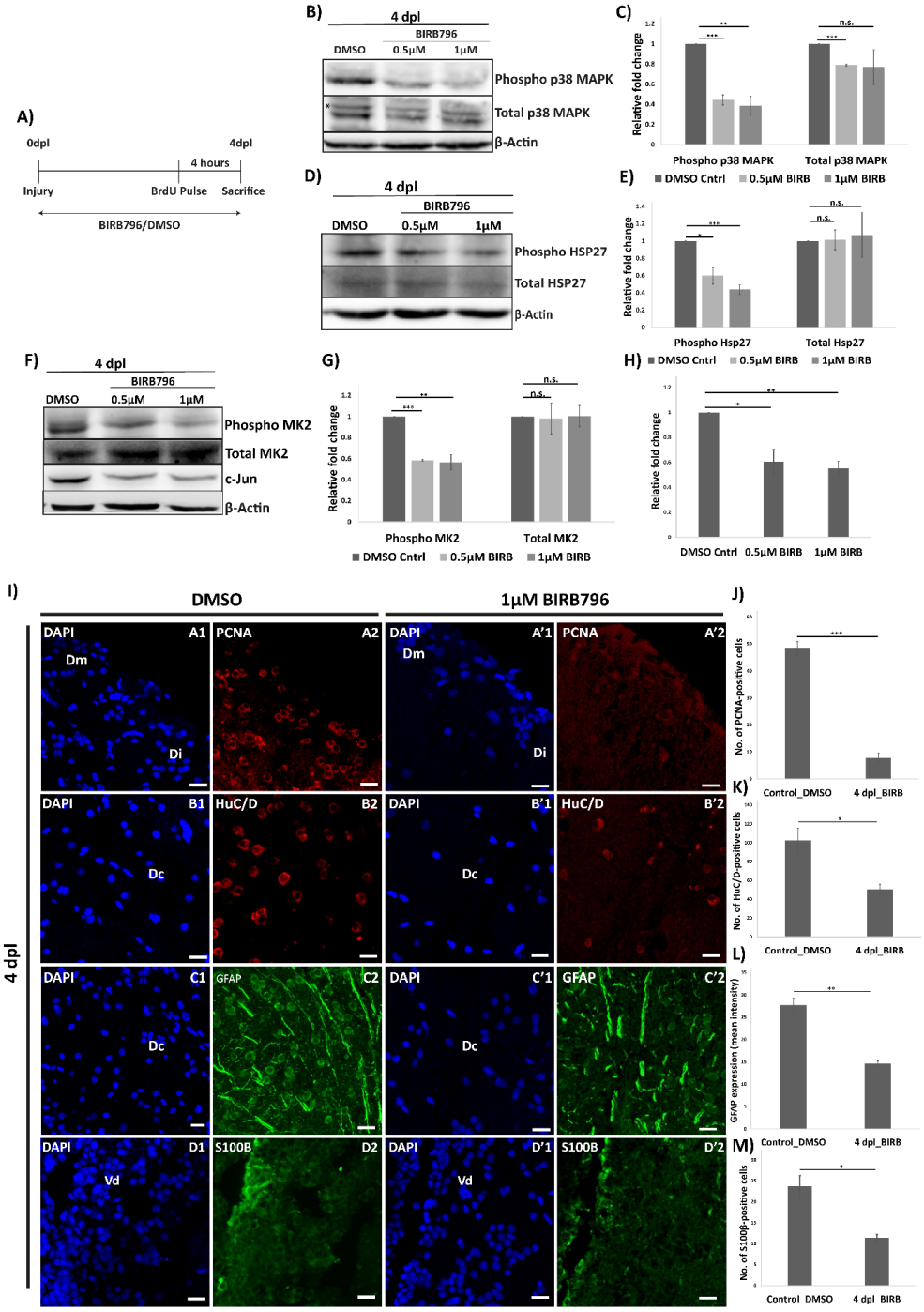

Figure 6.9: BIRB796-mediated inhibition of MAPK14a pathway impairs the regenerative response post traumatic brain injury A Schematic showing BIRB796 treatment after zebrafish brain injury and the brains harvested at 4 dpl. Treatment regimen: animals were immersed in system water containing 0.5 µM or 1 µM BIRB796 (or vehicle control, 0.1% DMSO) immediately after lesion induction and maintained until sacrifice at 4 dpl. **B** Immunoblot analysis showing the levels of phosphorylated (active) and total p38α MAPK protein upon BIRB796 treatment at 4 dpl;. *represents the band for p38α MAPK. **C** Quantification of Phosphorylated (active) and total p38α MAPK levels in control regenerating (4 dpl DMSO) brain and BIRB796 treated regenerating (4 dpl) brain is shown as a bar graph (n=3). **D** Immunoblot analysis showing the levels of phosphorylated (active) and total Hsp27 protein upon BIRB796 treatment at 4 dpl **E** Quantification of Phosphorylated (active) and total Hsp27 levels in control regenerating (4 dpl DMSO) brain and BIRB796 treated regenerating (4 dpl) brain is shown as a bar graph (n=3). **F** Immunoblot analysis showing the levels of phosphorylated (active)and total MK2 and c-Jun protein upon BIRB796 treatment at 4 dpl. **G** Quantification of Phosphorylated (active)and total MK2 levels

in control regenerating (4 dpl DMSO) brain and BIRB796 treated regenerating (4 dpl) brain is shown as a bar graph (n=3). **H** Quantification of c-Jun levels in control regenerating (4 dpl DMSO) brain and BIRB796 treated regenerating (4 dpl) brain is shown as a bar graph (n=3). Significance is represented as n.s. for p-value>0.05, * for p-value<0.05, ** for p-value<0.01 and *** for p-value<0.001.**I** Immunofluorescence staining on 4 dpl Zebrafish brains treated with DMSO (Control) or 1μM BIRB796. Panels show staining with the following markers: PCNA (red), HuC/D (red), GFAP (green), and S100B (green), with DAPI used to label nuclei. (A-D) DMSO control, (A'-D') BIRB796 treatment. Scale bar denotes 10μm. The following anatomical regions are indicated: **Dc** (central zone of the dorsal telencephalic area), **Dm** (medial zone of dorsal telencephalic area), **Dl** (lateral zone of dorsal telencephalic area), **Vd** (dorsal nucleus of ventral telencephalic area). **J-M** Quantification of immunostaining wherein injured hemisphere of 4 dpl regenerating brain has been compared to that of 4 dpl BIRB796 treated regenerating brain (n=3). Significance is represented as n.s. for p-value>0.05, * for p-value<0.05, ** for p-value<0.01 and *** for p-value<0.001. cntrl; control; dpl: days post-lesion.

As we previously proposed MAPK14a (p38α MAPK) was identified as a key player during zebrafish brain regeneration working at several stages of the regenerative reaction. Inhibition of MAPK14a activity with BIRB796 displayed a significant decrease of the regenerative capacity, shown by diminished progenitor proliferation of both glial and neuronal origin. Therefore, activation of MAPK14a seems essential in this context. Furthermore, preservation of the regenerative potential of progenitor cells implies activation of MAPK14a activity, indicated by diminished abundance of PCNA+, GFAP+, S100B+, and Olig2+ cells upon MAPK14a inhibition. In addition, successful integration and differentiation of neurons was strictly dependent upon MAPK14a activity evidenced by decreased HuC/D+ neuron density within the injured hemisphere.

The role of MAPK14a stretches beyond a facilitator of stem cell division; this protein regulates key signaling cascades driving regenerative repair. Inhibition of MAPK14a diminishes the presence of phosphorylated AKT and β-catenin within cells, signifying its regulation lies in the direct activation or modulation by upstream components like GSK3β, affecting Wnt/β-catenin and PI3K/AKT activity respectively. This establishes a central position for MAPK14a in orchestrating multiple processes central to efficient tissue revitalization following damage. This interpretation is consistent with studies in mammalian systems demonstrating a role for MAPK14a in regulating brain precursor cell proliferation and adult neurogenesis (72). Collectively, these observations indicate that MAPK14a contributes not only to neural stem cell activation and proliferation but also to progenitor cell survival, thereby preserving the integrity of the neurogenic niche during regeneration.

Signaling *via* MAPK aside from the temporal co-regulation of transcriptional profiles the stage-specific activation of signaling *via* FoxO and PPAR during the regenerative process has also emerged. Their temporal co-activation with MAPK signaling suggests potential crosstalk in coordinating metabolic regulation, cellular stress responses, and progenitor proliferation,

although the precise molecular interactions among these pathways remain to be defined. It is likely that multiple signaling cascades operate in parallel yet convergent manners to optimize regenerative outcomes, a hypothesis that warrants further investigation.

On the other hand, some critical points must be mentioned. Firstly, the stab-wound injury paradigm is an already validated approach, albeit inherently more physically manipulated than other models of lesions that involve mechanical perturbations (71,263). In addition, BIRB796 inhibits multiple p38 MAPK isoforms (α/β/γ), and thus contributions from isoforms other than MAPK14a cannot be fully excluded when interpreting the results. Finally, although zebrafish and mammalian brains differ substantially in regenerative capacity, the zebrafish model remains a powerful system for identifying conserved molecular pathways and regulatory principles that may inform strategies for enhancing brain repair in mammals. Transient knockdown of p38αMAPK will be integral in elucidating the exact mechanisms operating downstream (transcriptional and post-translational) of MAPK14a regulation and defining precise biological role of this isoform in zebrafish neuroregeneration, and future studies should utilize a combination of transgenic and isoform-specific methods to tackle these aims. The identification of additional pathways, including GnRH, NOD-like receptor, ErbB, and FoxO signaling, further expands the current understanding of regenerative regulation and suggests that brain regeneration is governed by a more complex and interconnected signaling network than previously appreciated.

6.6 Conclusion

The complexity of the interaction between localized injury signals and system-wide molecular processes across a regenerating zebrafish brain is demonstrated here. The time-course and spatial profile of various signaling molecules provides crucial insights into the mechanisms of restoration of neurogenesis upon brain injury. Instead of focusing on a single neurogenic niche the use of a whole-brain transcriptomic approach shows that global brain response underlies successful repair after damage. Such integrative approaches enable one to identify injury responsive and system-wide gene expression that would not be apparent by focusing solely on a single region or response. Although these findings identify p38α MAPK (MAPK14a) as a pivotal regulator of adult neural progenitor activation and neurogenesis, several experimental limitations should be recognized. First, the pharmacological inhibitor utilized in this study, BIRB796, targets multiple p38 MAPK isoforms (including p38α, β, and γ); therefore, the potential secondary contributions of non-alpha isoforms cannot be completely ruled out by

chemical inhibition alone. Second, whole-telencephalon bulk RNA sequencing was utilized, which, while capturing global injury-induced transcriptional transitions, does not resolve cell-type-specific transcriptomic trajectories across distinct radial glial subsets and neuronal lineages. Future research should prioritize the generation of cell-type-specific transgenic knockout lines (e.g., using Cre-loxP or CRISPR-Cas9 targeted specifically to radial glia) to genetically validate the cell-autonomous requirement of *mapk14a*. Additionally, integrating single-cell or spatial transcriptomics will be crucial to track progenitor lineage trajectories and identify precise downstream transcriptional targets of p38 MAPK signaling during regenerative neurogenesis.

The findings presented in this chapter are published in *BMC Journal of Translational Medicine*

Bhasin, S*., **Kaushal, S.*,** Srivastava, P. P.*, Menon, M. B., Ramachandran, R., Dhanjal, J. K., & Minocha, S. (2025). From injury to recovery: transcriptomic dynamics in zebrafish brain regeneration. Journal of translational medicine, 24(1), 87. https://doi.org/10.1186/s12967-025-07400-7

***** *equal contribution*

Chapter 7. Mapping the transcriptomic divergence between controlled regenerative exit and oncogenic persistence in zebrafish (*Danio rerio*).

7.1 Graphical abstract

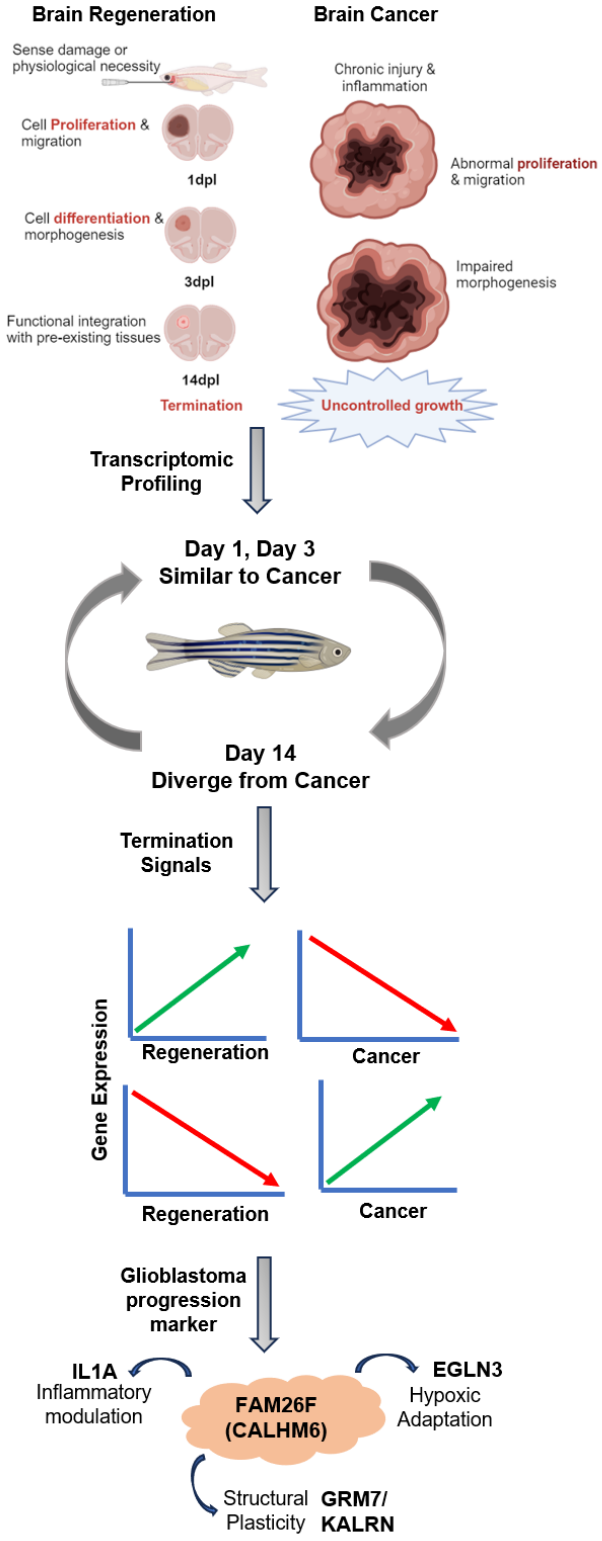

7.2 Background

A central question of biology is not only if there are shared molecular pathways for regeneration and tumorigenesis, but why similar proliferative states are self-limited in one case and perpetual in the other. Both processes are highly proliferative; the difference, however, lies in the proliferative states' self-limited nature in the first instance and non-self-limited proliferative state in the latter. In this scenario, the focus shifts from the regulation of pathway activity to that of proliferative exit, positioning the termination of cell division as the critical determinant separating physiological repair from pathological growth.

In regenerating systems, proliferative expansion is rigorously controlled in time and function. The initial response to injury results in a vigorous activation of cell cycle- and survival-promoting pathways, which is then switched off by sequential activation of apoptosis-, differentiation- and senescence-inducing pathways (343). Processes such as apoptosis-induced proliferation will increase the strength of early proliferative responses but are ultimately regulated within a tight regulatory system designed to ensure cessation of proliferations. Regeneration is therefore marked by an active termination of proliferation and a return to a tissue steady state (344), in contrast to tumorigenesis, which is marked by the collapse of these regulatory constraints, resulting in continued proliferative signaling and maintenance of an undifferentiated cellular state (345).

This divergence is mediated through differential regulation of conserved developmental signaling pathways. During regeneration these developmentally active signaling pathways (Wnt, Notch, and Hedgehog) are transiently stimulated to foster stem-cell progenitor proliferation and lineage specification but become inactivated as regeneration proceeds (345). In the zebrafish telencephalon, injury induces radial glial cells (RGCs) to re-enter the cell cycle and contribute to neural repair, followed by a return to quiescence (266). In contrast, sustained activation of these pathways in tumorigenesis supports the proliferation and stemness of glioma cells, maintaining them in a persistent regenerative-like state (346).

In fact, regeneration and tumorigenesis programs share important similarities in early stages of operation. Activation of Wnt/β-catenin signaling pathways, and pro-inflammatory networks immediately after wounding recapitulate some glioma-inductive pathways (269). Such overlap suggests a temporal mis- regulation of proliferation- resolving processes as an inductive force behind tumors.

In this analysis, the core hypothesis posits that what defines tumorigenesis is the lost capability to send termination signals necessary for regulating proliferative pathways during regeneration, which should otherwise be switched off and constrained. In the context of this problem, by comparing zebrafish brain regeneration with temporal resolution across stages 1, 3, and 14 days post-lesion, to a variety of brain cancer datasets, expression programs which are evanescent during regeneration but continuously expressed during tumorigenesis should be mapped.

Through this comparative approach, genes that are only transiently activated during the physiological regenerative phase but remain persistently expressed in the tumorigenic state may be identified, representing potential regulators of proliferative exit as well as candidate tumor drivers. This is analogous to recent research where genes that are specifically active only during embryogenesis but not in adult tissues can represent set of new drivers for cell proliferation.

7.3 Methods

7.3.1 Transcriptome Analysis

Transcriptomic datasets for zebrafish brain regeneration and brain cancer were obtained from publicly available repositories (ENA; project IDs PRJEB48872 and PRJNA301408). Raw sequencing reads were processed using Trim Galore (v0.6.4) and assessed for quality using FastQC (v0.11.8). High-quality reads were aligned to the zebrafish reference genome (GRCz11/danRer11) using STAR aligner (v2.7.9a). Reads with MAPQ scores of 255 (unique mapping), 3 (mapping to two locations), and 1 (mapping to multiple locations) were retained. Transcript quantification was performed using featureCounts (v2.0.3) (187). Differential expression analysis and normalization were conducted using DESeq2 (v1.42.0) (279), with Wald tests applied for the following comparisons - (i) 1 dpl *vs.* control; (ii) 3 dpl *vs.* control, (iii) 14 dpl *vs.* control, (iv) brain cancer *vs.* control. Genes with $|\log2FC| \geq 1$ and p-value < 0.05 were considered significant. Functional enrichment analyses were performed using clusterProfiler (v4.10.0), including Gene Ontology (GO) and KEGG pathway enrichment (347).

7.3.2 Data Acquisition and Survival Analysis of Glioblastoma Cohorts

RNA-seq expression data (Illumina HiSeq) for glioblastoma multiforme (GBM) were obtained from the University of California Santa Cruz (UCSC) Xena Browser (n = 172 patients).

Corresponding clinical data were integrated to generate a consolidated dataset containing patient ID, overall survival (OS), and gene expression values.

Patients were stratified into high- and low-expression groups (n = 86 each) based on median expression levels. Kaplan–Meier survival analysis and log-rank tests were used to assess survival differences. For evaluation of candidate genes, Cox proportional hazards regression was used to get hazard ratios (HR).

7.3.3 Identification of FAM26F-Regulated Downstream Effectors

The regulation of *FAM26F* (*CALHM6*) was uncovered *via* integrated analysis of KO (GSE223008) and OE (GSE249906) transcriptomics from murine bone marrow-derived macrophages (BMDMs). Genes that were upregulated in OE while downregulated in KO were identified *via* differential expression analysis as high-confidence direct targets.

The STRING database was used to construct protein-protein interaction networks, and Gene Ontology and KEGG functional enrichment to elucidate signaling pathways and downstream biological processes.

7.4 Results

7.4.1 Transcriptomic Landscape of Brain Regeneration in Zebrafish

Experimental Background and Scientific Rationale: Tissue regeneration and oncogenesis represent opposing outcomes of shared cellular and molecular mechanisms, both require rapid stem/progenitor cell expansion, dedifferentiation, extensive metabolic remodeling, and tissue invasion. However, while physiological regeneration culminates in timely proliferative shutdown, functional differentiation, and restored tissue homeostasis, tumorigenesis is characterized by a failure to engage these termination mechanisms, resulting in autonomous, unrestrained cellular proliferation. Comparing the temporal transcriptomic trajectory of a proficiently regenerating organ with the stable oncogenic profiles of human glioblastoma multiforme (GBM) provides an unbiased strategy to identify the elusive 'off-switches' that govern proliferative arrest. Adult zebrafish brain regeneration was therefore profiled across three key temporal stages: 1 dpl (acute injury response and wound healing), 3 dpl (active progenitor cell proliferation and peak neurogenesis), and 14 dpl (proliferative termination, differentiation, and tissue resolution). By systematically intersecting these stages with transcriptomes from human glioblastoma cohorts, this analysis sought to pinpoint genes that are resolved during late regeneration but remain constitutively active in cancer. Genome-wide

analysis across these post-lesion stages revealed widespread transcriptional reprogramming during zebrafish brain repair (**Figure 7.1**). At 1 dpl, 11,211 genes were differentially expressed (5048 upregulated and 6163 downregulated), indicating a robust early response to injury. At 3 dpl, 3439 genes were differentially expressed (2996 upregulated and 443 downregulated), while at 14 dpl, 1292 genes were differentially expressed (922 upregulated and 370 downregulated), reflecting a progressive reduction in transcriptional perturbation as regeneration advances (**Figure 7.1 A-C**).

Functional enrichment analysis demonstrated that the early stage (1 dpl) is dominated by stress response, immune activation, and tissue repair processes. Enriched biological processes included cellular response to stress, neuron development, apoptosis, axonogenesis, gliogenesis, chemotaxis, and synaptic signaling. Molecular functions such as enzyme regulator activity, signaling receptor binding, calcium ion binding, protein kinase activity, and peptidase activity were significantly enriched. KEGG pathway analysis revealed activation of MAPK, calcium signaling, mTOR, TGF-β signaling, apoptosis, and necroptosis pathways (**Figure 7.1 D-E**).

At 3 dpl, the transcriptional program shifted toward proliferation and tissue reconstruction (**Figure 7.2B**). Enriched biological processes included cell cycle regulation, DNA replication, DNA repair, mitotic division, stem cell differentiation, and tissue morphogenesis. Molecular functions such as phosphotransferase activity, protein kinase activity, and receptor signaling remained prominent. KEGG pathways included MAPK signaling, p53 signaling, FoxO signaling, focal adhesion, cytoskeletal regulation, and apoptosis (**Figure 7.1 F-G**).

By 14 dpl, regeneration progressed toward differentiation and structural remodeling (**Figure 7.2C**). Enriched processes included morphogenesis, axon development, nervous system development, and organ formation. KEGG pathways such as MAPK, Wnt, FoxO, insulin signaling, cellular senescence, and apoptosis remained active, reflecting a transition toward resolution (**Figure 7.1 H-I**).

7.4.2 Overlap Between Regeneration and Brain Cancer

Brain cancer transcriptome analysis identified 3298 differentially expressed genes **(Figure 7.2A)**, of which 2558 were upregulated and 740 were downregulated. Functional enrichment analysis revealed a broad spectrum of biological processes associated with tumorigenesis, including cell proliferation, angiogenesis, chemotaxis, immune response, cell differentiation, cell–cell signaling, defense response, growth, and homeostatic processes. In addition, several developmental processes related to vasculature, head, brain, and central nervous system

development were significantly enriched. Molecular function analysis further highlighted enrichment of phosphotransferase activity, enzyme regulator activity, and oxidoreductase activity **(Figure 7.2B)**. Consistent with these observations, KEGG pathway analysis revealed activation of key oncogenic and stress-response pathways, including MAPK signaling, calcium signaling, efferocytosis, apoptosis, ECM–receptor interaction, endocytosis, Wnt signaling, phagosome, and necroptosis pathways **(Figure 7.2C)**.

A substantial overlap was observed between regeneration and cancer, particularly at early stages. Specifically, 876 dysregulated genes were shared between 1 dpl and brain cancer, including 754 upregulated and 122 downregulated genes **(Figure 7.3A)**. At 3 dpl, 1098 dysregulated genes overlapped with cancer, with 1051 upregulated and 47 downregulated **(Figure 7.3B)**. In contrast, only 326 genes were shared at 14 dpl, including 285 upregulated and 41 downregulated genes **(Figure 7.3C)**, indicating a progressive reduction in overlap as regeneration advances. Functional characterization of the shared gene sets revealed stage-specific convergence patterns. At 1 dpl, mutual GO biological process terms were strongly enriched for proliferation- associated programs, including regulation of the MAPK cascade, regulation of kinase activity, regulation of cell development, growth, regeneration, tissue regeneration, and gliogenesis. In parallel, multiple immune-related processes such as inflammatory response, defense response, and response to cytokines were significantly enriched, indicating that early regenerative responses are accompanied by robust immune activation. These findings were further supported by KEGG pathway enrichment, which highlighted MAPK signaling, RHO GTPase effectors, IL4 signaling, immune system pathways, and nervous system development **(Figure 7.3D)**.

At 3 dpl, the shared transcriptional landscape shifted toward differentiation and developmental progression. Enriched GO biological processes included regulation of cell differentiation, mononuclear cell differentiation, leukocyte differentiation, glial cell differentiation, regulation of hemopoiesis, connective tissue development, lymphocyte activation, and developmental growth. KEGG pathway analysis supported these observations, revealing enrichment of VEGF signaling, MAPK signaling, receptor tyrosine kinase (RTK) pathways, and RHO GTPase signaling. In addition, immune-related pathways such as cytokine–cytokine receptor interaction, RIG-I-like receptor signaling, Toll-like receptor signaling, and NOD-like receptor signaling remained prominent, alongside cell death–associated pathways including necroptosis, efferocytosis, and apoptosis **(Figure 7.3E)**.

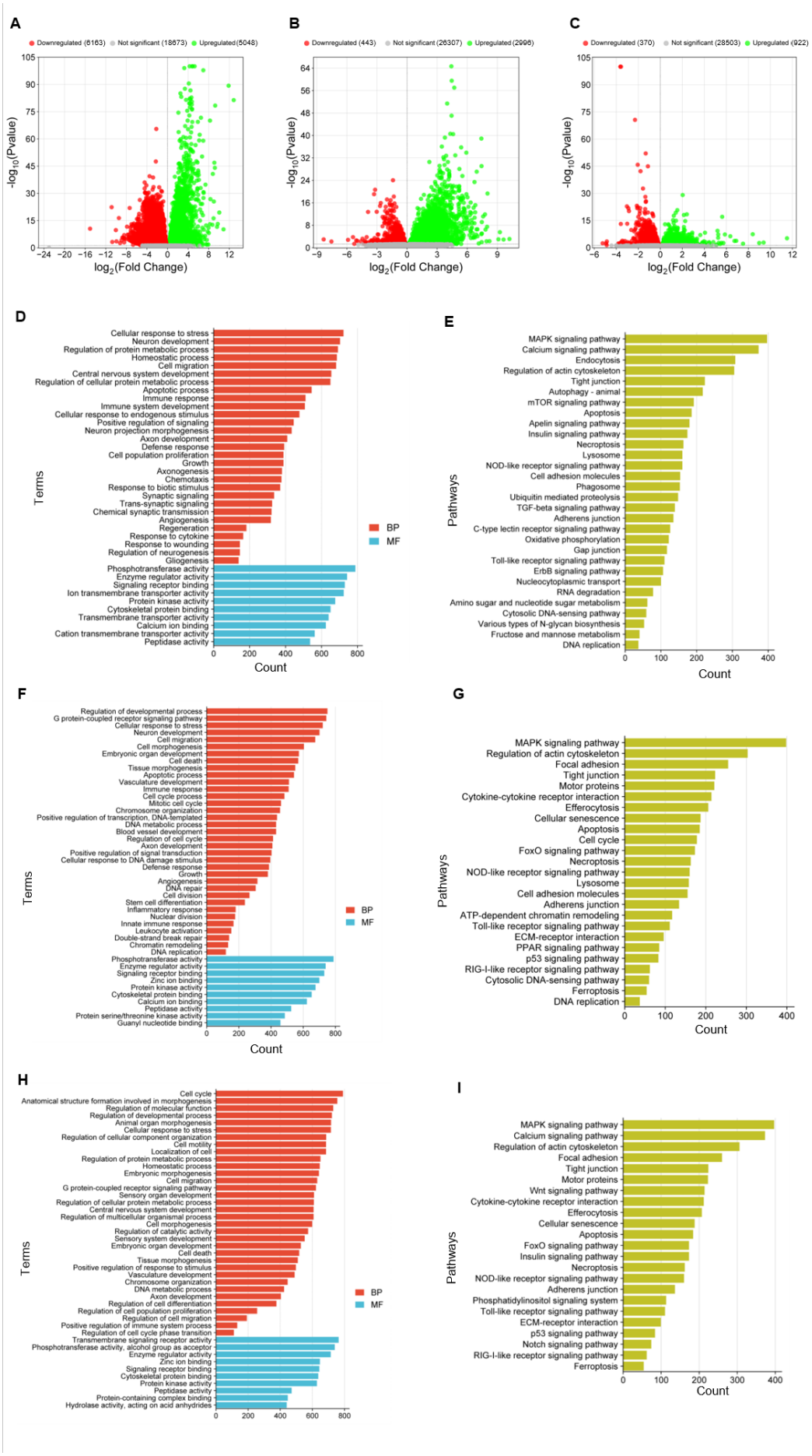
A
Downregulated (6163)
Not significant (18673)
Upregulated (5048)
-log10(Pvalue)
log2(Fold Change)
B
Downregulated (443)
Not significant (26307)
Upregulated (2998)
-log10(Pvalue)
log2(Fold Change)
C
Downregulated (370)
Not significant (28503)
Upregulated (922)
-log10(Pvalue)
log2(Fold Change)
D
Terms
Cellular response to stress
Neuron development
Regulation of protein metabolic process
Homeostatic process
Cell migration
Central nervous system development
Regulation of cellular protein metabolic process
Apoptotic process
Immune response
Immune system development
Cellular response to endogenous stimulus
Positive regulation of signaling
Neuron projection morphogenesis
Axon development
Defense response
Cell population proliferation
Growth
Axonogenesis
Chemotaxis
Response to biotic stimulus
Synaptic signaling
Trans-synaptic signaling
Chemical synaptic transmission
Angiogenesis
Regeneration
Response to cytokine
Response to wounding
Regulation of neurogenesis
Gliogenesis
Phosphotransferase activity
Enzyme regulator activity
Signaling receptor binding
Ion transmembrane transporter activity
Protein kinase activity
Cytoskeletal protein binding
Transmembrane transporter activity
Calcium ion binding
Cation transmembrane transporter activity
Peptidase activity
BP
MF
Count
E
Pathways
MAPK signaling pathway
Calcium signaling pathway
Endocytosis
Regulation of actin cytoskeleton
Tight junction
Autophagy - animal
mTOR signaling pathway
Apoptosis
Apelin signaling pathway
Insulin signaling pathway
Necroptosis
Lysosome
NOD-like receptor signaling pathway
Cell adhesion molecules
Phagosome
Ubiquitin mediated proteolysis
TGF-beta signaling pathway
Adherens junction
C-type lectin receptor signaling pathway
Oxidative phosphorylation
Gap junction
Toll-like receptor signaling pathway
ErbB signaling pathway
Nucleocytoplasmic transport
RNA degradation
Amino sugar and nucleotide sugar metabolism
Cytosolic DNA-sensing pathway
Various types of N-glycan biosynthesis
Fructose and mannose metabolism
DNA replication
Count
F
Terms
Regulation of developmental process
G protein-coupled receptor signaling pathway
Cellular response to stress
Neuron development
Cell migration
Cell morphogenesis
Embryonic organ development
Cell death
Tissue morphogenesis
Apoptotic process
Vasculature development
Immune response
Cell cycle process
Mitotic cell cycle
Chromosome organization
Positive regulation of transcription, DNA-templated
DNA metabolic process
Blood vessel development
Regulation of cell cycle
Axon development
Positive regulation of signal transduction
Cellular response to DNA damage stimulus
Defense response
Growth
Angiogenesis
DNA repair
Cell division
Stem cell differentiation
Inflammatory response
Nuclear division
Innate immune response
Leukocyte activation
Double-strand break repair
Chromatin remodeling
DNA replication
Phosphotransferase activity
Enzyme regulator activity
Signaling receptor binding
Zinc ion binding
Protein kinase activity
Cytoskeletal protein binding
Calcium ion binding
Peptidase activity
Protein serine/threonine kinase activity
Guanyl nucleotide binding
BP
MF
Count
G
Pathways
MAPK signaling pathway
Regulation of actin cytoskeleton
Focal adhesion
Tight junction
Motor proteins
Cytokine-cytokine receptor interaction
Efferocytosis
Cellular senescence
Apoptosis
Cell cycle
FoxO signaling pathway
Necroptosis
NOD-like receptor signaling pathway
Lysosome
Cell adhesion molecules
Adherens junction
ATP-dependent chromatin remodeling
Toll-like receptor signaling pathway
ECM-receptor interaction
PPAR signaling pathway
p53 signaling pathway
RIG-I-like receptor signaling pathway
Cytosolic DNA-sensing pathway
Ferroptosis
DNA replication
Count
H
Terms
Cell cycle
Anatomical structure formation involved in morphogenesis
Regulation of molecular function
Regulation of developmental process
Animal organ morphogenesis
Cellular response to stress
Regulation of cellular component organization
Cell motility
Localization of cell
Regulation of protein metabolic process
Homeostatic process
Embryonic morphogenesis
Cell migration
G protein-coupled receptor signaling pathway
Sensory organ development
Regulation of cellular protein metabolic process
Central nervous system development
Regulation of multicellular organismal process
Cell morphogenesis
Regulation of catalytic activity
Sensory system development
Embryonic organ development
Cell death
Tissue morphogenesis
Positive regulation of response to stimulus
Vasculature development
Chromosome organization
DNA metabolic process
Axon development
Regulation of cell differentiation
Regulation of cell population proliferation
Regulation of cell migration
Positive regulation of immune system process
Regulation of cell cycle phase transition
Transmembrane signaling receptor activity
Phosphotransferase activity, alcohol group as acceptor
Enzyme regulator activity
Zinc ion binding
Signaling receptor binding
Cytoskeletal protein binding
Protein kinase activity
Peptidase activity
Protein-containing complex binding
Hydrolase activity, acting on acid anhydrides
BP
MF
I
Pathways
MAPK signaling pathway
Calcium signaling pathway
Regulation of actin cytoskeleton
Focal adhesion
Tight junction
Motor proteins
Wnt signaling pathway
Cytokine-cytokine receptor interaction
Efferocytosis
Cellular senescence
Apoptosis
FoxO signaling pathway
Insulin signaling pathway
Necroptosis
NOD-like receptor signaling pathway
Adherens junction
Phosphatidylinositol signaling system
Toll-like receptor signaling pathway
ECM-receptor interaction
p53 signaling pathway
Notch signaling pathway
RIG-I-like receptor signaling pathway
Ferroptosis
Count

Figure 7.1: Transcriptome profiling and functional annotation of the brain during 1 dpl, 3 dpl, 14 dpl stages of zebrafish brain regeneration. **A-C** Volcano plots of differentially expressed genes (DEGs) comparing injured samples at **A** 1 dpl, **B** 3 dpl, and **C** 14 dpl with uninjured controls. The x-axis represents Log_2(fold-change), and the y-axis represents $-Log_{10}$(p-adjusted value). Vertical dashed lines mark the fold-change thresholds (≥1 for upregulated, ≤−1 for downregulated), and the horizontal dashed line marks the significance cutoff (p-adjusted < 0.05). Significant upregulated genes are shown in green (upper-right), and downregulated genes in red (upper-left). **D-I** Gene Set Enrichment Analysis (GSEA)-based functional annotations for GO terms and KEGG pathways at **D–E** 1 dpl, **F–G** 3 dpl, and **H–I** 14 dpl. Data associated with this present in additional file 7.1.

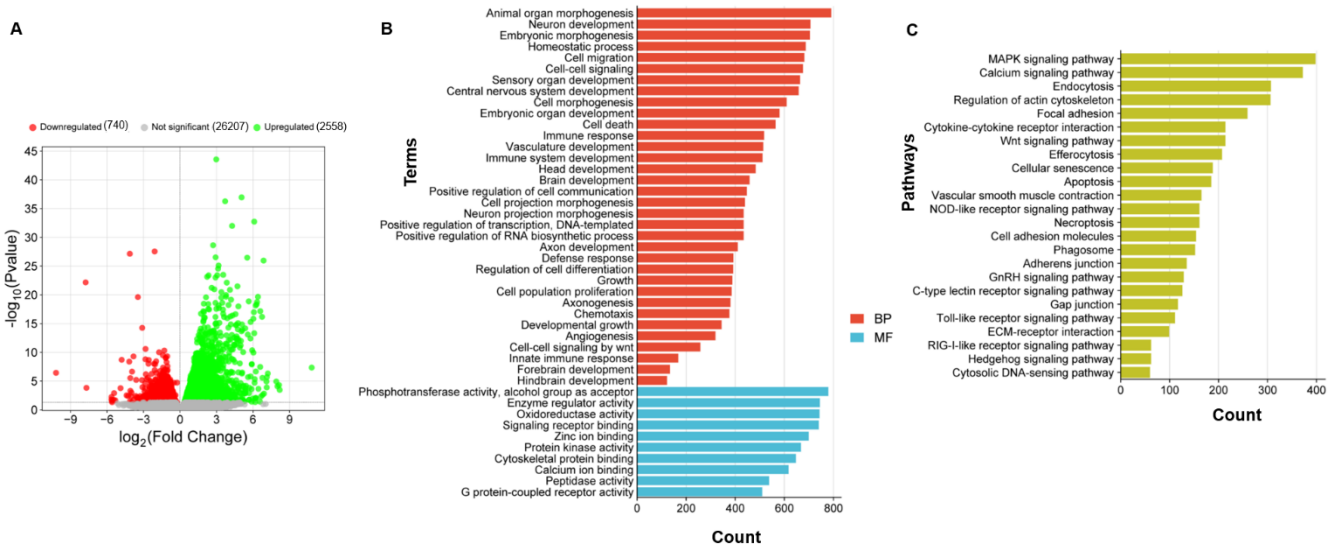

Figure 7.2: Transcriptome profiling and functional annotation of the brain during brain cancer A-C shows volcano plot, GSEA GO terms and KEGG pathways respectively. Data associated with this present in additional file 7.1.

In contrast, the overlap between regeneration and cancer at 14 dpl was markedly reduced. The few shared GO terms were predominantly restricted to immune-related processes, with minimal representation of proliferation or differentiation-associated pathways **(Figure 7.3F)**. This sharp decline in shared transcriptional programs indicates a clear divergence between regenerative and tumorigenic states at later stages.

Collectively, these findings demonstrate that early stages of wound healing closely recapitulate tumorigenic programs at both transcriptional and functional levels, particularly with respect to proliferation, immune activation, and signaling pathway engagement. However, as regeneration progresses, these shared programs are progressively attenuated, leading to a distinct transcriptional state that is no longer aligned with cancer. This temporal pattern supports the concept that tumorigenesis reflects the persistence of early regenerative programs, whereas successful regeneration is defined by their resolution.

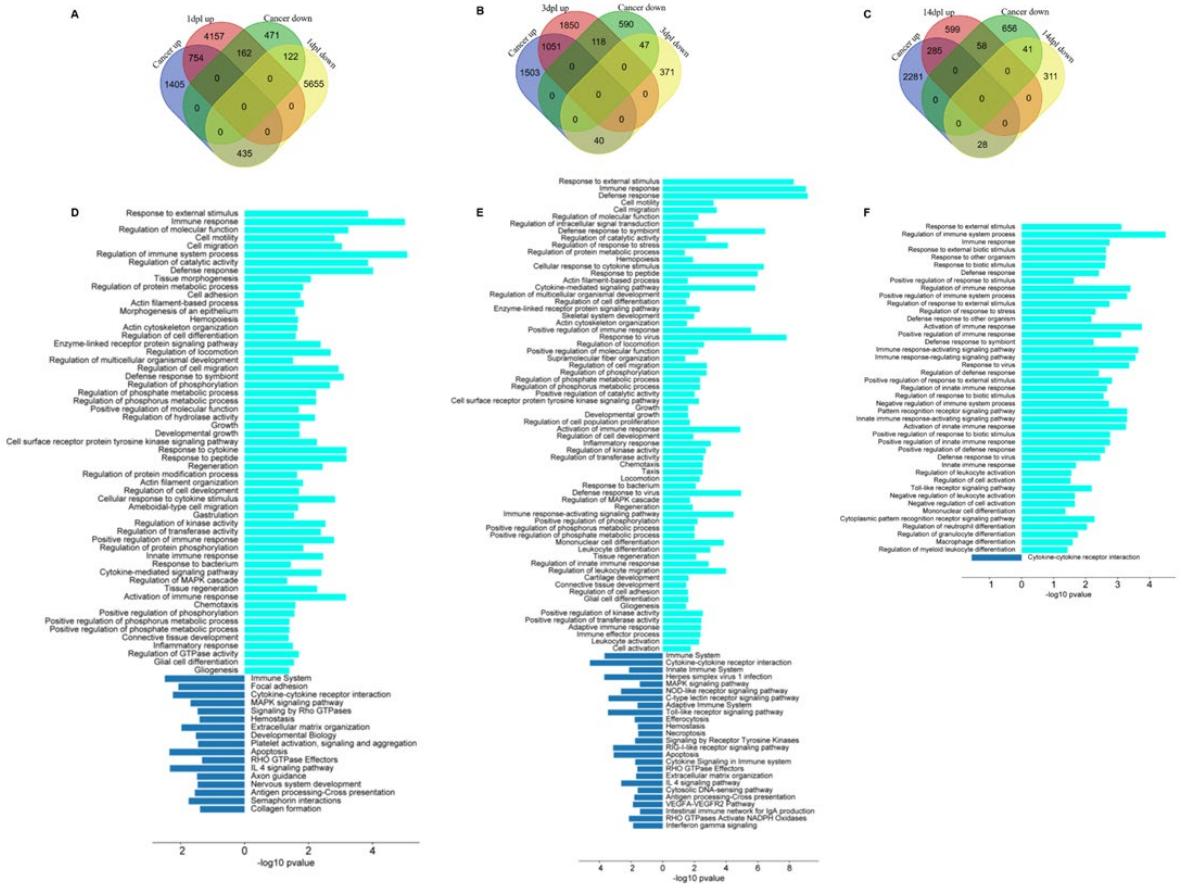

Figure 7.3: Intersection between regeneration and cancer. Upregulated and downregulated genes common between **A** 1dpl and cancer **B** 3dpl and cancer **C** 14dpl and cancer. The shared biological terms between **D** 1dpl and cancer **E** 3dpl and cancer **F** 14dpl and cancer. Data associated with this present in additional file 7.2.

7.4.3 Divergence Between Regeneration and Cancer at Late Stages

A defining feature of regeneration is the progressive downregulation of proliferative and stemness-associated genes from Day 1 to Day 14. In contrast, these genes remain persistently upregulated in cancer, indicating a failure to terminate proliferative signaling. This opposing trajectory highlights a fundamental divergence between physiological repair and pathological growth, wherein regeneration is characterized by resolution of cellular activity, while cancer sustains and amplifies processes that promote tumor progression.

Thus, genes showing this reverse differential expression are key for many of the cancer 'hallmarks' and define separate functional components of tumorigenesis, including stemness properties (*aldh1a2, anxa4, b2m, bdh2, cd99, clic1, ctsc, cyba, egln3, entpd1, etv4, gng10, mthfd1l, nenf, ptprc, tdgf1, tmem220, tnfrsf1a, tram2, zcchc14, bcl6b, il11,* and *il1b*) and sustained self-renewal programs. While such programs are transiently activated during

regeneration, they are constitutively maintained in cancer, supporting sustained stem-like states.

It also describes continuously active proliferation-related genes such as *yap1, csf3a, emp2, hbegfa, hlx1, il11a, irf8, ism1, klf1, nfkbiaa, pdgfaa, plxnd1, ptn6, rspo3, s100b, serpinh1b,* and *socs3b*. The genes which are related to transition to the mesenchymal state, for instance *adam8a, adam8b, snai1a, twist1a, twist1b,* and *twist2* also promote increased cell motility and invasiveness and support metastasis. Furthermore, cell cycle regulators which are still active, including *mvb12a, psme1, psme2, rac2, rad51b, rgs14a, stx11a,* stimulate persistent cell cycle activity (**Figure 7.4A**).

This grouping of genes then is key to driving sustained cell proliferation, invasiveness, immune-modulation, and survival of cancer cells. Functional summarization using treemap analysis further highlights enrichment of canonical cancer hallmarks (**Figure 7.4B**), including sustained proliferative signaling (e.g., cell cycle activation and JAK–STAT pathways), evasion of growth suppressors through maintenance of stemness and developmental dysregulation, activation of invasion and metastasis *via* mesenchymal transition and chemotaxis, resistance to cell death, induction of angiogenesis, tumor-promoting inflammation, and immune evasion.

In contrast, during regeneration, these pathways gradually weaken as tissue repair advances, reflecting the activation of regulatory mechanisms that enforce proliferative exit and restore homeostasis. The persistence of these programs in cancer therefore represents a failure of this regulatory transition, reinforcing the concept that tumorigenesis arises from the inability to resolve regenerative signaling.

Notably, 58 genes identified within this inverse expression set correspond to well-established therapeutic targets in cancer (**Additional File 7.3**). The recovery of such a substantial number of clinically validated targets underscores the robustness of the comparative framework and confirms that the analysis captures key drivers of tumorigenesis consistent with the established oncological landscape.

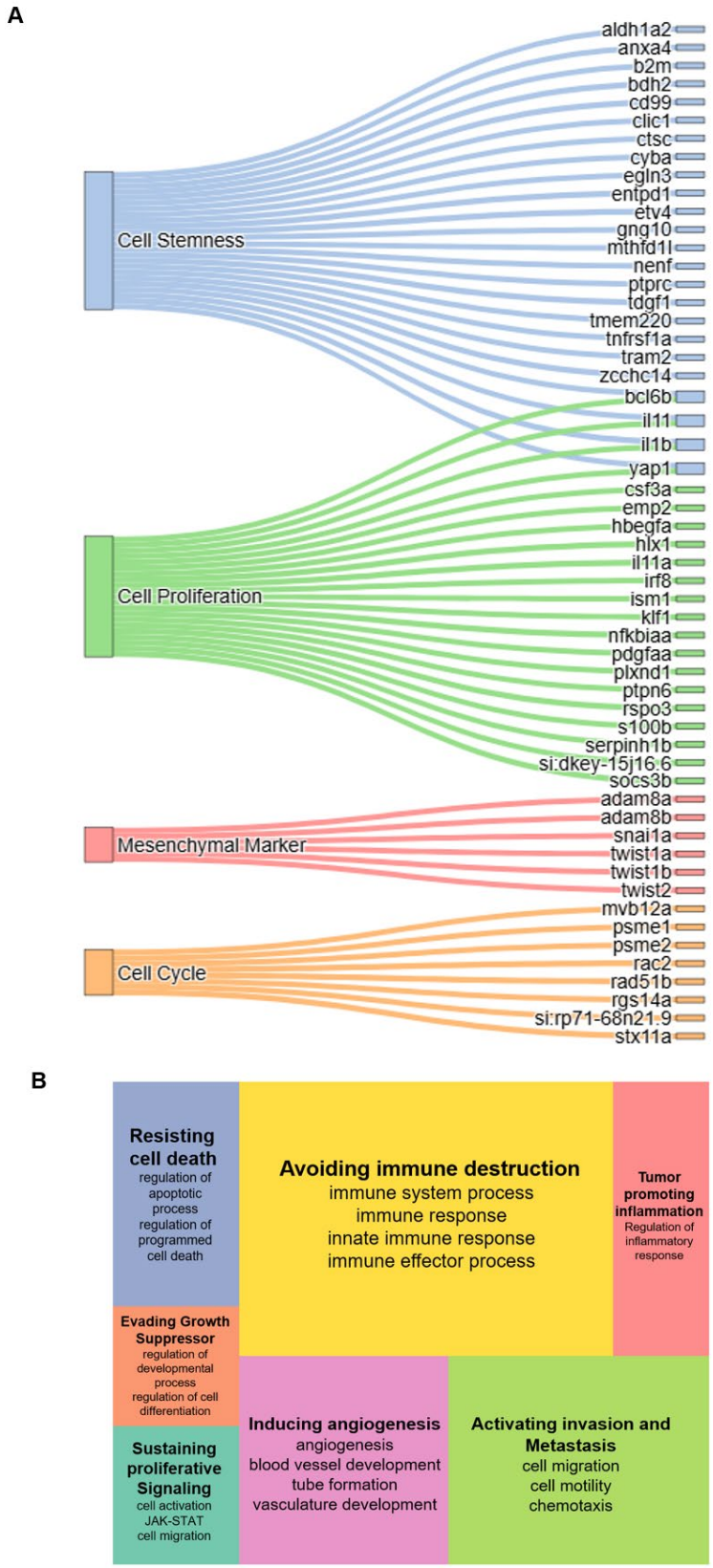

Figure 7.4: A Sankey plot shows genes downregulated from Day 1 to Day 14 and upregulated in cancer, associated with cancer hallmarks. **B** The treemap shows terms associated with the abovementioned genes.

7.4.4 Identification of FAM26F as a Novel Prognostic Marker

To identify regulators of regenerative termination, Genes that switched on during wound repair yet stayed high in tumors were given close attention. Specifically, genes that were progressively downregulated from day 1 to day 14 during regeneration, but remained upregulated in cancer, were considered candidates for mediating the transition from proliferative expansion to resolution. These genes were hypothesized to represent components of a "termination signal," the failure of which may contribute to sustained tumor growth.

From these results, a total of 23 genes without prior linkage to cancer were uncovered through a comprehensive literature search (PubMed). Validation of expression in the human genome utilized the Human Protein Atlas to identify human orthologues for the genes. Furthermore, they were analyzed for pan-cancer expression and prognostic significance/survival analyses. Among these, *FAM26F* (also known as *CALHM6*) emerged as the most promising candidate for further investigation.

Pan-cancer expression analysis revealed that *FAM26F* is consistently upregulated across multiple malignancies relative to corresponding normal tissues (**Figure 7.5A**). Notably, the highest expression levels were observed in DLBC, followed by substantial upregulation in LAML, TGCT, THCA, BRCA, KIRC, and SKCM. Moderate but clear increases were also detected in GBM, HNSC, LIHC, LUAD, and UCEC. Meanwhile, normal cells staying calm kept their message under 10 TPM nearly everywhere, remaining quiet despite surrounding disease activity.

This widespread tumor-associated overexpression suggests a potential role for *FAM26F* in tumorigenesis and supports its relevance as a candidate biomarker.

The prognostic significance of *FAM26F* was further evaluated in glioblastoma (GBM). Survival heatmap analysis demonstrated a positive association between *FAM26F* expression and patient risk, as indicated by hazard ratios greater than 1 (**Figure 7.5B**). Consistent with this observation, Kaplan–Meier survival analysis using the GEPIA2 database revealed that patients with high *FAM26F* expression exhibited significantly reduced overall survival compared to those with low expression (log-rank $p = 0.03$), with a hazard ratio of 1.5, corresponding to a 50% increased risk of mortality (**Figure 7.5C**). This analysis included 81 patients in each expression group.

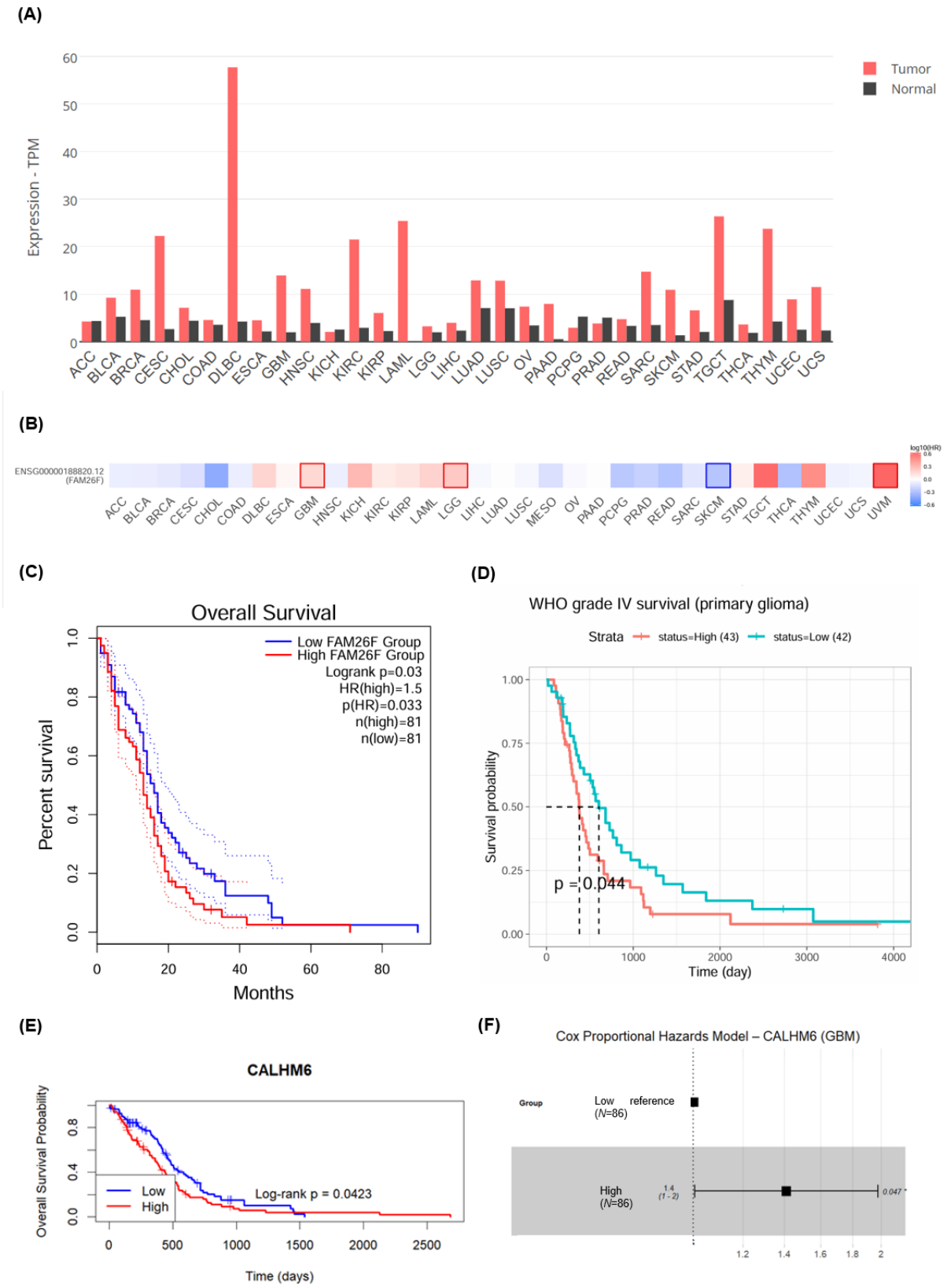

Figure 7.5: Expression and Prognostic Significance of FAM26F (CALHM6) in Glioblastoma. A Pan-cancer Expression. Bar plot comparing *FAM26F* expression (TPM) in tumor (red) and normal (black) tissues across multiple malignancies. **B** Survival Heatmap. Risk assessment across cancer types; the red box highlights the positive correlation between *FAM26F* expression and patient risk in GBM. **C–E** Survival Analysis. Kaplan-Meier

curves from GEPIA2 (C), CGGA (D), and TCGA (E) datasets consistently show that high *FAM26F* expression (red lines) predicts significantly poorer overall survival compared to low expression (blue/green lines). **F** Cox Proportional Hazards Model. Forest plot for GBM showing a Hazard Ratio (HR) of 1.4, confirming high FAM26F expression as a statistically significant independent risk factor (p=0.047).

These findings were independently validated using the CGGA dataset, where a similar survival trend was observed in WHO grade IV primary glioma patients. High *FAM26F* expression was associated with poorer survival (p = 0.044), further supporting its prognostic relevance (**Figure 7.5D**). The CGGA cohort comprised 43 patients in the high-expression group and 42 in the low-expression group.

Further validation using TCGA glioblastoma data confirmed the prognostic significance of *FAM26F*. Kaplan–Meier survival curves demonstrated a clear separation between high- and low-expression groups, with elevated expression associated with reduced overall survival (log-rank p = 0.042) (**Figure 7.5E**). Cox proportional hazards analysis, performed on a cohort stratified into equal groups (n = 86 per group), revealed a hazard ratio of 1.4 (95% CI: 1.0–2.0), indicating a 40% increased risk of death in the high-expression group. This association was statistically significant (p = 0.047) (**Figure 7.5F**), with a total of 138 events included in the analysis.

Collectively, these results identify *FAM26F* as a broadly upregulated gene across multiple cancer types and establish its significant association with poor prognosis in glioblastoma. The consistent validation across independent datasets (TCGA, GEPIA2, and CGGA) highlights its robustness as a prognostic biomarker. In the context of the comparative framework, the persistent upregulation of *FAM26F* in cancer, contrasted with its downregulation during regenerative resolution, supports its potential role as a regulator of proliferative termination whose dysregulation may contribute to tumor progression.

7.4.5 FAM26F Regulatory Network and Functional Mechanisms

To elucidate the molecular mechanisms underlying FAM26F (CALHM6)-mediated regulation, an integrated transcriptomic analysis was performed by combining overexpression (OE) and knockout (KO) datasets derived from *Mus musculus* bone marrow-derived macrophages (BMDMs). This reciprocal expression framework enabled the identification of high-confidence downstream effectors whose expression positively correlated with FAM26F levels, defined by significant upregulation in OE and downregulation in KO conditions. The internal consistency of the model was validated by *Fam26f* itself, which exhibited the most pronounced differential expression across both datasets (log2FC = 7.51 in OE; −2.40 in KO).

Table 7.1: Identification of High-Confidence FAM26F Downstream Effectors *via* Reciprocal Expression Analysis.

Gene	log2FC OE	P-value OE	log2FC KO	P-value KO
Il1a	2.991089729	1.72E-45	-1.616521209	0.013534714
Grm7	1.887099854	0.00023491	-5.008424003	0.030325903
Fam26f	7.516858803	3.07E-217	-2.400301816	0.000773444
Egln3	2.515836285	1.70E-11	-1.065241551	0.044246497
Kalrn	2.924587831	1.57E-06	-1.124144832	0.034930709

This reciprocal expression analysis identified a core quartet of downstream effectors namely *Il1a*, *Egln3*, *Grm7*, and *Kalrn* (**Table 7.1**), which link FAM26F activity to key hallmarks of glioblastoma. It is important to emphasize that all four downstream effectors (*Il1a*, *Egln3*, *Grm7*, and *Kalrn*) were identified purely through computational reciprocal-expression filtering across *in vitro* murine BMDM knockout and overexpression datasets, supported by STRING protein-protein network topology and public human glioblastoma survival correlations. Primary wet-lab biochemical validation such as direct chromatin binding assays, co-immunoprecipitation, or direct functional rescue in glioblastoma cell lines and *in vivo* orthotopic xenografts was not conducted in this thesis and remains designated as critical future work.

Among these, *Il1a* emerged as a central mediator of inflammatory signaling. It functions as a primary node coordinating neuroinflammatory responses, with strong induction observed in the OE model (log2FC = 2.99). Mechanistically, IL-1α activates NF-κB and major MAPK pathways (p38, ERK1/2, and JNK), thereby promoting tumor cell proliferation and resistance to apoptosis (348). In addition, *Il1a* acts as an "alarmin," released upon cellular damage to initiate inflammatory cascades that can paradoxically support tumor progression through necroptosis and senescence-associated pathways (349). Protein–protein interaction analysis further supports this role, with STRING network mapping identifying IL1A as a primary interactor of FAM26F, alongside secondary interactors such as *Serpina3n, Il1r2,* and *Pdgfra*

(**Figure 7.6A**). These interactions suggest that FAM26F amplifies cytokine-mediated signaling and facilitates immune modulation within the tumor microenvironment.

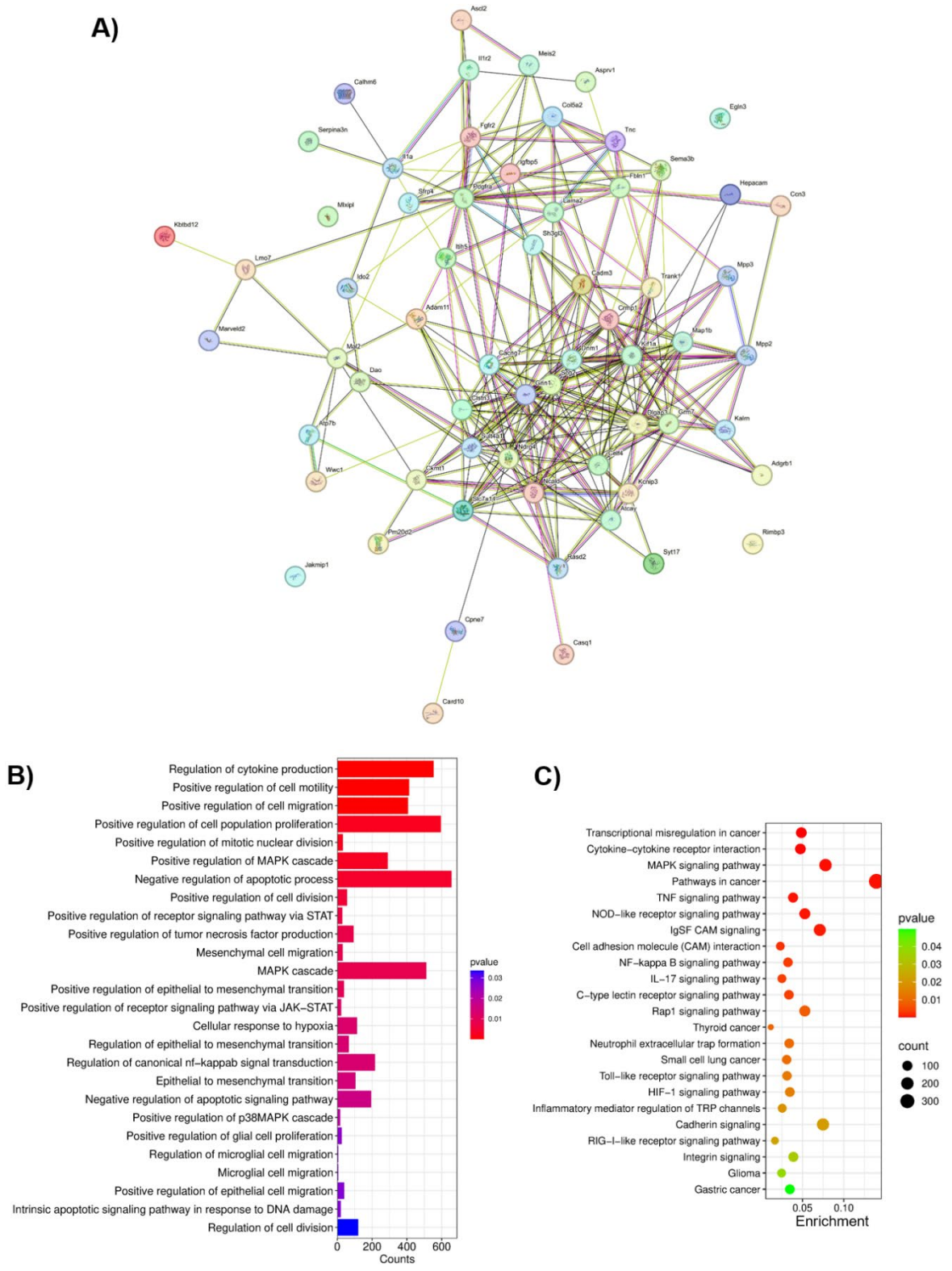

Figure 7.6: A Protein-Protein Interaction (PPI) Network: STRING database analysis illustrating the functional network of high-confidence downstream effectors regulated by FAM26F (CALHM6). **B** Gene Ontology (GO)

Enrichment Analysis: Bar plot representing the most significant Biological Process (BP) terms enriched in the FAM26F overexpression (OE) model. The color scale indicates p-value significance, and the x-axis shows gene count. **C** KEGG Pathway Enrichment Analysis: Dot plot displaying significantly enriched KEGG pathways associated with FAM26F regulation. The dot size corresponds to gene count, while the color indicates the p-value.

Beyond inflammatory regulation, FAM26F influences metabolic adaptation through the upregulation of *Egln3* (PHD3), a key regulator of hypoxia signaling. Enrichment of HIF-1 signaling pathways, along with gene ontology terms associated with cellular stress responses and RNA metabolism, indicates that FAM26F enhances the ability of tumor cells to adapt to hypoxic conditions. In the context of glioblastoma, this regulatory axis supports metabolic reprogramming, enabling tumor cells to maintain bioenergetic stability within hypoxic and necrotic tumor cores characteristic of high-grade lesions (350).

FAM26F also modulates structural and signaling integration through the regulation of *Grm7* and *Kalrn*. The marked downregulation of *Grm7* in the KO model (log2FC = −5.00) suggests that FAM26F facilitates the engagement of tumor cells with neuronal signaling networks, potentially enabling neural mimicry *via* glutamatergic signaling. Concurrently, *Kalrn* regulates cytoskeletal organization and cell motility through Rho GTPase signaling pathways. KEGG enrichment further supports these roles, highlighting pathways related to cell adhesion molecules (CAMs), integrin signaling, cadherin signaling, and axon guidance (**Figure 7.6C**), all of which contribute to cytoskeletal remodeling and invasive behavior.

Functional enrichment analysis of the *FAM26F* overexpression model revealed strong enrichment of pathways associated with ribosome biogenesis, translation, and rRNA processing (**Figure 7.6B**), indicating a global increase in cellular biosynthetic capacity. This enhanced translational machinery supports the elevated metabolic and proliferative demands of tumor cells. In parallel, KEGG pathway analysis identified activation of NF-κB, MAPK, TNF, IL-17, and cytokine–cytokine receptor interaction pathways (**Figure 7.6C**), reinforcing the role of FAM26F in establishing a pro-inflammatory and pro-survival signaling environment.

Additional enrichment of pathways such as leukocyte transendothelial migration and phagosome formation suggests that FAM26F also contributes to immune cell recruitment and microenvironment remodeling. Notably, the combined action of *Il1a* and *Egln3* establishes a functional link between inflammation and metabolic adaptation, forming a feedback loop that enhances tumor resilience. This coordinated regulation enables tumor cells to sustain proliferation and survival while bypassing environmental constraints that would otherwise induce differentiation or quiescence.

Collectively, these findings demonstrate that FAM26F functions as a central regulatory node integrating inflammatory, metabolic, and structural signaling pathways into a coordinated oncogenic program. Rather than acting as a passive marker, FAM26F actively orchestrates multiple hallmarks of glioblastoma, including immune modulation, hypoxic adaptation, enhanced biosynthetic capacity, and invasive growth. This integrated signaling axis represents a potential therapeutic vulnerability, where targeting FAM26F or its downstream network may disrupt multiple survival pathways simultaneously and sensitize glioblastoma to existing treatment strategies.

7.5 Discussion

The comparative transcriptomic analysis of zebrafish telencephalic regeneration and human glioblastoma (GBM) provides a unified framework for understanding tumorigenesis as a dysregulated regenerative process. The findings demonstrate that brain cancer does not arise from novel or cancer-specific pathways, but rather from the persistent activation of conserved regenerative programs that are normally tightly controlled. In this context, tumorigenesis can be conceptualized as a "wound that fails to resolve," wherein early injury-response mechanisms are aberrantly sustained.

During the early stages of regeneration (1 dpl and 3 dpl), there is extensive activation of developmental, immune, and proliferative signaling networks, including Wnt/β-catenin, Notch, Hedgehog, MAPK, and inflammatory pathways. These programs are essential for mobilizing radial glial cells into a proliferative and multipotent state required for tissue repair. Notably, the same pathways are constitutively active in glioblastoma, particularly within glioma stem cell populations, indicating that tumorigenesis co-opts the intrinsic regenerative capacity of the brain. The substantial overlap observed between early regenerative stages and cancer, including the identification of 58 established therapeutic targets, further reinforces the validity of regeneration as a proxy system for studying tumor biology.

The critical distinction between regeneration and cancer emerges at later stages. In the zebrafish model, the 14 dpl stage represents a resolution phase characterized by the activation of "termination signals" that suppress proliferation and promote differentiation, structural remodeling, and restoration of homeostasis. This transition is marked by the downregulation of key proliferative, stemness, and mesenchymal genes such as *yap1, snai1a,* and *twist*. In contrast, glioblastoma fails to execute this transition, maintaining persistent activation of these pathways and thereby sustaining uncontrolled growth. This failure to terminate proliferative

signaling represents the defining mechanistic divergence between physiological regeneration and pathological tumorigenesis.

A central finding of this study is the identification of *FAM26F* (CALHM6) as a key regulator of this divergence. The data indicate that *FAM26F* is transiently expressed during early regenerative phases but must be downregulated for successful completion of regeneration. In contrast, *FAM26F* is aberrantly and consistently upregulated in glioblastoma, as validated across TCGA, GEPIA2, and CGGA datasets, where its elevated expression is significantly associated with reduced overall survival. These observations position *FAM26F* as both a biomarker of aggressive disease and a candidate regulator of proliferative termination failure.

Mechanistically, FAM26F appears to function as a high-level signaling node that integrates multiple oncogenic processes into a coordinated program. Through its downstream effector *Il1a*, FAM26F establishes a pro-inflammatory microenvironment that supports tumor cell survival and immune modulation. The regulation of *Egln3* enables adaptation to hypoxic and metabolically stressed conditions characteristic of high-grade gliomas, contributing to bioenergetic stability and resistance to therapy. In parallel, modulation of *Grm7* suggests a mechanism of neural mimicry, allowing tumor cells to exploit endogenous glutamatergic signaling networks for survival and migration. The regulation of *Kalrn* further enhances cytoskeletal remodeling and invasive capacity *via* Rho GTPase signaling, facilitating diffuse infiltration into surrounding brain tissue.

These coordinated processes define a multi-dimensional fitness program that enables glioblastoma cells to sustain proliferation, resist cell death, adapt to environmental stress, and invade adjacent tissue. The persistence of FAM26F expression effectively prevents the transition from a proliferative to a differentiated state, thereby maintaining cells in a regenerative-like but pathological state. This supports a model in which tumorigenesis results from the failure of a regulatory switch that normally enforces the termination of regenerative programs.

In summary, this research shows regeneration and cancer are divided not by different active signals but because some signals remain active too long. FAM26F stands out because it ties together inflammatory, metabolic, and structural pathways into unified oncogenic network.

7.6 Conclusion

A deep look into gene activity shows how brain repair gone wrong can lead to brain tumors (glioblastoma). Not because growth switches turn on forever, but because a normal shut-off mechanism fails to activate. While fixing a damaged brain usually means turning off certain signals after a time, in cancers those brakes (termination) never apply. This lingering presence keeps cellular activities proliferative, stemness, and invasion-associated programs actively pushing tumors forward over time.

During this progression, FAM26F emerges as a critical junction linking regenerative processes to tumorigenic mechanisms. Its fleeting activation during initial regenerative events contrasts sharply with strong persistent elevation observed in glioblastoma, pointing toward a possible regulatory function in limiting excessive proliferation. The uniform correlation of elevated FAM26F levels with worse clinical results in three separate independent cohorts (TCGA, GEPIA2, and CGGA) firmly positions it as a reliable predictor of patient prognosis for GBM.

Functional interactions demonstrate that FAM26F drives a unified oncogenic program by modulating its target effectors. Modulation of *Il1a* results in an inflammatory environment beneficial to the tumor; meanwhile, control of *Egln3* enhances its metabolic flexibility while potentiating resilience under hypoxic conditions. Interaction with *Grm7* enables neural-cell-like characteristics and connectivity in brain circuitry, whereas activation of *Kalrn* induces changes in the cytoskeleton that underpin invasiveness. Cumulatively, these processes bestow a robust survival benefit allowing continuous growth, evasion of environmental insults, and migration into adjacent tissues.

The identification of this FAM26F-centered regulatory axis presents a promising avenue for both clinical biomarker development and therapeutic intervention in glioblastoma. To advance FAM26F (CALHM6) toward clinical translation, future research must establish its utility as a diagnostic and prognostic biomarker through standardized immunohistochemical and digital PCR quantification in prospective glioblastoma patient biopsies, correlating expression levels with patient stratification, molecular subtypes (e.g., IDH-wildtype vs. mutant), and temozolomide chemotherapy responsiveness. Therapeutically, given that FAM26F functions as a membrane-associated ion and signaling channel protein, structure-guided drug discovery offers an attractive strategy to identify small-molecule inhibitors or monoclonal neutralizing antibodies that block its channel pore or disrupt its protein interactome. Preclinical validation should evaluate whether pharmacological inhibition or targeted CRISPR/Cas9 ablation of

FAM26F suppresses glioma stem-cell self-renewal, alleviates hypoxia-driven invasiveness, and restores sensitivity to standard-of-care radiotherapy in patient-derived orthotopic xenograft models.

Chapter 8. Summary and future directions

The aim of this thesis was to study regeneration and identify the molecular determinants that distinguish successful tissue repair from pathological progression. A series of integrated studies in liver and brain systems were undertaken to examine the hypothesis that molecular processes supporting physiological repair are closely linked to processes that, when disrupted or persistently activated, can contribute to disease.

The first part of this work investigated the role of Host Cell Factor 1 (HCF-1) in liver regeneration and metabolic homeostasis. HCF-1 emerged as an important epigenetic regulator linking metabolic state with transcriptional programs required for hepatocyte proliferation. Loss of HCF-1 impaired efficient cell-cycle entry and compromised hepatocyte proliferation following partial hepatectomy, thereby reducing the regenerative capacity of the liver. At the epigenetic level, HCF-1 depletion altered H3K4 methylation and RNA polymerase II-associated transcriptional activity, disrupting gene-expression programs required for cell-cycle progression and normal hepatic function. These changes were accompanied by mitochondrial dysfunction, altered lipid metabolism, hepatic steatosis, inflammation, and other features associated with metabolic dysfunction-associated fatty liver disease (MAFLD). Thus, the findings demonstrate that successful liver regeneration requires close coordination between epigenetic regulation, metabolic homeostasis, and cell-cycle progression, and that disruption of this coordination can simultaneously impair regeneration and promote metabolic pathology.

The second study examined this relationship from the perspective of metabolic stress by establishing a zebrafish model of MAFLD using dietary palmitic acid supplementation. The model reproduced major histopathological and molecular characteristics of MAFLD, including hepatic steatosis, lipid accumulation, oxidative and endoplasmic reticulum stress, mitochondrial dysfunction, and inflammatory activation. Transcriptomic analysis further revealed alterations in lipid biosynthesis and transport, oxidative phosphorylation, cellular stress responses, and inflammatory pathways. Importantly, comparison with murine and human MAFLD datasets demonstrated conservation of several dysregulated genes and pathways across species. Together with the HCF-1 study, these findings show that both disruption of intrinsic regulatory mechanisms and sustained metabolic stress can disturb hepatic homeostasis and converge on molecular processes associated with metabolic liver disease. The zebrafish model therefore provides a complementary system for investigating the molecular progression of MAFLD and for future evaluation of potential interventions.

The third component of the thesis investigated the molecular regulation of brain regeneration using a zebrafish telencephalic stab-wound injury model. Temporal transcriptomic profiling revealed a highly dynamic regenerative response involving inflammatory signaling, cell-cycle activation, progenitor proliferation, neuronal differentiation, and subsequent tissue remodeling. Among the pathways identified, p38α MAPK (MAPK14a) emerged as a key regulator of the regenerative response. Its activation was temporally associated with the early proliferative phase and declined as regeneration progressed. Functional inhibition using BIRB796 significantly impaired cell proliferation, radial glial progenitor activation, neuronal regeneration, and oligodendrocyte maintenance, establishing the functional importance of p38α MAPK during brain repair. Reduced β-catenin and phosphorylated AKT following p38 inhibition further indicated its association with Wnt/β-catenin and PI3K/AKT signaling. These findings demonstrate that effective neural regeneration requires not only activation of injury-responsive signaling pathways but also their appropriate temporal regulation as the tissue progresses from proliferation toward differentiation and restoration.

Building on this temporal view of brain regeneration, the final study investigated its relationship with tumorigenesis through comparative transcriptomic analysis. Comparison of zebrafish brain regeneration at 1, 3, and 14 days post-lesion with human brain cancer revealed substantial molecular convergence during the early regenerative stages. Both processes showed activation of programs associated with proliferation, immune responses, developmental signaling, and progenitor-like cellular states. This similarity progressively declined as regeneration advanced, with a marked divergence at later stages when regenerative tissue reduced proliferative and stemness-associated programs and transitioned toward differentiation and tissue restoration. In contrast, many of these programs remained active in cancer.

Analysis of genes showing opposing temporal patterns between regeneration and cancer identified candidate regulators associated with this transition. In this context, proliferative termination refers to the coordinated exit of proliferating cells from active cell-cycle programs as regeneration progresses toward differentiation and tissue restoration, rather than simply a reduction in the overall rate of cell division. Genes associated with stemness, proliferation, mesenchymal characteristics, and cell-cycle regulation were progressively downregulated during late regeneration but remained elevated in cancer, supporting the concept that successful regeneration requires active resolution of proliferative programs.

Among the genes displaying this inverse expression pattern, FAM26F (CALHM6) emerged as a candidate regulator associated with the failure of proliferative termination in glioblastoma. Its expression decreased as regeneration progressed but remained elevated in glioblastoma, where higher expression was consistently associated with poorer survival across TCGA, GEPIA2, and CGGA datasets. Integration of FAM26F overexpression and knockout datasets further identified *Il1a*, *Egln3*, *Grm7*, and *Kalrn* as potential downstream effectors linking FAM26F with inflammatory signaling, hypoxic and metabolic adaptation, neuronal signaling, and cytoskeletal regulation. These findings provide a molecular link between the persistence of early regenerative-like programs and tumor progression and identify FAM26F as a candidate for further mechanistic investigation.

Taken together, the studies presented in this thesis highlight temporal regulation as an important feature of successful regeneration. In both liver and brain, tissue repair depends on coordinated activation of metabolic, transcriptional, signaling, and proliferative programs, together with their appropriate regulation as repair progresses. Disruption of these regulatory processes can compromise regeneration and contribute to pathological outcomes. In the liver, loss of epigenetic and metabolic coordination was associated with impaired regeneration and MAFLD-like pathology, whereas in the brain, persistence of proliferative and progenitor-associated programs distinguished tumorigenesis from the resolving regenerative response. Thus, rather than being defined solely by the presence or absence of individual pathways, regenerative and pathological outcomes appear to be strongly influenced by the timing, duration, and resolution of shared molecular programs.

Although this work identifies and functionally validates important molecular regulators of regeneration in both liver and brain, including HCF-1 and p38α MAPK, regeneration is governed by complex networks involving many additional factors. Several regulators identified through the transcriptomic, epigenomic, and network analyses presented in this thesis remain to be investigated experimentally. Further characterization of these molecules and their temporal interactions will help develop a more complete understanding of how regenerative responses are initiated, maintained, and ultimately resolved in different tissues.

The identification of FAM26F as a candidate regulator associated with proliferative persistence also provides a specific direction for future investigation. Functional perturbation of FAM26F in glioblastoma models will be required to establish its direct contribution to cell proliferation, survival, migration, and invasion. Further studies should also determine the functional

relationship between FAM26F and the identified downstream effectors *Il1a*, *Egln3*, *Grm7*, and *Kalrn*. Validation in appropriate *in vivo* models and larger clinical cohorts would further establish whether FAM26F has potential utility as a prognostic biomarker or therapeutic target in glioblastoma. Collectively, these studies would extend the observations made in this thesis and further clarify the molecular mechanisms that distinguish successful regenerative resolution from persistent pathological growth.

Bibliography

1. Gurtner GC, Werner S, Barrandon Y, Longaker MT. Wound repair and regeneration. Nature. 2008 May;453(7193):314–21.
2. Hanahan D, Weinberg RA. Hallmarks of cancer: the next generation. Cell. 2011 Mar;144(5):646–74.
3. Francoeur N, Sen R. Advances in Cardiac Development and Regeneration Using Zebrafish as a Model System for High-Throughput Research. J Dev Biol. 2021 Sep;9(4).
4. Janssens DH, Lee C-Y. It takes two to tango, a dance between the cells of origin and cancer stem cells in the Drosophila larval brain. Semin Cell Dev Biol. 2014 Apr;28:63–9.
5. Han M, Fu ML, Zhu Y, Choi AA, Li E, Bezney J, et al. Programmable control of spatial transcriptome in live cells and neurons. Nature. 2025 Jul;643(8070):241–51.
6. Zhou Y, Lin X, Jiao Y, Yang D, Li Z, Zhu L, et al. A brain-to-liver signal mediates the inhibition of liver regeneration under chronic stress in mice. Nat Commun. 2024 Nov;15(1):10361.
7. Srivastava PP, Dasari A, Kumar S, Gupta I, Jain D, Minocha S. Epigenetic co-regulator HCF-1 promotes lung cancer via O-GlcNAcylation-dependent pathways. Mol Ther Oncol. 2025 Dec;33(4):201046.
8. Diehl AM, Day C. Cause, Pathogenesis, and Treatment of Nonalcoholic Steatohepatitis. N Engl J Med. 2017 Nov;377(21):2063–72.
9. Kizil C, Kaslin J, Kroehne V, Brand M. Adult neurogenesis and brain regeneration in zebrafish. Dev Neurobiol. 2012 Mar;72(3):429–61.
10. Dvorak HF. Tumors: wounds that do not heal-redux. Cancer Immunol Res. 2015 Jan;3(1):1–11.
11. Sell S. Stem cell origin of cancer and differentiation therapy. Crit Rev Oncol Hematol. 2004 Jul;51(1):1–28.
12. Arenas Gómez CM, Echeverri K. Salamanders: The molecular basis of tissue regeneration and its relevance to human disease. Curr Top Dev Biol. 2021;145:235–75.
13. Tanaka EM, Reddien PW. The cellular basis for animal regeneration. Dev Cell. 2011 Jul;21(1):172–85.
14. Poss KD. Advances in understanding tissue regenerative capacity and mechanisms in animals. Nat Rev Genet. 2010 Oct;11(10):710–22.
15. Michalopoulos GK, Bhushan B. Liver regeneration: biological and pathological mechanisms and implications. Nat Rev Gastroenterol Hepatol. 2021 Jan;18(1):40–55.
16. Hanahan D. Hallmarks of Cancer: New Dimensions. Cancer Discov. 2022 Jan;12(1):31–46.
17. Wynn TA, Ramalingam TR. Mechanisms of fibrosis: therapeutic translation for fibrotic disease. Nat Med. 2012 Jul;18(7):1028–40.

18. Xu C, Su R, Song Y, Shu W, Yang M, Yang Z, et al. Integrating spatial transcriptomics and single-cell RNA-seq dissects immune microenvironment in fatty liver regeneration. Clin Transl Med. 2025 Jun;15(6):e70365.

19. Talman V, Ruskoaho H. Cardiac fibrosis in myocardial infarction-from repair and remodeling to regeneration. Cell Tissue Res. 2016 Sep;365(3):563–81.

20. Yassin NYS, AbouZid SF, El-Kalaawy AM, Ali TM, Almehmadi MM, Ahmed OM. Silybum marianum total extract, silymarin and silibinin abate hepatocarcinogenesis and hepatocellular carcinoma growth via modulation of the HGF/c-Met, Wnt/β-catenin, and PI3K/Akt/mTOR signaling pathways. Biomed Pharmacother. 2022 Jan;145:112409.

21. Pibiri M, Simbula G. Role of the Hippo pathway in liver regeneration and repair: recent advances. Inflamm Regen. 2022 Dec;42(1):59.

22. Michalopoulos GK. Hepatostat: Liver regeneration and normal liver tissue maintenance. Hepatology. 2017 Apr;65(4):1384–92.

23. Herranz-Itúrbide M, Peñuelas-Haro I, Espinosa-Sotelo R, Bertran E, Fabregat I. The TGF-β/NADPH Oxidases Axis in the Regulation of Liver Cell Biology in Health and Disease. Cells. 2021 Sep;10(9).

24. Forbes SJ, Newsome PN. Liver regeneration - mechanisms and models to clinical application. Nat Rev Gastroenterol Hepatol. 2016 Aug;13(8):473–85.

25. Trefts E, Gannon M, Wasserman DH. The liver. Curr Biol. 2017 Nov;27(21):R1147–51.

26. Tyagi S, Herr W. E2F1 mediates DNA damage and apoptosis through HCF-1 and the MLL family of histone methyltransferases. EMBO J [Internet]. 2009;28(20):3185–95. Available from: http://dx.doi.org/10.1038/emboj.2009.258

27. Goto H, Motomura S, Wilson AC, Freiman RN, Nakabeppu Y, Fukushima K, et al. A single-point mutation in HCF causes temperature-sensitive cell-cycle arrest and disrupts VP16 function. Genes Dev. 1997;11(6):726–37.

28. Frattini A, Faranda S, Redolfi E, Zucchi I, Villa A, Patrosso MC, et al. Genomic organization of the human VP16 accessory protein, a housekeeping gene (HCFC1) mapping to Xq28. Genomics. 1994 Sep;23(1):30–5.

29. Capotosti F, Guernier S, Lammers F, Waridel P, Cai Y, Jin J, et al. O-GlcNAc transferase catalyzes site-specific proteolysis of HCF-1. Cell. 2011;144(3):376–88.

30. Lamanilao GG, Dogan M, Patel PS, Azim S, Patel DS, Bhattacharya SK, et al. Key hepatoprotective roles of mitochondria in liver regeneration. Am J Physiol Gastrointest Liver Physiol. 2023 Mar;324(3):G207–18.

31. Zhou P, Wang Z, Yuan X, Zhou C, Liu L, Wan X, et al. Mixed lineage leukemia 5 (MLL5) protein regulates cell cycle progression and E2F1-responsive gene expression via association with host cell factor-1 (HCF-1). J Biol Chem. 2013 Jun;288(24):17532–43.

32. Dou Y, Milne TA, Tackett AJ, Smith ER, Fukuda A, Wysocka J, et al. Physical association and coordinate function of the H3 K4 methyltransferase MLL1 and the H4 K16 acetyltransferase MOF. Cell. 2005;121(6):873–85.

33. Narita T, Weinert BT, Choudhary C. Functions and mechanisms of non-histone protein acetylation. Nat Rev Mol Cell Biol. 2019 Mar;20(3):156–74.

34. Minocha S, Villeneuve D, Praz V, Moret C, Lopes M, Pinatel D, et al. Rapid Recapitulation of Nonalcoholic Steatohepatitis upon Loss of Host Cell Factor 1 Function in Mouse Hepatocytes. Mol Cell Biol. 2019;39(5).

35. Lane EA, Choi DW, Garcia-Haro L, Levine ZG, Tedoldi M, Walker S, et al. HCF-1 Regulates De Novo Lipogenesis through a Nutrient-Sensitive Complex with ChREBP. Mol Cell. 2019 Jul;75(2):357-371.e7.

36. Capotosti F, Guernier S, Lammers F, Waridel P, Cai Y, Jin J, et al. O-GlcNAc transferase catalyzes site-specific proteolysis of HCF-1. Cell [Internet]. 2011;144(3):376–88. Available from: http://dx.doi.org/10.1016/j.cell.2010.12.030

37. Bhuiyan T, Waridel P, Kapuria V, Zoete V, Herr W. Distinct OGT-Binding Sites Promote HCF-1 Cleavage. PLoS One. 2015;10(8):e0136636.

38. Daou S, Mashtalir N, Hammond-Martel I, Pak H, Yu H, Sui G, et al. Crosstalk between O-GlcNAcylation and proteolytic cleavage regulates the host cell factor-1 maturation pathway. Proc Natl Acad Sci U S A. 2011 Feb;108(7):2747–52.

39. Kapuria V, Ayushma, Herr W, Minocha S. HCF-1 as a key modulator of OGT function and O-GlcNAcylation in the liver. Sci Rep. 2025 Aug;15(1):28328.

40. Zargar ZU, Tyagi S. Role of host cell factor-1 in cell cycle regulation. Transcription. 2012;3(4):187–92.

41. Kaushal S, Bhattacharya D, Kumar S, Herr W, Dhanjal JK, Minocha S. Epigenetic modifications in the murine liver upon depletion of transcriptional coregulator host cell factor 1. BMC Genomics. 2025 Jul;26(1):654.

42. Ibrahim SH, Kohli R, Gores GJ. Mechanisms of lipotoxicity in NAFLD and clinical implications. J Pediatr Gastroenterol Nutr. 2011 Aug;53(2):131–40.

43. Younossi ZM, Henry L. The Impact of Obesity and Type 2 Diabetes on Chronic Liver Disease. Vol. 114, The American journal of gastroenterology. United States; 2019. p. 1714–5.

44. Eslam M, Newsome PN, Sarin SK, Anstee QM, Targher G, Romero-Gomez M, et al. A new definition for metabolic dysfunction-associated fatty liver disease: An international expert consensus statement. J Hepatol. 2020 Jul;73(1):202–9.

45. Berthier A, Vinod M, Porez G, Steenackers A, Alexandre J, Yamakawa N, et al. Combinatorial regulation of hepatic cytoplasmic signaling and nuclear transcriptional events by the OGT/REV-ERBα complex. Proc Natl Acad Sci U S A. 2018 Nov;115(47):E11033–42.

46. Iizuka K, Takao K, Yabe D. ChREBP-Mediated Regulation of Lipid Metabolism: Involvement of the Gut Microbiota, Liver, and Adipose Tissue. Front Endocrinol (Lausanne). 2020;11:587189.

47. Iwata TN, Cowley TJ, Sloma M, Ji Y, Kim H, Qi L, et al. The transcriptional co-regulator HCF-1 is required for INS-1 β-cell glucose-stimulated insulin secretion. PLoS One. 2013;8(11):e78841.

48. Denechaud P-D, Lopez-Mejia IC, Fajas L. [Cell cycle regulators CDK4 and E2F1 control glucose and lipid homeostasis]. Med Sci (Paris). 2016 Oct;32(10):815–8.

49. Maus M, López-Polo V, Mateo L, Lafarga M, Aguilera M, De Lama E, et al. Iron accumulation drives fibrosis, senescence and the senescence-associated secretory phenotype. Nat Metab. 2023 Dec;5(12):2111–30.

50. Ruan H Bin, Han X, Li MD, Singh JP, Qian K, Azarhoush S, et al. O-GlcNAc transferase/host cell factor C1 complex regulates gluconeogenesis by modulating PGC-1α stability. Cell Metab. 2012;16(2):226–37.

51. Moussaieff A, Rouleau M, Kitsberg D, Cohen M, Levy G, Barasch D, et al. Glycolysis-mediated changes in acetyl-CoA and histone acetylation control the early differentiation of embryonic stem cells. Cell Metab. 2015 Mar;21(3):392–402.

52. Flessa C-M, Kyrou I, Nasiri-Ansari N, Kaltsas G, Kassi E, Randeva HS. Endoplasmic reticulum stress in nonalcoholic (metabolic associated) fatty liver disease (NAFLD/MAFLD). J Cell Biochem. 2022 Oct;123(10):1585–606.

53. Flessa C-M, Nasiri-Ansari N, Kyrou I, Leca BM, Lianou M, Chatzigeorgiou A, et al. Genetic and Diet-Induced Animal Models for Non-Alcoholic Fatty Liver Disease (NAFLD) Research. Int J Mol Sci. 2022 Dec;23(24).

54. Lau JKC, Zhang X, Yu J. Animal models of non-alcoholic fatty liver disease: current perspectives and recent advances. J Pathol. 2017 Jan;241(1):36–44.

55. Holmer M, Lindqvist C, Petersson S, Moshtaghi-Svensson J, Tillander V, Brismar TB, et al. Treatment of NAFLD with intermittent calorie restriction or low-carb high-fat diet - a randomised controlled trial. JHEP reports Innov Hepatol. 2021 Jun;3(3):100256.

56. Ibrahim SH, Hirsova P, Malhi H, Gores GJ. Animal Models of Nonalcoholic Steatohepatitis: Eat, Delete, and Inflame. Dig Dis Sci. 2016 May;61(5):1325–36.

57. Miranda J, Eseberri I, Lasa A, Portillo MP. Lipid metabolism in adipose tissue and liver from diet-induced obese rats: a comparison between Wistar and Sprague-Dawley strains. J Physiol Biochem. 2018 Nov;74(4):655–66.

58. Lee L, Alloosh M, Saxena R, Van Alstine W, Watkins BA, Klaunig JE, et al. Nutritional model of steatohepatitis and metabolic syndrome in the Ossabaw miniature swine. Hepatology. 2009 Jul;50(1):56–67.

59. Goessling W, Sadler KC. Zebrafish: an important tool for liver disease research. Gastroenterology. 2015 Nov;149(6):1361–77.

60. Ma J, Deng Y, Yang T, Li M, Shang J. Esculetin Alleviates Nonalcoholic Fatty Liver Disease on High-Cholesterol-Diet-Induced Larval Zebrafish and FFA-Induced BRL-3A Hepatocyte. Int J Mol Sci. 2023 Jan;24(2).

61. Li X, Zhou L, Zheng Y, He T, Guo H, Li J, et al. Establishment of a non-alcoholic fatty liver disease model by high fat diet in adult zebrafish. Anim Model Exp Med. 2024 Dec;7(6):904–13.

62. Michalopoulos GK. Advances in liver regeneration. Expert Rev Gastroenterol Hepatol. 2014;8(8):897–907.

63. Marques IJ, Lupi E, Mercader N. Model systems for regeneration: zebrafish.

Development. 2019 Sep;146(18).

64. Ghaddar B, Lübke L, Couret D, Rastegar S, Diotel N. Cellular Mechanisms Participating in Brain Repair of Adult Zebrafish and Mammals after Injury. Cells. 2021 Feb;10(2).

65. Chen J, Sanchez-Iranzo H, Diotel N, Rastegar S. Comparative insight into the regenerative mechanisms of the adult brain in zebrafish and mouse: highlighting the importance of the immune system and inflammation in successful regeneration. FEBS J. 2024 Oct;291(19):4193–205.

66. Otsuki L, Brand AH. Quiescent Neural Stem Cells for Brain Repair and Regeneration: Lessons from Model Systems. Trends Neurosci. 2020 Apr;43(4):213–26.

67. Ghosh S, Hui SP. Regeneration of Zebrafish CNS: Adult Neurogenesis. Neural Plast. 2016;2016:5815439.

68. Chapouton P, Skupien P, Hesl B, Coolen M, Moore JC, Madelaine R, et al. Notch activity levels control the balance between quiescence and recruitment of adult neural stem cells. J Neurosci Off J Soc Neurosci. 2010 Jun;30(23):7961–74.

69. Palsamy K, Chen JY, Skaggs K, Qadeer Y, Connors M, Cutler N, et al. Microglial depletion after brain injury prolongs inflammation and impairs brain repair, adult neurogenesis and pro-regenerative signaling. Glia. 2023 Nov;71(11):2642–63.

70. Zupanc GKH. Neurogenesis and neuronal regeneration in the adult fish brain. J Comp Physiol A, Neuroethol sensory, neural, Behav Physiol. 2006 Jun;192(6):649–70.

71. März M, Schmidt R, Rastegar S, Strähle U. Regenerative response following stab injury in the adult zebrafish telencephalon. Dev Dyn an Off Publ Am Assoc Anat. 2011 Sep;240(9):2221–31.

72. Kase Y, Otsu K, Shimazaki T, Okano H. Involvement of p38 in Age-Related Decline in Adult Neurogenesis via Modulation of Wnt Signaling. Stem cell reports. 2019 Jun;12(6):1313–28.

73. Asih PR, Prikas E, Stefanoska K, Tan ARP, Ahel HI, Ittner A. Functions of p38 MAP Kinases in the Central Nervous System. Front Mol Neurosci. 2020;13:570586.

74. D'Mello SR. When Good Kinases Go Rogue: GSK3, p38 MAPK and CDKs as Therapeutic Targets for Alzheimer's and Huntington's Disease. Int J Mol Sci. 2021 May;22(11).

75. Schäfer M, Werner S. Cancer as an overhealing wound: an old hypothesis revisited. Nat Rev Mol Cell Biol. 2008 Aug;9(8):628–38.

76. Dvorak HF. Tumors: wounds that do not heal. Similarities between tumor stroma generation and wound healing. N Engl J Med. 1986 Dec;315(26):1650–9.

77. Yun MH, Gates PB, Brockes JP. Regulation of p53 is critical for vertebrate limb regeneration. Proc Natl Acad Sci U S A. 2013 Oct;110(43):17392–7.

78. Molchadsky A, Rivlin N, Brosh R, Rotter V, Sarig R. p53 is balancing development, differentiation and de-differentiation to assure cancer prevention. Carcinogenesis. 2010 Sep;31(9):1501–8.

79. Giakoustidis A, Giakoustidis D, Mudan S, Sklavos A, Williams R. Molecular signalling in hepatocellular carcinoma: Role of and crosstalk among WNT/ß-catenin, Sonic

Hedgehog, Notch and Dickkopf-1. Can J Gastroenterol Hepatol. 2015 May;29(4):209–17.

80. Li X, Ortiz MA, Kotula L. The physiological role of Wnt pathway in normal development and cancer. Exp Biol Med (Maywood). 2020 Mar;245(5):411–26.

81. Manfioletti G, Fedele M. Epithelial-Mesenchymal Transition (EMT). Vol. 24, International journal of molecular sciences. Switzerland; 2023.

82. Almstedt E, Rosén E, Gloger M, Stockgard R, Hekmati N, Koltowska K, et al. Real-time evaluation of glioblastoma growth in patient-specific zebrafish xenografts. Neuro Oncol. 2022 May;24(5):726–38.

83. Carén H, Stricker SH, Bulstrode H, Gagrica S, Johnstone E, Bartlett TE, et al. Glioblastoma Stem Cells Respond to Differentiation Cues but Fail to Undergo Commitment and Terminal Cell-Cycle Arrest. Stem cell reports. 2015 Nov;5(5):829–42.

84. Vander Heiden MG, Cantley LC, Thompson CB. Understanding the Warburg effect: the metabolic requirements of cell proliferation. Science. 2009 May;324(5930):1029–33.

85. Demirci Y, Heger G, Katkat E, Papatheodorou I, Brazma A, Ozhan G. Brain Regeneration Resembles Brain Cancer at Its Early Wound Healing Stage and Diverges From Cancer Later at Its Proliferation and Differentiation Stages. Front cell Dev Biol. 2022;10:813314.

86. Piccirillo SGM, Reynolds BA, Zanetti N, Lamorte G, Binda E, Broggi G, et al. Bone morphogenetic proteins inhibit the tumorigenic potential of human brain tumour-initiating cells. Nature. 2006 Dec;444(7120):761–5.

87. Li A, Wang R, Zhao Y, Zhao P, Yang J. Crosstalk between Epigenetics and Metabolic Reprogramming in Metabolic Dysfunction-Associated Steatotic Liver Disease-Induced Hepatocellular Carcinoma: A New Sight. Metabolites. 2024 Jun;14(6).

88. Shi L, Chen H, Zhang Y, An D, Qin M, Yu W, et al. SLC13A2 promotes hepatocyte metabolic remodeling and liver regeneration by enhancing de novo cholesterol biosynthesis. EMBO J. 2025 Mar;44(5):1442–63.

89. Berumen J, Baglieri J, Kisseleva T, Mekeel K. Liver fibrosis: Pathophysiology and clinical implications. WIREs Mech Dis. 2021 Jan;13(1):e1499.

90. Baffy G. Kupffer cells in non-alcoholic fatty liver disease: the emerging view. J Hepatol. 2009 Jul;51(1):212–23.

91. Puche JE, Saiman Y, Friedman SL. Hepatic stellate cells and liver fibrosis. Compr Physiol. 2013 Oct;3(4):1473–92.

92. Kristie TM. The mouse homologue of the human transcription factor C1 (host cell factor). Conservation of forms and function. J Biol Chem. 1997;272(42):26749–55.

93. Kapuria V, Röhrig UF, Waridel P, Lammers F, Borodkin VS, Van Aalten DMF, et al. The conserved threonine-rich region of the HCF-1PRO repeat activates promiscuous OGT:UDP-GlcNAc glycosylation and proteolysis activities. J Biol Chem [Internet]. 2018;293(46):17754–68. Available from: http://dx.doi.org/10.1074/jbc.RA118.004185

94. Bhuiyan T, Waridel P, Kapuria V, Zoete V, Herr W. Distinct OGT-binding sites promote

HCF-1 cleavage. PLoS One. 2015;10(8):1–24.

95. Liang Y, Quenelle D, Vogel JL, Mascaro C, Ortega A, Kristie TM. A novel selective LSD1/KDM1A inhibitor epigenetically blocks herpes simplex virus lytic replication and reactivation from latency. MBio. 2013;4(1).

96. Liang Y, Vogel JL, Narayanan A, Peng H, Kristie TM. Inhibition of the histone demethylase LSD1 blocks α-herpesvirus lytic replication and reactivation from latency. Nat Med. 2009;15(11):1312–7.

97. Liu W, Tanasa B, Tyurina O V., Zhou TY, Gassmann R, Liu WT, et al. PHF8 mediates histone H4 lysine 20 demethylation events involved in cell cycle progression. Nature [Internet]. 2010;466(7305):508–12. Available from: http://dx.doi.org/10.1038/nature09272

98. Yokoyama A, Wang Z, Wysocka J, Sanyal M, Aufiero DJ, Kitabayashi I, et al. Leukemia Proto-Oncoprotein MLL Forms a SET1 like Complex with Menin to Regulate Hox Gene Expression. Blood. 2004;104(11):2550–2550.

99. Smith ER, Cayrou C, Huang R, Lane WS, Côté J, Lucchesi JC. A Human Protein Complex Homologous to the Drosophila MSL Complex Is Responsible for the Majority of Histone H4 Acetylation at Lysine 16 . Mol Cell Biol. 2005;25(21):9175–88.

100. Machida YJ, Machida Y, Vashisht AA, Wohlschlegel JA, Dutta A. The deubiquitinating enzyme BAP1 regulates cell growth via interaction with HCF-1. J Biol Chem. 2009;284(49):34179–88.

101. Mangone M, Myers MP, Herr W. Role of the HCF-1 basic region in sustaining cell proliferation. PLoS One. 2010;5(2):1–9.

102. Lane EA, Choi DW, Garcia-Haro L, Levine ZG, Tedoldi M, Walker S, et al. HCF-1 Regulates De Novo Lipogenesis through a Nutrient-Sensitive Complex with ChREBP. Mol Cell [Internet]. 2019;75(2):357-371.e7. Available from: https://doi.org/10.1016/j.molcel.2019.05.019

103. Dejosez M, Krumenacker JS, Zitur LJ, Passeri M, Chu LF, Songyang Z, et al. Ronin Is Essential for Embryogenesis and the Pluripotency of Mouse Embryonic Stem Cells. Cell. 2008;133(7):1162–74.

104. Minocha S, Sung TL, Villeneuve D, Lammers F, Herr W. Compensatory embryonic response to allele-specific inactivation of the murine X-linked gene *Hcfc1*. Dev Biol [Internet]. 2016;412(1):1–17. Available from: http://dx.doi.org/10.1016/j.ydbio.2016.02.019

105. Yu HC, Sloan JL, Scharer G, Brebner A, Quintana AM, Achilly NP, et al. An X-linked cobalamin disorder caused by mutations in transcriptional coregulator HCFC1. Am J Hum Genet [Internet]. 2013;93(3):506–14. Available from: http://dx.doi.org/10.1016/j.ajhg.2013.07.022

106. Jolly LA, Nguyen LS, Domingo D, Sun Y, Barry S, Hancarova M, et al. HCFC1 loss-of-function mutations disrupt neuronal and neural progenitor cells of the developing brain. Hum Mol Genet. 2015;24(12):3335–47.

107. Dheekollu J, Wiedmer A, Sentana-Lledo D, Cassel J, Messick T, Lieberman PM. HCF1 and OCT2 Cooperate with EBNA1 To Enhance OriP-Dependent Transcription and Episome Maintenance of Latent Epstein-Barr Virus. J Virol. 2016 Jun;90(11):5353–67.

108. Le Martelot G, Canella D, Symul L, Migliavacca E, Gilardi F, Liechti R, et al. Genome-Wide RNA Polymerase II Profiles and RNA Accumulation Reveal Kinetics of Transcription and Associated Epigenetic Changes During Diurnal Cycles. PLoS Biol. 2012;10(11).

109. Wilson AC, LaMarco K, Peterson MG, Herr W. The VP16 accessory protein HCF is a family of polypeptides processed from a large precursor protein. Cell. 1993;74(1):115–25.

110. Krueger F, Galore T. Babraha. bioinformatics - trim galore! [Internet]. Available from: https://www.bioinformatics.babraham.ac.uk/projects/trim_galore/

111. Babraham Bioinformatics - FastQC A Quality Control tool for High Throughput Sequence Data [Internet]. [cited 2024 Jun 26]. Available from: https://www.bioinformatics.babraham.ac.uk/projects/fastqc/

112. Dobin A, Davis CA, Schlesinger F, Drenkow J, Zaleski C, Jha S, et al. STAR: ultrafast universal RNA-seq aligner. Bioinformatics. 2013 Jan;29(1):15–21.

113. Amemiya HM, Kundaje A, Boyle AP. The ENCODE Blacklist: Identification of Problematic Regions of the Genome. Sci Rep. 2019 Jun;9(1):9354.

114. Zhang Y, Liu T, Meyer CA, Eeckhoute J, Johnson DS, Bernstein BE, et al. Model-based analysis of ChIP-Seq (MACS). Genome Biol. 2008;9(9):R137.

115. Quinlan AR, Hall IM. BEDTools: a flexible suite of utilities for comparing genomic features. Bioinformatics. 2010 Mar;26(6):841–2.

116. Dennis GJ, Sherman BT, Hosack DA, Yang J, Gao W, Lane HC, et al. DAVID: Database for Annotation, Visualization, and Integrated Discovery. Genome Biol. 2003;4(5):P3.

117. Michaud J, Praz V, James Faresse N, Jnbaptiste CK, Tyagi S, Schütz F, et al. HCFC1 is a common component of active human CpG-island promoters and coincides with ZNF143, THAP11, YY1, and GABP transcription factor occupancy. Genome Res. 2013 Jun;23(6):907–16.

118. Parker JB, Yin H, Vinckevicius A, Chakravarti D. Host cell factor-1 recruitment to E2F-bound and cell-cycle-control genes is mediated by THAP11 and ZNF143. Cell Rep. 2014 Nov;9(3):967–82.

119. Lesurf R, Cotto KC, Wang G, Griffith M, Kasaian K, Jones SJM, et al. ORegAnno 3.0: a community-driven resource for curated regulatory annotation. Nucleic Acids Res. 2016 Jan;44(D1):D126-32.

120. Dejosez M, Levine SS, Frampton GM, Whyte WA, Stratton SA, Barton MC, et al. Ronin/Hcf-1 binds to a hyperconserved enhancer element and regulates genes involved in the growth of embryonic stem cells. Genes Dev. 2010 Jul;24(14):1479–84.

121. Blanc V, Sessa KJ, Kennedy S, Luo J, Davidson NO. Apobec-1 complementation factor modulates liver regeneration by post-transcriptional regulation of interleukin-6 mRNA stability. J Biol Chem. 2010;285(25):19184–92.

122. Kanchev I, Gregor M. Original Article ADAM10 / 17-Dependent Release of Soluble c-Met Correlates with Hepatocellular Damage. 2013;86:76–86.

123. Dong H-M, Xu C-S. Analysis of the relevance of e2fs and their target genes with rat liver regeneration. Vol. 27, Indian journal of gastroenterology: official journal of the Indian Society of Gastroenterology. India; 2008. p. 31–2.

124. Natarajan A, Wagner B, Sibilia M. The EGF receptor is required for efficient liver regeneration. Proc Natl Acad Sci U S A. 2007;104(43):17081–6.

125. Kurinna S, Stratton SA, Tsai WW, Akdemir KC, Gu W, Singh P, et al. Direct activation of forkhead box O3 by tumor suppressors p53 and p73 is disrupted during liver regeneration in mice. Hepatology. 2010;52(3):1023–32.

126. Bard-Chapeau EA, Yuan J, Droin N, Long S, Zhang EE, Nguyen T V., et al. Concerted Functions of Gab1 and Shp2 in Liver Regeneration and Hepatoprotection. Mol Cell Biol. 2006;26(12):4664–74.

127. Zerrad-Saadi A, Lambert-Blot M, Mitchell C, Bretes H, De L'Hortet AC, Baud V, et al. GH receptor plays a major role in liver regeneration through the control of EGFR and ERK1/2 activation. Endocrinology. 2011;152(7):2731–41.

128. Behrens A, Sibilia M, David JP, Möhle-Steinlein U, Tronche F, Schütz G, et al. Impaired postnatal hepatocyte proliferation and liver regeneration in mice lacking c-jun in the liver. EMBO J. 2002;21(7):1782–90.

129. Chou CH, Lai SL, Chen CN, Lee PH, Peng FC, Kuo ML, et al. IL-6 Regulates Mcl-1L Expression through the JAK/PI3K/Akt/CREB Signaling Pathway in Hepatocytes: Implication of an Anti-Apoptotic Role during Liver Regeneration. PLoS One. 2013;8(6).

130. Pierre KB, Jones CM, Pierce JM, Nicoud IB, Earl TM, Chari RS. NFAT4 Deficiency Results in Incomplete Liver Regeneration Following Partial Hepatectomy. J Surg Res. 2009;154(2):226–33.

131. Dayoub R, Vogel A, Schuett J, Lupke M, Spieker SM, Kettern N, et al. Nrf2 activates augmenter of liver regeneration (ALR) via antioxidant response element and links oxidative stress to liver regeneration. Mol Med. 2013;19(1):237–44.

132. Zhu R, Tu Y, Chang J, Xu H, Li JC, Liu W, et al. The Orphan Nuclear Receptor Gene NR0B2 Is a Favorite Prognosis Factor Modulated by Multiple Cellular Signal Pathways in Human Liver Cancers. Front Oncol. 2021;11(May):1–12.

133. Tan Y, Yoshida Y, Hughes DE, Costa RH. Increased Expression of Hepatocyte Nuclear Factor 6 Stimulates Hepatocyte Proliferation During Mouse Liver Regeneration. Gastroenterology. 2006;130(4):1283–300.

134. Haga S, Ozaki M, Inoue H, Okamoto Y, Ogawa W, Takeda K, et al. The survival pathways phosphatidylinositol-3 kinase (PI3-K)/phosphoinositide-dependent protein kinase 1 (PDK1)/Akt modulate liver regeneration through hepatocyte size rather than proliferation. Hepatology. 2009;49(1):204–14.

135. Kawao N, Okada K, Kawata S, Okamoto C, Tsuritani M, Ueshima S, et al. Plasmin decreases the BH3-only protein BimEL via the ERK1/2 signaling pathway in hepatocytes. Biochim Biophys Acta - Mol Cell Res. 2007;1773(6):718–27.

136. Anderson SP, Yoon L, Richard EB, Dunn CS, Cattley RC, Corton JC. Delayed liver regeneration in peroxisome proliferator-activated receptor-α-null mice. Hepatology. 2002;36(3):544–54.

137. Li B, Cai SY, Boyer JL. The role of the retinoid receptor, RAR/RXR heterodimer, in liver physiology. Biochim Biophys Acta - Mol Basis Dis. 2021;1867(5):166085.

138. Sun R, Jaruga B, Kulkarni S, Sun H, Gao B. IL-6 modulates hepatocyte proliferation via induction of HGF/p21 cip1: Regulation by SOCS3. Biochem Biophys Res Commun. 2005;338(4):1943–9.

139. Tsuchiya S, Tsukamoto Y, Taira E, LaMarre J. Involvement of transforming growth factor-β in the expression of gicerin, a cell adhesion molecule, in the regeneration of hepatocytes. Int J Mol Med. 2007;19(3):381–6.

140. Kwon HJ, Won YS, Yoon YD, Yoon WK, Nam KH, Choi IP, et al. Vitamin D3 up-regulated protein 1 deficiency accelerates liver regeneration after partial hepatectomy in mice. J Hepatol. 2011;54(6):1168–76.

141. Wang GQ, Chen QM, Minuk GY, Gong Y, Burczynski FJ. Enhanced expression of cytosolic fatty acid binding protein and fatty acid uptake during liver regeneration in rats. Mol Cell Biochem. 2004;262(1–2):41–9.

142. Schuchmann M, Rückert F, Garcia-Lazaro JF, Karg A, Burg J, Knorr N, et al. MORT1/FADD is involved in liver regeneration. World J Gastroenterol. 2005;11(46):7248–53.

143. Dai G, He L, Bu P, Wan YJY. Pregnane X receptor is essential for normal progression of liver regeneration. Hepatology. 2008;47(4):1277–87.

144. Minocha S, Sung TL, Villeneuve D, Lammers F, Herr W. Compensatory embryonic response to allele-specific inactivation of the murine X-linked gene *Hcfc1*. Dev Biol. 2016;412(1):1–17.

145. Byrne CD, Targher G. NAFLD: A multisystem disease. J Hepatol [Internet]. 2015;62(S1):S47–64. Available from: http://dx.doi.org/10.1016/j.jhep.2014.12.012

146. Hardy T, Oakley F, Anstee QM, Day CP. Nonalcoholic Fatty Liver Disease: Pathogenesis and Disease Spectrum. Annu Rev Pathol Mech Dis. 2016;11:451–96.

147. Teng MLP, Ng CH, Huang DQ, Chan KE, Tan DJH, Lim WH, et al. Global incidence and prevalence of nonalcoholic fatty liver disease. Clin Mol Hepatol. 2023;29(supp1):32–42.

148. Fausto N, Campbell JS, Riehle KJ. Liver regeneration. Hepatology. 2006;43(2 SUPPL. 1):45–53.

149. Michalopoulos GK. Liver regeneration after partial hepatectomy: Critical analysis of mechanistic dilemmas. Am J Pathol [Internet]. 2010;176(1):2–13. Available from: http://dx.doi.org/10.2353/ajpath.2010.090675

150. Forbes SJ, Newsome PN. Liver regeneration-mechanisms and models to clinical application. Nat Rev Gastroenterol Hepatol. 2016;13(8):473–85.

151. Taub R. Liver regeneration: From myth to mechanism. Nat Rev Mol Cell Biol. 2004;5(10):836–47.

152. Arechederra M, Berasain C, Avila MA, Fernández-Barrena MG. Chromatin dynamics during liver regeneration. Semin Cell Dev Biol [Internet]. 2020;97(December 2018):38–46. Available from: https://doi.org/10.1016/j.semcdb.2019.03.004

153. Bangru S, Kalsotra A. Cellular and molecular basis of liver regeneration. Semin Cell Dev Biol [Internet]. 2020;100(November):74–87. Available from: https://doi.org/10.1016/j.semcdb.2019.12.004

154. Tirnitz-Parker JEE, Viebahn CS, Jakubowski A, Klopcic BRS, Olynyk JK, Yeoh GCT, et al. Tumor necrosis factor-like weak inducer of apoptosis is a mitogen for liver progenitor cells. Hepatology. 2010;52(1):291–302.

155. Kumar R. Hard clinical outcomes in patients with NAFLD. Hepatol Int. 2013;7(2013):S790–9.

156. Germani G, Laryea M, Rubbia-Brandt L, Egawa H, Burra P, O'Grady J, et al. Management of Recurrent and de Novo NAFLD/NASH after Liver Transplantation. Transplantation. 2019;103(1):57–67.

157. Moghadam AD, Eslami P, Razavi-Khorasani N, Moazzami B, Zahedi-Tajrishi F, Farokhi E, et al. Recurrence of fatty liver disease following liver transplantation for nafld-related cirrhosis: Current status and challenges. Casp J Intern Med. 2020;11(4):346–54.

158. Tyagi S, Chabes AL, Wysocka J, Herr W. E2F Activation of S Phase Promoters via Association with HCF-1 and the MLL Family of Histone H3K4 Methyltransferases. Mol Cell. 2007;27(1):107–19.

159. Zargar ZU, Tyagi S. Role of host cell factor-1 in cell cycle regulation. Transcription. 2012;3(4).

160. Tyagi S, Herr W. E2F1 mediates DNA damage and apoptosis through HCF-1 and the MLL family of histone methyltransferases. EMBO J. 2009;28(20):3185–95.

161. Liang H, Ward WF. PGC-1α: A key regulator of energy metabolism. Vol. 30, American Journal of Physiology - Advances in Physiology Education. 2006. p. 145–51.

162. Wysocka J, Myers MP, Laherty CD, Eisenman RN, Herr W. Human Sin3 deacetylase and trithorax-related Set1/Ash2 histone H3-K4 methyltransferase are tethered together selectively by the cell-proliferation factor HCF-1. Genes Dev. 2003;17(7):896–911.

163. Liu W, Tanasa B, Tyurina O V., Zhou TY, Gassmann R, Liu WT, et al. PHF8 mediates histone H4 lysine 20 demethylation events involved in cell cycle progression. Nature. 2010;466(7305):508–12.

164. Narayanan A, Ruyechan WT, Kristie TM. The coactivator host cell factor-1 mediates Set1 and MLL1 H3K4 trimethylation at herpesvirus immediate early promoters for initiation of infection. Proc Natl Acad Sci U S A. 2007;104(26):10835–40.

165. Brown GT, Kleiner DE. Histopathology of nonalcoholic fatty liver disease and nonalcoholic steatohepatitis. Metabolism. 2016 Aug;65(8):1080–6.

166. Brunt EM. Pathology of nonalcoholic fatty liver disease. Nat Rev Gastroenterol Hepatol. 2010 Apr;7(4):195–203.

167. Lazarus J V, Colombo M, Cortez-Pinto H, Huang TT-K, Miller V, Ninburg M, et al. NAFLD - sounding the alarm on a silent epidemic. Nat Rev Gastroenterol Hepatol. 2020 Jul;17(7):377–9.

168. Hardy T, Oakley F, Anstee QM, Day CP. Nonalcoholic Fatty Liver Disease:

Pathogenesis and Disease Spectrum. Annu Rev Pathol. 2016 May;11:451–96.

169. Rinella ME. Nonalcoholic fatty liver disease: a systematic review. JAMA. 2015 Jun;313(22):2263–73.

170. Browning JD, Horton JD. Molecular mediators of hepatic steatosis and liver injury. J Clin Invest. 2004 Jul;114(2):147–52.

171. Byrne CD, Targher G. NAFLD: a multisystem disease. J Hepatol. 2015 Apr;62(1 Suppl):S47-64.

172. Powell EE, Wong VW-S, Rinella M. Non-alcoholic fatty liver disease. Lancet (London, England). 2021 Jun;397(10290):2212–24.

173. Teng ML, Ng CH, Huang DQ, Chan KE, Tan DJ, Lim WH, et al. Global incidence and prevalence of nonalcoholic fatty liver disease. Clin Mol Hepatol. 2023 Feb;29(Suppl):S32–42.

174. Matsuzawa N, Takamura T, Kurita S, Misu H, Ota T, Ando H, et al. Lipid-induced oxidative stress causes steatohepatitis in mice fed an atherogenic diet. Hepatology. 2007 Nov;46(5):1392–403.

175. Gao D, Wei C, Chen L, Huang J, Yang S, Diehl AM. Oxidative DNA damage and DNA repair enzyme expression are inversely related in murine models of fatty liver disease. Am J Physiol Gastrointest Liver Physiol. 2004 Nov;287(5):G1070-7.

176. Asgharpour A, Cazanave SC, Pacana T, Seneshaw M, Vincent R, Banini BA, et al. A diet-induced animal model of non-alcoholic fatty liver disease and hepatocellular cancer. J Hepatol. 2016 Sep;65(3):579–88.

177. Oka T, Nishimura Y, Zang L, Hirano M, Shimada Y, Wang Z, et al. Diet-induced obesity in zebrafish shares common pathophysiological pathways with mammalian obesity. BMC Physiol. 2010 Oct;10:21.

178. Schlegel A. Studying non-alcoholic fatty liver disease with zebrafish: a confluence of optics, genetics, and physiology. Cell Mol Life Sci. 2012 Dec;69(23):3953–61.

179. Wang S, Miller SR, Ober EA, Sadler KC. Making It New Again: Insight Into Liver Development, Regeneration, and Disease From Zebrafish Research. Curr Top Dev Biol. 2017;124:161–95.

180. Quinlivan VH, Farber SA. Lipid Uptake, Metabolism, and Transport in the Larval Zebrafish. Front Endocrinol (Lausanne). 2017;8:319.

181. Shimizu N, Shiraishi H, Hanada T. Zebrafish as a Useful Model System for Human Liver Disease. Cells. 2023 Sep;12(18).

182. Chang C, Li H, Zhang R. Zebrafish facilitate non-alcoholic fatty liver disease research: Tools, models and applications. Liver Int Off J Int Assoc Study Liver. 2023 Jul;43(7):1385–98.

183. Asaoka Y, Terai S, Sakaida I, Nishina H. The expanding role of fish models in understanding non-alcoholic fatty liver disease. Dis Model Mech. 2013 Jul;6(4):905–14.

184. Wang Y, Qian Y, Fang Q, Zhong P, Li W, Wang L, et al. Saturated palmitic acid induces myocardial inflammatory injuries through direct binding to TLR4 accessory protein

MD2. Nat Commun. 2017 Jan;8:13997.

185. Marra F, Svegliati-Baroni G. Lipotoxicity and the gut-liver axis in NASH pathogenesis. J Hepatol. 2018 Feb;68(2):280–95.

186. Hernández EÁ, Kahl S, Seelig A, Begovatz P, Irmler M, Kupriyanova Y, et al. Acute dietary fat intake initiates alterations in energy metabolism and insulin resistance. J Clin Invest. 2017 Feb;127(2):695–708.

187. Liao Y, Smyth GK, Shi W. featureCounts: an efficient general purpose program for assigning sequence reads to genomic features. Bioinformatics. 2014 Apr;30(7):923–30.

188. Szklarczyk D, Kirsch R, Koutrouli M, Nastou K, Mehryary F, Hachilif R, et al. The STRING database in 2023: protein-protein association networks and functional enrichment analyses for any sequenced genome of interest. Nucleic Acids Res. 2023 Jan;51(D1):D638–46.

189. Arguello G, Balboa E, Arrese M, Zanlungo S. Recent insights on the role of cholesterol in non-alcoholic fatty liver disease. Biochim Biophys Acta. 2015 Sep;1852(9):1765–78.

190. Min H-K, Kapoor A, Fuchs M, Mirshahi F, Zhou H, Maher J, et al. Increased hepatic synthesis and dysregulation of cholesterol metabolism is associated with the severity of nonalcoholic fatty liver disease. Cell Metab. 2012 May;15(5):665–74.

191. Mota M, Banini BA, Cazanave SC, Sanyal AJ. Molecular mechanisms of lipotoxicity and glucotoxicity in nonalcoholic fatty liver disease. Metabolism. 2016 Aug;65(8):1049–61.

192. Dabravolski SA, Bezsonov EE, Orekhov AN. The role of mitochondria dysfunction and hepatic senescence in NAFLD development and progression. Biomed Pharmacother. 2021 Oct;142:112041.

193. Yi HS. Implications of Mitochondrial Unfolded Protein Response and Mitokines: A Perspective on Fatty Liver Diseases. Endocrinol Metab (Seoul, Korea). 2019 Mar;34(1):39–46.

194. Petrescu M, Vlaicu SI, Ciumărnean L, Milaciu MV, Mărginean C, Florea M, et al. Chronic Inflammation-A Link between Nonalcoholic Fatty Liver Disease (NAFLD) and Dysfunctional Adipose Tissue. Medicina (Kaunas). 2022 May;58(5).

195. Chen Z, Tian R, She Z, Cai J, Li H. Role of oxidative stress in the pathogenesis of nonalcoholic fatty liver disease. Free Radic Biol Med. 2020 May;152:116–41.

196. Wang S, Sheng F, Zou L, Xiao J, Li P. Hyperoside attenuates non-alcoholic fatty liver disease in rats via cholesterol metabolism and bile acid metabolism. J Adv Res. 2021 Dec;34:109–22.

197. Shi L, Guo S, Zhang S, Gao X, Liu A, Wang Q, et al. Glycyrrhetinic acid attenuates disturbed vitamin a metabolism in non-alcoholic fatty liver disease through AKR1B10. Eur J Pharmacol. 2020 Sep;883:173167.

198. Perez-Robles M, Campos-Perez W, Rivera-Valdés JJ, Franco-Topete RA, Navarrete-Medina EM, Maldonado-González M, et al. Elevated Serum Low-Density Lipoproteins-Cholesterol Levels and B1B2/B2B2 CETP Genotype Are Positively Associated with Nonalcoholic Fatty Liver Disease in Women with Gallstone Disease. Metab Syndr Relat Disord. 2023 Feb;21(1):41–7.

199. Park K-H, Ye Z-W, Zhang J, Kim S-H. Palmitic Acid-Enriched Diet Induces Hepatic Steatosis and Injury in Adult Zebrafish. Zebrafish. 2019 Dec;16(6):497–504.

200. Nasiri-Ansari N, Nikolopoulou C, Papoutsi K, Kyrou I, Mantzoros CS, Kyriakopoulos G, et al. Empagliflozin Attenuates Non-Alcoholic Fatty Liver Disease (NAFLD) in High Fat Diet Fed ApoE((-/-)) Mice by Activating Autophagy and Reducing ER Stress and Apoptosis. Int J Mol Sci. 2021 Jan;22(2).

201. Hodson L, Brouwers MCGJ. Non-alcoholic fatty liver disease concerns with glucokinase activators. Vol. 6, The lancet. Diabetes & endocrinology. England; 2018. p. 684–5.

202. Zhang X, Zhang X, Jiang D, Zheng W, Wang H, Tian Y, et al. INHA acts as a novel and potential biomarker in lung adenocarcinoma and shapes the immune-suppressive tumor microenvironment. Transl Oncol. 2023 Jul;33:101679.

203. Looyenga BD, Wiater E, Vale W, Hammer GD. Inhibin-A antagonizes TGFbeta2 signaling by down-regulating cell surface expression of the TGFbeta coreceptor betaglycan. Mol Endocrinol. 2010 Mar;24(3):608–20.

204. Evans ET, Horst B, Arend RC, Mythreye K. Evolving roles of activins and inhibins in ovarian cancer pathophysiology. Am J Physiol Cell Physiol. 2023 Feb;324(2):C428–37.

205. Zhu L, Luu T, Emfinger CH, Parks BA, Shi J, Trefts E, et al. CETP Inhibition Improves HDL Function but Leads to Fatty Liver and Insulin Resistance in CETP-Expressing Transgenic Mice on a High-Fat Diet. Diabetes. 2018 Dec;67(12):2494–506.

206. Nakayama M, Matsumoto K, Tatsumi N, Yanai M, Yokouchi Y. Id3 is important for proliferation and differentiation of the hepatoblasts during the chick liver development. Mech Dev. 2006 Jul;123(7):580–90.

207. Pan C, Liu J, Gao Y, Yang M, Hu H, Liu C, et al. Hepatocyte CHRNA4 mediates the MASH-promotive effects of immune cell-produced acetylcholine and smoking exposure in mice and humans. Cell Metab. 2023 Dec;35(12):2231-2249.e7.

208. Vicente JB, Guerreiro ACL, Felgueiras B, Chapla D, Tehrani D, Moremen KW, et al. Glycosyltransferase 8 domain-containing protein 1 (GLT8D1) is a UDP-dependent galactosyltransferase. Sci Rep. 2023 Dec;13(1):21684.

209. Viloria K, Nasteska D, Briant LJB, Heising S, Larner DP, Fine NHF, et al. Vitamin-D-Binding Protein Contributes to the Maintenance of α Cell Function and Glucagon Secretion. Cell Rep. 2020 Jun;31(11):107761.

210. Hachero-Cruzado I, Rodríguez-Rua A, Román-Padilla J, Ponce M, Fernández-Díaz C, Manchado M. Characterization of the genomic responses in early Senegalese sole larvae fed diets with different dietary triacylglycerol and total lipids levels. Comp Biochem Physiol Part D Genomics Proteomics. 2014 Dec;12:61–73.

211. Chalhoub G, Jamnik A, Pajed L, Kolleritsch S, Hois V, Bagaric A, et al. Carboxylesterase 2a deletion provokes hepatic steatosis and insulin resistance in mice involving impaired diacylglycerol and lysophosphatidylcholine catabolism. Mol Metab. 2023 Jun;72:101725.

212. Pusec CM, Ilievski V, De Jesus A, Farooq Z, Zapater JL, Sweis N, et al. Liver-specific overexpression of HKDC1 increases hepatocyte size and proliferative capacity. Sci Rep. 2023 May;13(1):8034.

213. Agius L. Hormonal and Metabolite Regulation of Hepatic Glucokinase. Annu Rev Nutr. 2016 Jul;36:389–415.

214. Wang K, Fang S, Liu Q, Gao J, Wang X, Zhu H, et al. TGF-β1/p65/MAT2A pathway regulates liver fibrogenesis via intracellular SAM. EBioMedicine. 2019 Apr;42:458–69.

215. Leung IC-Y, Chong CC-N, Cheung TT, Yeung PC, Ng KK-C, Lai PB-S, et al. Genetic variation in ABCB5 associates with risk of hepatocellular carcinoma. J Cell Mol Med. 2020 Sep;24(18):10705–13.

216. Rong M-H, Li J-D, Zhong L-Y, Huang Y-Z, Chen J, Xie L-Y, et al. CCNB1 promotes the development of hepatocellular carcinoma by mediating DNA replication in the cell cycle. Exp Biol Med (Maywood). 2022 Mar;247(5):395–408.

217. Chiu Y-T, Husain A, Sze KM-F, Ho DW-H, Suarez EMS, Wang X, et al. Midline 1 interacting protein 1 promotes cancer metastasis through FOS-like 1-mediated matrix metalloproteinase 9 signaling in HCC. Hepatology. 2023 Nov;78(5):1368–83.

218. Zhou T, Cao L, Du Y, Qin L, Lu Y, Zhang Q, et al. Gypenosides ameliorate high-fat diet-induced nonalcoholic fatty liver disease in mice by regulating lipid metabolism. PeerJ. 2023;11:e15225.

219. Sobolewski C, Abegg D, Berthou F, Dolicka D, Calo N, Sempoux C, et al. S100A11/ANXA2 belongs to a tumour suppressor/oncogene network deregulated early with steatosis and involved in inflammation and hepatocellular carcinoma development. Gut. 2020 Oct;69(10):1841–54.

220. Margraf A, Chen J, Christoforou M, Claria-Ribas P, Henriques Schneider A, Cecconello C, et al. Formyl-peptide receptor type 2 activation mitigates heart and lung damage in inflammatory arthritis. EMBO Mol Med. 2025 May;17(5):1153–83.

221. Chen Y, Qian B, Sun X, Kang Z, Huang Z, Ding Z, et al. Sox9/INHBB axis-mediated crosstalk between the hepatoma and hepatic stellate cells promotes the metastasis of hepatocellular carcinoma. Cancer Lett. 2021 Feb;499:243–54.

222. Kimura M, Moteki H, Ogihara M. Role of Hepatocyte Growth Regulators in Liver Regeneration. Cells. 2023 Jan;12(2).

223. Gao Y, Shen W, Lu B, Zhang Q, Hu Y, Chen Y. Upregulation of hepatic VLDLR via PPARα is required for the triglyceride-lowering effect of fenofibrate. J Lipid Res. 2014 Aug;55(8):1622–33.

224. Chella Krishnan K, Floyd RR, Sabir S, Jayasekera DW, Leon-Mimila P V, Jones AE, et al. Liver Pyruvate Kinase Promotes NAFLD/NASH in Both Mice and Humans in a Sex-Specific Manner. Cell Mol Gastroenterol Hepatol. 2021;11(2):389–406.

225. Wu T-T, Zheng Y-Y, Ma X, Xiu W-J, Yang H-T, Hou X-G, et al. Mutated CYP17A1 promotes atherosclerosis and early-onset coronary artery disease. Cell Commun Signal. 2023 Jun;21(1):155.

226. Graham K, Murphy JI, Dhoot GK. SULF1/SULF2 reactivation during liver damage and tumour growth. Histochem Cell Biol. 2016 Jul;146(1):85–97.

227. Pham D-H, Zhang C, Yin C. Using zebrafish to model liver diseases-Where do we stand? Curr Pathobiol Rep. 2017 Jun;5(2):207–21.

228. Donnelly KL, Smith CI, Schwarzenberg SJ, Jessurun J, Boldt MD, Parks EJ. Sources of fatty acids stored in liver and secreted via lipoproteins in patients with nonalcoholic fatty liver disease. J Clin Invest. 2005 May;115(5):1343–51.

229. Steensels S, Qiao J, Ersoy BA. Transcriptional Regulation in Non-Alcoholic Fatty Liver Disease. Metabolites. 2020 Jul;10(7).

230. Ding R-B, Bao J, Deng C-X. Emerging roles of SIRT1 in fatty liver diseases. Int J Biol Sci. 2017;13(7):852–67.

231. Della Fazia MA, Servillo G. Foie gras and liver regeneration: a fat dilemma. Cell Stress. 2018 Jun;2(7):162–75.

232. Tian C, Huang R, Xiang M. SIRT1: Harnessing multiple pathways to hinder NAFLD. Pharmacol Res. 2024 May;203:107155.

233. Fulco M, Sartorelli V. Comparing and contrasting the roles of AMPK and SIRT1 in metabolic tissues. Cell Cycle. 2008 Dec;7(23):3669–79.

234. Chen D, Bruno J, Easlon E, Lin S-J, Cheng H-L, Alt FW, et al. Tissue-specific regulation of SIRT1 by calorie restriction. Genes Dev. 2008 Jul;22(13):1753–7.

235. Xu X, So J-S, Park J-G, Lee A-H. Transcriptional control of hepatic lipid metabolism by SREBP and ChREBP. Semin Liver Dis. 2013 Nov;33(4):301–11.

236. Cantó C, Auwerx J. PGC-1alpha, SIRT1 and AMPK, an energy sensing network that controls energy expenditure. Curr Opin Lipidol. 2009 Apr;20(2):98–105.

237. Zhang C, Chen X, Zhu R-M, Zhang Y, Yu T, Wang H, et al. Endoplasmic reticulum stress is involved in hepatic SREBP-1c activation and lipid accumulation in fructose-fed mice. Toxicol Lett. 2012 Aug;212(3):229–40.

238. Ibrahim SH, Hirsova P, Gores GJ. Non-alcoholic steatohepatitis pathogenesis: sublethal hepatocyte injury as a driver of liver inflammation. Gut. 2018 May;67(5):963–72.

239. Hirsova P, Gores GJ. Death Receptor-Mediated Cell Death and Proinflammatory Signaling in Nonalcoholic Steatohepatitis. Cell Mol Gastroenterol Hepatol. 2015 Jan;1(1):17–27.

240. Wei Y, Wang D, Gentile CL, Pagliassotti MJ. Reduced endoplasmic reticulum luminal calcium links saturated fatty acid-mediated endoplasmic reticulum stress and cell death in liver cells. Mol Cell Biochem. 2009 Nov;331(1–2):31–40.

241. Lebeaupin C, Vallée D, Hazari Y, Hetz C, Chevet E, Bailly-Maitre B. Endoplasmic reticulum stress signalling and the pathogenesis of non-alcoholic fatty liver disease. J Hepatol. 2018 Oct;69(4):927–47.

242. Fu S, Yang L, Li P, Hofmann O, Dicker L, Hide W, et al. Aberrant lipid metabolism disrupts calcium homeostasis causing liver endoplasmic reticulum stress in obesity. Nature. 2011 May;473(7348):528–31.

243. Patterson RE, Kalavalapalli S, Williams CM, Nautiyal M, Mathew JT, Martinez J, et al. Lipotoxicity in steatohepatitis occurs despite an increase in tricarboxylic acid cycle activity. Am J Physiol Endocrinol Metab. 2016 Apr;310(7):E484-94.

244. Moore MP, Cunningham RP, Meers GM, Johnson SA, Wheeler AA, Ganga RR, et al. Compromised hepatic mitochondrial fatty acid oxidation and reduced markers of

mitochondrial turnover in human NAFLD. Hepatology. 2022 Nov;76(5):1452–65.

245. Koliaki C, Szendroedi J, Kaul K, Jelenik T, Nowotny P, Jankowiak F, et al. Adaptation of hepatic mitochondrial function in humans with non-alcoholic fatty liver is lost in steatohepatitis. Cell Metab. 2015 May;21(5):739–46.

246. Hughey CC, Puchalska P, Crawford PA. Integrating the contributions of mitochondrial oxidative metabolism to lipotoxicity and inflammation in NAFLD pathogenesis. Biochim Biophys acta Mol cell Biol lipids. 2022 Nov;1867(11):159209.

247. Staňková P, Kučera O, Peterová E, Lotková H, Maseko TE, Nožičková K, et al. Adaptation of Mitochondrial Substrate Flux in a Mouse Model of Nonalcoholic Fatty Liver Disease. Int J Mol Sci. 2020 Feb;21(3).

248. Simões ICM, Amorim R, Teixeira J, Karkucinska-Wieckowska A, Carvalho A, Pereira SP, et al. The Alterations of Mitochondrial Function during NAFLD Progression-An Independent Effect of Mitochondrial ROS Production. Int J Mol Sci. 2021 Jun;22(13).

249. Lee K, Haddad A, Osme A, Kim C, Borzou A, Ilchenko S, et al. Hepatic Mitochondrial Defects in a Nonalcoholic Fatty Liver Disease Mouse Model Are Associated with Increased Degradation of Oxidative Phosphorylation Subunits. Mol Cell Proteomics. 2018 Dec;17(12):2371–86.

250. Boland ML, Oldham S, Boland BB, Will S, Lapointe J-M, Guionaud S, et al. Nonalcoholic steatohepatitis severity is defined by a failure in compensatory antioxidant capacity in the setting of mitochondrial dysfunction. World J Gastroenterol. 2018 Apr;24(16):1748–65.

251. Zhang X, Fan L, Wu J, Xu H, Leung WY, Fu K, et al. Macrophage p38α promotes nutritional steatohepatitis through M1 polarization. J Hepatol. 2019 Jul;71(1):163–74.

252. Tomita K, Kabashima A, Freeman BL, Bronk SF, Hirsova P, Ibrahim SH. Mixed Lineage Kinase 3 Mediates the Induction of CXCL10 by a STAT1-Dependent Mechanism During Hepatocyte Lipotoxicity. J Cell Biochem. 2017 Oct;118(10):3249–59.

253. Tsuchida T, Friedman SL. Mechanisms of hepatic stellate cell activation. Nat Rev Gastroenterol Hepatol. 2017 Jul;14(7):397–411.

254. Mi X-J, Hou J-G, Jiang S, Liu Z, Tang S, Liu X-X, et al. Maltol Mitigates Thioacetamide-induced Liver Fibrosis through TGF-β1-mediated Activation of PI3K/Akt Signaling Pathway. J Agric Food Chem. 2019 Feb;67(5):1392–401.

255. Finnson KW, Almadani Y, Philip A. Non-canonical (non-SMAD2/3) TGF-β signaling in fibrosis: Mechanisms and targets. Semin Cell Dev Biol. 2020 May;101:115–22.

256. David CJ, Massagué J. Contextual determinants of TGFβ action in development, immunity and cancer. Nat Rev Mol Cell Biol. 2018 Jul;19(7):419–35.

257. Chen B, Zheng Y-M, Zhang J-P. Comparative Study of Different Diets-Induced NAFLD Models of Zebrafish. Front Endocrinol (Lausanne). 2018;9:366.

258. Gao X, Wang X, Zhang S. Bioinformatics identification of crucial genes and pathways associated with hepatocellular carcinoma. Biosci Rep. 2018 Dec;38(6).

259. Wang Z, Qin H, Yang Q, Jia J, Yang L, Zhong S, et al. Identification of Basement

Membrane Genes and Related Molecular Subtypes in Nonalcoholic Fatty Liver Disease. Horm Metab Res = Horm und Stoffwechselforsch = Horm Metab. 2023 Aug;55(8):546–54.

260. Wan Y, Ceci L, Wu N, Zhou T, Chen L, Venter J, et al. Knockout of α-calcitonin gene-related peptide attenuates cholestatic liver injury by differentially regulating cellular senescence of hepatic stellate cells and cholangiocytes. Lab Invest. 2019 Jun;99(6):764–76.

261. Day K, Seale LA, Graham RM, Cardoso BR. Selenotranscriptome Network in Non-alcoholic Fatty Liver Disease. Front Nutr. 2021;8:744825.

262. Bidooki SH, Sánchez-Marco J, Martínez-Beamonte R, Herrero-Continente T, Navarro MA, Rodríguez-Yoldi MJ, et al. Endoplasmic Reticulum Protein TXNDC5 Interacts with PRDX6 and HSPA9 to Regulate Glutathione Metabolism and Lipid Peroxidation in the Hepatic AML12 Cell Line. Int J Mol Sci. 2023 Dec;24(24).

263. Kishimoto N, Shimizu K, Sawamoto K. Neuronal regeneration in a zebrafish model of adult brain injury. Dis Model Mech. 2012 Mar;5(2):200–9.

264. Grandel H, Kaslin J, Ganz J, Wenzel I, Brand M. Neural stem cells and neurogenesis in the adult zebrafish brain: origin, proliferation dynamics, migration and cell fate. Dev Biol. 2006 Jul;295(1):263–77.

265. Adolf B, Chapouton P, Lam CS, Topp S, Tannhäuser B, Strähle U, et al. Conserved and acquired features of adult neurogenesis in the zebrafish telencephalon. Dev Biol. 2006 Jul;295(1):278–93.

266. Zhang G, Lübke L, Chen F, Beil T, Takamiya M, Diotel N, et al. Neuron-Radial Glial Cell Communication via BMP/Id1 Signaling Is Key to Long-Term Maintenance of the Regenerative Capacity of the Adult Zebrafish Telencephalon. Cells. 2021 Oct;10(10).

267. Hentig J, Campbell LJ, Cloghessy K, Lee M, Boggess W, Hyde DR. Prophylactic Activation of Shh Signaling Attenuates TBI-Induced Seizures in Zebrafish by Modulating Glutamate Excitotoxicity through Eaat2a. Biomedicines. 2021 Dec;10(1).

268. Di Giaimo R, Durovic T, Barquin P, Kociaj A, Lepko T, Aschenbroich S, et al. The Aryl Hydrocarbon Receptor Pathway Defines the Time Frame for Restorative Neurogenesis. Cell Rep. 2018 Dec;25(12):3241-3251.e5.

269. Demirci Y, Cucun G, Poyraz YK, Mohammed S, Heger G, Papatheodorou I, et al. Comparative Transcriptome Analysis of the Regenerating Zebrafish Telencephalon Unravels a Resource With Key Pathways During Two Early Stages and Activation of Wnt/β-Catenin Signaling at the Early Wound Healing Stage. Front cell Dev Biol. 2020;8:584604.

270. Kyritsis N, Kizil C, Zocher S, Kroehne V, Kaslin J, Freudenreich D, et al. Acute inflammation initiates the regenerative response in the adult zebrafish brain. Science. 2012 Dec;338(6112):1353–6.

271. Gence L, Fernezelian D, Meilhac O, Rastegar S, Bascands J-L, Diotel N. Insulin signaling promotes neurogenesis in the brain of adult zebrafish. J Comp Neurol. 2023 Dec;531(17):1812–27.

272. Cacialli P, Palladino A, Lucini C. Role of brain-derived neurotrophic factor during the regenerative response after traumatic brain injury in adult zebrafish. Neural Regen Res.

2018 Jun;13(6):941–4.

273. Srivastava PP, Bhasin S, Shankaran SS, Roger C, Ramachandran R, Minocha S. A reproducible method to study traumatic injury-induced zebrafish brain regeneration. Biol methods Protoc. 2024;9(1):bpae073.

274. Hussain G, Akram R, Anwar H, Sajid F, Iman T, Han HS, et al. Adult neurogenesis: a real hope or a delusion? Neural Regen Res. 2024 Jan;19(1):6–15.

275. Faigle R, Brederlau A, Elmi M, Arvidsson Y, Hamazaki TS, Uramoto H, et al. ASK1 inhibits astroglial development via p38 mitogen-activated protein kinase and promotes neuronal differentiation in adult hippocampus-derived progenitor cells. Mol Cell Biol. 2004 Jan;24(1):280–93.

276. Albert-Gascó H, Ros-Bernal F, Castillo-Gómez E, Olucha-Bordonau FE. MAP/ERK Signaling in Developing Cognitive and Emotional Function and Its Effect on Pathological and Neurodegenerative Processes. Int J Mol Sci. 2020 Jun;21(12).

277. Wang H, Engstrom AK, Xia Z. Cadmium impairs the survival and proliferation of cultured adult subventricular neural stem cells through activation of the JNK and p38 MAP kinases. Toxicology. 2017 Apr;380:30–7.

278. Langfelder P, Horvath S. WGCNA: an R package for weighted correlation network analysis. BMC Bioinformatics. 2008 Dec;9:559.

279. Love MI, Huber W, Anders S. Moderated estimation of fold change and dispersion for RNA-seq data with DESeq2. Genome Biol. 2014;15(12):550.

280. Li A, Horvath S. Network neighborhood analysis with the multi-node topological overlap measure. Bioinformatics. 2007 Jan;23(2):222–31.

281. Baumgart EV, Barbosa JS, Bally-Cuif L, Götz M, Ninkovic J. Stab wound injury of the zebrafish telencephalon: a model for comparative analysis of reactive gliosis. Glia. 2012 Mar;60(3):343–57.

282. Winter CD, Pringle AK, Clough GF, Church MK. Raised parenchymal interleukin-6 levels correlate with improved outcome after traumatic brain injury. Brain. 2004 Feb;127(Pt 2):315–20.

283. Kossmann T, Hans V, Imhof HG, Trentz O, Morganti-Kossmann MC. Interleukin-6 released in human cerebrospinal fluid following traumatic brain injury may trigger nerve growth factor production in astrocytes. Brain Res. 1996 Mar;713(1–2):143–52.

284. Hasegawa T, Hall CJ, Crosier PS, Abe G, Kawakami K, Kudo A, et al. Transient inflammatory response mediated by interleukin-1β is required for proper regeneration in zebrafish fin fold. Elife. 2017 Feb;6.

285. Chen X-K, Kwan JS-K, Wong GT-C, Yi Z-N, Ma AC-H, Chang RC-C. Leukocyte invasion of the brain after peripheral trauma in zebrafish (*Danio rerio*). Exp Mol Med. 2022 Jul;54(7):973–87.

286. Wu Y-H, Hsieh H-L. Roles of Heme Oxygenase-1 in Neuroinflammation and Brain Disorders. Antioxidants (Basel, Switzerland). 2022 May;11(5).

287. Bouhlel MA, Derudas B, Rigamonti E, Dièvart R, Brozek J, Haulon S, et al. PPARgamma activation primes human monocytes into alternative M2 macrophages

with anti-inflammatory properties. Cell Metab. 2007 Aug;6(2):137–43.

288. Koenis DS, Medzikovic L, van Loenen PB, van Weeghel M, Huveneers S, Vos M, et al. Nuclear Receptor Nur77 Limits the Macrophage Inflammatory Response through Transcriptional Reprogramming of Mitochondrial Metabolism. Cell Rep. 2018 Aug;24(8):2127-2140.e7.

289. Rostad KO, Trognitz T, Frøyset AK, Bifulco E, Fladmark KE. Accelerated Sarcopenia Phenotype in the DJ-1/Park7-Knockout Zebrafish. Antioxidants (Basel, Switzerland). 2024 Dec;13(12).

290. Weijts BGMW, Bakker WJ, Cornelissen PWA, Liang K-H, Schaftenaar FH, Westendorp B, et al. E2F7 and E2F8 promote angiogenesis through transcriptional activation of VEGFA in cooperation with HIF1. EMBO J. 2012 Oct;31(19):3871–84.

291. Melincovici CS, Boşca AB, Şuşman S, Mărginean M, Mihu C, Istrate M, et al. Vascular endothelial growth factor (VEGF) - key factor in normal and pathological angiogenesis. Rom J Morphol Embryol = Rev Roum Morphol Embryol. 2018;59(2):455–67.

292. Fernández-Hernando C, Suárez Y. ANGPTL4: a multifunctional protein involved in metabolism and vascular homeostasis. Curr Opin Hematol. 2020 May;27(3):206–13.

293. Nicolas CS, Peineau S, Amici M, Csaba Z, Fafouri A, Javalet C, et al. The Jak/STAT pathway is involved in synaptic plasticity. Neuron. 2012 Jan;73(2):374–90.

294. Liao P, Han S, Qu H. Expression, Prognosis, and Immune Infiltrates Analyses of E2Fs in Human Brain and CNS Cancer. Biomed Res Int. 2020;2020:6281635.

295. Bonfanti L, Seki T. The PSA-NCAM-Positive "Immature" Neurons: An Old Discovery Providing New Vistas on Brain Structural Plasticity. Cells. 2021 Sep;10(10).

296. Overlack K, Primorac I, Vleugel M, Krenn V, Maffini S, Hoffmann I, et al. A molecular basis for the differential roles of Bub1 and BubR1 in the spindle assembly checkpoint. Elife. 2015 Jan;4:e05269.

297. Du L, Jing J, Wang Y, Xu X, Sun T, Shi Y, et al. Knockdown of SASS6 reduces growth of MDA-MB-231 triple-negative breast cancer cells through arrest of the cell cycle at the G2/M phase. Oncol Rep. 2021 Jun;45(6).

298. Li L, Liu C, Carr AL. STIL: a multi-function protein required for dopaminergic neural proliferation, protection, and regeneration. Cell death Discov. 2019;5:90.

299. Feng Y, Tang D, Wang J. Emerging role and function of SPDL1 in human health and diseases. Open Med (Warsaw, Poland). 2024;19(1):20240922.

300. Yasuhara T, Suzuki T, Katsura M, Miyagawa K. Rad54B serves as a scaffold in the DNA damage response that limits checkpoint strength. Nat Commun. 2014 Nov;5:5426.

301. Zhang J, Wang Z, Liu Z, Chen Z, Jiang J, Ji Y, et al. CENPF promotes the proliferation of renal cell carcinoma in vitro. Transl Androl Urol. 2023 Feb;12(2):320–9.

302. Fattahi F, Grailer JJ, Parlett M, Lu H, Malan EA, Abe E, et al. Requirement of Complement C6 for Intact Innate Immune Responses in Mice. J Immunol. 2020 Jul;205(1):251–60.

303. Brand FJ 3rd, de Rivero Vaccari JC, Mejias NH, Alonso OF, de Rivero Vaccari JP. RIG-I contributes to the innate immune response after cerebral ischemia. J Inflamm (Lond).

2015;12:52.

304. Goto M, Mizuno M, Matsumoto A, Yang Z, Jimbo EF, Tabata H, et al. Role of a circadian-relevant gene NR1D1 in brain development: possible involvement in the pathophysiology of autism spectrum disorders. Sci Rep. 2017 Mar;7:43945.

305. Yu T, Gao M, Yang P, Liu D, Wang D, Song F, et al. Insulin promotes macrophage phenotype transition through PI3K/Akt and PPAR-γ signaling during diabetic wound healing. J Cell Physiol. 2019 Apr;234(4):4217–31.

306. Akram R, Anwar H, Javed MS, Rasul A, Imran A, Malik SA, et al. Axonal Regeneration: Underlying Molecular Mechanisms and Potential Therapeutic Targets. Biomedicines. 2022 Dec;10(12).

307. Vafaee F, Zarifkar A, Emamghoreishi M, Namavar MR, Shirzad S, Ghazavi H, et al. Insulin-Like Growth Factor 2 (IGF-2) Regulates Neuronal Density and IGF-2 Distribution Following Hippocampal Intracerebral Hemorrhage. J stroke Cerebrovasc Dis Off J Natl Stroke Assoc. 2020 Oct;29(10):105128.

308. Aberg ND, Brywe KG, Isgaard J. Aspects of growth hormone and insulin-like growth factor-I related to neuroprotection, regeneration, and functional plasticity in the adult brain. ScientificWorldJournal. 2006 Jan;6:53–80.

309. Yin Y, Kong D, He K, Xia Q. Aurora kinase A regulates liver regeneration through macrophages polarization and Wnt/β-catenin signalling. Liver Int Off J Int Assoc Study Liver. 2022 Feb;42(2):468–78.

310. Pérez de Castro I, Aguirre-Portolés C, Fernández-Miranda G, Cañamero M, Cowley DO, Van Dyke T, et al. Requirements for Aurora-A in tissue regeneration and tumor development in adult mammals. Cancer Res. 2013 Nov;73(22):6804–15.

311. Gwee SSL, Radford RAW, Chow S, Syal MD, Morsch M, Formella I, et al. Aurora kinase B regulates axonal outgrowth and regeneration in the spinal motor neurons of developing zebrafish. Cell Mol Life Sci. 2018 Dec;75(23):4269–85.

312. Guo Z, Chen M, Chao Y, Cai C, Liu L, Zhao L, et al. RGCC balances self-renewal and neuronal differentiation of neural stem cells in the developing mammalian neocortex. EMBO Rep. 2021 Sep;22(9):e51781.

313. Ro EJ, Cho Y-H, Jeong W-J, Park J-C, Min DS, Choi K-Y. WDR76 degrades RAS and suppresses cancer stem cell activation in colorectal cancer. Cell Commun Signal. 2019 Jul;17(1):88.

314. Jeong W-J, Park J-C, Kim W-S, Ro EJ, Jeon SH, Lee S-K, et al. WDR76 is a RAS binding protein that functions as a tumor suppressor via RAS degradation. Nat Commun. 2019 Jan;10(1):295.

315. Kearsey SE, Maiorano D, Holmes EC, Todorov IT. The role of MCM proteins in the cell cycle control of genome duplication. Bioessays. 1996 Mar;18(3):183–90.

316. Wasilewska I, Gupta RK, Palchevska O, Kuźnicki J. Identification of Zebrafish Calcium Toolkit Genes and their Expression in the Brain. Genes (Basel). 2019 Mar;10(3).

317. Glaser T, Arnaud Sampaio VF, Lameu C, Ulrich H. Calcium signalling: A common target in neurological disorders and neurogenesis. Semin Cell Dev Biol. 2019 Nov;95:25–33.

318. Mason I. The RET receptor tyrosine kinase: activation, signalling and significance in neural development and disease. Pharm Acta Helv. 2000 Mar;74(2–3):261–4.

319. Sato T, Sato F, Kamezaki A, Sakaguchi K, Tanigome R, Kawakami K, et al. Neuregulin 1 Type II-ErbB Signaling Promotes Cell Divisions Generating Neurons from Neural Progenitor Cells in the Developing Zebrafish Brain. PLoS One. 2015;10(5):e0127360.

320. Mei L, Nave K-A. Neuregulin-ERBB signaling in the nervous system and neuropsychiatric diseases. Neuron. 2014 Jul;83(1):27–49.

321. Gomez GA, Veldman MB, Zhao Y, Burgess S, Lin S. Discovery and characterization of novel vascular and hematopoietic genes downstream of etsrp in zebrafish. PLoS One. 2009;4(3):e4994.

322. Roy NM, Sagerström CG. An early Fgf signal required for gene expression in the zebrafish hindbrain primordium. Brain Res Dev Brain Res. 2004 Jan;148(1):27–42.

323. Itoh N, Konishi M. The zebrafish fgf family. Zebrafish. 2007;4(3):179–86.

324. Choi C, Benveniste EN. Fas ligand/Fas system in the brain: regulator of immune and apoptotic responses. Brain Res Brain Res Rev. 2004 Jan;44(1):65–81.

325. Iribarne M, Hyde DR. Different inflammation responses modulate Müller glia proliferation in the acute or chronically damaged zebrafish retina. Front cell Dev Biol. 2022;10:892271.

326. Jeffrey KL, Camps M, Rommel C, Mackay CR. Targeting dual-specificity phosphatases: manipulating MAP kinase signalling and immune responses. Nat Rev Drug Discov. 2007 May;6(5):391–403.

327. Huang C-Y, Tan T-H. DUSPs, to MAP kinases and beyond. Cell Biosci. 2012 Jul;2(1):24.

328. Jakaria M, Haque ME, Cho D-Y, Azam S, Kim I-S, Choi D-K. Molecular Insights into NR4A2(Nurr1): an Emerging Target for Neuroprotective Therapy Against Neuroinflammation and Neuronal Cell Death. Mol Neurobiol. 2019 Aug;56(8):5799–814.

329. Fernezelian D, Rondeau P, Gence L, Diotel N. Telencephalic stab wound injury induces regenerative angiogenesis and neurogenesis in zebrafish: unveiling the role of vascular endothelial growth factor signaling and microglia. Neural Regen Res. 2025 Oct;20(10):2938–54.

330. Fernezelian D, Pfitsch S, Rastegar S, Diotel N. Mapping the cellular expression patterns of vascular endothelial growth factor aa and bb genes and their receptors in the adult zebrafish brain during constitutive and regenerative neurogenesis. Neural Dev. 2024 Sep;19(1):17.

331. Gupta A, Bansal A, Hashimoto-Torii K. HSP70 and HSP90 in neurodegenerative diseases. Neurosci Lett. 2020 Jan;716:134678.

332. Shurin MR, Esche C, Lotze MT. FLT3: receptor and ligand. Biology and potential clinical application. Cytokine Growth Factor Rev. 1998 Mar;9(1):37–48.

333. Yanase S, Yasuda K, Ishii N. Interaction between the ins/IGF-1 and p38 MAPK signaling pathways in molecular compensation of sod genes and modulation related to

intracellular ROS levels in C. elegans. Biochem Biophys reports. 2020 Sep;23:100796.

334. Mills BN, Albert GP, Halterman MW. Expression Profiling of the MAP Kinase Phosphatase Family Reveals a Role for DUSP1 in the Glioblastoma Stem Cell Niche. Cancer Microenviron Off J Int Cancer Microenviron Soc. 2017 Dec;10(1–3):57–68.

335. Stokoe D, Engel K, Campbell DG, Cohen P, Gaestel M. Identification of MAPKAP kinase 2 as a major enzyme responsible for the phosphorylation of the small mammalian heat shock proteins. FEBS Lett. 1992 Nov;313(3):307–13.

336. Grierson PM, Dodhiawala PB, Cheng Y, Chen TH-P, Khawar IA, Wei Q, et al. The MK2/Hsp27 axis is a major survival mechanism for pancreatic ductal adenocarcinoma under genotoxic stress. Sci Transl Med. 2021 Dec;13(622):eabb5445.

337. Zhao M, New L, Kravchenko V V, Kato Y, Gram H, di Padova F, et al. Regulation of the MEF2 family of transcription factors by p38. Mol Cell Biol. 1999 Jan;19(1):21–30.

338. Humar M, Loop T, Schmidt R, Hoetzel A, Roesslein M, Andriopoulos N, et al. The mitogen-activated protein kinase p38 regulates activator protein 1 by direct phosphorylation of c-Jun. Int J Biochem Cell Biol. 2007;39(12):2278–88.

339. Bikkavilli RK, Feigin ME, Malbon CC. p38 mitogen-activated protein kinase regulates canonical Wnt-beta-catenin signaling by inactivation of GSK3beta. J Cell Sci. 2008 Nov;121(Pt 21):3598–607.

340. Chen S, Liu Y, Rong X, Li Y, Zhou J, Lu L. Neuroprotective Role of the PI3 Kinase/Akt Signaling Pathway in Zebrafish. Front Endocrinol (Lausanne). 2017;8:21.

341. Attilio PJ, Snapper DM, Rusnak M, Isaac A, Soltis AR, Wilkerson MD, et al. Transcriptomic Analysis of Mouse Brain After Traumatic Brain Injury Reveals That the Angiotensin Receptor Blocker Candesartan Acts Through Novel Pathways. Front Neurosci. 2021;15:636259.

342. Hamanoue M, Morioka K, Ohsawa I, Ohsawa K, Kobayashi M, Tsuburaya K, et al. Cell-permeable p38 MAP kinase promotes migration of adult neural stem/progenitor cells. Sci Rep. 2016 Apr;6:24279.

343. Vriz S, Reiter S, Galliot B. Chapter Five - Cell Death: A Program to Regenerate. In: Galliot BBT-CT in DB, editor. Mechanisms of Regeneration [Internet]. Academic Press; 2014. p. 121–51. Available from: https://www.sciencedirect.com/science/article/pii/B9780123914989000024

344. Ryoo HD, Bergmann A. The role of apoptosis-induced proliferation for regeneration and cancer. Cold Spring Harb Perspect Biol. 2012 Aug;4(8):a008797.

345. Charni M, Aloni-Grinstein R, Molchadsky A, Rotter V. p53 on the crossroad between regeneration and cancer. Cell Death Differ. 2017 Jan;24(1):8–14.

346. Feng J, Yang J. Glioma-neuron interactions: insights from neural plasticity. Front Oncol. 2025;15:1661897.

347. Yu G, Wang L-G, Han Y, He Q-Y. clusterProfiler: an R package for comparing biological themes among gene clusters. OMICS. 2012 May;16(5):284–7.

348. Chiu JW, Binte Hanafi Z, Chew LCY, Mei Y, Liu H. IL-1α Processing, Signaling and Its Role in Cancer Progression. Cells. 2021 Jan;10(1).

349. Gelfo V, Romaniello D, Mazzeschi M, Sgarzi M, Grilli G, Morselli A, et al. Roles of IL-1 in Cancer: From Tumor Progression to Resistance to Targeted Therapies. Int J Mol Sci. 2020 Aug;21(17).

350. Högel H, Miikkulainen P, Bino L, Jaakkola PM. Hypoxia inducible prolyl hydroxylase PHD3 maintains carcinoma cell growth by decreasing the stability of p27. Mol Cancer. 2015 Jul;14:143.

Publications

* *equal contribution*

Thesis Publications

1. Kaushal, S*., Bhattacharya, D*., Kumar, S., Herr, W., Dhanjal, J. K., & Minocha, S. (2025). Epigenetic modifications in the murine liver upon depletion of transcriptional coregulator host cell factor 1. BMC genomics, 26(1), 654. https://doi.org/10.1186/s12864-025-11786-5

2. Bhattacharya, D*., **Kaushal, S*.,** Chakraborty, B., Raha, A., Dutta, T., Shekhar, H., Koner, A. L., Kumar, S., Ramachandran, R., Kaur Dhanjal, J., & Minocha, S. (2025). Zebrafish model of palmitic acid induced MAFLD recapitulates pathways conserved in mice and humans. Scientific reports, 15(1), 33343. https://doi.org/10.1038/s41598-025-13154-5

3. Bhasin, S*., **Kaushal, S.*,** Srivastava, P. P.*, Menon, M. B., Ramachandran, R., Dhanjal, J. K., & Minocha, S. (2025). From injury to recovery: transcriptomic dynamics in zebrafish brain regeneration. Journal of translational medicine, 24(1), 87. https://doi.org/10.1186/s12967-025-07400-7

Other Publications

1. Ayushma, Srivastava, P. P., **Kaushal, S**., Dhanjal, J. K., Kapuria, V., & Minocha, S. (2026). The HCF-1:OGT axis regulates neuronal proliferation and differentiation. *Neurobiology of disease*, *220*, 107308. https://doi.org/10.1016/j.nbd.2026.107308

2. Kaushal, S.*, Gupta, S.*, Shefrin, S., Vora, D. S., Kaul, S. C., Sundar, D., Wadhwa, R., & Dhanjal, J. K. (2024). Synthetic and Natural Inhibitors of Mortalin for Cancer Therapy. *Cancers*, *16*(20), 3470. https://doi.org/10.3390/cancers16203470

3. Hemlata, Murali, N., Roy, S., Joshi, Y. C., Das, R. N., Hariharan, A., Shankaran, S., Mudgal, P., Shekhar, H., **Kaushal, S**., Dhanjal, J. K., Tanwar, P., Batra, A., Kumar, S., Betal, S., & Minocha, S. (2026). pH-responsive dual-drug-loaded bovine serum albumin nanoparticles for targeted cancer therapy. *International journal of biological macromolecules*, 365, 152319. Advance online publication. https://doi.org/10.1016/j.ijbiomac.2026.152319

4. Gupta, S.*, **Kaushal, S.*,** Bhargava, P., Ishida, Y., Terao, K., Kaul, S.C., Dhanjal, J. K., Wadhwa, R. (2025). Molecular Insights into the Neurogenic Potential of Alpha-Lipoic Acid (2025). *Current Topics in Medicinal Chemistry*, 26(15):1649 - 1663.

https://doi.org/10.2174/0115680266426195260219062738

5. Roy, S., **Kaushal, S.,** Tandon, R., Dhanjal, J. K., Herr, W., Kumar, S., & Minocha, S. (2026). Metabolomic insights into HCF-1-dependent regulation of liver homeostasis. *Journal of Clinical and Experimental Hepatology*, 16(5):103602. https://doi.org/10.1016/j.jceh.2026.103602

6. Kaushal, S*.; Gupta, S.*; Shefrin, S.; Vora, D.S.; Kaul, S.C.; Sundar, D.; Wadhwa, R.; Dhanjal, J.K. (2024). Synthetic and Natural Inhibitors of Mortalin for Cancer Therapy. *Cancers*, *16*, 3470. https://doi.org/10.3390/cancers16203470

7. Raha, A.*, Paul, P.*, Gupta, S.*, **Kaushal, S.*** and Dhanjal, J.K., (2024). Paradigm shift in stem cell research with computational tools, techniques, and databases. In *Computational Biology for Stem Cell Research*, Raghav, P.K, Kumar, R., Lathwal, A. and Sharma, S. (Eds.), *pp. 17-32. Academic Press. (Book ISBN: 9780443132223).* https://doi.org/10.1016/B978-0-443-13222-3.00019-8

8. Nofita Sari, A., Yi, J., **Kaushal, S**., Ishida, Y., Nakata, D., Terao, K., Kaul, S. C., Yun, C.-O., Dhanjal, J. K., Yoon, A.-R., & Wadhwa, R. A low dose combination of Withaferin A and Caffeic Acid Phenethyl Ester inhibits cancer cell stemness: In vitro and in vivo evidence. (Manuscript communicated for publication)

9. Ayushma, **Kaushal S**, Venkatraman R, Dhanapal S, Thankachan R, Sehrish S, Shankaran SS, Sachidanandan C, Dhanjal JK, Ramachandran R, Minocha S. HCF-1:OGT-mediated transcriptional regulation of WDR91 coordinates neuronal differentiation and CNS regeneration. (Manuscript communicated for publication)